Investigation of Energy Storage Options for Sustainable Energy Systems

By

Mehdi Hosseini

A Thesis Submitted in Partial Fulfillment

of the Requirements for the degree of Doctor of Philosophy

in

Mechanical Engineering

Faculty of Engineering and Applied Science

University of Ontario Institute of Technology

Oshawa, Ontario, Canada

Abstract

Determination of the possible energy storage options for a specific source of energy requires a thorough analysis from the points of energy, exergy, and exergoeconomics. The main objective of this thesis is to investigate energy storage options for sustainable energy systems. A technology description and illustration of concerns regarding each system is presented. Moreover, the possibility of implementing each option into different sources of energy is investigated. Thus, integrated energy systems are developed, utilizing energy storage options with the aim of achieving more efficient systems.

Energy and exergy analyses are performed for three novel, integrated renewable energy-based systems. Energy storage methods investigated here include hydrogen storage, thermal energy storage, compressed air energy storage, and battery. Solar, wind, and biomass are the energy sources considered for the integrated systems. In this research, a discussion on various energy storage systems is presented, and the potential of each storage option in the current and future energy market is studied.

Each of the integrated systems is described and its operating strategy is presented. The components of the integrated systems are first modeled to obtain their operating characteristics. The energy, exergy, and exergoeconomic equations are applied to the components to calculate the rates of energy and exergy flows. The efficiencies are subsequently calculated. The results of energy and exergy analyses are combined with exergoeconomic equations to report the unit exergy cost of flows in the components.

System 1 consists of a PV system, a water electrolyser and a fuel cell to generate electricity for a house. Hydrogen and thermal energy storage are considered as the storage options. The results show that the capacities of the components depend on weather data and electric power demand. In System 1, the PV electric power output exceeds demand during months with high-solar irradiance. The results of a case study based on the weather data in Toronto, Canada, and the electricity demand pattern of a Canadian house (5.74 kW maximum demand) are presented. The photovoltaic system capacity and the electrolyser nominal hydrogen production rate are 37.17 kW and 4.5 kg/day, respectively. The economic investigation of the hybrid system reports an average cost of electricity of 0.84 $/kWh based on 25 years of operation. The optimal

nominal capacity of the fuel cell is found to be 1.5 kW, according to the optimization results. The optimal exergy efficiency varies from 9.91 to 9.94%.

System 2 consists of a wind park, a PV-fuel cell and a biomass-fuel cell-gas turbine system. This integrated renewable energy-based system is developed for baseload power generation and utilizes wind, solar and biomass energy resources. For a 64 bar compressed air storage system, and a 36 bar gas turbine inlet air pressure, 356 wind turbines are required. The lower the pressure difference between the compressed air in the cavern and the gas turbine inlet air pressure, the fewer the number of wind turbines required in the Wind-CAES system. The results also show that 5.4×10^5 PV modules (covering 0.66 Mm^2 of land) are required to generate 5 MW of baseload electric power. Optimization of System 2 provides a range of optimal points at which the exergy efficiency and the total purchase cost of the system are optimum. At an optimal point, the overall exergy efficiency of the integrated system is reported as 36.85%. At this point, the optimal values of compression ratio, gas turbine expansion ratio, and CAES storage capacity are 8, 6.5, and 240 h, respectively.

System 3 consists of a biomass gasifier integrated with a gas turbine cycle (biomass-GT). As another sub-part of System 3, a PV-electrolyser module is integrated with a compressed air energy storage system. The overall hybrid system supplies 10 MW baseload electric power, and 7730 MWh thermal energy. The PV is accountable for 56% of the annual exergy destruction in the hybrid system, and 38% of the annual exergy destruction occurs in the biomass-GT system. The overall energy and exergy efficiencies of System 3 are 34.8 and 34.1%, respectively. The hybrid PV-biomass system is sensitive to some parameters such as the steam-to-carbon ratio of the biomass gasifier, and the gas turbine inlet temperature and expansion ratio. A 29% increase in energy and exergy efficiencies is reported with the increase in SC from 1 to 3 mol/mol. The related specific carbon dioxide emission reduction is from 1441 to 583 g/kWh.

Acknowledgments

I would like to express my deep and sincere gratitude to my supervisor, Dr. Ibrahim Dincer and my co-supervisor, Dr. Marc A. Rosen, for their resourceful guidance and never-ending support.

I also acknowledge the support provided by the Natural Sciences and Engineering Research Council of Canada.

I would like to thank my family for their support and encouragement throughout my education.

Table of Contents

List of Figures

List of Tables

Nomenclature

a	Completion factor
c_p	Constant pressure specific heat, kJ/kgK
D	Diameter, m
ex	Specific exergy, kJ/kg
$\dot{E}n$	Energy flow rate, kW
$\dot{E}x$	Exergy flow rate, kW
G	Solar irradiance, kW/m^2
h	Specific enthalpy, kJ/kg
I_L	PV light current, A
I_0	Reverse saturation current, A
I	Electric current, A
$\dot{I}$	Exergy destruction rate, kW
K	Boltzmann constant
k_t	Temperature coefficient of short-circuit current, A/°C
LHV	Lower heating value, kJ/kg
$\dot{m}$	Mass flow rate, kg/s
P	Power, kW; Pressure, bar
$\dot{Q}$	Heat transfer rate, kW
r_c	Compression ratio
r_{GT}	Expansion ratio
R_s	Series resistance of the PV cells, Ohm
SC	Steam to carbon ratio, mol/mol
T	Temperature, K
TIT	Turbine inlet temperature, K
v	Velocity, m/s
w	Specific work, kJ/kg
W	Work, kJ
$\dot{W}$	Work rate, kW

Greek letters

ρ	Density, kg/m^3
γ	PV cell shape factor
η	Energy efficiency, %
ψ	Exergy efficiency, %
ω	Moisture fraction of biomass, $kg_{water}/kg_{biomass}$

Subscripts

0	Ambient condition
bm	Biomass
c	Compressor
cell	PV cells
c.a	Compressed air stored in the cavern
DH	District heating
EL	Electrolyser
evap	Evaporator
f	Fuel
g	Gas
FWP	Feed water pump
h	Heat
H_2	Hydrogen
in, el	Input to the electrolyser
L,C	Loss during charging phase
L,D	Loss during discharging phase
L,S	Loss during storage phase
mb	Moist biomass
mp	Maximum power
S	Steam
SOFC	Solid oxide fuel cell
wb	Wet biomass
WP	Wind park

Acronyms

CAES	Compressed air energy storage
CGH_2	Compressed gaseous hydrogen
CHP	Combined heat and power
DG	Distributed generation
GT	Gas turbine
HEV	Hybrid electric vehicle
HRSG	Heat recovery steam generator
LH	Liquid hydrogen
MCFC	Molten carbonate fuel cell
MED	Multi-effect desalination
MGT	Micro gas turbine
PEM	Proton exchange membrane
PV	Photovoltaic

PV-FC	Photovoltaic-fuel cell
PV-H_2- FC	Photovoltaic-hydrogen-fuel cell
SOFC	Solid oxide fuel cell
STC	Standard test condition
TIT	Gas turbine inlet temperature
TVC	Thermal vapour compression
WP	Wind park

Chapter 1: Introduction

With today's production and use of energy, the environment faces the threat of global warming and depletion of energy resources. Accordingly, industrial countries are trying to find ways to keep the environment "sustainable". In the effort to promote sustainability, in 1997, representatives of 160 countries gathered in Kyoto at the United Nations Framework Convention on Climate Change to discuss methods to decrease the threat of global warming. The results of the convention were named the Kyoto Protocol which put a limit on CO_2 emissions in industrialized countries. As another example, in 2007 the European Union (EU) issued a Communication on a "Strategy for Energy Policy for Europe", consisting of a reliable plan into securing a sustainable energy future. One example of important legislation on the matter of mitigating global warming by the use of energy storage, is the Commission's communication, which state that efficient and sustainable energy use requires energy storage to play a major role (Naish et al., 2007).

1.1 Why Energy Storage?

The type of energy used in daily life usually is in a converted form. Conversion and storage are the two main steps in energy utilization. Chemical energy stored in well-known fossil fuels is a form of abundant solar energy stored underneath the Earth's surface for millions of years. Despite the difficulties in extracting fossil fuels, the rate of consumption is increasing annually. In addition, the by-products of burning fossil fuels are the main cause of greenhouse gas emissions and environment pollution. Thinking of less polluting, more abundant and non-diminishing sources of energy the direct use of renewable energy arises. Solar and wind energy are available everywhere; as long as the Sun shines and the wind blows. Unlike fossil fuels, biomass does not require millions of years to form. It is formed from living plants and animals. Biomass is a renewable energy resource since it can be harvested and replanted. Biomass is formed during the photosynthesis process in plants, where they take in sunlight, water, and carbon dioxide from their environment. Therefore,

burning or gasification of biomass only releases the amount of CO_2 that was absorbed by the plant. That is the reason biomass consumption is considered a carbon-neutral process (Basu, 2010). Unfortunately, renewable energies are intermittently available. Many technologies have emerged to convert renewable energies; e.g. photovoltaic for converting solar energy, and wind turbines for converting wind energy into electricity. Afterwards, the generated electric energy can be stored in different ways: as electrochemical energy stored in batteries, or as chemical energy stored in hydrogen produced by water electrolysis.

Energy storage options are not only implemented to renewable energies, but also can be used to store other forms of energy. For instance, heavy fossil fuels can be converted into the less polluting and more environmentally friendly energy carrier, hydrogen. Next, the produced hydrogen is stored in hydrogen storage systems for later use. The generated electric energy surplus by the base power generation plants can be converted into potential energy of elevated water behind a hydroelectric dam during off-peak hours. Whenever required, the stored water flows down a hydro turbine producing electricity. In addition, this off-peak, low-price electricity can be stored in high technology batteries, in super-capacitors, or it can be used in an electrolyser to produce hydrogen for later use.

Since sustainability deals with managing resources and a healthy environment, the idea of energy storage can help to achieve these goals. The concept is apparent; surplus or intermittent forms of energy are stored for a more efficient use while required. However, the storage process and the storage system must meet all the regulations of sustainability. Thus, different methods and systems should be examined to cover all the concerns in this matter.

The interest in energy storage is inspired by at least five factors (Krein, 2007):

- advancement of storage technologies
- dramatic change in fossil fuel prices
- change in the pattern of energy utilization and the development of off-grid electricity generation
- problems with the available transmission and distribution facilities and the difficulties with their development

Energy storage systems can be implemented in power generation, transmission, and distribution to increase power supply reliability. Table 1.1 illustrates some main points regarding the benefits of energy storage to the electricity distribution sector.

Table 1.1: Some applications of energy storage systems in electricity distribution sector

Transmission and Distribution	The distribution lines are designed for high-peak loads. However, peak demand grows relatively with the growth of societies. Therefore, either new systems should be constructed, or the available transmission and distribution systems , which are mostly expensive or technically impossible, should be re-designed and reconstructed,. With the aim of energy storage systems near the load, these difficulties can be avoided or deferred. Off-peak energy can be stored when the transmission and distribution lines are lightly loaded, and discharged during peak periods when the system may otherwise be overloaded (Nourai, 2007).
Black Out	Even power plants require a source of electricity to start up and provide the grid with electricity. An energy storage system (batteries, pumped-hydro powers) can meet such demands.
Power Quality and Stability	Energy storage can be used to assist in a general class of services referred to as power quality and stability. Electric power systems experience some oscillations and disturbances in frequency. Energy storage systems can be used to off-set the disturbances, and provide stability.

There are many valuable applications for energy storage systems. Providing emergency and backup power for increased reliability is but one example. Energy storage systems can be categorized based on the form of energy. A simple classification with some examples of the respective storage options are presented here (Dincer and Rosen, 2011c):

- ***Mechanical storage:*** pumped hydro storage, compressed air storage, flywheels
- ***Chemical:*** hydrogen, biofuels, electrochemical batteries, organic molecular storage
- ***Biological:*** starch, glycogen
- ***Thermal:*** ice, latent heat, sensible heat, seasonal thermal storage
- ***Magnetic:*** superconducting magnetic energy storage

In the next section, a brief description of the most available forms of energy storage is presented.

1.2 Energy Storage Systems

As discussed before, energy is stored in different forms, depending on the type of the energy source and application. Not all the types of energy storage systems are used for large scale storage, and many of them are not economically available. Here brief descriptions of the most common energy storage systems in the electricity generation market are presented. The section starts with batteries, continues with hydrogen storage, and ends with compressed air energy storage systems.

1.2.1 Batteries

In batteries, electric energy is converted to chemical energy (charging phase) and vice versa (discharging phase) in which, the stored chemical energy is converted back to electricity. A battery cell has a specified nominal voltage and electric current, and cells are stacked-up to build a larger battery with the desired output. Energy and power density, charging and discharging efficiencies, battery operational temperature, and self-discharging are among the important features of batteries. Tremendous research and development efforts are put into the development of batteries, and many different kinds of batteries have emerged as a result. Some of these batteries are not commercially available despite their significant characteristics. Some types of batteries are introduced below (Divya and Østergaard, 2009; Wagner, 2007).

1.2.1.1 Supercapacitors

In a supercapacitor energy is stored in an electric field. The field is created between two charged plates. The surface area of a supercapacitor is considerably larger than a conventional capacitor. The charging and discharging time of supercapacitors is significantly short, and there is no degradation during cycling phenomena. The charging time of a supercapacitor is about 10 seconds. Although the energy efficiency of super or ultracapacitors is 80-90%, the small scale size of these valuable energy storage systems is yet a challenge. As with any other new developing technologies, supercapacitors found their way in industry through military applications. Other applications serve as starters in diesel trucks and locomotives. Transient load levelling of hybrid electric vehicles (HEV) is among the most recent applications of super or ultracapacitors. Increasing the operational temperature increases the storage capacity of this kind of battery. This issue is important in

developing electric vehicles; a considerable amount of energy is lost in the vehicle braking system. Supercapacitors can be utilized to recover that energy, thus reducing fuel consumption.

1.2.1.2 Nickel batteries

Nickel batteries are electrochemical devices with energy densities of 20-120 Wh/kg. The charging/discharging cycles of batteries determine their life time. Ni-Cd and Ni-MH batteries can have around 1500 deep charging/discharging cycles. The life time of Ni-Zn and Na-$NiCl_2$ is shorter in comparison to Ni-Cd and Ni-MH batteries. However, the efficiency of Ni-Zn and Na-$NiCl_2$ batteries is higher (almost 90%). Furthermore, the cost of manufacturing Ni-Cd and Ni-MH batteries is twice as much as lithium batteries and four times as much as lead acid batteries. Use of the highly toxic material, cadmium, is a major drawback for Ni-Cd batteries.

1.2.1.3 Lithium batteries

These batteries are produced in different types where four main categories are lithium metal, lithium metal polymer, lithium-ion polymer and lithium-ion batteries. Lithium-ion (Li-ion) batteries are used in laptops, cellular phones and other electronic applications such as electric vehicles. Li-ion and lithium polymer (Li-pol) batteries have high energy densities (100-150 Wh/kg). Moreover the energy efficiency is 90-98% for charging and discharging phases. The operating temperature of lithium batteries is limited to a narrow range, due to conductivity and cell degradation dependency on temperature. Therefore due to safety and cost concerns, the widespread use of lithium batteries is limited. These kinds of batteries are very sensitive to overcharging, compared to Ni-MH or other Li-ion polymer batteries. Higher cycle life and specific energy give Li-ion batteries superiority over other kinds of batteries such as Ni-MH. As electrochemical systems, they are very dependent on temperature variations within the cell. Lithium oxides and salts are easily recoverable, thus lithium batteries have a limited environmental impact.

1.2.1.4 Lead acid batteries

Lead acid batteries are the oldest and most developed batteries. The energy density of this type of battery is the lowest, 25-45 Wh/kg, and their charging/discharging efficiency is 60-95% with 2-5% self-discharging rates. Lead acid batteries have

dominated the market due to their very low cost, which is almost 8 times less expensive than Li batteries and 13 times less costly than Ni batteries. In a lead acid battery, lead and lead oxide serve as negative and positive electrodes, respectively, and sulphuric acid is used as the electrolyte. Since lead is toxic, recovery of lead acid batteries is very important. Also, the sulphuric acid used in lead acid batteries is highly corrosive.

1.2.1.5 Metal air batteries

Metal air batteries are the most available compact batteries. The energy density of these batteries reaches 110-420 Wh/kg. However, these batteries have a major disadvantage due to their low charging/discharging energy efficiency around 50%. The application of metal air batteries, e.g. zinc air battery, has been limited to a small scale mostly due to difficulties in the charging and discharging of these systems. Metal air batteries are totally environment friendly since the metal used in its composition is highly recoverable.

1.2.1.6 Sodium-sulphur batteries

High temperature sodium sulphur batteries are electrochemical devices with 150-240 Wh/kg energy densities and 90% charging/discharging efficiency. These batteries are built for long discharge cycles, and have a 15 year lifetime.

A comparison is made in Table 1.2 for various battery technologies.

Table 1.2: Comparison of various battery technologies

Characteristics	Li-ion	Ni-MH	Lead-acid
Gravimetric energy density, Wh/kg	110-250	60-120	30-50
Number of cycles during lifetime (80% of initial capacity)	500-1000	300-500	200-300
Nominal cell voltage, V	3.6	1.25	2
Maintenance requirement	Not required	2-3 months	3-6 months
Overcharge tolerance	Very low	Low	high
Self-discharge/month, %	1 - 5	20	4 - 8
Efficiency, %	90 - 98	80	85

Adapted from: Javani (2011)

The electric efficiency of charging/discharging phases of lithium batteries (90-98%) is higher than the other types, which makes it an effective system for energy storage (Javani, 2011; Krein, 2007). Li-ion batteries have energy densities higher than lead acid batteries. In addition, if temperature management issues are sufficiently addressed, they can be a better choice for hybrid electric vehicles, since their energy densities are almost twice that of Ni-MH batteries (Javani, 2011).

1.2.2 Thermal energy storage systems

Thermal energy storage (TES) is a method for harnessing thermal energy with the advantage of heat regeneration and reducing environmental pollution. TES is illustrated as storage of thermal energy in the form of a cold, hot, or a chemical media (Haji Abedin, 2010). TES can play a significant role in meeting society's needs for more efficient and environmentally benign energy use in various sectors. A potential application of TES is integration with renewable energy systems. Since the energy from renewable resources is mostly intermittent, a TES system provides the consumer with thermal energy whereas the energy source is not available. In general TES is helpful in balancing between supply and demand of energy (Dincer and Rosen, 2011c). TES provides a reliable method to use waste or renewable energy in the growing heating and cooling demand (Rosen et al., 2004).

Sensible energy storage is one of the two types of TES systems. The amount of energy stored by sensible heat devices is proportional to the difference between the storage input and output temperatures, the mass of the storage medium, and the medium's heat capacity. The heat capacity of water is almost double that of the heat capacity of rock or ceramic. However, since no phase change takes place in rocks or ceramics in storage systems, they can be used to temperatures as high as 800°C (Dincer and Dost, 1996).

The other common type of TES is through latent heat storage, in which thermal energy is stored by phase change of the storing media. For example, energy is stored in a cold storage system as ice, or as a hot storage system by melting paraffin waxes. The selection of a TES system for a particular application depends on many factors, including storage duration, economics, temperature requirements, storage capacity, heat losses and available space. In addition, thermal energy can be stored in the form of an endothermic chemical reaction. Thermal energy is provided to some reversible

chemical reactions to produce other forms of chemical products. A part of this energy will be recuperated later in the process, when synthesis reaction takes place.

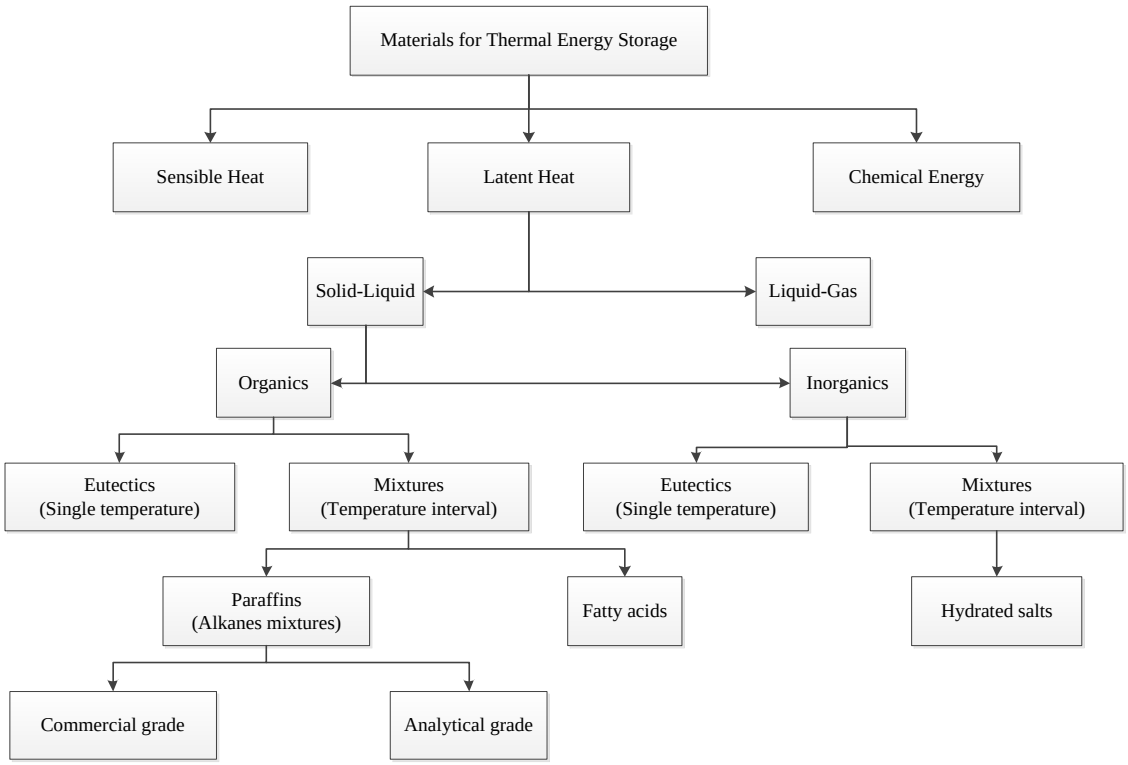

Figure 1.1: Thermal energy storage material (adapted from Zalba et al., 2003)

Zalba et al. (2003), Abhat (1983), Lane (1983) and Dincer and Rosen (2011c) are among the researchers who particularly addressed the proper materials for TES systems. The classification presented in these references provides detailed and current information on the materials for the storage of thermal energy. Figure 1.1 illustrates the classification presented by Zalba et al. (2003). They present a comprehensive table, listing all the organic/inorganic materials in the TES market. The list provides information about materials and their thermophysical properties.

Paraffin as an organic material for latent heat storage suffers certain limitations; i.e. flammability, low thermal conductivity and volumetric change during phase change. Therefore, most research on phase change materials (PCMs) for TES focuses on salt hydrates. The long term stability of phase change materials used as storing media is an important concern. The instability concerns arise due to the thermal cycling and corrosive nature of most PCMs. Based on the experimental studies, nano particles enhance the thermal conductivity of most liquid solvents. The analysis of PCM-based,

nano-fluids for solar thermal energy storage is of interest to Shin and Banerjee (2010). They investigate the optimum performance of different nano-fluids for solar thermal storage applications.

Heat transfer calculations and solving energy equations in TES systems are important due to the complexity of heat transfer regimes. Moreover, the determination of the boundary of heat transfer phenomena is a concern in determining temperature gradient within the storing media. Dincer and Rosen (2011c) point out that exergy analysis based on thermodynamic laws can provide a more sophisticated understanding of thermodynamic efficiencies. Thus, for all the phases of the storage process, exergy analysis gives a good insight of the process irreversibility.

One of the applications of TES systems is to store the intermittent energy of renewable energies. Numerous literatures are available on this matter (Chidambaram et al., 2011; Grazzini and Milazzo, 2008; Kamimoto et al., 1985). Ice storage is among the methods for TES. Although pure substances, e.g. water, are used for ice storage, the development of this method by implementing other substances is a point of interest (Zalba et al., 2003). Moreover different geometries are used in order to enhance storage capacity and heat transfer phenomena. Spheres, ice on coils containing water with glycol are the two popular geometries in the market used for ice storage. Random character of crystallization and the delay in the start of solidification are among the problems of ice storage addressed in the literature. Many parameters affect the performance of an ice storage system, including inlet fluid temperature, initial temperature of PCM, and thermal conductivity of the tube (Ismail and de Jesus, 2001).

Conservation and transportation of temperature sensitive materials bring in thermal storage or PCM systems as a viable option. Food transportation requires a specific range of low temperature environment which can be simply provided by PCMs. The operation of electronic devices strongly depends on temperature. For most devices, operation at high temperature causes severe damage to their components.

Thermal storage systems can also be used in buildings for smoothing thermal demand. Providing a part of hot water supply, or room temperature control are just two examples of the applications of TES in buildings. With the aim of geothermal heat pumps and solar energy, TES systems can be very promising in decreasing the

fuel costs of buildings. Thermal stratification is an interesting method in the storage of thermal energy for heating or cooling purposes. In a simple description, lower density warm water above a layer of higher density cold water is stored in an above ground storage tank. During peak demands of cooling, the lower layer, cold water, is withdrawn from the bottom of the tank. The cold water gives up its cooling energy to the target environment, and returns to the top of the storage tank. During off-peak hours, when low cost electricity is available, the warm water is cooled down using a simple inexpensive cooling system and is returned to the bottom of the storage tank. To provide lower cooling temperatures, other types of fluids with lower freezing points are used. Water based fluids containing sodium nitrite, sodium nitrate, and other additives can be used instead of water providing stratified storage. Rosen et al. (2004) report a thermodynamic analysis of thermal stratification in a TES system. They utilize a design based temperature-distribution model which could facilitate exergy and energy analysis. In their study, they investigate the increase of exergy content of the storage system by using different storage fluids.

1.2.3 Hydrogen Storage

As a carbonless energy carrier, hydrogen is likely to be an important element for future energy systems, which are being designed to be free of air pollution, CO_2, and other greenhouse gases (Mori and Hirose, 2009). Widespread use of hydrogen has been challenging, however, because of its low energy density relative to conventional (hydrocarbon) fuels. Since hydrogen is a very low density gas, storage and delivery becomes a great concern, especially for automotive engineering. Of the applications of hydrogen are power generation, and serving as fuel in hydrogen cars. In both cases, hydrogen is supplied from a storage tank. Conventionally hydrogen is stored as compressed gas or as a cryogenic liquid. Storing hydrogen in a hydride form is another method, which still is in the development phase. Although there are still many limitations in developing compressed gaseous and liquid hydrogen storage technologies, these systems are in a good phase of development. Today hydrogen is stored in pressures up to 700 bar (Di Profio et al., 2009). Moreover, hydrogen is stored in the liquid form in highly isolated liquid hydrogen storage tanks. A 68 L internal volume LH_2 storage tank with 4% boil-off allowance in 300 K ambient temperature must have 10 cm wall thickness with $3.2 \times 10^{-5}\,\mathrm{W/mK}$ thermal

conductivity. With these design specifications, the heat ingress rate is 1 W. In order to design a similar tank with the same size and heat ingress rate and 5 cm wall thickness, the thermal conductivity of the tank material should be 1.9×10^{-5} W/mK (EERE, 2008a).

Carbon-fibre-reinforced tanks, with 350 bar and 700 bar storage pressures, are under development for compressed hydrogen gas storage. The inner liner is a hydrogen permeation barrier made of high-molecular-weight polymer. Around the liner is a shell of carbon fibre-epoxy resin composite serving as the pressure load-bearing component of the tank. The compressed hydrogen gas storage tank is protected by an outer shell layer. The temperature of the CGH_2 is monitored by an internal sensor placed at the inside of the tank. In automotive applications, the driving range with CGH_2 tanks depends on the storage tank volume and pressure, and the vehicle type. High pressure, volumetric capacity and cost are the main challenges in the development of compressed hydrogen storage tanks (Ahluwalia et al., 2012).

The cost of the storage tank is mostly affected by finding low cost carbon-fibre reinforcement. However, lowering cost without compromising weight and volume is a key challenge. In order to achieve desired gravimetric and volumetric densities, efforts are being made to develop cryo-compressed hydrogen storage tanks, in which the tank is cooled to 77 K. The cooling process decreases the volume of the stored hydrogen, thus increasing the volumetric capacity of the tank. Carbon fibre tanks with 350 and 700 bar storage pressures are approved by several standard organizations; e.g. ISO (ISO 11439 Europe), NGV-2 (US), and TUV (Germany). Jensen et al. (2007) review a number of hydrogen storage technologies to compare their limitations and advantages in terms of energy efficiency. For each system, they calculate the amount of energy required for storage and the energy consumption in the hydrogen discharging (release) phase. They compare systems efficiencies as a percentage of hydrogen lower heating values, based on the energy demand of an on-board hydrogen storage system.

Hua et al. (2011) report that compressed gaseous hydrogen systems do not meet the U.S. Department of Energy's 2010 and 2015 volumetric capacity targets, based on an assessment of 350 bar and 700 bar hydrogen storage tanks (EERE, 2008b). The study also shows that the 700 bar CGH_2 storage tank can meet the 2010 gravimetric

capacity target, while the 350 bar storage tank meets both the 2010 and 2015 gravimetric capacity targets.

A thermodynamic analysis of gaseous and liquid hydrogen storage by Klell et al. (2007) examined concerns regarding temperature rise, pressure build-up, and boil-off rates in the storage tanks. Numerical models are used for analyses and parametric optimizations with respect to pressure, temperature and filling level in the presence of pressure build-up, boil-off and chilling. The results show that gaseous hydrogen compression to high pressures uses up to 15% of its calorific energy content.

Compressed hydrogen can be stored in closed tank systems at volumetric densities of around 20–50 kg/m³ and gravimetric densities (kg H_2/kg of the tank) of around 5–10%. Klell et al. (2007) state that liquid hydrogen can be stored with densities up to 70 kg/m^3, whereas the energy used in the liquefaction process is as much as 30% of the hydrogen lower heating value (LHV). A major concern with liquid hydrogen is hydrogen boil-off during periods when the tank is refilled and is not in service. Liquid hydrogen boils off readily when exposed to heat, causing a significant pressure increment in the storage tank. To keep the tank's pressure below its maximum pressure, a part of the hydrogen vapor must be vented as "back gas".

Although the back gas is normally directed to a supplementary system, this process involves a significant loss in the exergy content of the stored hydrogen in the tank. Moreover, exergy is lost due to vaporization, which further decreases the total exergy efficiency of the storage process. A comprehensive investigation of the storage of compressed gaseous hydrogen requires consideration of the filling (charging), storing and discharging phases. Filling a CGH_2 tank requires compliance to safety regulations. Moreover, customer expectations exist regarding filling time and maximum filling capacity.

1.2.3.1 Compressed gaseous hydrogen storage

Storing 1 kg of hydrogen at 100 kPa and 25°C requires a tank with 12.3 m^3 of volume. Compressing hydrogen to 350 bar decreases the required storage volume by 99.6%. Further pressure increases lower the required storage volume, but increase compression work input and safety concerns.

Atomic hydrogen can diffuse into the material and cause embrittlement. Materials suitable for hydrogen applications are mainly austenitic stainless steel and aluminum alloys. Most compressed hydrogen tanks are presently made of steel. Stainless steel CGH_2 storage tanks are called "Type I" tanks, and their volume ranges from 2.5 to 50 L (Hirscher, 2010). Composite containers, which consist of a thin inner layer of steel or aluminum, have lower storage tank weights. Composite tanks (type II and III tanks) may be composed of carbon fibre in order to achieve strength requirements. Type IV hydrogen storage tanks are made of composite materials which are lighter than types I and II, but more expensive. Table 1.3 shows the main characteristics of CGH_2 storage tanks.

Table 1.3: Major characteristics of commercially available CGH_2 storage tanks for automotive applications

Net volume, dm^3	34	100	50	100	36	65	30	120
Type	III	III	III	III	IV	IV	IV	IV
Nominal pressure, bar	350	350	700	700	350	350	700	700
Test pressure, bar	525	525	1050	1050	525	525	1050	1050
Tank system weight, kg	18	48	55	95	18	33	26	84
Tank system volume, dm^3	50	150	80	150	60	100	60	200
H_2 density at 25° C, kg/m^3	23.3	23.3	39.3	39.3	23.3	23.3	39.3	39.3
H_2 content, Nm^3	8.83	26	21.84	43.69	9.35	16.96	13.5	51.7
H_2 content, kg	0.79	2.33	1.96	3.83	0.84	1.52	1.21	4.65
Grav. H_2 content, kgH_2/kg	0.044	0.049	0.036	0.041	0.047	0.047	0.047	0.055
Vol. H_2 content, kgH_2/dm^3	0.016	0.016	0.025	0.026	0.014	0.015	0.021	0.023
Grav. energy density, kWh/kg	1.467	1.633	1.200	1.367	1.567	1.567	1.567	1.833
Vol. energy density, kWh/dm^3	0.533	0.533	0.833	0.867	0.467	0.500	0.700	0.767

Adapted from Hirscher (2010)

1.2.3.2 Liquid hydrogen storage

The energy density of hydrogen can be improved by storing hydrogen in a liquid state. Storage of hydrogen in liquid form seems quite promising; however, several issues regarding liquid hydrogen boil-off, liquefaction energy demand, weight, volume and cost are limiting the development of liquid hydrogen storage tanks. Minimizing hydrogen boil-off is necessary to achieve higher storage efficiencies and lower cost. Volumetric capacity of LH_2 storage tanks (0.07 kg/L) is more than twice of the CGH_2 tanks at 700 bar (0.035 kg/L).

One way to liquefy hydrogen is to cool it down to 20 K (saturation temperature at 1 bar), and then condense it to saturated liquid state. The minimum theoretical work requirement to liquefy hydrogen gas to 20 K is about 14,280 kJ/kg, which is almost 12% of hydrogen LHV. Liquefaction of hydrogen requires removing heat from hydrogen using a combination of refrigeration techniques available to the cryogenics industry (EERE, 2008b). Three different techniques are commonly used for large scale operations. The first is Joule-Thomson expansion, where compressed hydrogen is throttled to a lower pressure through a nozzle or valve. The point here is that hydrogen cannot be liquefied only based on the Joule-Thomson expansion, since hydrogen temperature increases while passing through an expansion device at ambient temperature. Therefore, hydrogen needs to be cooled down to 204 K before the expansion process. The second technique is the use of an auxiliary refrigerating fluid from a source external to the hydrogen liquefaction process. Liquid nitrogen is commonly used for this purpose and the liquefaction process for the nitrogen may, in turn, employ an auxiliary refrigerant such as a halogenated hydrocarbon. Liquid nitrogen can provide the necessary pre-cooling to permit liquefaction of the hydrogen via Joule-Thomson expansion. The third technique is expansion of compressed hydrogen to a lower pressure by means of an expansion engine. In a perfectly efficient engine, this is an isentropic process that results in a reduction in enthalpy of the expanding gas. The work developed is recoverable for external use. Expanders may be either reciprocating or centrifugal but economics favors centrifugal turbines in large scale use. An electric generator coupled to the turbine shaft can be used to recover energy. A detailed study on hydrogen liquefaction is presented by Baker and Shaner (1978).

Liquid storage requires highly sophisticated tank systems. Heat transfer through conduction, convection and radiation has to be minimized. Nevertheless, due to the inevitable inward heat leakage, hydrogen evaporates in the container leading to an increase in pressure. Liquid hydrogen containers must therefore always be equipped with a suitable pressure relief system and safety valve. Krainz et al. (2003) present a comprehensive information on the development of liquid hydrogen storage tanks.

1.2.4 Compressed Air Storage

Compressed air energy storage (CAES) systems can be used for load levelling of electricity generation systems. As a modification of gas turbine cycles, in compressed air storage systems, low cost, off-peak electricity is used for compression of air. The compressed air is stored in underground caverns. The underground compressed air reservoir can be constant pressure type or constant volume. The constant pressure underground reservoir could be an aquifer or depleted natural gas storage. Salt domes or abandoned mines can be used for compressed air energy storage as a constant volume type.

During electrical peak-demand hours, the stored high pressure air is heated up and is expanded in a gas turbine to generate electricity. According to literature, by 2009, two plants of compressed air storage systems were available worldwide; a 390 MW gas turbine power output in Germany, and a 110 MW plant in US (Beaudin et al., 2010; Lund et al., 2009). These systems have demonstrated reliable operation, high efficiency, and economic feasibility, thus the interest in the installation of more systems of this type is growing. As an instance, the first compressed air energy storage system that stores compressed air in an aquifer will be installed in Iowa in 2015 (Beaudin et al., 2010). It is expected that by installing this system in a 75-150 MW wind farm, the emission will be reduced by 60% in comparison to a system other than CAES for energy management.

Recently the implementation of CAES into wind power technology has been considered to compensate for electricity generation fluctuations (Cavallo, 2007). The capital cost of a CAES system is estimated to be 890 $/kW, and it is reported as the least expensive storage option for intermittent renewable energy sources (Cavallo, 2007). The response time of compressed air storage systems is fast enough to be considered as a reliable option for storage of the generated electricity by these energy sources (Beaudin et al., 2010). A simple schematic of compressed air energy storage systems is shown in Figure 1.2. When needed, compressed air is heated up to a desired temperature, either by combustion gas or by waste heat recovery. Thus, compressed air energy storage systems are not pure storage systems. However, since the compressor and the turbine are de-coupled, almost all the gas turbine's power

output is fed to the electricity grid. Also, the compressed air can be pre-heated in a recuperator while released to flow into the gas turbine.

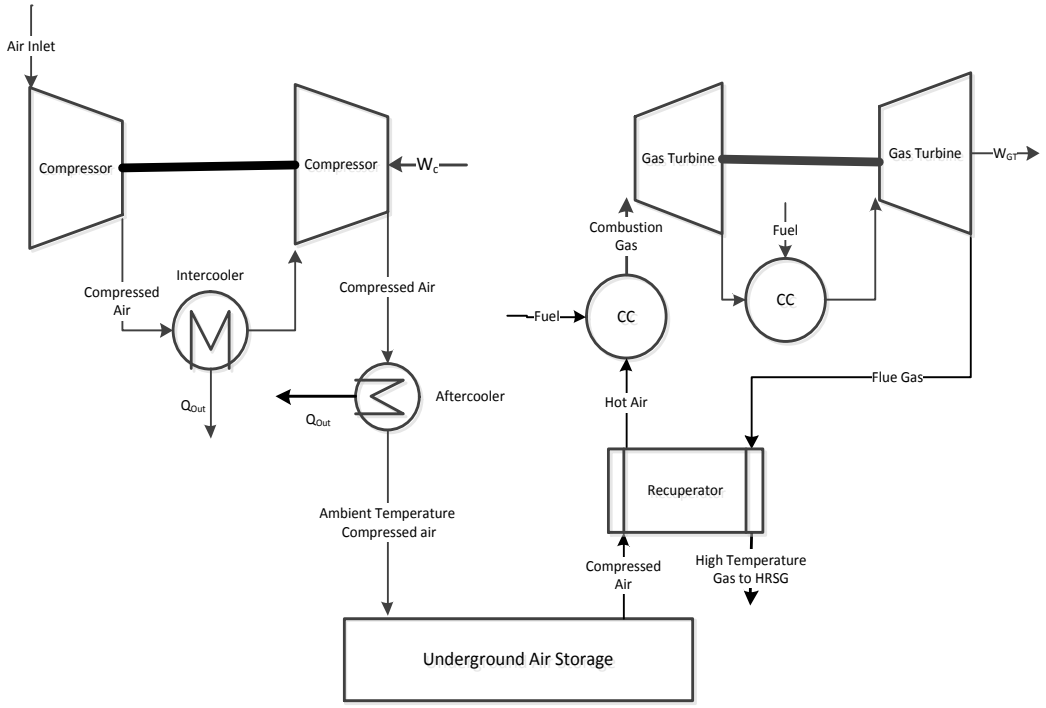

Figure 1.2: A simple schematic of compressed air energy storage system with its components (adapted from Wang and Yu (2012))

Table 1.4 gives a summary of electric energy storage technologies. In the summary, some of the available options for the storage of electric energy are considered and their advantages and disadvantages are reported, also.

Table 1.4: Comparison of different energy storage systems by their performance characteristics

EES Technology	Advantages	Disadvantages	Major Applications	Potential Improvements
Lead Acid	- Developed technology - Inexpensive - Commercially available	- Low energy density - Short cycle life - Sensitive to low temperatures	- Automobile -UPS - Telecom - reserve power	- Cycle Life -Depth of Discharge - Low temperature Performance
Li-ion (Phosphate based)	- High energy and power density - High efficiency	- Expensive - Requires complex battery management - Safety issues	- Electronics - HEV - Utility applications	- Lower costs - Safety - Thermal management
NiMH	- Relatively mature technology - High energy density	- More expensive than lead acid - Expensive material	- Utility - Telecom - Electronics	- Lower costs - Recyclability
CAES	- Large energy and power capacity	- Geographically limited - Requires fuel input	- Load levelling - Frequency regulation	- Adiabatic capability

1.3 Applications of Energy Storage Systems

Energy is stored in fossil fuels in the form of chemical energy. When required, the chemical energy of these fuels is released by relevant processes. Handling and transportation of fossil fuels is relatively easy, and they may be stored until such time as they are required and may be transported by rail, road or pipeline to where they are to be used. In contrast, most renewable energies require at least one time conversion to electricity (or another convenient form of energy) to be stored and transported. Using electric energy is very versatile and preferred, thus it is of great interest to convert, store, and transport renewable energies into electricity through available technologies. This makes renewable energies and electric energy bound together. However, it is not always easy to match the demand with supply of electricity and renewable energy availability is intermittent. Thus, the need for efficient, reliable, and cost effective energy storage systems emerges with these concerns.

Table 1.5: Renewable energy resources and their main utilization

Energy source	Energy utilization	Availability
Agriculture and forestry waste, Landfill and sewage gas, Energy crops	Combustion process	Now
Municipal solid waste	Combustion process	Now
Direct solar (active and passive)	Heating	Now
Geothermal	Heating/electricity	Now/limited scope
Hydro power	Electricity	Now
Wind power	Electricity	Now and developing
Hydrogen/fuel cells	Electricity	Now and developing
Solar photovoltaic	Electricity	Now and developing
Solar-thermal	Electricity, Hydrogen production	Medium-/long-term
Wave power	Electricity	Medium-/long-term

Adapted from Dell and Rand (2001)

Meeting short-term, random fluctuation in energy demand, load levelling, eliminating the need for part-loaded plants (e.g. gas turbines to meet peak-hour demands), and storage of renewable energy are among the significant applications of energy storage systems.

The various renewable sources of energy are listed in Table 1.5, together with their method of utilization and the likely timescale of early commercial use. According to

Dell and Rand (2001), the total contribution of renewable energies in responding to the growing demand for electricity by 2020 will be one third of the world's electricity generation. In addition, they predict that almost half of this contribution will be through burning or gasification of biomass; although the interest toward renewable energies varies by geographical locations.

However, the main points beyond all the available forms of renewable energy are their temporal behaviour, and the absence of well-developed technologies to utilize them (Lund, 2005). For example, solar energy is only available during day time, and solar insolation strongly depends on the location. Moreover, the most high-tech photovoltaic systems have efficiencies slightly higher than 25%, while the efficiency of commercial ones are as low as 10% (Green et al., 2012).

Aside from all these concerns, the utilization of renewable energies is moving on its development path. Most countries put maximum effort in order to increase the development rate of these systems. Energy storage systems have their own deficiencies, and require more experimental and modeling research. Renewable energy and energy storage systems are inter-related and growing fast. There will be one day when the share of renewable energies with the aim of energy storage in the energy sector is significant.

Energy storage is not limited to renewable energies. Waste heat from industry can be recovered and stored in proper thermal energy storage systems. The off-peak electricity in power grids can be stored in batteries, as hydro-power behind hydro-storage dams, or can be used in electrolysers for hydrogen production. Countries such as France and England, which have fully interconnected electricity network, are interested in having surplus electricity generation capacity. A specific capacity is generated for base load, and while required higher-cost plants are brought into the network to meet the peak hours demand. In such countries, the electricity is restricted to hydro-storage. The number of these pumped hydro-storage plants is limited due to the problems regarding location, space, and construction time. Many countries are interested in batteries for electricity storage, however, economic aspects of lead-acid batteries (as the most dominant battery worldwide) is still stringent. Also, the volumetric energy density of batteries is still far from expectations.

When energy storage systems are used in fossil fuel systems the fuel consumption decreases significantly. For example, thermal energy storage systems can be used to recover and store heat loss from the diesel engines exhaust gas (Clark and Isherwood, 2004). It is very common worldwide to use low-price, off-peak electricity produced by base power plants (mostly steam and combined cycles) in pumped-hydro storage stations. Waste heat recovery from gas turbine flue gas and utilizing it in an absorption chiller for ice storage is a feasible, economic method for energy storage. The thermal energy stored in the form of ice is used for gas turbine inlet air cooling in hot summer days. Ameri and Hejazi (2004) report that the overall GT power output increases by 11.3%.

1.4 Sustainability Aspects of Energy Storage

With the increase in energy consumption since the 1970s, environmental concerns became a major issue in 1980s. Acid rain, ozone layer depletion, and global climate change were the primary reasons for these concerns, thus shifting the attention of governments and societies toward the relationship between energy and sustainability of the environment. The connection between energy consumption rate and environment has been more recognized since then. Although production, transmission and use of energy resources are all beneficial to human life, the consequences are severe on climate change by thermal, chemical and nuclear emissions. Developing sustainable societies requires significant attention to manipulating energy resources in a well-developed, high efficient way. Thus attaining sustainable development requires that sustainable energy resources be used. Many suggest that in order to have a sustainable future, the use of fossil fuels should be limited and be substituted by renewable energies. In other words, for a sustainable environment, the energy resources should be reliable and safe, flexible in use, and affordable and limitless (Dell and Rand, 2001), which all are characteristics of renewable energies. However, energy storage becomes an important method to overcome the problems regarding temporal availability of renewable energies, and the mismatch between energy demand and supply (Caliskan et al., 2011). Thus environmental sustainability can be linked to energy storage systems through increasing renewable energy use.

Sustainability assessments include the definition and calculation of sustainability indicators. Sustainability indicators include: Resource Indicator, Environment

Indicator,

Economic Indicator, and Social Indicator (Begić and Afgan, 2007). Each of these indicators has sub-indicators, breaking down all the parameters affecting sustainability. When assessing sustainability of renewable energy resources indicators such as unit cost of electricity generation, energy and exergy efficiency, and greenhouse gas emission savings seem to be important, because the performance of renewable energy-based electricity generation systems varies with geographical location. Energy storage, as discussed before, improves renewable energy use, thus affecting sustainability of the systems, although there are many other aspects of sustainability.

Chapter 2: Motivation and Objectives

2.1 Motivation

As a part of larger energy generation/utilization sectors, the performance of energy storage systems is highly dependent on the other components. The form of the available/input energy is important to define the type of ESS. The determination of the optimized ESS for a specific source of energy requires a thorough analysis from the point of thermodynamics and economics. Several literature and research studies are available on analyzing individual energy storage systems. However, none of these works performed thermodynamic and economic analysis for different storage options integrated with renewable energy resources. The available analyses in the literature are mostly based on the first law of thermodynamics and economic analysis. Even the performed analyses based on exergy or exergoeconomic analysis have considered individual storage options, while ESSs are meant to be a part of integrated energy systems. These concerns are the main motivations of this research. Due to the importance of ESSs in providing societies with safe, reliable and environmentally friendly energy streams, the analysis of these systems, considering all the aspects of energy, exergy, and exergoeconomics, is of great importance. Moreover, future energy systems require improving energy utilization, decreasing exergy losses and destruction, and capital and operating costs of the systems' components. Thus, the need to perform such a complete and comprehensive analysis is realized.

2.2 Objectives

The main objective of this research is to investigate energy storage options for sustainable energy systems. A description of technology and illustration of concerns about each system is presented. Moreover, the possibility of implementing each technology into renewable energy resources is investigated. The analyses are based on the laws of thermodynamics. The thermodynamic modeling differentiates the systems based on their efficiencies and exergy destruction rates.

Furthermore, the results are used to investigate environmental impacts of integrated systems under study. However, this requires economic analyses along with thermodynamic modeling. This concept is investigated as exergoeconomic analysis, which specifies the relationship between exergy content and cost of each system. Thus, by exergoeconomic analysis, one can compare different technologies and make a corresponding choice of energy storage options for a specified energy source.

The specific objectives of the thesis, along with their detailed explanations, are as follows:

- To discuss the main concepts and importance of energy storage in developing sustainable energy systems

A detailed description of the available energy storage, along with a brief historical review of each system, is performed. A comprehensive literature review shows the history and the development path of each system, which helps to build a road map in modeling and analyzing the systems. Furthermore, application of each system, their ranges of operation, and development potentials and environmental obstacles against the available energy systems is determined.

- To perform energy and exergy analyses for some energy storage system: hydrogen, and compressed air energy storage, and thermal energy storage

The selected storage options will be studied based on the thermodynamic analyses, considering operating parameters, charging, storage, and discharging phases. The systems will be modeled so the energy and exergy flows of each stream is calculated, revealing the rates of irreversibility and exergy losses. The results are used to determine the systems efficiencies.

- To determine the effects of operating parameters on the energy and exergy efficiencies of the integrated systems

Several energy systems that are integrated with various energy storage options are developed. A parametric study is performed based on energy, exergy, and exergoeconomic analyses to investigate the effects of operating parameters on the systems' efficiencies. The effect of different operating scenarios on the overall efficiency of the integrated systems is also examined.

Since the storage systems are implemented into integrated renewable energy systems, the objective of this section is to provide detailed analyses of the integrated energy systems, which is the originality of the proposed research. Unit exergy cost of fuels, products, and flows are determined with the aid of available capital cost functions for the systems' components. Moreover, the CO_2 emission rate of the integrated systems is calculated.

- To investigate how the integrated systems help in mitigating the environmental impacts of energy consumption

Considering different layouts and operating scenarios for integrated renewable energy-based systems, the savings on greenhouse gas emission of the integrated systems are compared with the systems that run on fossil fuels. The comparison is used to illustrate the share of energy storage systems in addressing environmental issues.

- To optimize the novel, integrated renewable energy-based systems based on exergoeconomics

The results of the energy, exergy, and exergoeconomic analyses are used to optimize the novel systems. The optimization is multi-objective, and is based on exergy efficiencies and levelized costs of the systems.

Presenting hybrid scenarios based on the parametric study results, and the storage systems' capabilities in order to aid developing sustainable energy systems, is another objective of the proposed research.

Chapter 3: Literature Review

A summary of the relevant literature works on energy storage systems is presented below. The review is started with a brief discussion on the renewable energy resources, and their role in the world's energy market. The summary includes the study of renewable energy storage by various storage options. The chapter is organized based on the studies regarding the implementation of energy storage options into renewable energy systems, and the performed analyses are reviewed briefly. Sustainability aspects of energy storage systems form the closing of this chapter.

3.1 Role of Renewable Energy Resources

Reviewing the renewable forms of energy which are used for electricity generation (Table 1.5), tidal and geothermal sources are restricted to very few sites in the world and so may be discounted from this global discussion. Wave and solar-thermal generation are practical, and may eventually prove economic, but at present they are still in the developmental stage. Thus, given these considerations, wind and solar photovoltaic have emerged as the two dynamic and growing sources of renewable electricity generation, which require a storage component and are presently cost-effective in certain situations (Dell and Rand, 2001). Wind and solar energy have great potentials in the electric power generation sector by reducing fossil fuel consumption and decreasing the level of greenhouse gas emissions. However, both of these energy resources have variable and uncertain outputs. Therefore, there is a need for energy storage, which happens to receive much of the current attention on its potential application with renewable energy: primarily solar and wind (Denholm et al., 2010; Nourai, 2007).

There are only few plants around the world that utilize geothermal and tidal energy for electricity generation. Therefore, it is preferred not to consider them in this report for analysis. Solar-thermal and wave are in the developmental phase, although they

are practical and may eventually be economically reliable. Thus, with these considerations, wind and solar photovoltaic are analyzed due to their potential in generating electricity with the aim of developing technologies. Biomass is another renewable source that is considered in this research for electric power generation. If harvested enough, biomass feed to the electricity generation systems would be continuous and non-temporal. Therefore, the intermittency problems that occur with wind and solar energy are not a big issue with biomass energy.

3.1.1 Solar Photovoltaic Electricity Generation and Storage

The potential of solar energy as an intense and abundant renewable energy resource is apparent to everyone. Nevertheless, the current use of solar energy for electricity generation is less than 1% of the global energy consumption. Despite tremendous efforts toward development of photovoltaic systems, high capital cost, modest conversion efficiency, and intermittency are major drawbacks for dominant use of solar energy (GCEP, 2006). The market for solar energy electricity generation is still low, compared to the other forms of renewable energy. The PV share of 1465 GW electricity generations by renewable energies in 2011 was only 0.93%. However, developed countries' interest and investments in solar energy is increasing, and the International Energy Agency has predicted 600 GW of electricity generation by PV and solar thermal power plants by 2035 (IEA, 2012).

Solar energy can be used for electricity generation with PV systems. Such systems normally require supplementary devices to meet peak demands or to harvest surplus electricity generation. Producing the energy carrier hydrogen is one method for storing electricity from solar PV systems. Surplus electricity can be converted to hydrogen via water electrolysis, and the hydrogen can be stored and used to generate electricity in a fuel cell when required.

Lu and Yang (2010) report the results of an economic and environmental analysis of a rooftop building integrated renewable energy system in Hong Kong. The system consists of 126 mono-crystalline PV cells in series and parallel, and is connected to the local grid with an annual power output of 28,154 kWh. They report the energy payback period and greenhouse gas payback period as 7.3 and 5.2 years, respectively. Also, the results show that the installation orientation and location affect the sustainability of the PV system. They also suggest the increase in PV installations due

to their carbon free operation, although there are certain levels of greenhouse gas emission during manufacturing and installing the PV panels.

Uzunoglu et al. (2009) propose an integrated system to meet the power demand of a building. A solar PV system is integrated with a water electrolyser, an ultracapacitor bank, and a fuel cell for sustainable power generation. The hourly difference in the PV output and the load demand is calculated, along with the hydrogen production rate in the electrolyser. The dynamic behaviour of the hybrid system is tested under varying solar radiation and load demand conditions, where the solar radiation and power demand data are based on real-world data.

Direct coupling of electrolysers to solar PV systems for hydrogen production is studied by Clarke et al. (2009), which eliminates most of the interfacing electronic systems and reduces the cost of the PV-electrolyser system. The experimental set-up follows the maximum power generated by the PV system, which is directly introduced to the electrolyser. The efficiency of the PEM electrolyser is affected by cell degradation due to repetitive variations of the load, and an overall electrolyser stack efficiency of 65% is reported.

Solar-PV hydrogen systems can also be integrated with solid oxide fuel cells (SOFCs), due to their high efficiency and capability as distributed power generators. Hawkes et al. (2007) consider using an SOFC as the power and heat generator for a residential area in the United Kingdom. Different thermal demand profiles are considered, along with the environmental and economic investigation of the combined heat and power systems. The results show that the system has its best performance with slow, steady thermal demand. Numerous integration strategies for SOFCs are reviewed by Zhang et al. (2010). They conclude that integrated SOFC systems have higher efficiencies and lower environmental loads. Reversible solid oxide fuel cells integrated with solar PV power generation systems are said to be a promising substitute for solar PV-battery systems. In these systems, a reversible SOFC acts as the electrolyser for hydrogen generation when excess electricity from the PV system is available and as a power generation system when the PV power is unavailable.

Load variations and changes in weather conditions affect the performance of solar PV-hydrogen systems. Sudden load variations result in component degradation and reduction of the system’s lifetime. Tesfahunegn et al. (2011) propose the use of an

existing peak shaving battery to suppress short term the PV output and load fluctuations. This enables the fuel cell and electrolyser to operate under more favourable power conditions, which improves performance and lifetime.

Some other solar PV-hydrogen systems and their integration with fuel cells have been reported that focus on PV characteristic curves, power output and hourly hydrogen production (Gibson and Kelly, 2008; Shabani et al., 2010). The fuel cell behaviour and payback time are also reported in the literature. However, these integrated systems require to be analyzed from a thermodynamic point of view to understand their efficiencies and effectiveness, based on both energy and exergy.

Radchik et al. (2013) investigate the economic feasibility of baseload solar power generation systems for large scale applications as a path towards green electricity. They state that the intermittency of solar power output is a major factor in economic development of baseload PV systems, and propose market-based solutions for baseload PV electricity generation systems integrated with virtual non-intermittent generators, i.e. gas-fired power plants. This provides a financially attractive option for integration of a solar generator with the existing electricity market. Solar PV electric power generation can be at any scale and can contribute to a significant share in power demand supply. This will be achieved through proper integration with energy storage options, and improving cell efficiency, and lowering purchase costs.

The application of energy storage in solar energy systems is not restricted to electricity storage. Öztürk (2004) performs a thermodynamic analysis of an underground solar thermal storage system. An experimental setup was used to store energy in the form of sensible heat in volcanic materials. The heat storage unit consisted of a packed-bed with 7.2 m^3 volume, and energy and exergy analyses were applied to evaluate the system's efficiency. The reported values for average daily energy and exergy efficiencies are 39.7% and 2.03%, respectively.

Energy storage can also be implemented into solar heat pumps, which are available to meet thermal demands of buildings. However, there is an inconsistency between the availability of solar energy (daylight availability), and the demand for heat (regular time demand). Moreover, depending on the location of the building, this discrepancy may be seasonal, and the seasonal temperature of underground is small after a certain depth. Thus seasonal storage of the solar energy in an underground

vessel during summer season addresses the inconsistency between seasonal energy availability and demand. Yumrutaş et al. (2003) investigate thermal performance of a ground-coupled heat pump with a cylindrical energy storage tank. Their investigation consists of both analytical and computational analyses. Water is used as storage medium, and its temperature is calculated with the change in different parameters. It is reported that the area of the solar collector plays an important role in the maximum obtainable temperature of the stored water. Maximum variations in water temperatures were achieved while using smaller storage tanks. Thus, the stored water had higher mean temperature in summer and lower mean temperature in winter, for a smaller tank volume.

Thermal water splitting is a method for hydrogen production, in which the thermal energy can be provided by solar thermal energy. Wang et al. (2011) investigate the temperature range of solar thermal technologies for solar hydrogen production. The results show that the temperature requirements by the chemical reactions in the oxygen production step of the copper-chlorine cycle can be provided by the available solar thermal technologies. The required heat is provided by a molten salt that captures solar energy. The molten salt is a part of the solar thermal storage system.

Hacatoglu et al. (2011a) propose hydrogen storage with activated carbon in a residential solar power generation system. The assessment of the proposed system based on thermodynamic modeling is illustrated. Although the reported value for the overall solar-PV hydrogen storage system is 11%, the environmental benefits of the system are good inspiration for further developments. López et al. (2007) perform an optimization on solar hydrogen storage systems. The analysis is based on exergy and energy. Hydrogen is produced in an alkaline electrolyser and is stored in storage tanks or on activated carbon. Exergy flow of each state and component and specific exergy destruction are calculated. Since the produced hydrogen is used in a low pressure fuel cell, the results show that the best choice for hydrogen storage is low pressure gaseous storage, followed by activated carbon storage method.

Several other literatures are available on the utilization of solar energy through energy storage, of which one may refer to the works performed by Arias et al. (2008), and Zurigat et al. (1989).

3.1.2 Wind Power Generation and Storage

Wind energy is different from solar energy because it is available 24 hours a day; however, its intensity is variable. Large wind turbines are capable of generating 1-6 MW of electricity in a strong breeze, but in light air the output falls off dramatically. Thus, several wind turbines are required to replace a conventional power station.

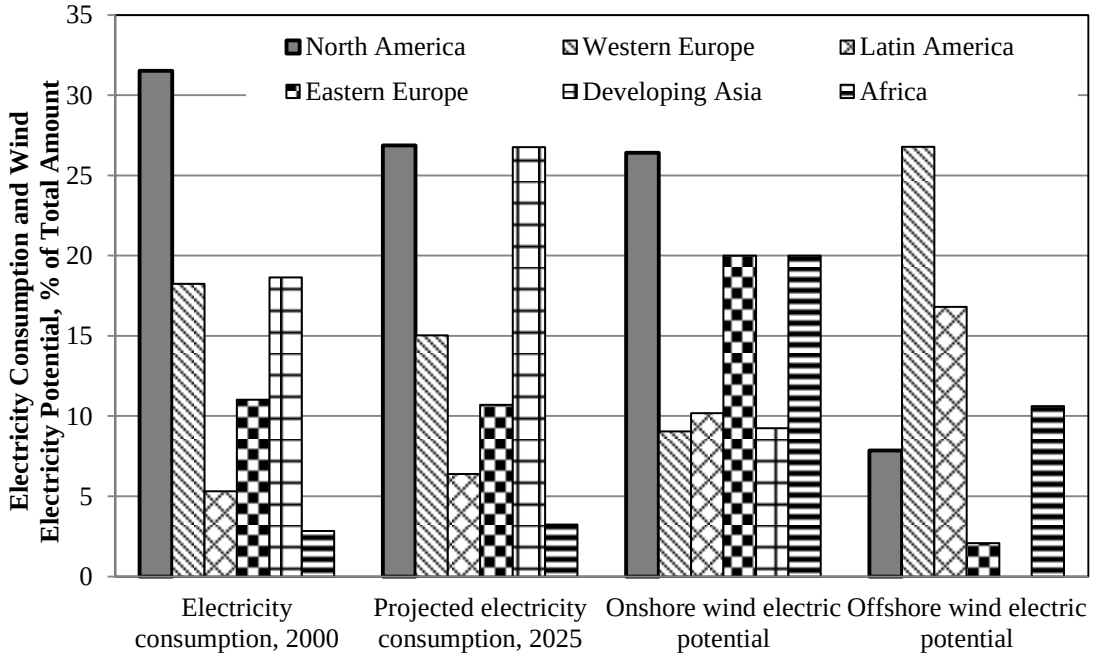

Figure 3.1: Projected electricity consumption and wind electricity potential, percentage of the total electric consumption (adapted from Cavallo, 2007)

Figure 3.1 shows the percentage of projected worldwide electricity consumption and wind electric potential regarding the total consumption. The first two sets of bars on the left side of Figure 3.1 present the share of each region on global electricity consumption (in years 2000 and 2025, respectively), and the latter two sets of bars on the right side represent the wind energy potential. With these predictions, onshore wind electric resources are clearly substantial, comparable to projected world electricity demand, and are specifically of interest to developed countries in North America and Europe. In Western Europe, there is a good potential for off-shore wind electricity generation, according to Figure 3.1.

Global wind power generation is 342 TWh in 2010, and the International Energy Agency predicts a total generation of 2680 TWh in 2035. The installation of new wind parks will increase its share in global energy production from 1.6% to 7.3% (IEA, 2012).

According to IEA (2012), some regions such as Europe will have the highest wind power penetration by 2035, which is estimated to be 20%. The global installed capacity was 238 GW in 2011, and 1100 GW of wind turbines will be installed by 2035.

A good way to utilize this great, however intermittent, resource for electricity generation is by using large scale storage systems (Cavallo, 2007; Clark and Isherwood, 2004; Lund, 2005). Different types of storage systems including pumped hydroelectric storage, batteries, supercapacitors, flywheels, fuel cells and compressed air energy storage are evaluated as potential candidates for this application. Considering its cost, high reliability and environmental effects, compressed air energy storage system is a good candidate for wind electricity storage. There is no need to make space for air storage; it simply can be stored underground in a natural salt dome (Cavallo, 2001).

In 2006, the national renewable energy laboratory of the United States proposed a baseload wind power system utilizing advanced compressed air energy storage systems (Denholm et al., 2010). They investigated the integration of a 2000 MW wind power plant with a 900 MW CAES. The integrated system has 900 MW net power output. The results show that the actual performance of the base-load wind power system strongly depends on the optimum size of the components, and the trade-off between high annual capacity factor and utilization of wind energy. The research was performed to investigate substituting conventional base-load fossil power plants with a renewable power generation site.

Madlener and Latz (2013) perform a feasibility analysis of CAES systems to improve wind power grid integration. Two scenarios are considered; a centralized CAES system, with its input electricity supplied by the wind park, and a decentralized CAES system, where for every wind turbine a separate air compressor is provided. The analyses are optimized by a profit-maximizing algorithm taking the economic aspects into account. The study shows that if the hourly contracts for the electricity are made, the centralized CAES systems would be economically feasible. Moreover, heat recovery from the compressed air is strongly recommended by the authors.

Lund and Salgi (2009) investigate the role of CAES systems in developing sustainable energy systems. The study is based on a detailed analysis of Denmark's

hourly energy supply. The role of CAES in providing Danish power grid with electricity is investigated and compared with other storage options. The results show that the economic feasibility of CAES is less than the value for other energy storage options provided that the systems are applied to wind energy storage.

McDowall (2006) discusses the use of short to long term energy storage options to support high penetrations of wind energy into the electricity grid. The results show that lithium-ion batteries are suitable, long term storage options for intermittent wind energy storage, especially in weak power grids. As an example of the storage of wind energy in the form of hydrogen, Calderón et al. (2010) present the experimental results of a hybrid PV-wind power system. The experiment was carried out in Spain for the hybrid system producing hydrogen in a water electrolyser. The results show that by storage of solar and wind energy in the form of hydrogen gas and by re-generating electricity in a fuel cell, the efficiencies of electricity generations by solar and wind energies are 2.24% and 9.71%, respectively.

3.1.3 Biomass

Organic materials derived from animals or plants are called biomass. An important fact about biomass is that in contrast to fossil fuels, the organic materials are not fossilized. Therefore, biomass is produced the moment a plant sprouts or an animal is born. The by-products, products, wastes, and residues from agriculture and bio-industries are also considered as biomass (Basu, 2010). Biofuels can be solids, liquids or gases recovered from biodegradable, non-fossilized materials. It is a renewable energy resource, since it is formed constantly as a result of interactions of animals and plants with carbon dioxide, water, sunlight, and soil. Low gravimetric energy density of biomass is a barrier to rapid increase in biomass use. Therefore, biochemical and thermochemical biomass conversion methods have developed for easier biomass handling, transportation, and use. The biochemical biomass conversion is called fermentation, and the thermochemical method is gasification. Fermentation is an ancient way of producing methane from digesting plants and animal waste. Gasification is a modern method in which biomass is heated in the presence of a gasification medium to produce syngas, which is a mixture of carbon monoxide and hydrogen. The product gas can later be synthesized to any other type of desired fuel. Ethanol is one of the post-processing products of biomass gasification.

Gasification is not just limited to biomass, since fossil fuels can benefit from gasification. The gasification medium can be air, pure oxygen, or steam. Gasification increases the heating value of fuels by removing non-combustible components. Moreover, the energy density of the fuel is improved, since gasification removes oxygen from the components. The fact that biomass is a renewable resource along with environmental and socio-political advantage of its utilization drives the interest toward biomass use through gasification. Many worked on biomass gasification modeling, analysis, optimization, and integration. The chemical reaction in the gasifier is usually modeled based on equilibrium models. Thermodynamic equilibrium model is independent of the gasifier design; therefore, it provides a convenient way of performance study of the process. Equilibrium constant and Gibb's free energy minimization are the two major modeling approaches (Basu, 2010). Biomass gasification is a complicated process, which is affected by many parameters, including gasification medium, biomass composition and moisture content, gasification temperature and pressure, and process configuration. A good understanding of the effects of these parameters on the performance of the gasification system is required for effective design work. Thermodynamic modeling, based on exergy as well as energy, is one approach to develop such an understanding.

Various studies have been performed on biomass gasification from the point of energy and exergy. Cohce et al. (2010) report an analysis for a hydrogen production unit based on biomass gasification. A simplified model is presented for biomass gasification based on chemical equilibrium considerations, with the Gibbs free energy minimization approach, and hydrogen production rate and exergy destruction rate in each component are found to be significant.

Abuadala et al. (2010) present an exergy analysis of a hydrogen production system via biomass gasification in a range of 10-32 kg/s from sawdust. The study focuses on the influence of gasification temperature, biomass feed and steam injection on the hydrogen yield and energy efficiencies. The results indicate that the performance of hydrogen production from steam-fed biomass gasification depends on the quantities of steam and biomass input to the gasifier. Rao et al. (2004) report results from an investigation of the change in exergy content of the produced gas in gasification for various biomass sources. Air-blown gasification is considered with a counter-current fixed-bed gasifier for municipal residue-based refuse derived fuel (RDF) pellets and

compared with the mass and energy performance of a gasifier using other biomass and residual fuels. Empirical stoichiometric equations are developed to describe the gasification of various fuels. The energy content of the produced gas generated from RDF pellets is found to be close to that from wood chips. When compared with the wood chip and charred soybean straw (CSS) pellets, the energy dissipated in the system is observed to be lowest and the exergy efficiency highest for RDF pellets, indicating that RDF can be a competitive fuel for thermal energy conversion through gasification.

Other researchers have reported thermodynamic analyses of gasification of other types of biomass (Abuadala and Dincer, 2010; Ptasinski et al., 2007; Puig-Arnavat et al., 2010). In these works, parametric studies are performed based on the change in such parameters as biomass feed rate, gasification temperature and biomass content. Important parameters in biomass gasification are shown to be biomass moisture content and amount of gasification medium. Abuadala and Dincer (2012) consider the use of biomass gasification product gas as the fuel feed to a SOFC, as a potential, integrated application. Solid oxide fuel cells are capable of operating with such fuels as natural gas, hydrogen, and syngas. The latter is produced with biomass gasification, and can be directly used after post-processing in SOFCs. Colpan et al. (2010) investigate effects of gasification medium on systems integrating biomass gasification and SOFCs. Steam gasification is found to have higher exergy efficiency, relative to air gasification. Also, the results show that a higher electricity generation rate in the SOFC is achieved with steam as the biomass gasification medium.

3.2 Sustainability

Sustainability has become an interest to societies since the 1980s, and the attention toward developing methods to achieve sustainability has grown accordingly. Experimental, analytical, and case studies of energy systems were performed based on sustainability development indices. Since the role of energy storage in sustainability was realized, efforts are made to address the relation between energy storage and sustainable systems (Dincer and Rosen, 2007).

Evans et al. (2009) assess the sustainability indicators for renewable energy technologies. The work is performed using data available in literature. The following sustainability indicators are taken into account:

- Price of generated electricity
- Greenhouse gas emissions during full lifecycle of the technology
- Availability of renewable sources
- Efficiency of energy conversion
- Land requirements
- Water consumption and
- Social impacts

The data for sustainability indicators of renewable energies were compared with those for coal and gas, as well. The ranking revealed that wind power is the most sustainable, followed by hydropower, photovoltaic and then geothermal. Although the assessment is quite complete and covers reasonable data available from literature, it lacks the consideration of the role of energy storage system in measuring the indicators.

The assessment of utilization of batteries in residential sectors as small scale energy storage systems is of interest to Nair and Garimella (2010). Therefore, they provide a paper to identity the benefits of the integration of renewable energies with various small-scale energy storage technologies. Simulation results by Simulink and HOMER reveal that Nickel Metal hydride batteries have high potentials for serving as small-scale energy storage system provided that the capital costs are lowered. Moreover, it was shown that the two factors resulting in dominant use of lead-acid batteries in renewable energy systems are affordability and availability, although their technical performance is poor. Li-ion batteries have a plausible potential to attain renewable energy market, thanks to the worldwide investment and improvements in performance of technology.

Denholm and Kulcinski (2004) perform life cycle assessment of energy storage systems to evaluate energy requirements and greenhouse gas emission. The results were used to understand energy sustainability and environmental impacts of constructing these systems. The results show that energy requirement for construction of battery energy storage is substantially greater compared to equivalent size CAES or

pumped-hydro storage (PHS). PHS and CAES use essentially energy free storage media (water or air) as opposed to the BES electrolytes, which require energy intensive mining and ore processing. The greenhouse gas emissions of pumped hydro storage systems are reported to be the least among the others, followed by batteries and then CAES.

Hydrogen systems and sustainability are bound together, since hydrogen, as an energy carrier, can contribute in developing a better environment through renewable energy utilization and by increasing efficiency of the systems. Dincer and Rosen (2011b) describe sustainability aspects of hydrogen and fuel cell system. They discuss the role of hydrogen and fuel cell systems toward the way of sustainability development. The discussion of the importance and usefulness of exergy methods in increasing the efficiency and sustainability of hydrogen systems is also a part of their work. Moreover, considerations were presented regarding production, transport and storage, and utilization of hydrogen.

The potential for providing sustainable energy systems using hydrogen energy is reported by Dunn (2002). In addition, the prohibiting role of hydrogen in climate change and environmental issues has been the objective of an investigation by Scott (2007). One major barrier on development of hydrogen communities is hydrogen transportation and storage. Hydrogen density is very low in ambient conditions and its storage and transportation in liquid or compressed gaseous hydrogen tanks is expensive (Dell and Rand, 2001; Dincer and Rosen, 2011b). Nevertheless, many efforts are made towards minimizing storage cost and lower transportation difficulties.

According to Dincer and Rosen (2011a; 2011c), energy, environment and sustainability are strictly bounded with exergy analysis. Sustainability increases and environmental impact decreases as the exergy efficiency of a process increases. Exergy modeling of energy storage systems will help in understanding of system deficiencies and finding methods to decrease them, thus attaining energy systems sustainability.

3.3 Closing Remarks

Renewable energy can help with developing sustainability, and will have a better performance if integrated with energy storage systems to address their temporal behaviour. As discussed above, wind, solar, and biomass energy have greater potential due to their local availability and recent technology improvements. Utilizing renewable energy decreases the level of greenhouse gas emission and dependency on fossil fuels, both of which are major indices of sustainability. Compressed air energy storage shows a good potential for integration with wind energy and hydrogen production storage can be integrated with solar PV electricity generation. Batteries, as the third energy storage system, can be considered for developing sustainability when integrated with renewables. Therefore, based on the needs for developing sustainable energy systems, and the literature review, three novel, integrated renewable energy-based systems are proposed, developed, modeled, and analyzed in this research. These three novel systems can contribute to supplying electricity and thermal energy for different energy sectors. Wind, solar, and biomass are the renewable energy resources, and hydrogen, compressed air, TES, and batteries are the electricity storage systems considered. Chapter 4 provides details of each system, along with their schematics.

Chapter 4: Descriptions of Systems

The inputs to energy storage systems are the outputs of the other systems. Therefore, the performance of the sources of energy and energy storage systems are inter-related. Since the objective of the present research is to investigate energy storage options for sustainable energy systems, some configurations of the energy systems are considered for this study, in which renewable energies are used for power and heat generation and are integrated with various storage options for better efficiency, economy, and environmental sustainability. Energy storage systems are gaining interest worldwide. Different technologies are emerging, with the aim of improving energy utilization and supply reliability, and mitigating environmental impacts of energy usage. Thus, hydrogen storage, batteries, and compressed air energy storage methods are considered in this research. In Chapter 1, a brief discussion about each of these storage systems was presented. In this chapter, storage systems are implemented in renewable energy systems, and are analyzed from energy, exergy, and exergoeconomic aspects. Therefore, different configurations with different scenarios are developed.

Detailed descriptions of the integrated systems under study are presented. The general purpose of the proposed systems is to increase renewable energy utilization. Thus energy storage options are considered in the schematics. It is expected that these integrated systems meet a part of the requirements for developing sustainable energy systems.

Three different systems are presented here, each consisting of several sub-systems and energy storage options. Solar, wind, and biomass energy are the main sources of energy in the integrated systems and depending on the application, different energy components are added. System 1 is selected according to the considerable share of residential areas in the global energy consumption. Developing renewable energy-based system to power houses will contribute to the mitigation of greenhouse gas emissions and the decrease in the dependency on fossil fuels. Baseload power

generation using renewable energies is gaining interest, due to the global energy problems and environmental concerns. Wind, solar, and biomass energy can contribute to the movement towards increasing the share of renewables in electricity generation, which is the main reason behind the selection of System 2. Local communities have access to abundant biomass and solar energy, and they can benefit from these great resources to meet their electricity demand, which is the main purpose of System 3. Moreover, they can benefit from heat recovery through thermal energy storage and water desalination. The three developed systems are described below.

4.1 System 1: Residential Hybrid PV-Fuel Cell-Battery System

Energy efficiency improvement and utilizing alternative energies result in energy savings and GHG mitigation (Martinot, 2013). According to Martinot (2013), renewable energy has 20% share in energy consumption in almost 30 countries around the world. Moreover, high-renewable scenarios project 50–95% energy shares of renewables by 2050. In 2005, 17% of the total energy used in Canada was for residential applications. This contributed to more than 70 million tons of greenhouse gas emission (NRC, 2008). Low and zero emission buildings are gaining interest by Canadian cities. Vancouver (British Columbia) and Calgary (Alberta) are only two examples of the Canadian cities aiming to implement more renewables into their energy sector (Martinot, 2013). Solar energy is plentiful and easily accessible. The residential sector can easily benefit from this emission free, renewable energy resource. Solar energy is actively used for space heating, and it is used for electricity generation by photovoltaic cells. In Canada, interest in electricity generation by renewable energy has increased. For instance, the Ontario government has initiated programs that increase reliance on renewables and decrease fossil fuel consumption.

Asides from the costs associated with generating electricity, transmission and distribution costs raise the levelized cost of electricity. One way to reduce/eliminate the transmission and distribution costs is distributed generation. Micro-gas turbines (MGT), internal combustion engines (ICE), fuel cells, and solar photovoltaic systems are examples of power generation devices that can reliably supply electricity to a remote/residential area (Van Thong and Belmans, 2006). Micro-gas turbines and ICEs typically use fossil fuels to operate and generate electricity. They also produce high-level noises and exhaust gas, both of which may be higher than the local standards.

On the other hand, fuel cells are electrochemical devices that are quiet, highly efficient, and when used with hydrogen as fuel, are very environment-friendly power generation systems. However, the hydrogen source can come from water electrolysis, which itself requires electricity. The electricity requirement by the water electrolyser can be supplied by solar energy via photovoltaic systems. Therefore, a renewable energy based electricity generation system will form.

System 1 is conceptually developed based on the following needs and reasons:

- Residential areas account for a significant share of energy consumption of a community. Developing a renewable energy-based system that suits the residential areas will help with decreasing fossil fuel consumption and greenhouse gas emission.
- Solar energy is considered as the renewable energy resource to power System 1. Solar power is available everywhere on the planet, although its intensity can be different. All the energy on the Earth, in any form, is a conversion of solar energy; therefore, direct use of solar energy increases energy utilization and removes/decreases the difficulties regarding energy transportation and conversion. Systems that use solar energy as their prime energy source are emission free.
- Despite all the benefits of direct use of solar energy, it is temporarily available. Solar irradiance is zero during cloudy days or night hours, and may change rapidly due to weather conditions. Therefore, the developed system is equipped with energy storage options to increase power reliability. Hydrogen storage is a potential choice of energy storage technology that can be produced and stored on-site. It has a high gravimetric energy density (120 MJ/kg, compared to 50 MJ/kg for methane). Hydrogen storage is chosen over battery, due to its higher energy density. The gravimetric energy storage potential of hydrogen is six times larger than lithium ion batteries (770 Wh/L vs. 130 Wh/L, respectively).
- Hydrogen production is accomplished using water electrolysers. Although there are other developed and developing methods, water electrolysers are well-developed, due to the significant need for hydrogen in the chemical and petrochemical industries. Electrolysers are available in a large range of production capacities. A Proton exchange membrane electrolyser is selected

due to its high flexibility in load variation. Also, the operating pressure of these electrolysers can be as high as 100 bar.

- When solar power is not available, another power generation system must cover the electricity demand of the residential area. Hydrogen, which is produced by the electrolyser, can be used as fuel for an internal combustion engine or a micro-gas turbine. Both ICEs and MGTs are well-developed and commercially available; however, they generate high level noise, as well as greenhouse gas emission. Fuel cells, which are electrochemical devices and operate at very low noise levels, are selected for the hybrid system. Their efficiency reaches 80% when heat recovery is applied to fuel cells.

The schematic diagram in Figure 4.1 is a simple description of the first novel system, which is a hybrid photovoltaic-fuel cell-battery (PV-FC-Battery) system. This system is considered to be independent from local electric power grids, and the total electricity of the residential system is provided by renewable energy resources. This configuration consists of a solar photovoltaic system, a water electrolyser, hydrogen storage, fuel cell, and a battery pack. The detailed explanation of the system is presented below. The main scenario is to supply the electricity demand of a house or a residential area with the electricity generated by the solar photovoltaic system.

Solar irradiance is the total solar radiation received by the surface of the Earth in a unit of time. The solar irradiance at a specific location depends on the location's latitude. Solar irradiance is measured in W/m^2. The solar irradiance is shown with yellow arrows in Figure 4.1. The PV system capacity depends on solar irradiance, which is related to climate, and residential electricity demand. It is possible to size the PV system in such a way that electricity generated during the day time exceeds demand, and surplus electricity can be harvested and stored as gaseous hydrogen. Thus the PV system generates as much electricity to meet the peak electricity demand of the house. The intermittency characteristic of solar energy is surpassed by the hydrogen-fuel cell system. The electrolyser utilizes the surplus electricity of the PV during off-peak hours, splitting water into hydrogen and oxygen. Interest in substitution of fossil fuels with hydrogen is growing rapidly.

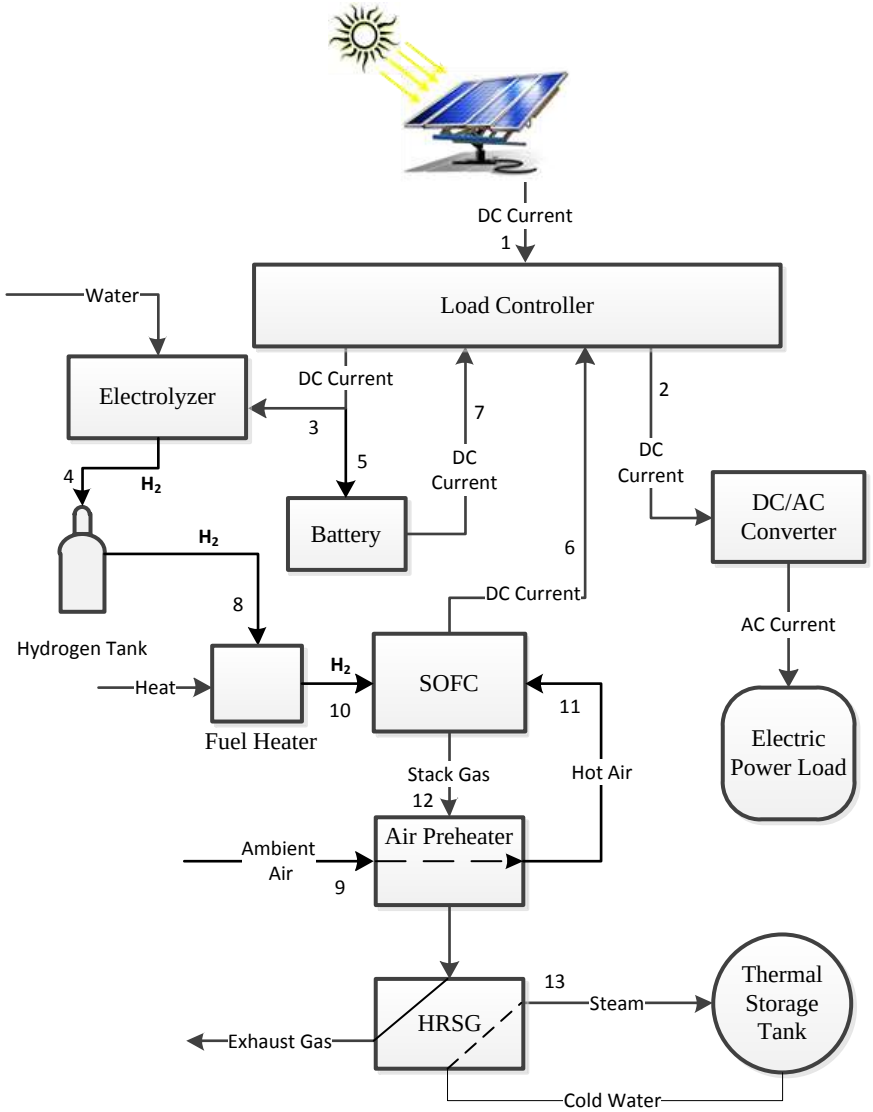

Figure 4.1: Schematic of System 1; residential hybrid PV-fuel cell-battery system

However, hydrogen storage is a challenge in developing sustainable energy systems. Hydrogen is stored and transported in bulk as compressed gas or liquid forms, even though new storage methods are under development. These storage methods require tremendous efforts through compression and liquefaction processes, and require high-tech storage tanks. In contrast, on-site utilization of hydrogen eliminates most of these difficulties. In the illustrated system in Figure 4.1, hydrogen is produced in an electrolyser installed in the residential area. The stored hydrogen is fed to the fuel cell system for electricity generation. Solid oxide fuel cells are capable of providing the residential area with DC electricity. In addition, the high temperature exhaust gases leaving the fuel cell stack can be used for space heating or hot water production with the aid of the thermal energy storage system.

It is worth noting that in the novel hybrid system, there still is some space for improvement. In fact, fuel cells are slow-response devices to the change in electricity demand. The electricity demand of the house may change suddenly; however, the power output of the fuel cell cannot rapidly follow the changes (Mueller et al., 2006). Moreover, high temperature fuel cells suffer from thermal stresses if abrupt changes in demand occur. Therefore, batteries can be used as electric energy storage systems to compensate for the fuel cell during spontaneous changes in the demand. The batteries are charged by the PV system using excess generated electricity. In some studies, PV systems are equipped only with batteries for energy storage and back-up. This simply implies that all the energy demand of the house during the periods of solar unavailability is supplied by the battery system. At first, this combination (PV-battery) seems simple and less complex, since the electrolyser and the fuel cell systems are eliminated. However, relying only on batteries will cause problems to power reliability. The shortcoming of batteries is their shorter lifetime and higher degradation rate compared to stationary fuel cells. Fuel cells can generate electricity as long as fuel is continuously provided but, while the battery is discharging, its power availability decreases. Moreover, the volumetric and gravimetric energy storage potential of hydrogen (as an energy storage medium) is higher than batteries. The gravimetric energy storage potential of hydrogen is six times greater than a lithium ion battery (770 Wh/L vs. 130 Wh/L, respectively).

Based on the schematic of the hybrid system in Figure 4.1, the operation strategy of System 1 is as follows:

- Solar energy is converted to electricity by the PV modules (Point 1).
- The generated electricity is directed to a load controller, which makes the decision of energy distribution within the system components and the house.
- If the PV electric output is more than the demand of the house, the load controller directs a part of the generated electricity (Point 2) to supply the power demand of the house. The electrolyser converts the surplus electricity (Point 3) to hydrogen, which is stored in a pressurized hydrogen tank (Point 4). Moreover, the batteries are charged (Point 5), if required.
- During periods of solar unavailability (e.g. PV output is less than the demand) the fuel cell and the battery cover the load (Point s 6 and 7). The

operation of the battery is limited to the conditions where the electric load exceeds the solid oxide fuel cell (SOFC) nominal power.

- The SOFC is fed with hydrogen (Point 8) as fuel (which is stored in the storage tank) and ambient air (Point 9) as the oxidant. Hydrogen is preheated (Point 10) via heat transfer from an external source, while air preheating is performed (Point 11) using the heat from the SOFC stack gas. The SOFC stack gas (Point 12) still has some energy to be recovered for space heating or hot water production. This is accomplished using a heat recovery steam generator, which generates low pressure saturated steam (Point 13). As shown in Figure 4.1, the steam generated in the HRSG is stored in a thermal energy storage tank.

The operating algorithm is simplified and illustrated in Figure 4.2.

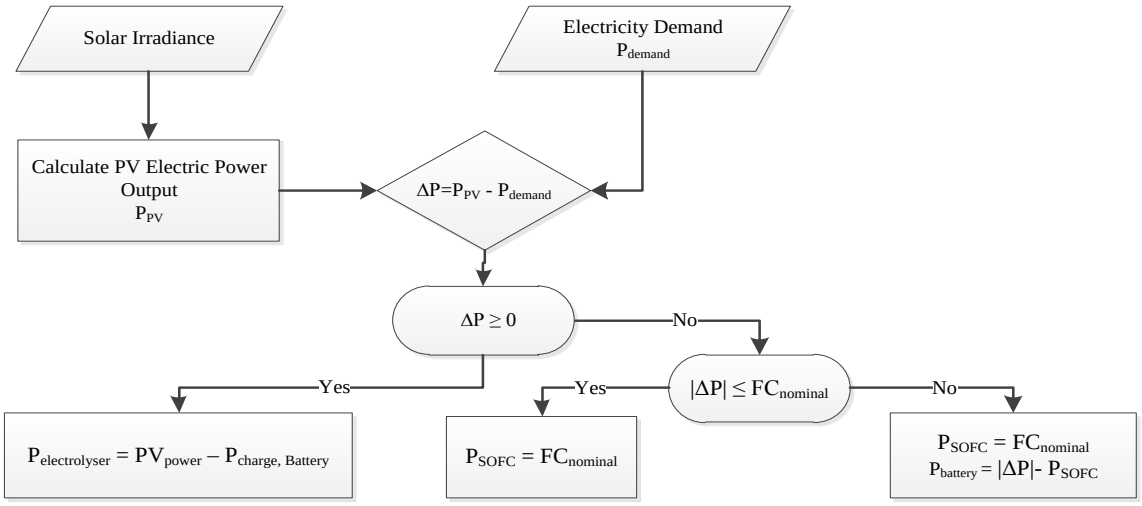

Figure 4.2: Solving algorithm for modeling and analyses of System 1

Once the PV output power and the load demand are calculated, the control system decides on the operation of the system components. A demand, lower than the PV output, results in the operation of the electrolyser or the charging of the battery pack. If the demand is higher than the electric power of the photovoltaic system, the fuel cell and the battery generate electricity for the house.

Table 4.1 presents the predicted, nominal capacities of the main components of System 1. These values may change, since an optimization is required to obtain optimal sizes and operating parameters.

Table 4.1: Predicted nominal capacities of components of System 1, based on 5.75 kW maximum electricity demand

Component	PV	Electrolyser	SOFC	Battery
Nominal Capacity	18.4, kW	12.6, kW	2, kW	13.8 kWh

Table 4.2: Flow type, thermodynamic state and nominal operating conditions of points shown in Figure 4.1

Point	Flow type	Thermodynamic state	Nominal operating conditions
1	Electricity	-	P=18.4 kW
2	Electricity	-	5.8 kW
3	Electricity	-	12.6
4	Hydrogen	Compressed gas	P=30 bar, 0.24 kg/hr
5	Electricity	-	13.8 kWh
6	Electricity	-	2 kW
7	Electricity	-	3.8 kW
8	Hydrogen	Atmospheric gas	0.12 kg/hr
9	Air	Ambient air	0.44 kg/hr
10	Hydrogen	High temperature gas	T=1073 K
11	Air	High temperature gas	T=1073 K
12	Stack gas	High temperature gas	T=1173 K, 0.56 kg/hr
13	Steam	Saturated steam	P=10 bar, 1.4 kg/s

Table 4.2 gives the type of flows at the points shown in Figure 4.1. The thermodynamic states of these points are also illustrated. The mass flow rates and nominal capacities presented in Table 4.2 may change once the analysis is performed for a specific geographical location and house demand.

The main components of the hybrid PV-FC-battery system are described in section 4.1.1. Moreover, the reasons for selecting these components for System 1 are discussed. Some of the components illustrated here, are also used in the other two novel integrated systems.

4.1.1 System Components

4.1.1.1 PV panel

Photovoltaic technology is a potential alternative for conventional power generation (mostly small scale) systems. PV panels directly convert solar energy to DC electric current. Three different PV cells are available in the market:

monocrystalline, polycrystalline, and amorphous. Monocrystalline PV cells are cut from a single silicon crystal. They are very effective in generating electricity (i.e. >25%) (Green et al., 2012); however, they are very expensive. Polycrystalline PV cells are cut from a silicon block; therefore, they contain a large number of crystals. Polycrystalline cells are not as expensive as monocrystalline ones; however, they are less efficient in generating electricity (15-20%). The third type of available PV cells, amorphous cells, are inefficient (10-15%) but not expensive, and are made by spreading non-crystalline silicon on a surface of choice.

PV panels must be installed in shade-free areas, whether or not they are installed on a roof. The performance of PV systems strongly depends on solar irradiance, wind speed, and ambient temperature. These factors may result in overestimation or underestimation of the PV system capacity. However, with careful consideration of these meteorological conditions and energy storage options, the PV panel will be able to effectively supply the electricity demand.

The residential PV panel capacity is selected after daily average electricity consumption is calculated, along with the electricity need of other system components. A PV system with 210 W/m^2 power density requires a total of 5.9 m^2 surface area for maximum output power of 1.0 kW. The electricity demand should include the consumption of all AC loads running at the same time, plus the wattage from the surge of starting motors, plus all DC loads operating at the same time; this demand is further increased by 1.2 to account for inverter losses. The inverter converts DC electricity to AC.

4.1.1.2 Electrolyser

Hydrogen can be produced from water electrolysis. Proton exchange membrane (PEM) and solid-oxide steam electrolysers (SOSE) are two available water electrolysers in the market. PEM electrolysers operate at low temperatures (<100°C), while SOSEs require higher operating temperatures (800-1000°C). Water electrolysers operate with DC electricity, and require a minimum cell voltage to operate. The irreversibility in the electrolyser cells results in higher operating voltage requirements. These losses are mainly due to ohmic, concentration, and activation voltage losses. In a PEM electrolyser, hydrogen cations are charge carrier particles, and the cell electrolyte is composed of polymer. The operating current density and

cell voltage requirements are 0.5-2 A/cm^2 and 1.7-2.1 V, respectively. The operating pressure can be as high as 20 MPa. One major advantage of PEM electrolysers is their fast response to load variation and proper operation at partial-load conditions. This major advantage makes them a great candidate for their implementation into renewable energy-based systems. Also, PEM electrolysers are low-temperature operating systems; therefore, their heat requirement is less than the SOSE systems (Nieminen et al., 2010). Moreover, Nieminen et al. (2010) report 60% exergy efficiency at a current density of 4000 A/cm^2 for a PEM electrolyser, while SOSE has 50% exergy efficiency at the same current density. In the residential hybrid PV-FC-battery, the PEM electrolyser is considered.

4.1.1.3 Hydrogen storage–fuel cell system

For residential applications, the choice of hydrogen storage in liquid form is eliminated due to the complexity and cost of the liquefaction process. Care should be considered regarding the space availability for storage tanks. The performance of solid oxide fuel cells increases slightly by the increase in their operating pressure. However, higher stack pressures require consumption of energy for air and fuel compression.

Hydrogen storage:

Storing 1 kg of hydrogen at 100 kPa and 25°C requires a tank volume of 12.3 m^3. Compressing hydrogen to 350 bar decreases the required storage volume by 99.6%. Further pressure increase lowers the required storage volume, but increases the compression work input and safety concerns. Hydrogen can be compressed with various processes, among which an isothermal process is ideal, exhibiting the lowest work consumption.

Hydrogen has a tendency to adsorb and dissociate at material surfaces. Atomic hydrogen can diffuse into the material and cause embrittlement. Materials suitable for hydrogen applications are mainly austenitic stainless steel and aluminum alloys. Most compressed hydrogen tanks are presently made of steel (Hirscher, 2010; Klell et al., 2007). Stainless steel CGH_2 storage tanks are called “Type I” tanks, and their volume ranges from 2.5 to 50 L, which consist of a thin inner layer of steel or aluminum, and have lower storage tank weights (Hirscher, 2010; Klell et al., 2007). Composite tanks (type II and III tanks) may be composed of carbon fibre in order to achieve strength

requirements. Type IV hydrogen storage tanks are made of composite materials which are lighter than types I and II, but more expensive.

Solid oxide fuel cells:

Solid oxide fuel cells are expensive power generation systems; yet, the interest in their implementation in small scale power generation units is increasing. With the advances in material technology, and development of proper catalyst and electrodes, the problems regarding response time and thermal degradation will be overcome. The available SOFC-CHP systems, run by Siemens and other manufacturers, show the feasibility of building more integrated energy systems with fuel cells and heat recovery units.

In a solid oxide fuel cell, hydrogen is ionized and forms H^+ cations and releases electrons, which flow through an electric circuit toward the cathode, where oxygen reacts with the electrons and forms an oxygen anion (O^{-2}). The oxygen anions flow through the electrolyte to the anode, where hydrogen and oxygen ions react and form water. The electrolyte is designed so that only negative ions can flow through it, forcing the electrons to flow through the external electric circuit. The electrolyte is a solid, non-porous metal oxide, which is usually made of yttria-stabilized zirconia (Larminie and Dicks, 2003). The anode is typically nickel-based zirconia, and the cathode is lanthanum strontium manganite (LSM) with a general chemical formula of Sr-doped $LaMnO_3$. The cells operate at 600-1000°C, and since there is no liquid electrolyte, cell corrosion and liquid management is not an issue. Solid oxide fuel cells use a wide range of fuels, including some hydrocarbon fuels. The high-temperature operating range of the SOFCs allows for internal reforming, and cogeneration with bottoming cycles due to their high-temperature stack gas. Recent developments have led to manufacture and installation of lower temperature SOFCs, which benefit from lower material and fabrication costs. Solid oxide fuel cells can be scaled-up from less than 1 kW to 100 MW, depending on the application. This is simply achieved since each cell itself is an electricity generation unit. Siemens Westinghouse is a pioneer in developing tubular solid oxide fuel cells, which overcome the sealing problems that occur in planar cells. SOFCs are by far the most efficient types of fuel cells, and taking advantage of cogeneration processes, the overall energy efficiency can reach as high as 80%. Solid oxide fuel cells are very

compact in size; therefore, their power density is considerably high, i.e. 0.7 kW/kg for 1.4 kW peak power GE-SOFCs (Minh, 2002), although it may be slightly less than the lithium ion batteries with almost 1 kW/kg power density (Gaines and Cuenca, 2000).

Other types of fuel cells can be potential candidates for the residential hybrid PV-FC-battery system, which may be referred to as proton exchange membrane (PEM) and molten carbonate fuel cells. However, based on the specifications of these fuel cells, solid oxide fuel cells have a higher potential for residential, stationary power generation. The solid electrolyte of SOFCs eliminates electrolyte management problems. SOFCs are less vulnerable to H_2S, and do not require CO_2 recirculation from anode to cathode as with the MCFCs. The solid oxide fuel cells life time is considerably high and can operate up to 100,000 hours with almost no degradations (Larminie and Dicks, 2003).

4.1.1.4 Thermal storage systems

Hot water storage can be used in the heat storage unit. Hot water storage tanks include two bundles of submerged heat exchanger tubes. The high temperature exhaust gases of the fuel cell unit produce saturated steam in a heat recovery unit. The steam is delivered to the storage tank through one of the bundles. The other bundle transfers stored heat in the storage tank to the heat utilization unit, when heat is required. Thermal stratification can be used to achieve higher efficiencies. Seasonal thermal energy storage is suitable for the conditions where thermal energy is abundant in a period of time, and there is a large demand when it is not available. For instance, solar thermal energy is abundant in spring-summer months in Canada, while in fall-winter months its availability decreases. Therefore, a seasonal TES system can store solar thermal energy during the months with higher solar availability, and the stored thermal energy can be utilized when required. Water is suggested as a good storage medium since it can be both the heat transfer medium and the heat storage medium. Water is also nontoxic, noncorrosive, and chemically stable and has high specific heat capacity, all of which are requirements for a good thermal storage medium. Proper sizing of the seasonal storage tank is important, and tanks with lower surface-to-volume ratio are more favoured.

The analysis of the energy storage systems integrated into the residential hybrid system requires good understanding of the energy demand of the residential area. The transient behaviour of the energy demand causes difficulties in proper sizing of the systems. The idea of analyzing these integrated renewable energy systems is to minimize grid dependency. It is reasonable to perform optimization analyses for proper selection of the system components.

4.2 System 2: Integrated Renewable Energy-based System for Baseload Power Generation

The philosophy behind baseload power generation systems is to maximize the implementation of renewable energy into electricity power grids. In other words, renewable energy resources are used to produce a share of the power consumption of a district area. As a movement toward a greener society, for example, the government of Ontario has set some regulations and policies such as "Go Green: Ontario Action Plan on Climate Change" and "Green Energy Act". Other provinces and territories have similar policies and regulations (Blackwell, 2013; NRC, 2008). These actions set targets for overall greenhouse gas emissions, and motivate increasing use of renewable energy. These result in less carbon dioxide emissions and environmental pollutants because a part of the energy demand is provided by renewable sources rather than fossil fuels. Furthermore, to achieve a higher level of sustainability, efforts have been made to use waste heat recovery systems and energy storage options.

One application of renewable energy is baseload power generation. This may not seem practical since these resources, i.e. wind and solar energy, have intermittent characteristics. In fact, a report by Peters and Burda (2007) argues the common strict idea of energy management companies in Ontario, Canada that baseload electric power should be solely supplied by nuclear and fossil power plants(Peters and Burda, 2007).

The report suggests that a distributed mix of renewable and conventional power plants can provide a reliable baseload power generation. Increasing renewable energy power plants, reducing peak demand by proper demand management methods, and installing adequate gas-fired thermal power plants to meet the peak demand will increase the share of renewable energies in baseload power generation. However, a

continuous supply of baseload electricity by renewable energy-based power plants requires compensating for the lack of power output during the unavailability of the renewable resource. For instance, solar energy is not available during cloudy days and night hours. Therefore, proper measures should be taken to overcome this intermittent behaviour, which energy storage is one of them.

The second novel system, proposed in this research, is an integrated renewable energy-based system for baseload power generation; System 2. This system is unique in its configuration and integration of different renewable energy resources with energy storage options.

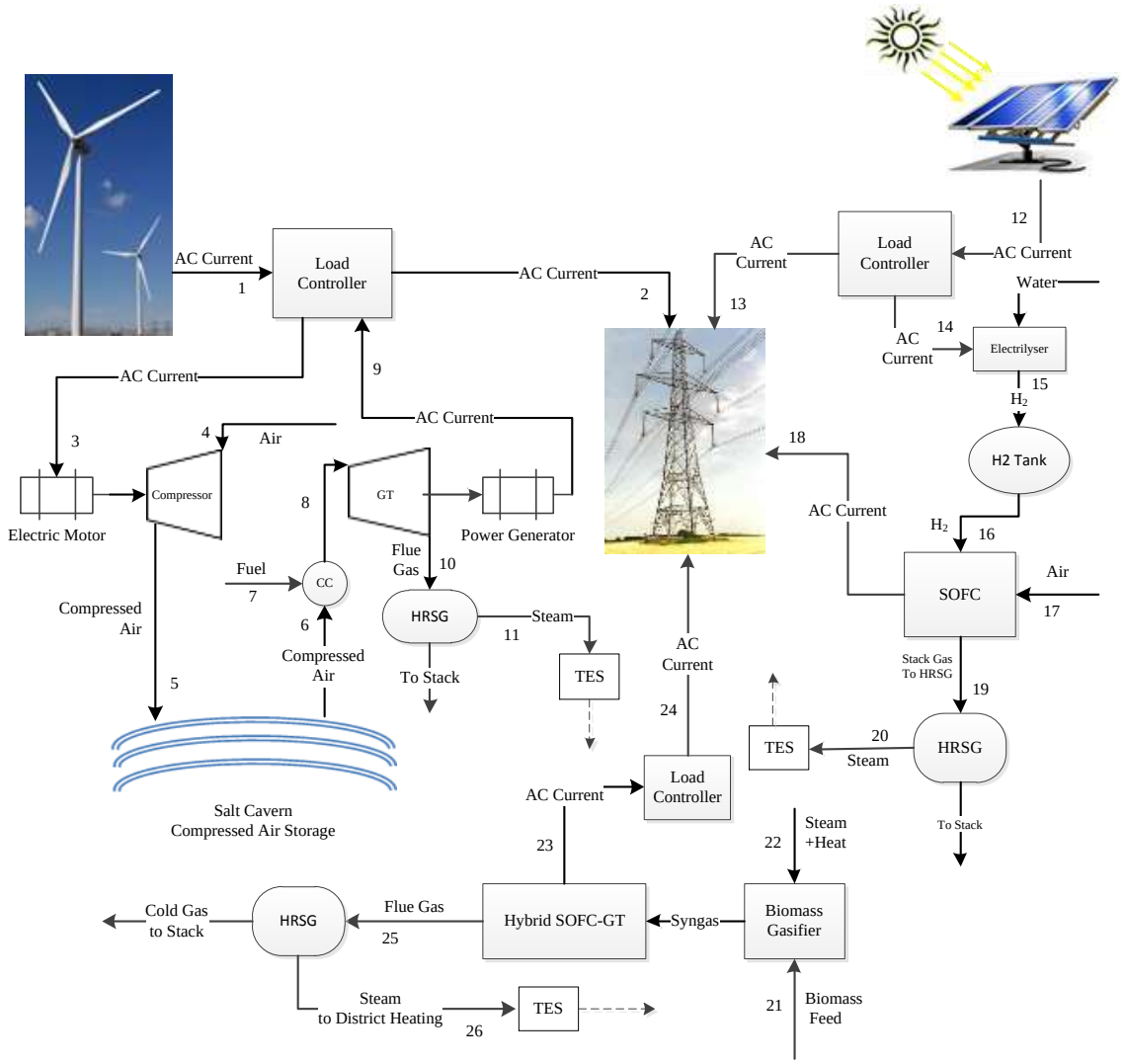

Figure 4.3: Simple schematic of the integrated renewable energy-based system for baseload power generation: System 2

Although many other configurations can be chosen, the proposed integrated system is selected for its simplicity in integrating different renewable energy resources.

System 2 contains three different power generation systems; each utilizing a renewable energy resource. As shown in Figure 4.3, wind, solar and biomass are the renewable energy resources. The integrated system is meant to supply the baseload electric power of a district area and the system components are selected so the wind park has the greatest share in meeting the power demand.

Moreover, thermal energy recovery from the system's components is considered to increase energy efficiency. The recovered thermal energy is stored in a seasonal TES system, and is supplied to a district area during fall-winter months. System 2 is developed based on the following needs and/or requirements:

- The increasing demand for energy, depletion of fossil fuel resources, and global warming concerns initiate the interest in renewable energy, of which solar, wind and biomass are three globally available resources. They can be easily accessed and utilized with solar photovoltaic systems, wind turbines, and direct or indirect use of biomass, respectively.
- Central, renewable energy-based power plants can benefit from local grids by feeding the generated electricity to the grid lines. There are countries that use renewable energy to power their houses and industries, and the wave towards baseload power generation through renewable energy is propagating.
- The potential of solar energy for electricity generation through solar photovoltaics were discussed in Section 4.1. Wind energy has shown itself as a great potential for power generation, as countries such as Denmark and Germany supply 20% of their electricity with wind power. However, wind speed varies with time of the day, and geographical locations. Therefore, energy storage is introduced to System 2, to overcome wind power intermittency.
- Among different storage options, e.g. battery and hydrogen energy storage, compressed air energy storage is selected for System 2. Air compressors can simply compress large flow rates of ambient air, and the compressed air can be stored in air storage vessels or underground caverns. The cavern can be an abandoned mine or a salt cavern; therefore, there is no need for building

storage tanks. Moreover, the start-up time of gas turbines can be as quick as 5 minutes, and natural gas can be used as fuel. Gas turbines are also flexible with power output fluctuation.

- The third power generation component of System 2 is a SOFC-GT system. Solid oxide fuel cells are reliable power generation systems and have integration capabilities. They have proven to work reliably when integrated with gas turbines and can be fed with different types of fuel such as syngas. Syngas, a mixture of hydrogen and carbon monoxide, can be produced through biomass gasification. Therefore, the integrated biomass-SOFC-GT system is selected to supply a part of the baseload electricity. This system can fit into the configuration of System 2, due to its reliable and clean electric power generation.

Table 4.3 illustrates the flow type, thermodynamic states and operating conditions of the Wind-CAES system shown in Figure 4.3. The relevant data for the PV-H_2-FC and biomass-SOFC-GT systems are given in Table 4.4.

Table 4.3: Flow type, thermodynamic state and operating conditions of the Wind-CAES system

Point	Flow type	Thermodynamic state	Operating condition
1	Electricity	-	662 MW
2	Electricity	-	470 MW
3	Electricity	-	192 MW
4	Air	Ambient air	290 Kg/s
5	Air	Compressed air	290 Kg/s, P=64 bar, T=331 K
6	Air	Compressed air	436 Kg/s, P=36 bar, T=298
7	Fuel	Gaseous methane	10 Kg/s
8	Combustion gas	High enthalpy gas	446 kg/s, P=36 bar, T=1300
9	Electricity	-	470 MW
10	GT flue gas	Moderate temperature gas	446 kg/s, P=1, T=900 K
11	Steam	Saturated steam	P=10 bar, $\dot{Q} = 49$ MW

The operation and reasons for selecting the components of System 2 is described below.

4.2.1 Wind-CAES

Wind energy is a cubic function of wind speed. Therefore, any fluctuation in the wind speed leads to a significant change in its available energy. Wind turbines are usually in operation 80% of the year, and produce nearly 30% of their nominal power capacity throughout the year (Munteanu et al., 2008). Wind power density (W/m^2) is an index quantifying the level of wind resource, and can be related to the cube of wind speed and the Weibull distribution function. The efficiency of wind turbines is limited to a maximum of 59%, known as the Betz limit (Munteanu et al., 2008).

Table 4.4: Flow type, thermodynamic state, and operating condition of the PV-H_2-FC and biomass-SOFC-GT system

Point	Flow type	Thermodynamic state	Operating condition
PV-H_2-FC			
12	Electricity	-	28 MW
13	Electricity	-	5.0 MW
14	Electricity	-	23 MW
15	Hydrogen	Compressed gas	0.12 kg/s, *P*=30 bar
16	Hydrogen	Atmospheric gas	0.083 kg/s
17	Air	Atmospheric gas	0.31 kg/s
18	Electricity	-	5.0 MW
19	Stack gas	High temperature gas	0.39 kg/s, *T*=1173 K
20	Steam	Saturated steam	*P*=10 bar, 2.3 MW
Biomass-SOFC-GT			
21	Biomass feed	Moist biomass	$\omega = 0.5$, 3.9 kg/s
23	Electricity	-	25 MW
26	Steam	Saturated steam	*P*=10 bar, 16 MW

Wind power generation is gaining interest worldwide and the projected plans promise a 3% share in global power generation by wind energy in the next five years. Although Asian countries, especially China, are planning to double their wind power installations, Europe still has the greatest share of global wind power generation. United States and Canada are also planning on generating 15 GW annual markets after rising from the financial recession in 2008. In Denmark, wind energy reached 20% electric power penetration in 2007, while in Canada only 1% of the electricity demand is supplied by wind power, despite its significant wind power resources. According to the Canadian Wind Energy Association, wind energy can generate 20% of the Canadian electric energy demand by 2025 (CanWEA, 2008). Therefore, wind

energy is selected as one of the potential renewable resources in this research. However, generating baseload power requires a continuous electric power output, which wind turbines may lack in such a requirement, due to the variations in wind speed.

Energy storage is one option to compensate for the intermittency of the wind energy, of which battery electric energy storage, hydrogen storage, and compressed air energy storage (CAES) are among the potential options. Batteries, as small scale power generation systems, could be a good option to store the excess generated electricity by the wind turbine(s) and meet the demand when needed. However, in large scale scenarios (baseload power), batteries are very bulky, expensive, and require continuous maintenance. Hydrogen storage is another option, which requires electrolysers, hydrogen tanks, and fuel cells or gas turbines for power generation. In large scale baseload power generation, the size of the hydrogen tanks will be significantly large, and work of compression will be considerable. Compressed air energy storage seems promising, since the compressed air is stored in abandoned mines or underground salt caverns.

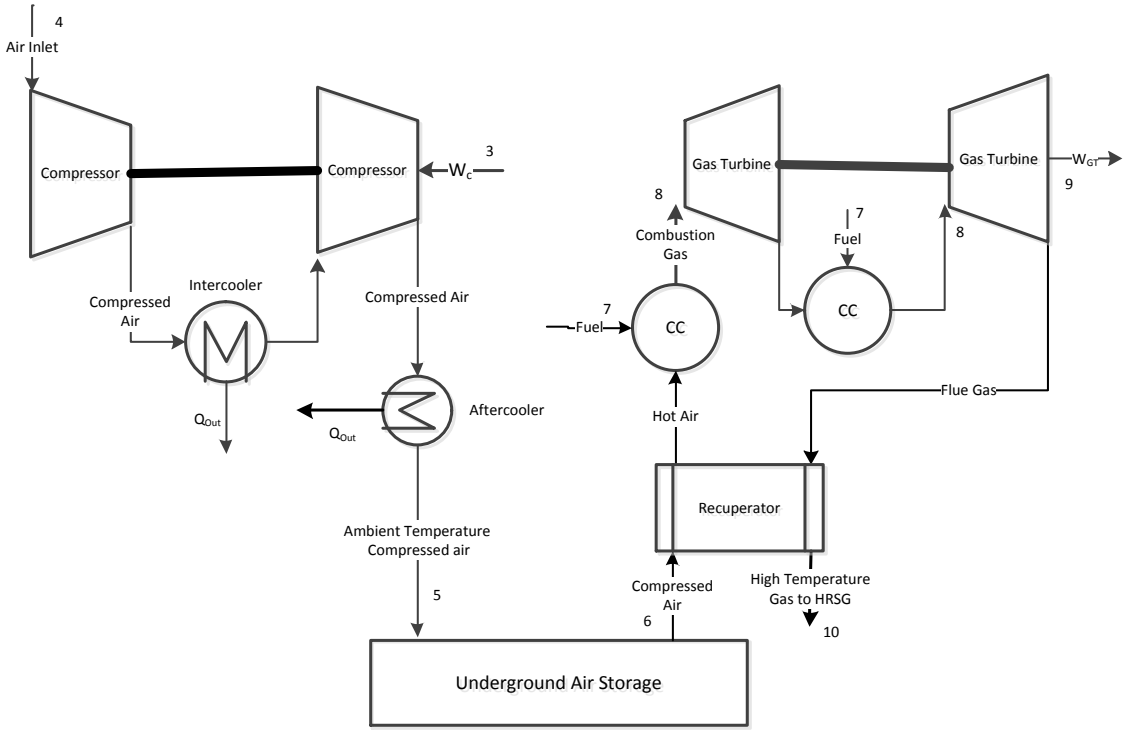

Figure 4.4: A simple schematic of the compressed air energy storage system

CAES utilizes the familiar gas turbine cycle, with a simple modification. When integrated with wind turbines, excess generated electricity by the wind turbines is consumed by the compressors to compress ambient air, which is stored in the salt cavern or the abandoned mine. When needed, the compressed air is heated and expanded in a gas turbine in order to produce electricity. Figure 4.4 shows a schematic of the compressed air energy storage system. The points indicated on Figure 4.4 refer to the mass and energy flows in Figure 4.3.

The operating strategy of the Wind-CAES system is illustrated using Figure 4.3. The power output of the wind park (Point 1) is fed to a load controller. The controller decides if the power output should be delivered to the grid (Point 2) or to the CAES system (Point 3). When the electric power output of the wind park is higher than demand, the surplus electricity is fed to the CAES system for ambient air compression in two steps (Point 4). First, the ambient air is compressed to a medium pressure (pressure ratio of r_c), and is cooled in the heat-exchanger. Water-air heat exchangers will best fulfill the purpose of removing heat from the compressed air. The heat removed from the compressed air in the heat exchanger can be used for district heating, or can be stored in a thermal storage system. The medium pressure, low temperature air enters the next compressor for further compression, where it gains energy. To decrease the required volume for storage, the high pressure compressed air is cooled in the second heat exchanger, and stored in the underground salt cavern (Point 5).

If the power output of the wind park is less than demand, the gas turbine operates, extracting compressed air (Point 6) from the salt cavern. The compressed air enters a combustion process with natural gas (Point 7), and is fed to the gas turbine (point 8) for electric power generation (Point 9). The gas turbine inlet temperature (*TIT*) depends on the type the turbine and the manufacturer. The *TIT* of a typical gas turbine is able to reach 1100°C, while the flue gas temperature can be as high as 550-650°C. To increase efficiency, the gas turbine flue gas (Point 10) is fed to the HRSG for low pressure steam generation (Point 11). The generated steam is stored in a thermal energy storage system. Due to the intermittency of power generation by the gas turbine, an advantageous way to utilize the generated steam is energy storage, as it gives more flexibility in meeting a part of the district's thermal demand. The compressor must produce enough compressed air so there is a net positive amount of

stored air in the salt cavern throughout the year, considering air consumption by the gas turbine.

4.2.2 PV-H_2-FC System

The photovoltaic-hydrogen-solid oxide fuel cell (PV-H_2-FC) is considered to supply a small part of the electricity demand (as 5 MW). This decision is made due to the high land use of the photovoltaic system (as 5.92 m^2/kWe). The PV system electricity output depends on solar irradiance, which is related to climate. It is possible to size the PV so that electricity generated during the day time exceeds demand, and surplus electricity can be harvested and stored as hydrogen gas. Thus the PV generates as much electricity as needed to meet the electricity demand. The intermittent characteristic of solar energy is overcome by the hydrogen–fuel cell system. The electrolyser utilizes the surplus electricity of the PV system (Point 14) during those times of the day when PV output exceeds the electricity demand of the grid. The electrolyser splits water into hydrogen and oxygen (Point 15). Interest in the substitution of fossil fuels with hydrogen is growing; however, hydrogen storage is a challenge in developing sustainable energy systems. Hydrogen can be stored and transported in bulk as a compressed gas or liquid, and new storage methods are under development. These storage methods require significant inputs through compression and liquefaction processes, and require high-tech storage tanks. In contrast, on-site utilization of hydrogen eliminates most of these difficulties. In the system illustrated in Figure 4.3, hydrogen is produced in an electrolyser installed at the PV-H_2-FC site. Therefore, there is no need for long term storage of hydrogen, because it is consumed by the fuel cell system on demand. Moreover, with proper sizing of the system components, a high pressure compressed gas is not required. The stored hydrogen is fed (Point 16) to the SOFC system for electricity generation (Point 18).

Solid oxide fuel cells are capable of generating baseload electric power. In addition, the high temperature exhaust gases leaving the fuel cell stack (Point 19) can be used for space heating or hot water production in a heat utilization unit. Since the fuel cell is in operation only when required, the heat gained by the heat utilization unit is stored in a thermal energy storage system (Point 20).

4.2.3 Biomass-Fuel Cell-Gas Turbine (Biomass-FC-GT) System

Gasification is a chemical process that converts materials like biomass into convenient gaseous fuels. In this process biomass is broken into simpler substances such as CO, H_2, CH_4 and CO_2. The process occurs in the presence of a gasification medium. Biomass gasification is a complicated process, which is affected by many parameters, including gasification medium, biomass composition and moisture content, gasification temperature and pressure, and process configuration. A schematic of the considered biomass gasification process is shown in Figure 4.5. Unlike fossil fuels, biomass does not require millions of years to form, and is formed from living plants and animals.

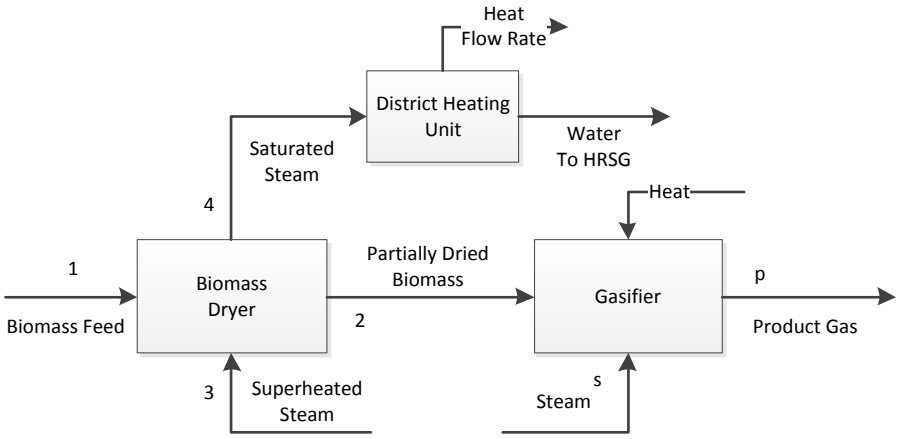

Figure 4.5: Simple schematic of a biomass gasification process

Biomass is a renewable energy resource since it can be harvested and replanted. Biomass is formed during the photosynthesis process in plants, while they take in sunlight, water, and the carbon dioxide in their environment. Therefore, burning or gasification of biomass only releases the amount of the CO_2 which was absorbed by the plant. Hence, biomass consumption is considered a carbon neutral process (Basu, 2010). Depending on the type (liquid or solid, animal or plant based) biomass contains moisture from 15-98% of its mass content. The biomass moisture fraction is defined as the ratio of the mass of water in the biomass to the mass of the total wet biomass. Sawdust, as a waste biomass, can contain 15-65% moisture content. The water content in the biomass significantly affects its potential as a fuel. Therefore, before the gasification process, a drying system is placed to remove a part of the biomass moisture from its structure. Air and steam drying are the two main options for

biomass drying. Steam drying is of more interest due to the potential for heat recovery from the steam and the additional steam added to it during the drying process. The additional steam is technically the evaporated water from the biomass feed (Tock et al., 2010).

To improve the performance of the gasification process, the moisture content of the biomass feed is controlled via a biomass dryer. A direct steam-biomass dryer is used to decrease biomass moisture content before it enters the gasifier. According to Figure 4.5, the superheated steam (Point 3) is supplied by a heat recovery steam generator. The steam exiting the dryer (Point 4) has considerable energy, which is used in a district heating (DH) system for efficient energy utilization. Dried biomass (Point 2), which still has 10-20% moisture content, enters the gasifier. Pressurized, superheated steam (Point 5) is used as the gasification medium. Gasification occurs in the absence of oxygen; however, the process requires a significant amount of heat to be initiated. The required heat can be supplied by an external heat source, or by the combustion of a portion of the biomass in the gasifier. In the steam-biomass gasification a controlling parameter is steam-to-carbon ratio (*SC*), which is defined as the ratio of molar flow rate of steam to the molar flow rate of carbon content of the biomass feed. Changing the amount of steam supplied to the gasifier affects the gasification process significantly (Basu, 2010; Tock et al., 2010). The product is in the gaseous phase. In this analysis CO, H_2, CO_2, CH_4, H_2O, and C (as char) are considered as constituents of the product gas from the gasification process.

Although only 5% of the global biomass resources can be transported to produce energy, these can still produce 26% of the world's energy consumption (Basu, 2010). Hacatoglu et al. (2011b) estimated that the available lignocellulosic biomass in Ontario can produce enough energy to substitute for all the coal-fired thermal power plants in the province, without significant impact on the food and fibre production. Therefore, biomass offers a great potential in supplying the electric energy demand taking advantage of the modern, high-efficiency gasification processes, and integration with downstream power generation cycles. Biomass gasification is integrated with solid oxide fuel cells, since this type of fuel cell can operate with syngas, a product of biomass gasification. Colpan et al. (2007) present the result of modeling a solid oxide fuel cell operating with syngas. Internal reforming is considered, due to the high operating temperature of the fuel cell stack. A parametric

analysis is performed to study the effect of main parameters on the I-V characteristic curves and cell power output. McIlveen-Wright et al. (2011) report the results of a thermo-economic analysis of biomass gasification integrated with medium and high temperature SOFCs. Two types of biomass, willow and miscanthus, are considered as biomass feeds, and the energy efficiencies are reported as 39 and 38%, respectively. Air gasification is considered in their study, and 841 g/kWh of CO_2 is emitted for a net 250 kW fuel cells output. SOFCs are high-temperature electrochemical devices, which generate electricity. The by-product of the SOFC stack is mostly hot water, depending on the type of the fuel. Heat recovery from SOFC stack gas is possible through heat recovery units for steam or hot water generation. Motahar and Alemrajabi (2009) and Dincer et al. (2009) propose the integration of SOFCs with bottoming gas turbine cycles. The energy and exergy efficiencies of the integrated system reach 70–80%, which compares well to the efficiencies of approximately 55% of conventional combined-cycle power generation systems. System 2 in this research consists of an SOFC-GT cycle integrated with biomass gasification.

4.2.4 Operating Strategy of System 2

The heat recovered from the gas turbine flue gas of the CAES-GT and SOFC-GT systems is stored in the form of hot water in thermal energy storage systems. Based on Figure 4.3, the overall operation of System 2, the integrated renewable based-energy system for baseload power generation can be described as follows:

- The wind turbines power output is estimated (Point 2) and compared with the electricity demand from the wind park.
- If the wind park's power output is greater than demand, the excess electricity is fed to the CAES system (Point 3) for electric energy storage in the form of compressed air (Point 5). Heat is recovered from the compressed air.
- If the wind park's power output is less than demand, the gas turbine of the CAES-GT system extracts the compressed air from the air cavern (Point 6). The extracted air participates in a combustion process with natural gas, which is supplied to the combustion chamber of the gas turbine (Point 7). The combustion gases (Point 8) are expanded in the gas turbine, which results in electric power generation. Heat is recovered from the GT flue gas (Point 9).

- Solar energy is converted to electricity by the PV modules (Point 12).
- The generated electricity is directed to a load controller, which compares the PV power output and the electricity demand from the solar PV system
- If the PV electric output is more than demand, the load controller directs a part of the generated electricity to supply the power demand (Point 13). The electrolyser converts the surplus electricity to hydrogen (Point 14), which is stored in a pressurized hydrogen tank (Point 15). During periods of solar unavailability (e.g. PV output is less than demand) the fuel cell covers the load (Point 18).
- The SOFC is fed with hydrogen (Point 16) as fuel (which is stored in the storage tank) and ambient air (Point 17) as the oxidant. Hydrogen is preheated via heat transfer from an external source, while air preheating is performed utilizing the heat from the SOFC stack gas.
- Heat is recovered from the SOFC stack gas (Point 19).
- Wood dust or crop waste is used as biomass in the biomass gasification unit (Point 21).
- The gasification process occurs in the presence of pressurized steam (Point 22).
- The product syngas (Point 23) is fed to the fuel cell system for power generation (Point 24).
- The gases leaving the fuel cell stack enter the combustion chamber and the gas turbine cascade, for further electricity generation. The biomass-SOFC-GT system is assumed to supply a fixed portion of the electricity demand of the grid. This means that, in contrast to the wind-CAES and PV-H_2-FC systems, the biomass-SOFC-GT system has steady, non-intermittent, operation.
- The SOFC-GT exhaust gas feeds a heat recovery steam generator (Point 25) for further renewable energy utilization. The generated steam is fed to the thermal storage system for thermal management (Point 26).

4.3: System 3: Hybrid PV-biomass System with Thermal Desalination and Energy Storage Options

Small communities can benefit from renewable energy-based systems since they have access to abundant renewable resources and landscapes. Energy consumption patterns of the dwellings may have similar trends because the life style is almost similar in the small communities. Therefore, developing integrated renewable energy-based systems for local communities can reduce dependency on fossil fuels, maintains environmental sustainability, and increase renewable energy use in general. Canada has significant solar and biomass energy resources (Hacatoglu et al., 2011b; OAGO, 2011), both of which are abundantly available in local, small communities. Solar photovoltaic power generation has gained much of interest in Canada due to the changing targets for greenhouse gas emissions and restructuring of energy companies (NRC, 2011). Utility scale solar PV systems, exploiting Canada's solar PV potential, collaborating with local and international solar PV industries, and codes and regulations development are among the main activities carried out by CanmetEnergy, a Canadian leader in clean energy research and technology development (NRC, 2011). However, utility scale solar PV power plants require vast landscapes to install the PV modules. For instance, if SunPower 210W monocrystalline-silicon PV cells are used, 5.92 m^2/kW of installation space is required. Moreover, solar energy is not available always, and energy storage systems are required to overcome its intermittency. Biomass has great potential in producing energy for local communities, since most of the natural biomass resources are located at those areas. Gasification is a technique that converts biomass into liquid or gaseous fuels, which can be used in internal combustion engines, gas turbines and fuel cells (Abuadala and Dincer, 2012). To increase renewable energy utilization, and overcome solar PV shortcomings, a hybrid PV-biomass system is developed and proposed to supply electricity on a small community scale. Furthermore, heat recovery from the hybrid system components will improve energy and exergy efficiencies.

The hybrid PV-biomass system, System 3, contains a biomass gasifier integrated with a gas turbine (biomass-GT), a solar photovoltaic system linked to a water electrolyser for hydrogen production (PV-EL), and a compressed air energy storage system linked to an air compressor and gas turbine (CAES-GT). The CAES system

acts as the main energy storage component of System 3, which is selected based on the following needs and/or requirements:

- Distributed generation (DG) is of growing interest in the electricity power industry. The costs related to power transmission and distribution are reduced when DG is implemented in small, local communities.
- Internal combustion engines and gas turbines are potential power generation systems for distributed generation. However, these systems are accompanied by high-level noise and greenhouse gas emission. Therefore, clean and noise-free renewable energy is a candidate as the driver of DG systems. Solar energy is globally available and abundant and local communities usually have access to great resources of biomass. Thus, solar and biomass energy are used as the sources of energy.
- To supply a specific baseload power for the community, energy storage is required to compensate for solar energy unavailability. Hydrogen is a potential energy carrier and can be produced by water electrolysis. It is chosen over battery energy storage due to its higher energy density. Moreover, battery lifetime is considerably shorter than hydrogen storage tanks.
- Excess electricity is generated by the PV system for hydrogen production in the electrolyser, which is selected due to its reasonably high efficiency. Moreover, the energy input to the electrolyser comes from a green energy source, which is solar energy.
- The compressed air energy storage is selected for excess energy storage during hours of high solar availability. The gas turbine of the CAES system powers a part of the demand, when required. By feeding the gas turbine with the generated hydrogen in the solar PV-electrolyser system, two renewable energy resources are integrated: solar and biomass. This way the combustion gases in the gas turbine contain only water and air.
- A thermal desalination system is selected based on its capability in operating with waste heat. Moreover, access to clean, fresh, and distilled water is required in every community.

The schematic of the hybrid PV-biomass system with energy storage options is shown in Figure 4.6. A direct steam biomass dryer feeds the gasifier with partially dried biomass, and the pressurized, produced syngas is fed to the combustion chamber of the GT. Gas turbine inlet temperature plays a major role in efficiency and electric power output (Borgnakke and Sonntag, 2008). Since a continuous operation is expected from the biomass-GT system, the biomass feed is estimated so that a continuous flow rate of syngas is provided to the gas turbine. Combustion gases then enter the gas turbine and produce work.

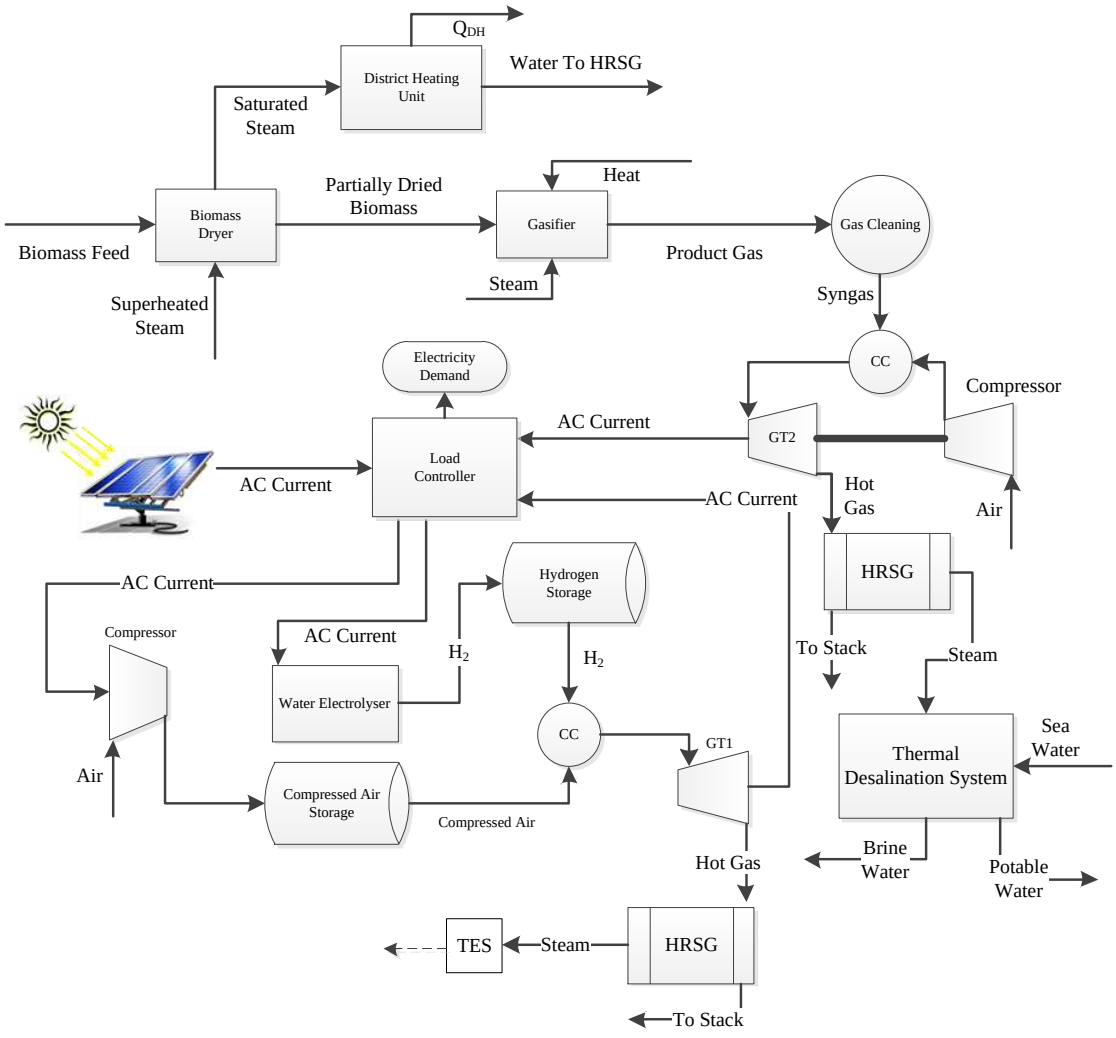

Figure 4.6: Hybrid PV-biomass system with thermal desalination and energy storage

During the hours of sufficient solar irradiance availability, the solar PV system generates electricity, while the biomass-GT system operates at its nominal capacity. The electricity demand is supplied by both the biomass-GT and the PV systems. A

part of the gas turbine power output is consumed by demand, and the rest is fed to the air compressor for energy storage. The PV power output is meant to feed both its share of the demand and the electrolyser.

However, when solar energy is not sufficiently available, the PV power output can be less than demand. Thus, the gas turbine of the compressed air energy storage system covers the power difference. During the hours of solar unavailability (e.g. night hours, cloudy periods), the biomass-GT and the CAES-GT systems operate and generate electricity. The gas turbine of the CAES system extracts hydrogen and compressed air, which both are produced during daylight hours. As shown in Figure 4.6, System 3 has two separate gas turbines, one in the biomass-GT system, and the other one in the CAES-GT system. The gas turbine of the biomass-GT system works continuously and its power output may change from a minimum to nominal capacity.

Conversely, the gas turbine of the CAES-GT system generates electricity only at times when the solar PV system is unable to supply its share of electricity demand. Heat recovery from both of these gas turbines is applicable through separate heat recovery steam generator. GT flue gas still contains enough energy to be recovered, since its temperature is approximately 600˚C, therefore it is used to produce saturated steam in the HRSG. The heat recovered from the CAES-GT cycles is stored in thermal storage units, and is used for district heating or hot water production. The thermal storage unit is considered in this case because the operation of the CAES-GT system is intermittent and its heat recovery potential is not continuous. An effective way of utilizing such a varying source of heat is thermal storage, which can be accessed later at a time of need.

In contrast, the heat recovery potential from the flue gas of the biomass-GT system is higher and more continuous. Therefore, a continuous application can be considered for the generated steam in the HRSG of the biomass-GT system. The generated steam can be used in a thermal water desalination system. Thermal desalination units can provide communities with clean water at reasonable prices. The energy requirement of thermal desalination systems can be any kind of available heat, e.g. waste heat from GT flue gas. Hosseini et al. (2013a) proposed an integrated system containing a hybrid SOFC–GT and a multi-effect desalination (MED) system. Along with power

generation by the hybrid system, waste heat recovery from the gas turbine gives the opportunity to produce potable water.

Table 4.5 presents the nominal capacities of the main components of System 3. The data given in Table 4.5 are based on 1000 W/m^2 solar irradiance, and 10 MW net electric power output. Table 4.6 presents the flow type, thermodynamic state, and operating conditions of the main components of System 3.

Table 4.5: Nominal capacities of main component of System 3

Component	GT1	PV	Electrolyser	Air Compressor	GT2
Capacity	8510 kW	3664 kW	1664 kW	510 kW	2000

Table 4.6: Flow type, thermodynamic state and operating conditions of components of System 3

Point	Flow type	Thermodynamic state	Operating condition
1	Biomass	Moist biomass	$\omega = 0.5$, 4500 kg/hr
2	Electricity	-	8510 kW
3	Electricity	-	3664 kW
4	Electricity	-	510 kW
5	Air	Ambient air	3149 kg/hr
6	Air	Compressed air	*P*=64 bar, 3149 kg/hr
7	Air (GT)	Compressed air	*P*=36 bar, 6298 kg/hr
8	Electricity	-	1664 kW
9	Hydrogen (EL)	Compressed gas	*P*=40 bar, 32.4 kg/hr
10	Hydrogen (GT)	Compressed gas	*P*=36 bar, 63.7 kg/hr
11	Electricity	-	2000 kW
12	GT flue gas	High temperature gas	*T*=900 K, 870 kW
13	Steam	Saturated Steam	*P*=10 bar, 770 kW
14	GT flue gas	High temperature gas	*T*=900 K, 129 kW
15	Steam	Saturated Steam	*P*=10 bar, 116 kW

The product of the thermal desalination system is distilled water, which has various applications. It can be used by pharmaceutical companies, oil and gas industries, or it can be used as drinking water after some post-treatments. In System 3, the HRSG of the biomass-GT system is integrated with a multi-effect desalination system for distilled water production. A detailed description of the MED system is presented below.

4.3.1 Description of Thermal Desalination Systems

The flow-diagram of the multi-effect desalination system is shown in Figure 4.7. The desalination system has four evaporator/condenser effects and a final condenser. It also consists of a thermal vapour compressor (TVC), which is added to the system to increase its performance. The TVC is a steam ejector that extracts a part of the produced steam in the 4^{th} effect.

The extracted steam is mixed with main-steam coming from the HRSG. The pressure of the mixture rises in the TVC and finally leaves at a superheated state. Thereafter, saturated steam leaves the de-superheater, and enters the horizontal tubes of the first effect.

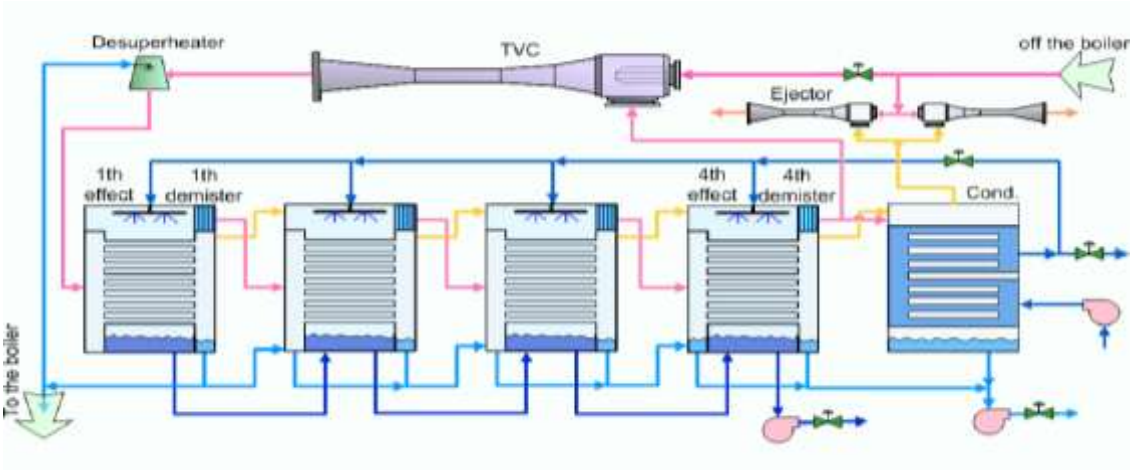

Figure 4.7: Flow diagram of Multi-Effect Desalination system; source: Hosseini et al. (2013a)

Condensation occurs inside the tubes, and saturated water leaves the first effect. The condensation latent heat is transferred to the feed water, which is sprayed over the horizontal tubes. Falling film evaporation is the result of heat transfer to the feed water, thus a specific portion of it evaporates and leaves the effect. The produced water vapour at the first effect is free of salt (ideally) and enters the horizontal tubes of the second effect. Again, condensation occurs inside the tubes and feed water evaporation occurs on the tubes outer surface. The condensed water accumulates outside the effect as pure water, and generated steam outside the tubes enters the next effect's tubes to serve as an evaporation heat source, while condensing inside the tubes. Therefore, a sequential evaporation/condensation process is formed so that pure water is produced from sea water. A part of the generated steam at the fourth effect is

extracted by TVC, and the remnant enters the final condenser to preheat the feed water, while film condensation occurs on the condenser tubes. Feed water, which now has a higher temperature than sea water, is equally distributed over the effects. To improve the MED-TVC system's performance, pure and brine water streams leaving each effect are directed to separate flash boxes in which flash evaporation occurs. Due to pressure drop in the flash boxes from the pressure of the upstream effect to the pressure of the downstream, water vapour gives its condensation heat to the sprayed feed water. Remaining brine water leaves the desalination system with a higher concentration than the inlet sea water.

The energy storage systems are studied in the three proposed integrated systems illustrated in Figures 4.1, 4.3, and 4.6. The analyses will include energy, exergy, and exergoeconomics of which the relevant equations are presented in Chapter 5.

Chapter 5: Analyses and Optimization

The investigation is based on energy and exergy analyses, and exergoeconomic concepts are applied to the developed models. The systems under study include various energy systems from renewable energy sources to district heating systems. These systems are integrated into more complex energy systems to achieve maximum energy utilization. The main tools for the analyses, thermodynamic concepts are the same for all the systems under study. In the next section, the basics of the governing equations are illustrated. Thereafter, these equations are applied to the components of the novel, integrated systems, which are illustrated in Chapter 4.

5.1 Thermodynamic Equations

Considering Figure 5.1, which has multiple inputs and outputs of the possible energy flows, the general mass, energy and exergy balance equations are respectively written as

$$\frac{dm_{\mathrm{CV}}}{dt} = \sum \dot{m}_{\mathrm{i}} - \sum \dot{m}_{\mathrm{e}} \tag{5.1}$$

$$\frac{dE_{\mathrm{CV}}}{dt} = \dot{Q}_{\mathrm{CV}} - \dot{W}_{\mathrm{CV}} + \sum \dot{m}_{\mathrm{i}} \left(h_{\mathrm{i}} + \frac{1}{2} V_{\mathrm{i}}^2 + g Z_{\mathrm{i}} \right) + \sum \dot{m}_{\mathrm{e}} \left(h_{\mathrm{e}} + \frac{1}{2} V_{\mathrm{e}}^2 + g Z_{\mathrm{e}} \right) \tag{5.2}$$

$$\frac{dEx_{\mathrm{CV}}}{dt} = \sum \left(1 - \frac{T_0}{T} \right) \dot{Q}_{\mathrm{CV}} - \dot{W}_{\mathrm{CV}} + P_0 \frac{dV_{\mathrm{CV}}}{dt} + \sum \dot{m}_{\mathrm{i}} ex_{\mathrm{i}} - \sum \dot{m}_{\mathrm{e}} ex_{\mathrm{e}} - T_0 \dot{S}_{\mathrm{gen}} \tag{5.3}$$

where the physical illustration of the terms are: $\sum \left(1 - \frac{T_0}{T} \right) \dot{Q}_{\mathrm{CV}}$: exergy transfer by heat; $-\dot{W}_{\mathrm{CV}} + P_0 \frac{dV_{\mathrm{CV}}}{dt}$: exergy transfer by shaft or boundary work; $\sum \dot{m}_{\mathrm{i}} ex_{\mathrm{i}} - \sum \dot{m}_{\mathrm{e}} ex_{\mathrm{e}}$: exergy transfer by flow; and $T_0 \dot{S}_{\mathrm{gen}}$: exergy destruction. The term exergy destruction, which is also called as irreversibility, is obtained as

$$\dot{I} = T_0 \dot{S}_{\mathrm{gen}} \tag{5.4}$$

The property E has a significant physical meaning by representing all forms of the energy of the system in a given state. The forms of energy might include kinetic or potential energy, energy of the moving molecules, energy associated with the structure of the atom, chemical energy, electrical energy, or other forms of energy.

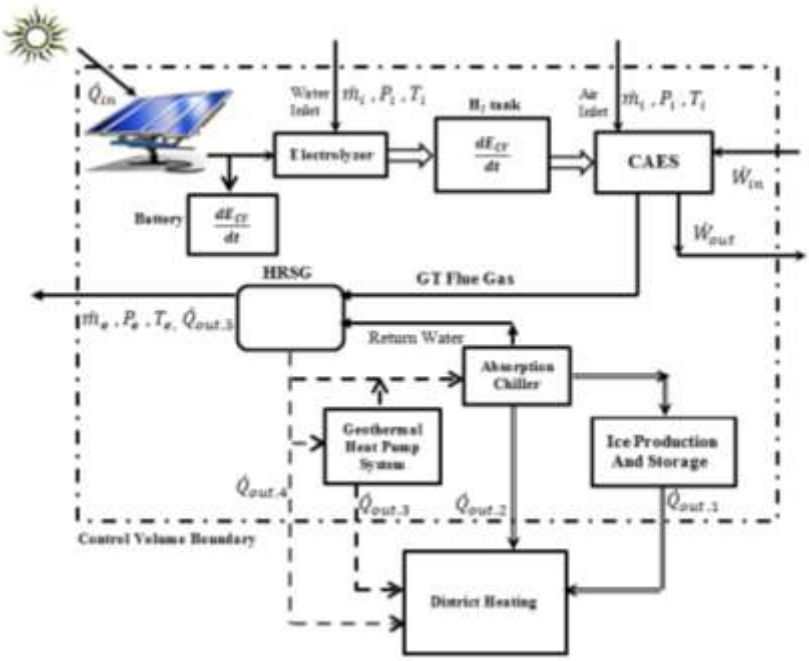

Figure 5.1: A schematic of a control volume consisting of various energy flows for illustration of energy equation

Depending on the type of the processes, the terms in Eqs. 5.1-5.3 may be reduced or broken down into proper formats. Energy analysis is performed based on the thermodynamic state of each point/flow of the system, and with the aid of Eq. 5.2. Performing exergy analysis requires the understanding of the exergy of flows and streams, which have some clarifications and categorizations to be made.

5.1.1 Exergy of Flows and Streams

The exergy content of a flow is a summation of its chemical and physical exergy values. Physical exergy is an extent of the temperature and pressure difference from the environment/reference state. Chemical exergy is measured according to a reference environment; the nature, the oceans, or the earth. In fact, its value is defined based on the equilibrium of the chemical content of the substance, the flow or the system with the components available in the environment. Any difference between the

chemical components of the flow, or the system from the reference environment initiates the appearance of chemical exergy.

5.1.1.1 Reference environment

The intensive property of the reference environment, which exergy is evaluated based on, determines the exergy of a stream. The reference environment acts an infinite system and is a sink or source for energy and material flow. The exergy of the reference environment is zero, thus the exergy of any stream and system with the same temperature, pressure and chemical composition as the reference environment is also zero. The ability of a stream or a system to perform work is measured based on its deviation from the reference environment. It is a requirement of a system to be a reference environment by having constant intensive properties. However, even the natural environment is not practically a reference environment, since its properties change by the by-products of processes. Thus several reference environments have been proposed by scientists (Dincer and Rosen, 2007). Determination of the reference environment depends on the process and the tools for analyzing the processes.

5.1.1.2 Exergy of material flow

The exergy content of a material flow is a combination of the flow and the material characteristics. Chemical exergy of the material is considered in exergy calculations and physical exergy is measured as a function of the thermodynamic state of the flow. The exergy of kinetic and potential energy of the flow is the same as the calculated values for these energies as given below:

$$\dot{E}x_{\text{flow}} = \dot{E}x_{\text{ph}} + \dot{E}x_{\text{ch}} + \dot{E}x_{\text{KE}} + \dot{E}x_{\text{PE}} \tag{5.5}$$

where

$$\dot{E}x_{\text{PE}} = \dot{m}g(Z_2 - Z_1)$$

$$\dot{E}x_{\text{KE}} = \dot{m}\left(\frac{v_2^2 - v_1^2}{2}\right)$$

$$\dot{E}x_{\text{ch}} = \Delta G_0 + \sum_{\text{i}} \dot{n}_{\text{i}} ex_{\text{ch,i}} \tag{5.6}$$

$$\dot{E}x_{\text{ph}} = \dot{m}[(h - h_0) - T_0(s - s_0)] \tag{5.7}$$

Here, ΔG_0 is the change in Gibbs free energy of the chemical compound, $Ex_{\mathrm{ch,i}}$ is the reference chemical exergy of each component of the chemical compound of the flow, and n_{i} is the molar amount of each component.

5.1.2.3 Exergy of work

The exergy of shaft or electricity work equals to the amount of work. However, the exergy of work due to the change of the control volume from V_1 to V_2, W_{net}, is

$$W_{\mathrm{net}} = W_{1-2} - P_0(V_2 - V_1) \tag{5.8}$$

where W_{1-2} is work done by the system due to the change in volume.

5.1.1.4 Exergy of thermal energy

Consider a system having heat interaction with its immediate environment. If the temperature of the control mass surface is considered to be constant, the minimum work required by the control mass and its environment to bring the control mass to the next state is the thermal exergy

$$\dot{E}x_{\mathrm{Q}} = \left(1 - \frac{T_0}{T}\right)\dot{Q} \tag{5.9}$$

where $\dot{Q}$ is the amount of heat transfer to the system.

5.1.2 Energy and Exergy Efficiencies

Efficiency is a measure of the effectiveness of a system or process in producing useful work with minimum input energy and waste. In thermodynamic systems, efficiency is defined as the ratio of useful produced energy/work over the total energy input to the system. Energy efficiencies are not qualitative ratios of energy. This matters since quantity and quality of energy streams are different, according to the second law of thermodynamics. Therefore, defining the efficiencies of systems based on the exergy contents of the outputs and inputs provides a better insight in defining performance of systems.

Energy and exergy efficiencies of steady state processes are often written as (Dincer and Rosen, 2007)

$$\eta = \frac{\text{useful energy output}}{\text{input energy}} \tag{5.10}$$

$$\psi = \frac{\text{useful exergy output}}{\text{input exergy}} \tag{5.11}$$

Exergy efficiencies differentiate the losses due to irreversibility from effluent losses, thus they illustrate the potential for improvement in the system by decreasing the effluent losses.

5.1.3 Procedure for Energy and Exergy Analyses

A simple procedure for performing energy and exergy analyses involves the following steps (Dincer and Rosen, 2007):

- Subdivide the processes into many desired sections so that the simplest forms of processes are considered for each section.
- Determine all quantities such as work and heat transfer rates by performing mass and energy balances on the sections.
- Define the reference environment (dead state condition) based on the materials of the processes and the range of temperature and pressure in the system.
- Evaluate energy and exergy values relative to the selected reference-environment model.
- Perform exergy balance equation on each section, and determine the rates of irreversibility.
- Define the efficiency of the processes considering the merit of the streams and purpose of each process, and evaluate the values of efficiencies.
- Interpret the results, and draw appropriate conclusions and recommendations, relating to such issues as design changes, retrofit plant modifications, etc.

5.1.4 Exergoeconomic Analysis

In economic calculations of energy systems, unit costs based on energy have been used conventionally. Since these systems are encountered with losses that can be better qualified based on exergy concepts, the use of exergy based unit costs would better distribute costs among outputs. With thermodynamic analyses the thermodynamic inefficiencies of the energy systems are evaluated. However, the cost of these inefficiencies, exergy destruction and exergy losses are important to us. The combination of exergy analysis and economic calculations represents a useful tool for

optimization of energy systems. This combination forms the basis of the relatively new field of exergoeconomics. The exergy model calculates the exergy content of each point in the system, and the economic model takes into account all the costs relevant to capital, operation and maintenance (O&M) of the system under study.

The objectives of exergoeconomic analysis are listed as (Bejan et al., 1996)

- to separately calculate the cost of each product of a system with multiple products
- to determine the flow of costs in the system by understanding how costs of flows in the system are formed
- to optimize specific variable in a specific component
- to optimize the overall system

In the exergoeconomic models, each exergy stream has a cost value. Thus, the cost of exergy of all inlet streams plus the capital and O&M costs equals to the cost of exergy of all exiting streams (Bejan et al., 1996):

$$\sum_{\mathrm{i}} \dot{C}_{\mathrm{i,k}} + \dot{C}_{\mathrm{Q,k}} + \dot{Z}_{\mathrm{k}} = \sum_{\mathrm{e}} \dot{C}_{\mathrm{e,k}} + \dot{C}_{\mathrm{w,k}} \tag{5.12}$$

where i and e represent inlet and exit streams, respectively. The other terms are defined as follows: $\sum_{\mathrm{i}} \dot{C}_{\mathrm{i,k}}$: total costs of exergy flows entering component k, $\dot{C}_{\mathrm{Q,k}}$: total costs associated with thermal exergy flow; $\dot{Z}_{\mathrm{k}}$: capital and O&M cost rates of the component; $\sum_{\mathrm{e}} \dot{C}_{\mathrm{e,k}}$: total costs of exergy flows exiting component k; and $\dot{C}_{\mathrm{w,k}}$: total costs associated with work in component. According to the exergy-costing principle, the cost rate of an exergy stream is given as

$$\dot{C} = c\dot{E}x \tag{5.13}$$

where *c* is the unit cost of exergy, and $\dot{E}$ is the exergy flow rate. A cost balance for the *k*th component of a system can be written as

$$\sum_{\mathrm{k}}\left(c_{\mathrm{e}}\dot{E}x_{\mathrm{e}}\right)_{\mathrm{k}} + c_{\mathrm{w,k}}\dot{W}_{\mathrm{k}} = c_{\mathrm{q,k}}\dot{E}x_{\mathrm{q,k}} + \sum_{\mathrm{k}}\left(c_{\mathrm{i}}\dot{E}x_{\mathrm{i}}\right)_{\mathrm{k}} + \dot{Z}_{\mathrm{k}} \tag{5.14}$$

where i and e represent inlet and exit streams, respectively. The other terms can be interpreted as follows: $\sum_{\mathrm{k}}\left(c_{\mathrm{i}}\dot{E}x_{\mathrm{i}}\right)_{\mathrm{k}}$ denotes the total costs of exergy flows entering component k; $c_{\mathrm{q,k}}\dot{E}x_{\mathrm{q,k}}$ is the total costs associated with thermal exergy flow for component k; $\dot{Z}_{\mathrm{k}}$ is he levelized capital and O&M costs of the component;

$\sum_{\mathrm{k}}\left(c_{\mathrm{e}}\dot{E}x_{\mathrm{e}}\right)_{\mathrm{k}}$ is the total costs of exergy flows exiting component k; and $c_{\mathrm{w,k}}\dot{W}_{\mathrm{k}}$ is the total costs associated with work for component k.

Writing the exergy cost balance equation for all the components of a system, conducts a set of non-linear algebraic system of equations, which is solved for $\dot{C}_{\mathrm{k}}$ and c_{k}. The unit for $\dot{C}$ is in \$/s, and thus *c* is defined as \$/kWh basis. The exergy cost balance equation quantifies the quality of a stream both exergetically and economically. This gives out a good insight of the economic feasibility of the processes under investigation.

Defining the exergy flows of the main outputs (purposes) of a component as "product" and the exergy flows that are spent (consumed) to achieve them as "fuel" often provides a better understanding of the processes occurring in the component in terms of exergy and exergoeconomics. For the PV system, for example, the solar exergy is considered as "fuel" and the power output of the modules is the "product", and the costs associated with each of these exergy flows can be expressed per unit of exergy. Because of the capital and O&M costs and the rates of irreversibility in a component, the cost per unit of exergy of the products is higher than the cost of unit of exergy of the fuel for the same component. The relative increase in the product's cost to the fuel's cost is called relative cost difference (*r*):

$$r_{\mathrm{k}} = \frac{c_{\mathrm{p}} - c_{\mathrm{f}}}{c_{\mathrm{f}}} \tag{5.15}$$

Exergoeconomic factor, *f* relates the costs associated with exergy destruction and exergy losses to the levelized capital costs. The exergoeconomic factor of component k, f_{k}, is defined as

$$f_{\mathrm{k}} = \frac{\dot{Z}_{\mathrm{k}}}{\dot{Z}_{\mathrm{k}} + c_{\mathrm{f,k}}(\dot{I}_{\mathrm{k}} + \dot{E}x_{\mathrm{loss}})} \tag{5.16}$$

where $c_{\mathrm{f,k}}$ is the unit cost of exergy of fuel provided to the component, k. The values of the exergoeconomic factor fall between zero and one. A small value for *f* suggests that the system needs to be improved in terms of irreversibility, although this may require capital cost investments. Higher values for *f* signify that, no matter how efficient the component is, its purchase cost is significantly high.

The concepts of exergoeconomic analysis discussed in this section are applied to the components of the integrated systems. The flows of exergy inlet and outlet from

each component are considered in the analyses, and are assigned with the relevant unit cost of exergy. Section 5.2 presents the application of the thermodynamic tools to the components of the novel, integrated system. Section 5.2 deals only with the modeling, and energy and exergy analyses of the systems' components.

5.2 Energy and Exergy Analyses of System Components

The basic, general equations of energy and exergy flows in thermodynamic systems were discussed in section 5.1. Here these principals are applied to specific components of the proposed, novel integrated systems. The analyses are presented for the components in order of appearance in the integrated systems. For components that are implemented in more than one integrated system, the same analysis and approach is used. However, redundancy in presenting equations is avoided.

5.2.1 Photovoltaic System

5.2.1.1 PV cell modeling

A primary electric model of a PV cell contains a current source and a diode (see Figure 5.2). Applying basic circuit laws gives the cell terminal voltage as

$$I = I_{\mathrm{L}} - I_{\mathrm{D}} \tag{5.17}$$

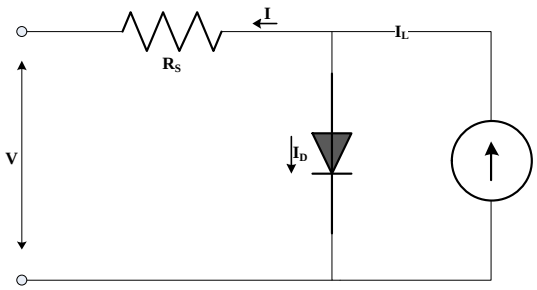

Figure 5.2: Equivalent circuit of the PV cell (adapted from Chenni et al. 2007)

The light current, I_{L} depends on the solar irradiance G and the cell temperature T_{c}, and is calculated according to design reference conditions:

$$I_{\mathrm{L}} = \left(\frac{G}{G_{\mathrm{ref}}}\right)\left(I_{\mathrm{L,ref}} + k_{\mathrm{t}}(T_{\mathrm{cell}} - T_{\mathrm{ref}})\right) \tag{5.18}$$

The values of G_{ref}, $I_{\mathrm{L,ref}}$, T_{ref}, and k_{t} are given by the manufacturer. The cell temperature (in °C) is a function of wind speed, solar irradiance and ambient temperature, and can be determined using the following correlation:

$$T_{\mathrm{cell}} = 0.943T_0 + 0.028G - 1.528V_{\mathrm{wind}} + 4.3 \tag{5.19}$$

which is developed by TamizhMani et al. (2003) as a result of an experiment on six different solar cell technologies. The researchers state that the dependency of the cell temperature on the ambient temperature, solar irradiance, and wind speed are fairly independent from the site location.

The diode current I_{D} is given as a function of the reverse saturation current I_0, and the cell terminal voltage and current. Details of the derivation of the equations are presented by Chenni et al. (2007). Therefore, the I-V characteristics of the PV modules can generally be expressed as (Chenni et al., 2007):

$$I = \left(\frac{G}{G_{\mathrm{ref}}}\right)\left(I_{\mathrm{L,ref}} + k_{\mathrm{t}}(T_{\mathrm{cell}} - T_{\mathrm{ref}})\right) - I_0\left[\exp\left(\frac{q(V+IR_{\mathrm{s}})}{\gamma k T_{\mathrm{cell}}}\right) - 1\right] \tag{5.20}$$

where q and k are the electron charge and the Boltzmann constant, respectively, R_{s} is the series resistance and γ, is the shape factor, which is a function of the completion factor and the number of cells in the module. Such data are usually available in PV module catalogues. The power output of the PV cell is the product of its terminal current and voltage. Equation 5.20 has a non-linear characteristic and the point at which the maximum current and voltage occur is called the maximum power point:

$$P_{\mathrm{mp}} = I_{\mathrm{mp}}V_{\mathrm{mp}} \tag{5.21}$$

Chenni et al. (2007) present an implicit expression to calculate the maximum current of the PV cell. The following expression can be solved using the Newton-Raphson method:

$$I_{\mathrm{mp}} + \frac{(I_{\mathrm{mp}} - I_{\mathrm{L}} - I_0)\left[\ln\left(\frac{I_{\mathrm{L}} - I_{\mathrm{mp}}}{I_0} + 1\right) - \frac{qI_{\mathrm{mp}}R_{\mathrm{s}}}{k\gamma T_{\mathrm{ref}}}\right]}{1 + (I_{\mathrm{L}} - I_{\mathrm{mp}} + I_0)\frac{qR_{\mathrm{s}}}{k\gamma T_{\mathrm{ref}}}} = 0 \tag{5.22}$$

At the maximum power point, the first derivation of power with respect to voltage is zero. Rearranging all the consequent equations results in an explicit equation for the maximum voltage as a function of the maximum terminal current obtained from

$$V_{\mathrm{mp}} = \frac{kT_{\mathrm{ref}}}{q}\ln\left(\frac{I_{\mathrm{L}} - I_{\mathrm{mp}}}{I_0} + 1\right) - I_{\mathrm{mp}}R_{\mathrm{s}} \tag{5.23}$$

The control system for the PV system is designed so that the system operates at the maximum power point.

5.2.1.2 PV system energy and exergy analyses

The laws of thermodynamics are applied to the PV system separately to determine the energy and exergy flows and the system's efficiencies. The energy and exergy solar input rates are

$$\dot{E}_{solar} = P_{\mathrm{PV}} + \dot{\mathrm{Q}}_{\mathrm{loss}} \tag{5.24}$$

The term $\dot{\mathrm{Q}}_{\mathrm{loss}}$ in Eq. 5.24 accounts for all heat transfer forms in the PV cell. The received solar energy is converted to electricity, thermal radiation, heat convection, and thermal energy stored in the PV cell. The extent of each of the above mentioned forms of energy depends on cell characteristics, e.g. material, specific heat, absorption coefficient.

$$\dot{E}x_{solar} = P_{\mathrm{PV}} + \dot{E}x_{\mathrm{Q}} + \dot{I}_{\mathrm{PV}} \tag{5.25}$$

where $\dot{E}x_{\mathrm{Q}}$ is thermal exergy loss due to radiation, convection and conduction to the environment (surroundings), and $\dot{I}_{\mathrm{PV}}$ is exergy destruction due to internal irreversibility of the PV cell.

The energy and exergy efficiencies of the PV cell at the maximum power point are given by:

$$\eta_{\mathrm{PV,mp}} = \frac{P_{\mathrm{mp}}}{\dot{E}_{\mathrm{solar}}} = \frac{I_{\mathrm{mp}} \times V_{\mathrm{mp}}}{G \times A_{\mathrm{PV}}} \tag{5.26}$$

$$\psi_{\mathrm{PV,mp}} = \frac{P_{\mathrm{mp}}}{\dot{E}x_{\mathrm{solar}}} = \frac{I_{\mathrm{mp}} \times V_{\mathrm{mp}}}{G \times A_{\mathrm{PV}} \times \left(1 - \frac{4}{3}\frac{T_0}{T_{\mathrm{sun}}} + \frac{1}{3}\left(\frac{T_0}{T_{\mathrm{sun}}}\right)^4\right)} \tag{5.27}$$

Maximum points of current, voltage and power are obtained according to Eqs. 5.21-5.23.

5.2.2 Water Electrolyser

The energy efficiency relation of the electrolyser is used to calculate the hydrogen production rate:

$$\eta_{\mathrm{el}} = \frac{\dot{m}_{\mathrm{H_2}} LHV_{\mathrm{H_2}}}{P_{\mathrm{in,el}}} \tag{5.28}$$

The exergy efficiency of the electrolyser is obtained using

$$\psi_{\mathrm{el}} = \frac{\dot{m}_{\mathrm{H_2}} ex_{\mathrm{ch,H_2}}}{P_{\mathrm{in,el}}} \tag{5.29}$$

where $P_{\mathrm{in,el}}$ is the surplus electricity from the PV system.

5.2.3 Solid Oxide Fuel Cell

Solid oxide fuel cell is a major component in Systems 1 and 2. In the first system, the SOFC acts as major electric power generation component, and supplies a residential area (house) with electricity during the periods of solar unavailability. In this research, SOFC is modelled based on the relations presented in literatures. This provides the relationships between current density, voltage, power output, and fuel consumption. In addition, the energy and exergy analyses equations are applied to the solid oxide fuel cell to determine energy and exergy flows, efficiencies, and the rates of exergy destructions.

5.2.3.1 SOFC modeling

The overall electrochemical reaction in the solid-oxide fuel cell is the oxidation of hydrogen, which results in water formation and the release of electrons (Larminie and Dicks, 2003):

$$\mathrm{H_2} + \frac{1}{2}\mathrm{O_2} \rightarrow \mathrm{H_2O} + 2\mathrm{e} \tag{5.30}$$

The reversible, open-circuit voltage of the cell is related to the change in the Gibbs free energy of formation of the reaction, and the electric charge of 2 moles of electrons:

$$E = \frac{-\Delta \bar{g}_{\mathrm{f}}}{2F} \tag{5.31}$$

where F is Faraday's constant. Here, 2 moles of electrons are considered, because for each mole of hydrogen 2 moles of electrons are released according to Eq. 5.31. The change of the specific Gibbs free energy of formation of the reaction is expressed as

$$\Delta \bar{g}_{\mathrm{f}} = \bar{g}_{\mathrm{f}}(\mathrm{products}) - \bar{g}_{\mathrm{f}}(\mathrm{reactants}) \tag{5.32}$$

The reversible open circuit voltage, E, is a function of temperature and pressure. Therefore, the operating temperature and pressure of the fuel cell affects its voltage output. The terminal voltage of the cell is calculated considering all the voltage losses

in the cell. The three main types of voltage losses are ohmic, activation, and concentration.

Ohmic losses are proportional to the current density in the cell, and are caused by resistance to the flow of electrons through the electrodes, the interconnections, and resistance to the flow of ions through the electrolyte. Activation losses are voltage drops due to the slow rate of the electrochemical reactions at the surfaces of the electrodes. These losses behave nonlinearly, with a decrease of the reactants at the surface of electrodes resulting in a change of the cell voltage. The corresponding losses are called concentration losses. Colpan et al. (2007) present three equations to calculate the voltage losses in the solid oxide fuel cell, which are not repeated here.

The cell terminal voltage is expressible as

$$V_{\mathrm{SOFC}} = E - V_{\mathrm{ohmic}} - V_{\mathrm{activation}} - V_{\mathrm{concentration}} \tag{5.33}$$

The voltage losses are functions of the cell current density, and the cell terminal voltage changes with the change of the current density. Therefore, knowing the current-voltage characteristic curve is important in modeling and analysis of the fuel cell. The cell power output is the product of its terminal voltage and current:

$$\dot{W}_{\mathrm{SOFC}} = N_{\mathrm{cell}} V_{\mathrm{cell}} I_{\mathrm{cell}} \tag{5.34}$$

where N_{cell} is the number of cells in the fuel cell stack. Note that the net power output of the fuel cell stack is less than the value calculated using Eq. 5.34, due to the internal power consumption.

5.2.3.2 SOFC energy and exergy analyses

The inputs to the fuel cell are hydrogen, air, and heat, and the outputs are SOFC net electric power and high temperature by-products. The thermodynamic balance equation for the fuel cell stack is as follows:

$$\dot{m}_{\mathrm{H_2}} LHV_{\mathrm{H_2}} + \dot{Q}_{\mathrm{H_2-preheat}} = \dot{W}_{\mathrm{net-SOFC}} + \dot{Q}_{\mathrm{o,SOFC}} \tag{5.35}$$

where $\dot{Q}_{\mathrm{H_2-preheat}}$ is the required heat to preheat the fuel to the cell temperature and $\dot{Q}_{\mathrm{o,SOFC}}$ is the thermal energy of the gases leaving the fuel cell stack. The lower heating value of hydrogen is considered in the analyses due to the existence of water

vapor in the fuel cell stack gas. A corresponding exergy rate balance can be written as follows:

$$\dot{m}_{\mathrm{H_2}} ex_{\mathrm{ch,H_2}} + \dot{E}x_{\mathrm{Q,H_2-preheat}} = \dot{W}_{\mathrm{net-SOFC}} + \dot{E}x_{\mathrm{o,SOFC}} + \dot{I}_{\mathrm{SOFC}} \quad (5.36)$$

When performing an energy and exergy analyses for the SOFC, the fuel cell power is an input to the calculation procedures. Current density is a characteristics of the type of the fuel cell (depends on the manufacturer) and it is an input as well. The voltage drops, as discussed above, are functions of current density, cell material, and fuel type. With these inputs, the required fuel feed rate is calculated, knowing that the SOFC stack temperature is an input value in the calculations. The extents of exergy destruction are thus calculated using Eq. 5.31. The energy and exergy efficiencies for the fuel cell system are

$$\eta_{\mathrm{SOFC}} = \frac{\dot{W}_{\mathrm{net-SOFC}}}{\dot{m}_{\mathrm{H_2,SOFC}} LHV_{\mathrm{H_2}} + \dot{Q}_{\mathrm{H_2-preheat}}} \quad (5.37)$$

$$\psi_{\mathrm{SOFC}} = \frac{\dot{W}_{\mathrm{net-SOFC}}}{\dot{m}_{\mathrm{H_2,SOFC}} ex_{\mathrm{H_2}} + \dot{E}x_{\mathrm{H_2-preheat}} - \dot{E}x_{\mathrm{o,SOFC}}} \quad (5.38)$$

5.2.4 Wind Park

The power output of the wind turbine is a function of wind speed, blade geometry and turbine efficiency, and is illustrated as

$$\dot{W}_{\mathrm{wt}} = \frac{\pi}{8} C_{\mathrm{p}} \rho D^2 v^3 \quad (5.39)$$

where C_{p} is the wind turbine efficiency and is related to aerodynamic characteristics of the blades. The wind turbine efficiency is limited to a maximum value of 59% as shown by Betz. Due to the quality of electric power output of the wind turbine, the energy and exergy efficiencies are the same; therefore, the exergy destruction rate of the wind turbine is calculated using:

$$\dot{I}_{\mathrm{wt}} = \left(\frac{1}{C_p} - 1\right) \dot{W}_{\mathrm{wt}} \quad (5.40)$$

5.2.5 Compressed Air Energy Storage System

The compressed air energy storage system has three main components; compressor, gas turbine, and intercooler. The energy and exergy balance equations for

these components are presented below, according to the descriptions and numberings in Figure 5.3.

5.2.5.1 Compressor

The energy balance equations for the compressors in the CAES system are written as

$$(\dot{m}_{\mathrm{air}} h_{\mathrm{air}})_1 + \dot{W}_{\mathrm{C1}} = (\dot{m}_{\mathrm{air}} h_{\mathrm{air}})_2 \tag{5.41}$$

$$(\dot{m}_{\mathrm{air}} h_{\mathrm{air}})_3 + \dot{W}_{\mathrm{C2}} = (\dot{m}_{\mathrm{air}} h_{\mathrm{air}})_4 \tag{5.42}$$

The relevant exergy balance equations for the compressors are given as follows:

$$(\dot{m}_{\mathrm{air}} ex_{\mathrm{air}})_1 + \dot{W}_{\mathrm{C1}} = (\dot{m}_{\mathrm{air}} ex_{\mathrm{air}})_2 + \dot{I}_{\mathrm{C1}} \tag{5.43}$$

$$(\dot{m}_{\mathrm{air}} ex_{\mathrm{air}})_2 + \dot{W}_{\mathrm{C2}} = (\dot{m}_{\mathrm{air}} ex_{\mathrm{air}})_4 + \dot{I}_{\mathrm{C2}} \tag{5.44}$$

Here, exergy of the inlet air to the compressor is zero, considering the ambient conditions be the same as the reference environment. Ideal gas assumption is made to calculate the air enthalpy using

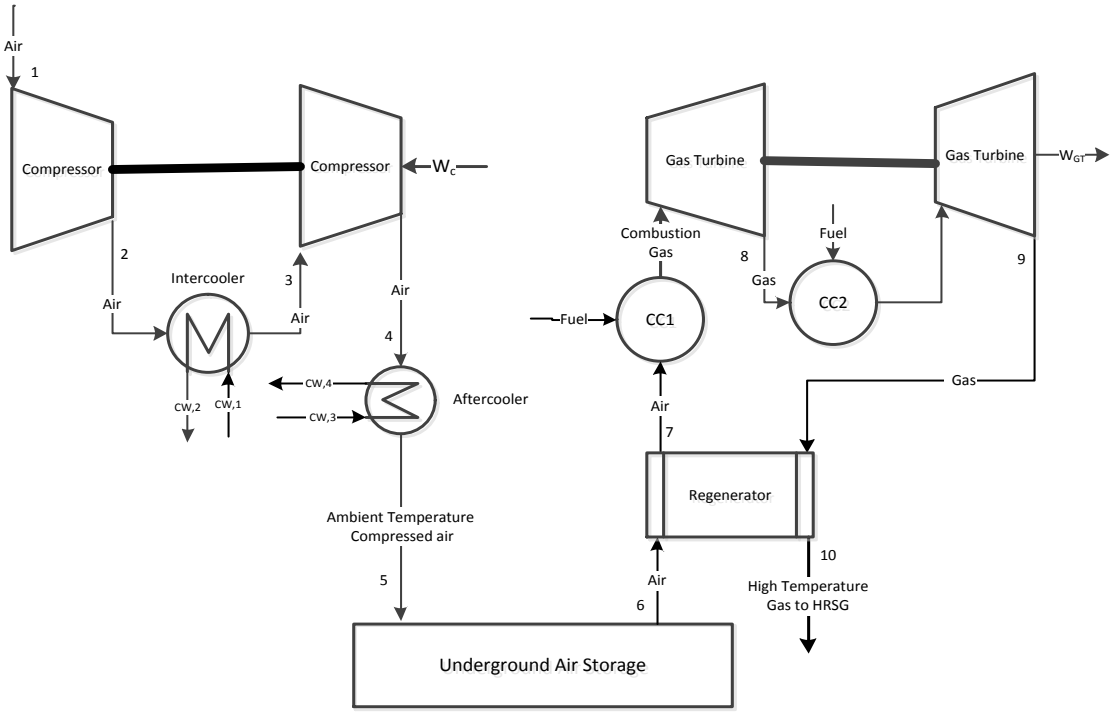

Figure 5.3: Flows of materials in the CAES-GT system for the energy and exergy analyses

$$\Delta h = c_{\mathrm{p}} \Delta T \tag{5.45}$$

where ΔT is obtained using the isentropic relations for ideal gases:

$$T_{\text{out}} = T_{\text{in}}\left[1 + \frac{1}{\eta_{\text{C}}}\left(r_{\text{c}}^{\frac{\gamma_{\text{a}}-1}{\gamma_{\text{a}}}} - 1\right)\right] \tag{5.46}$$

The constant pressure specific heat of air is a function of temperature and the empirical correlations presented in Borgnakke and Sonntag (2008) are used. The electric power consumption of the compressors are obtained using

$$\dot{W}_{\text{C1}} = \dot{m}_{\text{air}} w_{\text{C1}} \tag{5.47}$$

$$\dot{W}_{\text{C2}} = \dot{m}_{\text{air}} w_{\text{C2}} \tag{5.48}$$

The mass flow rates of air in both of the compressors are the same; however, the specific work consumptions can be different as presented as

$$w_{\text{C1}} = (h_{\text{air}})_1 - (h_{\text{air}})_2 \tag{5.49}$$

$$w_{\text{C2}} = (h_{\text{air}})_3 - (h_{\text{air}})_4 \tag{5.50}$$

Substituting Eq. 5.45 into equation 5.50 and using Eq. 5.46 to calculate the air temperature, the following equation is obtained for specific work of compression:

$$w_{\text{C1}} = \left(c_{\text{p}} T_{\text{air}}\right)_1 - \left(c_{\text{p}} T_{\text{air}}\right)_2 = (T_{\text{air}})_1\left[c_{\text{p1}} - c_{\text{p2}}\right]\left[1 + \frac{1}{\eta_{\text{C}}}\left(r_{\text{c}}^{\frac{\gamma_{\text{a}}-1}{\gamma_{\text{a}}}} - 1\right)\right] \tag{5.51}$$

where $(T_{\text{air}})_1$ is the inlet air temperature to the first stage of the compressor, c_{p1} and c_{p2} are the constant pressure specific heat at the inlet and outlet of the compressor stage, respectively, and r_{c} is the compression ratio of the compressor stage. A similar equation is obtained to calculate the specific work of compression of the second compressor:

$$w_{\text{C2}} = \left(c_{\text{p}} T_{\text{air}}\right)_3 - \left(c_{\text{p}} T_{\text{air}}\right)_4 = (T_{\text{air}})_3\left[c_{\text{p3}} - c_{\text{p4}}\right]\left[1 + \frac{1}{\eta_{\text{C}}}\left(r_{\text{c}}^{\frac{\gamma_{\text{a}}-1}{\gamma_{\text{a}}}} - 1\right)\right] \tag{5.52}$$

Eqs. 5.51 and 5.52 are substituted in Eqs. 5.47-5.48 to calculate the work of compression of each stage of the compressor. The total work of compression is the sum of the electric power consumption of the individual stages of the compressor:

$$\dot{W}_{\text{C}} = \dot{W}_{\text{C1}} + \dot{W}_{\text{C2}} \tag{5.53}$$

5.2.5.1 Intercooler

The following energy balance equations are written for the intercoolers:

$$(\dot{m}_{\text{air}}h_{\text{air}})_2 + (\dot{m}_{\text{cw}}h_{\text{cw}})_1 = (\dot{m}_{\text{air}}h_{\text{air}})_3 + (\dot{m}_{\text{cw}}h_{\text{cw}})_2 \quad (5.54)$$

$$(\dot{m}_{\text{air}}h_{\text{air}})_4 + (\dot{m}_{\text{cw}}h_{\text{cw}})_3 = (\dot{m}_{\text{air}}h_{\text{air}})_5 + (\dot{m}_{\text{cw}}h_{\text{cw}})_4 \quad (5.55)$$

where $\dot{m}_{\text{cw}}h_{\text{cw}}$ refers to the enthalpy of the cooling water.

The following exergy balance equations are written for the intercoolers:

$$(\dot{m}_{\text{air}}ex_{\text{air}})_2 + (\dot{m}_{\text{cw}}ex_{\text{cw}})_1 = (\dot{m}_{\text{air}}ex_{\text{air}})_3 + (\dot{m}_{\text{cw}}ex_{\text{cw}})_2 + \dot{I}_{\text{HEX,1}} \quad (5.56)$$

$$(\dot{m}_{\text{air}}ex_{\text{air}})_4 + (\dot{m}_{\text{cw}}ex_{\text{cw}})_3 = (\dot{m}_{\text{air}}ex_{\text{air}})_5 + (\dot{m}_{\text{cw}}ex_{\text{cw}})_4 + \dot{I}_{\text{HEX,2}} \quad (5.57)$$

Since, there is no chemical reaction or change involved in the intercoolers, only physical exergy of the compressed air and the cooling water are considered in the calculations. $\dot{I}_{\text{HEX}}$ is the exergy destruction in the intercooler.

5.2.5.3 Gas turbine

The inlets to the gas turbine (combustion chamber + turbine stages) are compressed air and fuel, and the outlets are electricity and high temperature exhaust gas. The gas turbine has two stages, and the energy balance equations for each stage are given as

$$(\dot{m}_{\text{air}}h_{\text{air}})_7 + (\dot{m}_{\text{fuel}}LHV_{\text{fuel}})_{\text{CC1}} = \left(\dot{m}_{\text{gas}}w_{\text{T}}\right)_{\text{GT1}} + \left(\dot{m}_{\text{gas}}h_{\text{gas}}\right)_8 \quad (5.58)$$

$$\left(\dot{m}_{\text{gas}}h_{\text{gas}}\right)_8 + (\dot{m}_{\text{fuel}}LHV_{\text{fuel}})_{\text{CC2}} = \left(\dot{m}_{\text{gas}}w_{\text{T}}\right)_{\text{GT2}} + \left(\dot{m}_{\text{gas}}h_{\text{gas}}\right)_9 \quad (5.59)$$

The notations and numbering in the above mentioned equations refer to Figure 5.2. The change in enthalpy of the combustion gases is calculated as $\Delta h = c_{\text{p,gas}}\Delta T$, where ΔT is obtained using the isentropic relations for the gas turbine.

The following give the exergy balance equations for each stage of the gas turbine:

$$(\dot{m}_{\text{air}}ex_{\text{air}})_7 + (\dot{m}_{\text{fuel}}ex_{\text{fuel}})_{\text{CC1}} = \left(\dot{m}_{\text{gas}}w_{\text{T}}\right)_{\text{GT1}} + \left(\dot{m}_{\text{gas}}ex_{\text{gas}}\right)_8 + \dot{I}_{\text{GT1}} \quad (5.60)$$

$$(\dot{m}_{\text{air}}ex_{\text{air}})_8 + (\dot{m}_{\text{fuel}}ex_{\text{fuel}})_{\text{CC2}} = \left(\dot{m}_{\text{gas}}w_{\text{T}}\right)_{\text{GT2}} + \left(\dot{m}_{\text{gas}}ex_{\text{gas}}\right)_9 + \dot{I}_{\text{GT2}} \quad (5.61)$$

where $\dot{I}_{\text{GT1}}$ and $\dot{I}_{\text{GT2}}$ are the exergy destruction rates in the gas turbine stages, and $\dot{m}_{\text{fuel}}ex_{\text{fuel}}$ refers to the chemical exergy of the fuel.

The energy and exergy efficiencies of the compressed air energy storage system are obtained using

$$\eta_{\mathrm{CAES-GT}} = \frac{\dot{W}_{\mathrm{GT}} + \dot{Q}_{\mathrm{HR}}}{\dot{W}_{\mathrm{C}} + \dot{m}_{\mathrm{fuel}} LHV} \tag{5.62}$$

$$\psi_{\mathrm{CAES-GT}} = \frac{\dot{W}_{\mathrm{GT}} + \dot{E}x_{\mathrm{q,HR}}}{\dot{W}_{\mathrm{C}} + \dot{m}_{\mathrm{fuel}} ex_{fuel}} \tag{5.63}$$

5.2.6 Biomass Gasification

Systems 2 and 3 include biomass gasification units. The gasification system has two main components; the dryer and the gasifier. Here the analyses of these two main components of the gasification process are presented, separately. Wood dust or crop waste is used as biomass in the biomass gasification unit. As discussed in Chapter 4, the dryer improves the performance of the gasification process. Figure 5.4 shows a simple schematic of the biomass gasification unit, which includes a dryer and a gasifier as the main components.

5.2.6.1 Biomass Dryer

According to Figure 5.4, the mass balances in the dryer can be written as follows:

$$\dot{m}_{\mathrm{db},1} = \dot{m}_{\mathrm{db},2} \tag{5.64}$$

$$\dot{m}_{\mathrm{m},1} + \dot{m}_{\mathrm{s},3} = \dot{m}_{\mathrm{m},2} + \dot{m}_{\mathrm{s},4} \tag{5.65}$$

$$\dot{m}_{\mathrm{m},1} = \dot{m}_{\mathrm{db},1}\omega_1 \tag{5.66}$$

$$\dot{m}_{\mathrm{m},2} = \dot{m}_{\mathrm{db},2}\omega_2 \tag{5.67}$$

$$\dot{m}_1 = \dot{m}_{\mathrm{db},1} + \dot{m}_{\mathrm{m},1} \tag{5.68}$$

$$\dot{m}_2 = \dot{m}_{\mathrm{db},2} + \dot{m}_{\mathrm{m},2} \tag{5.69}$$

In the sets of equations 5.64 to 5.69, subscript db stands for dry biomass, m is the water moisture in biomass, s illustrates steam provided for biomass drying process, and ω is the moisture content of biomass.

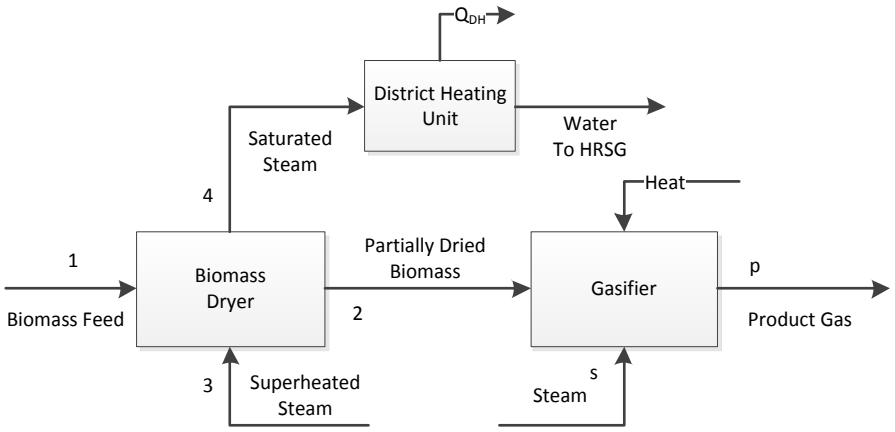

Figure 5.4: Schematic of the biomass gasification process

Accordingly the energy and exergy balance equations for the dryer can be written as follows:

$$\dot{m}_1 h_1 + \dot{m}_{s,3} h_{s,3} = \dot{m}_{s,4} h_{s,4} + \dot{m}_2 h_2 \tag{5.70}$$

where is expanded to a more specific (in terms of biomass contents) equation:

$$\dot{m}_{db,1} h_{db,1} + \dot{m}_{m,1} h_{m,1} + \dot{m}_{s,3} h_{s,3} = \dot{m}_{db,2} h_{db,2} + \dot{m}_{m,2} h_{m,2} + \dot{m}_{s,4} h_{s,4} \tag{5.71}$$

There is no change in chemical composition of dry biomass in the dryer. Therefore, the enthalpy of biomass is calculated as a function of its specific heat, which can be expressed as (Basu, 2010):

$$c_{p,db} = 0.266 + 0.00116T \tag{5.72}$$

Thus, enthalpy of dry biomass is obtained as:

$$h_{db} = c_{p,db} T \tag{5.73}$$

where *T* is absolute temperature of biomass. An exergy balance for the dryer follows:

$$\dot{m}_1 ex_1 + \dot{m}_{s,3} \mathrm{ex}_{s,3} = \dot{m}_{s,4} ex_{s,4} + \dot{m}_2 ex_2 + \dot{I}_{dryer} \tag{5.74}$$

Substituting the mass balance equations into Eq. 5.74 gives the following equation:

$$\dot{m}_{db,1} \mathrm{ex}_{db,1} + \dot{m}_{m,1} ex_{m,1} + \dot{m}_{s,3} ex_{s,3} = \dot{m}_{db,2} ex_{db,2} + \dot{m}_{m,2} ex_{m,2} + \dot{m}_{s,4} ex_{s,4} + \dot{I}_{dryer} \tag{5.75}$$

Rearranging Eq. 5.75 based on the exergy flows of biomass and drying steam yields the exergy destruction rate in the dryer as

$$\dot{I}_{\text{dryer}} = \dot{m}_{\text{db,1}} \times \left(ex_{\text{db,1}} - ex_{\text{db,2}}\right) +$$

$$\left(\dot{m}_{\text{m,1}} ex_{\text{m,1}} - \dot{m}_{\text{m,2}} ex_{\text{m,2}}\right) + \left(\dot{m}_{\text{s,3}} ex_{\text{s,3}} - \dot{m}_{\text{s,4}} ex_{\text{s,4}}\right) \quad (5.76)$$

Here, changes in exergy content of the biomass are expressed only as the change in its physical exergy, which is a function of enthalpy and entropy as

$$ex_{\text{db,1}} - ex_{\text{db,2}} = \left(h_{db,1} - h_{db,2}\right) - T_0\left(s_{db,1} - s_{db,2}\right) \quad (5.77)$$

The change of entropy of biomass is calculated as a function of the change in temperature:

$$s_{\text{db,1}} - s_{\text{db,2}} = c_{\text{p,db}} \ln\left(\frac{T_1}{T_2}\right) \quad (5.78)$$

5.2.6.2 Gasifier

The following main chemical reactions take place in biomass gasification (Abuadala and Dincer, 2012):

$$\text{C} + 2\text{H}_2 \rightarrow \text{CH}_4 \qquad \Delta\text{H} = -74.9\ \text{kJ/kmol} \quad (5.79)$$

$$\text{C} + \text{O}_2 \rightarrow \text{CO}_2 \qquad \Delta\text{H} = -393.5\ \text{kJ/kmol} \quad (5.80)$$

$$\text{C} + \text{CO}_2 \rightarrow 2\text{CO} \qquad \Delta\text{H} = +172.6\ \text{kJ/kmol} \quad (5.81)$$

$$\text{C} + \text{H}_2\text{O} \rightarrow \text{CO} + \text{H}_2 \qquad \Delta\text{H} = +131.4\ \text{kJ/kmol} \quad (5.82)$$

The above mentioned chemical reactions can be shown in an overall chemical reaction as will be discussed below. In the case of using steam as the gasification medium, the chemical reaction equation is written as

$$\text{C}_\text{a}\,\text{H}_\text{b}\text{O}_\text{c}\text{N}_\text{d} + SC \times \text{H}_2\text{O(steam)} + \dot{Q}_{\text{gasifier}} \rightarrow$$

$$\dot{n}_1\,\text{CO} + \dot{n}_2\,\text{H}_2 + \dot{n}_3\text{CH}_4 + \dot{n}_4\,\text{CO}_2 + \dot{n}_5\,\text{H}_2\text{O} + \dot{n}_6\,\text{N}_2 + \dot{n}_7\,\text{C} \quad (5.83)$$

Here, $\dot{n}_\text{i}$ is the molar flow rate of each component in the products. These coefficients are calculated based on atomic balance of species and minimization of Gibbs free energy discussed by Basu (2010). The inlet steam to the gasifier is controlled by steam-to-carbon ratio.

To calculate the gasifier heat input, the steady-state energy balance is used:

$$\dot{n}_{\mathrm{mb,2}}\left(h^{f}_{\mathrm{mb,2}}+\bar{h}_{\mathrm{mb,2}}-h^{0}_{\mathrm{mb,2}}\right)+\dot{n}_{\mathrm{s}}\left(h^{f}_{\mathrm{s}}+\bar{h}_{\mathrm{s}}-h^{0}_{\mathrm{s}}\right)+\dot{Q}_{\mathrm{gasifier}}=$$

$$\left[\sum_{\mathrm{i}=1}^{7}\dot{n}_{\mathrm{i}}\left(h^{f}_{\mathrm{i}}+\bar{h}_{\mathrm{i}}-h^{0}_{\mathrm{i}}\right)\right]_{\mathrm{p}} \tag{5.84}$$

and

$$\dot{E}x_{\mathrm{mb,2}}+\dot{E}x_{\mathrm{s}}+\dot{E}x_{\mathrm{Q}}=\dot{E}x_{\mathrm{P}}+\dot{I}_{\mathrm{gasifier}} \tag{5.85}$$

Here, $h^{f}_{\mathrm{mb,2}}$ is the enthalpy of formation of biomass, which is affected by the moisture content of the biomass, $\bar{h}-h^{0}$ is the sensible heat of the material relative to the reference state, which is ambient condition. Also, $\dot{n}$ denotes the molar flow rate of the species in the reaction. Here, mb refers to moist biomass, and s to steam. Enthalpy of formation and sensible heat of the product gas are calculated on a molar basis for the gas mixture.

The enthalpy of formation of dry biomass is calculated as (Basu, 2010):

$$h^{f}_{\mathrm{db}}=349.1C+1178.2H-103.4O-15.1N+100.5S \tag{5.86}$$

where *C*, *H*, *O*, *N*, and *S* are the weight fractions of the ultimate compositions in the biomass, as given in the assumptions. The following correlation specifies the enthalpy of formation of moist biomass:

$$h^{f}_{\mathrm{mb}}=h^{f}_{\mathrm{db}}(1-\omega)-2.44\omega-21.83H(1-\omega) \tag{5.87}$$

The values of molar coefficients of the products are also a function of the gasification temperature. Since gasification is considered to be adiabatic, the gasifier temperature is the adiabatic gasification temperature. In the minimization of Gibb's free energy method, the temperature of the product species is required; therefore, Eq. 5.84 is used as a checking parameter in obtaining both the molar coefficients and the required heat for gasification. It is worth noting that calculated values for heat input and molar coefficients must satisfy the energy balance, Eq. 5.84. Enthalpy of formation of the product gas is calculated as

$$h^{f}_{\mathrm{p}}=\sum_{\mathrm{i}}y_{\mathrm{i}}h^{f}_{\mathrm{i}} \tag{5.88}$$

where y_{i} is the molar fraction of each component of the product gas, consistent with Eq. 5.83, and

$$y_i = \frac{n_{\mathrm{i}}}{\sum n_{\mathrm{i}}} \tag{5.89}$$

The general exergy rate balance for the gasifier can be written as follows:

$$\sum_i \dot{E}x_{\mathrm{i}} = \sum_{\mathrm{e}} \dot{E}x_{\mathrm{e}} + \dot{\mathrm{I}}_{\mathrm{gasifier}} \tag{5.90}$$

Therefore,

$$\dot{E}x_{\mathrm{mb},2} + \dot{E}x_{\mathrm{s}} + \dot{E}x_{\mathrm{q,gasifier}} = \dot{E}x_{\mathrm{P}} + \dot{I}_{\mathrm{gasifier}} \tag{5.91}$$

The exergy content of the biomass entering the gasifier is a summation of physical and chemical exergy. The physical exergy is calculated using the concept of Eq. 5.77. The chemical exergy of biomass is a function of its lower heating value (Abuadala and Dincer, 2012; Cohce et al., 2010):

$$ex_{\mathrm{mb}} = \beta \times LHV_{\mathrm{mb}} \tag{5.92}$$

$$LHV_{\mathrm{mb}} = 349.1C + 1178.3H - 103.4O\ - 15.1N - \ h_{\mathrm{g}}\left(\frac{9H}{100} + \frac{m}{100}\right) \tag{5.93}$$

where *C*, *H*, *O*, and *N* are percentages of carbon, hydrogen, oxygen, and nitrogen in dry biomass, respectively. Also, h_{g} is latent heat of steam (2260 kJ/kg), and *m* is moisture percentage in moist biomass. Here, β is a correlation factor for biomass with a carbon to oxygen ratio (C/O) less than 2 (Szargut, 2005). The chemical exergy of other relevant substances are presented elsewhere (Bejan et al., 1996).

Since the species in the product gas are considered ideal, their enthalpy is only a function of temperature (Borgnakke and Sonntag, 2008). The purpose of a biomass gasification system is to produce syngas, a combination of CO, H_2 and CH_4 here. In fact, syngas conventionally is a mixture of carbon monoxide and hydrogen gases. Some methane often results from syngas production, although in relatively small quantities in comparison to hydrogen and carbon monoxide.

The lower heating value and chemical exergy content of the produced syngas are calculated based on the thermodynamic rules of gas mixtures:

$$LHV_{\mathrm{syngas}} = y_1 LHV_{\mathrm{CO}} + y_2 LHV_{\mathrm{H_2}} + y_3 LHV_{\mathrm{CH_4}} \tag{5.94}$$

$$\mathrm{ex}_{\mathrm{ch,syngas}} = \mathrm{y}_1 \mathrm{ex}_{\mathrm{ch,CO}} + \mathrm{y}_2 \mathrm{ex}_{\mathrm{ch,H_2}} + \mathrm{y}_3 \mathrm{ex}_{\mathrm{ch,CH_4}} +$$

$$RT_0(y_1 \ln y_1 + y_2 \ln y_2 + y_3 \ln y_3) \tag{5.95}$$

Since the exergy efficiency gives a better insight of the effectiveness of the system, the overall exergy efficiency of the process presented here is defined based on exergy of the produced syngas. In addition, the presence of district heating is considered in the efficiency relation. Hence,

$$\eta_{\text{gasification}} = \frac{\dot{m}_{\text{syngas}} \times LHV_{\text{syngas}} + \dot{Q}_{\text{DH}}}{\dot{m}_{\text{mb}} \times LHV_{\text{mb}} + \dot{Q}_{\text{gasifier}} + \dot{Q}_{\text{Steam}}} \tag{5.96}$$

$$\psi_{\text{gasification}} = \frac{\dot{m}_{\text{syngas}} \times ex_{\text{syngas}} + \dot{E}x_{\text{q,DH}}}{\dot{m}_{\text{mb}} \times ex_{\text{mb}} + \dot{E}x_{\text{q,gasifier}} + \dot{E}x_{\text{Steam}}} \tag{5.97}$$

Here, $\dot{E}x_{\text{q,gasifier}}$ accounts for heat input to the gasifier, and $\dot{E}x_{\text{Steam}}$ is the exergy of steam, for biomass drying and biomass gasification.

5.2.7 Hydrogen Storage

Refilling hydrogen storage tanks can be studied from two different points of view; uniform flow-uniform state and transient. The first point of view sees the refilling process as an initial-final process, while the latter deals with the transient thermodynamic states of the refilling process. In this section, the relevant equations are presented for refilling a hydrogen tank. First, transient behaviour of filling a compressed gaseous hydrogen (CGH_2) tank is modeled thermodynamically. Governing equations are applied to an open system and temperature, pressure, energy and exergy flow rates are determined for hydrogen gas at each time step during filling. Secondly, tank filling is assumed as a uniform flow, uniform state process, in which only the initial and final states of the process are investigated.

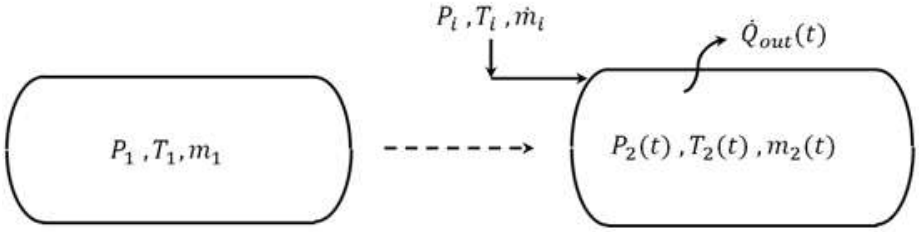

Figure 5.5: Simplified schematic of filling a hydrogen storage tank.

5.2.7.1 Transient process of filling a compressed hydrogen storage tank

Figure 5.5 shows an idealized filling process. The analysis is based on the modeling presented by Yang (2009). Since the filling process is relatively fast (3 min, according to DOE 2010 target (CEC, 2004; Dicken and Mérida, 2007; Maus et al.,

2008), it is considered adiabatic. Hydrogen properties are obtained based on the equation of state presented by Jacobsen et al. (2007) and Lemmon et al. (2005).

According to Figure 5.5, the conservation of mass can be written as follows:

$$\frac{dm}{dt} = \frac{dm_{\mathrm{i}}}{dt} \tag{5.98}$$

The left hand side of Eq. 5.98 represents the temporal change of hydrogen mass inside the storage tank. Neglecting changes in kinetic and potential energies, the first law of thermodynamics can be written for the filling of the storage tank as

$$\frac{dU}{dt} = \dot{Q} + h_{\mathrm{i}} \frac{dm_{\mathrm{i}}}{dt} \tag{5.99}$$

where $\frac{dU}{dt}$ is the rate of change of internal energy. Equation 5.85 can be expressed in the form of specific internal energy (u) and the hydrogen mass content of the storage tank (m):

$$\frac{d(mu)}{dt} = m\frac{du}{dt} + u\frac{dm}{dt} = \dot{Q} + h_{\mathrm{i}} \frac{dm_{\mathrm{i}}}{dt} \tag{5.100}$$

For a constant hydrogen mass flow rate, *k*, integrating Eq. 5.98 results in:

$$m(t) = m_1 + kt \tag{5.101}$$

Substituting Eq. 5.101 into Eq. 5.100 gives an ordinary differential equation for the transient filling of a compressed hydrogen tank:

$$(m_1 + kt)\frac{du}{dt} + u(t)k = \dot{Q} + h_{\mathrm{i}}k \tag{5.102}$$

where $\dot{Q}$ is the heat transfer rate from/to the storage tank, and h_{i} is the specific enthalpy of the supply hydrogen.

The solution to Eq. 5.102, which is solved at any time step for *u*, the specific internal energy of the stored hydrogen inside the tank, follows:

$$u(t) = \frac{m_1 u_1}{m_1 + kt} + \frac{t(h_{\mathrm{i}}k + \dot{Q})}{m_1 + kt} \tag{5.103}$$

where u_1 is the initial specific internal energy of hydrogen in the storage tank.

If the filling process is fast enough and/or the tank is insulated, the process can be assumed to be adiabatic, and Eq. 5.103 reduces to:

$$u(t) = h_{\mathrm{i}} + \frac{u_1 - h_{\mathrm{i}}}{1 + kt/m_1} \tag{5.104}$$

A solution to the above equation is obtained in the form of the temperature of the hydrogen gas inside the storage tank. The equations of states for hydrogen reported by Jacobsen et al. (2007) are used in this study to relate the specific internal energy to the temperature of hydrogen, as follows:

$$RT_{\mathrm{c}}\left[\left(\frac{\partial \alpha^0}{\partial \tau}\right)_{\delta} + \left(\frac{\partial \alpha^r}{\partial \tau}\right)_{\delta}\right] = h_{\mathrm{i}} - \frac{h_{\mathrm{i}} - u_1}{1 + (kt/m_1)} \tag{5.105}$$

where α^0 and α^r are the ideal gas and residual contributions of the reduced Helmholtz free energy, and $\alpha = A/(RT_{\mathrm{c}})$. Also,

$$\tau = \frac{T_{\mathrm{c}}}{T} \tag{5.106}$$

and

$$\delta = \frac{\rho}{\rho_{\mathrm{c}}} \tag{5.107}$$

where T_{c} and ρ_{c} are the critical temperature and density of normal hydrogen, respectively. For a constant feed of hydrogen gas into the storage tank, the density of the hydrogen content of the tank at each time step is expressed by:

$$\rho = \frac{m_1 + kt}{V} \tag{5.108}$$

With Eq. 5.107, one can calculate the temperature of hydrogen as a function of time (Eq. 5.105), for an adiabatic filling process.

The thermodynamic state of the compressed hydrogen gas inside the storage tank is determined by two independent variables, temperature and density. Therefore, relations for the enthalpy, internal energy and pressure of hydrogen as functions of temperature and density can be written as follows (Jacobsen et al., 2007; Lemmon and Jacobsen, 2005; Yang, 2009):

$$u(\tau, \delta) = RT_{\mathrm{c}}\left[\left(\frac{\partial \alpha^0}{\partial \tau}\right)_{\delta} + \left(\frac{\partial \alpha^r}{\partial \tau}\right)_{\delta}\right] \tag{5.109}$$

$$h(\tau, \delta) = RT\left\{\tau\left[\left(\frac{\partial \alpha^0}{\partial \tau}\right)_{\delta} + \left(\frac{\partial \alpha^r}{\partial \tau}\right)_{\delta}\right] + \delta\left(\frac{\partial \alpha^r}{\partial \delta}\right)_{\tau} + 1\right\} \tag{5.110}$$

$$P(\tau, \delta) = \rho RT\left[\left(\frac{\partial \alpha^r}{\partial \delta}\right)_{\tau} + 1\right] \tag{5.111}$$

With the thermodynamic states of hydrogen determined based on Eqs. 5.105 and 5.109-5.111, one can perform an exergy analysis according to exergy balances for the filling process. Thus, the amount of exergy input to the tank plus the tank initial exergy equals to the total amount of the exergy inside the tank plus the amount of exergy destruction during the filling process. Exergy destruction is calculated using the following time-dependent exergy balance for the adiabatic filling process:

$$m_1 ex_1 + (\dot{m}_i t) ex_{\mathrm{i}} = m_2 ex_2 + I_{\mathrm{filling}} \tag{5.112}$$

where m_1 and m_2 are the mass content of the tank before and after t seconds from the start of the filling process, respectively. Also, ex_2 is the exergy of the hydrogen in the tank at each time, *t*. Since the chemical exergy of hydrogen remains constant during the filling process, only physical exergy is taken into account as follows:

$$ex_1 = (u_1 - u_0) - T_0(s_1 - s_0) + P_0(v_1 - v_0) \tag{5.113}$$

$$ex_{\mathrm{i}} = (h_{\mathrm{i}} - h_0) - T_0(s_{\mathrm{i}} - s_0) \tag{5.114}$$

$$ex_2 = (u_2 - u_0) - T_0(s_2 - s_0) + P_0(v_2 - v_0) \tag{5.115}$$

The exergy efficiency of the filling process after t seconds from which the filling process starts can be evaluated by

$$\psi_{\mathrm{filling}} = \frac{m_2 ex(t)_2}{m_1 ex_1 + (\dot{m}_{\mathrm{i}} \times t) ex_{\mathrm{i}}} \tag{5.116}$$

Here, $m_2 ex(t)_2$ represents the total exergy content (not the exergy flow rate) of the hydrogen tank after t seconds from the start of the filling process. Moreover, the term in the denominator of this equation, is the total exergy of hydrogen entering the storage tank in *t* seconds. The above equations are used to study the temporal behaviour of hydrogen during filling a compressed hydrogen storage tank. These equations yield valuable information on the thermodynamic states of hydrogen and the exergy destruction and exergy efficiency of the transient process.

5.2.7.2 Uniform flow-uniform state refilling of a compressed hydrogen tank

To perform a parametric study, the uniform flow, uniform state process is considered for filling a compressed hydrogen tank. The uniform state, uniform flow process is useful in the analysis of unsteady processes, which involve rapid mixing within the control volume, e.g., filling tanks and discharging from pressure vessels.

The initial temperature and pressure of the storage tank determine its initial condition and the quantity of the initial hydrogen content.

The analysis is thus performed only for the initial and final points of the process. The governing equations for this analysis are now described as

$$m_1 u_1 + (\dot{m}_{\mathrm{i}} t) h_{\mathrm{i}} = m_2 u_2 + t\dot{Q} \tag{5.117}$$

Here, t is the filling time and m_1 is the initial hydrogen mass in the storage tank. Also, $m_2 u_2$ is the internal energy of the stored hydrogen at the end of the filling process, and $\dot{Q}$ represents the heat removal rate. Moreover, $\dot{Q}$ is zero if the process considered as adiabatic.

The exergy balance, in this case, is used to calculate the total final state exergy destruction rate during the filling process of a compressed hydrogen tank:

$$m_1 ex_1 + (\dot{m}_{\mathrm{i}} t) ex_{\mathrm{i}} = m_2 ex_2 + t\dot{Q}\left(1 - \frac{T_0}{T_{\mathrm{s}}}\right) + I_{1-2} \tag{5.118}$$

The exergy efficiency of the filling process in a uniform flow, uniform state process can be written as

$$\psi_{\mathrm{filing},1-2} = \frac{m_2 ex_2}{m_1 ex_1 + (\dot{m}_{\mathrm{i}} \times t) ex_{\mathrm{i}}} \tag{5.119}$$

The exergy value for each state is calculated using Eqs. 5.113-5.115.

5.2.8 Battery Energy Storage

The internal resistances of the battery lead to terminal voltage drops during discharging phase. The terminal voltage, therefore, is expressed as the open circuit voltage minus the voltage losses:

$$(V_{\mathrm{Bat}})_{\mathrm{discharging}} = V_{\mathrm{oc}} - I_{\mathrm{Bat}} R_{\mathrm{Bat}} \tag{5.120}$$

where I is the battery electric current.

Alternatively, the battery internal resistances impose a higher voltage requirement during the charging phase. The open circuit voltage is expressed as a function of the state of charge of the battery, which is defined as the ratio of the instantaneous battery charge to the nominal charge capacity of the battery. Sukamongkol et al. (2002) present an empirical relation for the open circuit voltage:

$$V_{\mathrm{oc}} = V_{\mathrm{F}} + \mathrm{B} \times \log(\mathrm{SOC}) \tag{5.121}$$

where V_F is the battery full charge voltage, B is an empirical coefficient, and SOC is the state of charge of the battery. Substituting Eq. 5.121 into Eq. 5.120 and accounting for the relation of SOC with the battery charge (Q_{Bat}) and the battery capacity (BC), one can have a final relation for the terminal voltage of the battery:

$$(V_{\mathrm{Bat}})_{\mathrm{discharging}} = V_{\mathrm{F}} + \mathrm{B} \times \log\left(\frac{Q_{\mathrm{Bat}}}{\mathrm{BC}}\right) - I_{\mathrm{Bat}} R_{\mathrm{Bat}} \tag{5.122}$$

Sukamongkol et al. (2002) also relate the internal resistance of the battery to the battery SOC with some empirical relations. It is important to note that the empirical coefficient, B, in Eq. 5.122 is different for the charging and the discharging phases. These values are reported as 0.810, and 0.724, respectively.

The operation of the battery has a transient behaviour. Therefore, the uniform flow-uniform state condition fits the thermodynamic analyses. Considering the initial and final energy of the battery during the charging phase as $E_{\mathrm{Bat},1}$ and $E_{\mathrm{Bat},2}$ the energy balance equation for the battery is:

$$E_{\mathrm{Bat},1} + (IV)_{\mathrm{charging}} \times t = E_{\mathrm{Bat},2} + Q_{\mathrm{loss}} \tag{5.123}$$

which calculates the final electric energy stored in the battery, $E_{\mathrm{Bat},2}$, in a period of time, t. Moreover, Q_{loss} is the heat generation in the battery during the charging phase, which is dissipated to the battery's immediate surroundings. A similar approach is used to calculate the final energy level of the battery during the discharge phase:

$$E_{\mathrm{Bat},1} = E_{\mathrm{Bat},2} + (IV)_{\mathrm{discharging}} \times t + Q_{\mathrm{loss}} \tag{5.124}$$

During this phase, the energy level of the battery decreases by supplying the power demand, and the internal resistances of the battery. The related exergy balance equations for the charging and discharging of a battery system are presented in Eqs. 5.125 and 5.126, respectively:

$$Ex_{\mathrm{Bat},1} + (IV)_{\mathrm{charging}} \times t = Ex_{\mathrm{Bat},2} + Ex_{\mathrm{q,loss}} \tag{5.125}$$

$$Ex_{\mathrm{Bat},1} = Ex_{\mathrm{Bat},2} + (IV)_{\mathrm{discharging}} \times t + Ex_{\mathrm{q,loss}} \tag{5.126}$$

Since the exergy of electricity has the same value as its energy, the exergy content of the battery equals its energy storage.

5.2.9 Thermal Energy Storage

Figure 5.6 shows a simple schematic of the three main phases in thermal storage systems. The charging process involves heat transfer from saturated steam to the storage medium. The saturated steam is produced in the HRSG via heat recovery from the integrated systems. Therefore the latent heat of condensation of steam is transferred to the water in the storage tank. The water temperature rises accordingly, and the high temperature water is stored in the storage tank.

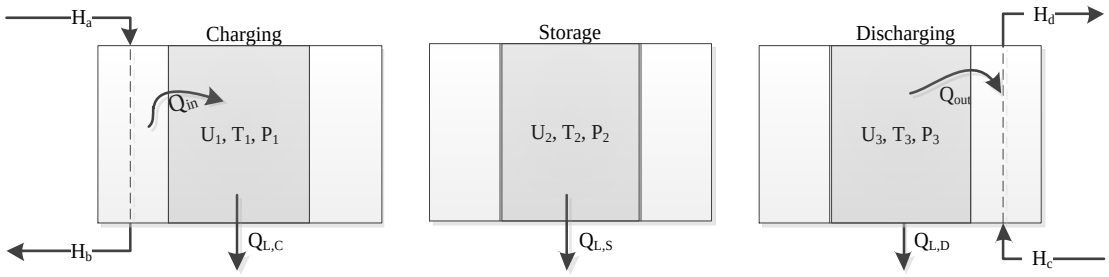

Figure 5.6: Three main phases in thermal energy storage systems

The storage phase is the dormant period in which the high temperature water is stored for later use. Heat loss to the surroundings may occur through the system boundary. During the discharge process, depending on the demand, hot water is extracted from the storage tank. In this research the size of the storage tank is large enough to provide a steady flow of thermal energy to the demand.

Overall energy balance equation for the thermal energy storage system shown in Figure 5.6 is written as

$$Q_{\mathrm{in}} + U_1 = Q_{\mathrm{out}} + Q_{\mathrm{L,C}} + Q_{\mathrm{L,S}} + Q_{\mathrm{L,D}} + U_3 \tag{5.127}$$

where $Q_{\mathrm{in}} = H_{\mathrm{a}} - H_{\mathrm{b}}$ is the thermal energy input to the TES system, and $Q_{\mathrm{out}} = H_{\mathrm{d}} - H_{\mathrm{c}}$ is the thermal energy recovered from the TES system. The three heat flows shown as $Q_{\mathrm{L,C}}, Q_{\mathrm{L,S}},$ and $Q_{\mathrm{L,D}}$ are the heat losses to the surroundings during charging, storage, and discharging phases, respectively. Here, U_1 and U_3 are the initial and final thermal energy content of the storage tank, respectively. The change in enthalpy of water (the storage medium) is considered as a function of its constant pressure specific heat and temperature difference:

$$H_{\mathrm{a}} - H_{\mathrm{b}} = m_{\mathrm{c}} c_{\mathrm{p}} (T_{\mathrm{a}} - T_{\mathrm{b}}) \tag{5.128}$$

$$H_{\mathrm{d}} - H_{\mathrm{c}} = m_{\mathrm{d}} c_{\mathrm{p}} (T_{\mathrm{d}} - T_{\mathrm{c}}) \tag{5.129}$$

One may notice that the values of c_{p} are different at different storage temperatures. The exergy balance equation is obtained according to Figure 5.6:

$$Ex_{\mathrm{in}} + Ex_1 = Ex_{\mathrm{out}} + Ex_{\mathrm{Q,L,C}} + Ex_{\mathrm{Q,L,S}} + Ex_{\mathrm{Q,L,D}} + Ex_3 + I_{\mathrm{TES}} \tag{5.130}$$

where Ex_{in} and Ex_{out} are the thermal exergy input to the TES and the thermal exergy recovered from the TES system, respectively:

$$Ex_{\mathrm{in}} = m_{\mathrm{c}} c_{\mathrm{p}} \left[(T_{\mathrm{a}} - T_{\mathrm{b}}) - T_0 \ln \frac{T_{\mathrm{a}}}{T_{\mathrm{b}}} \right] \tag{5.131}$$

$$Ex_{\mathrm{out}} = m_{\mathrm{d}} c_{\mathrm{p}} \left[(T_{\mathrm{d}} - T_{\mathrm{c}}) - T_0 \ln \frac{T_{\mathrm{d}}}{T_{\mathrm{c}}} \right] \tag{5.132}$$

Here, Ex_1 and Ex_3 are the exergy content of the thermal energy storage system right before the charging process and after the discharging process, respectively. Also, $Ex_{\mathrm{Q,L,C}}, Ex_{\mathrm{Q,L,S}},$ and $Ex_{\mathrm{Q,L,D}}$ are the exergy losses through the system boundary during different phases of energy storage. These quantities are obtained based on the relation for thermal exergy, Eq. 5. 9. Equation 5.130 also presents the exergy destruction in the TES system as I_{TES}, which is the total destruction during the overall thermal energy storage process. Exergy destruction accounts for the internal irreversibility in the storage system due to pressure drops or heat transfer with finite temperature differences. Dincer and Rosen (2011a) define the overall energy and exergy efficiencies of thermal energy storage systems as

$$\eta_{\mathrm{TES}} = \frac{Q_{\mathrm{out}}}{Q_{\mathrm{in}}} \tag{5.133}$$

$$\psi_{\mathrm{TES}} = \frac{Ex_{\mathrm{out}}}{Ex_{\mathrm{in}}} \tag{5.134}$$

Other forms of the efficiency equations can be obtained using the balance equations Eqs. 5.127 and 5.130. The choice of efficiencies presented above are due to the fact that the TES system is considered to supply seasonal thermal energy, and the net energy stored in the storage tank(s) is zero year around. The energy and exergy flows in the TES, and therefore the efficiencies, are functions of temperature and pressure of the storage tank. Therefore, any variations in these two parameters affect the performance of the TES system. Thermal energy storage systems must be well-insulated to reduce heat loss from the system boundary.

In open-type TES systems, the storage medium is used for both charging and discharging of materials as shown in Figure 5.7. Water is heated in a HRSG and is fed to the storage tank in high-temperature, liquid form. Heat is lost during the charging phase, and the relevant energy and exergy balance equations follow:

$$m_1 u_1 + \dot{m}_\mathrm{i} h_\mathrm{i} \Delta t = m_1^{'} u_1^{'} + Q_{\mathrm{L,C}} \tag{5.135}$$

$$m_1 ex_1 + \dot{m}_\mathrm{i} ex_\mathrm{i} \Delta t = m_1^{'} ex_1^{'} + Ex_{\mathrm{Q,L,C}} + I_\mathrm{C} \tag{5.136}$$

where $m_1^{'} u_1^{'}$ is the internal energy, and Δt, $Q_{\mathrm{L,C}}$, and $Ex_{\mathrm{Q,L,C}}$ are the charging period, the heat loss, and the thermal exergy loss, right after the end of the charging period, respectively.

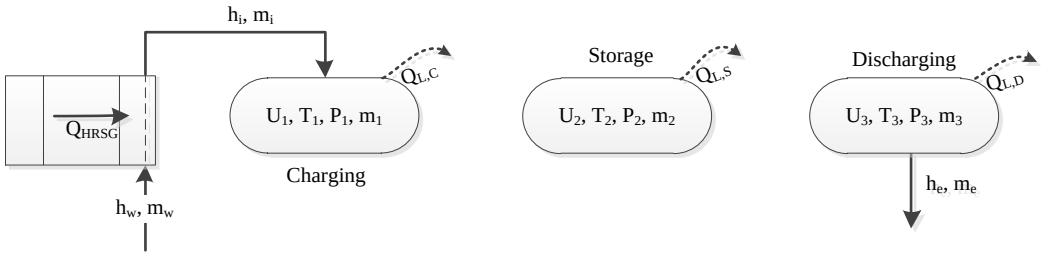

Figure 5.7: A schematic of an open TES system

The final state of the tank (after the charging phase is finished) is the initial state of the storage phase. The balance equations are written as follows:

$$m_1^{'} u_1^{'} = m_2 u_2 + Q_{\mathrm{L,S}} \tag{5.137}$$

$$m_1^{'} ex_1^{'} = m_2 ex_2 + Ex_{\mathrm{Q,L,S}} + I_\mathrm{S} \tag{5.138}$$

where u_2 and ex_2 are the specific internal energy and exergy of the medium at the end of the storage phase. The corresponding state is the initial state of the discharging phase, for which the relevant equations are given below:

$$m_2 u_2 = \dot{m}_\mathrm{e} h_2 \Delta t + m_3 u_3 + Q_{\mathrm{L,D}} \tag{5.139}$$

$$m_2 ex_2 = \dot{m}_\mathrm{e} ex_2 \Delta t + m_3 ex_3 + Ex_{\mathrm{Q,L,D}} + I_D \tag{5.140}$$

where $\dot{m}_\mathrm{e} h_2 \Delta t$ and $\dot{m}_\mathrm{e} ex_2 \Delta t$ represent the energy and exergy of the flow leaving the TES, and point 3 illustrates the final state of the tank after the discharging phase. Pressure drops are neglected, and the enthalpy and physical exergy of the liquid medium are obtained as

$$h = c_{\mathrm{p}} T \tag{5.141}$$

$$ex_{\mathrm{ph}} = c_p(T - T_0) - c_p T_0 \ln \frac{T}{T_0}) \tag{5.142}$$

5.3 Overall Energy and Exergy Efficiencies of Integrated Systems

The effectiveness of integrated renewable energy-based systems is measured by calculating the ratio of outputs to the inputs to the system. As an instance, for a simple steam power plant, energy efficiency is the ratio of the generated electricity output to the rate of energy consumption in the boiler. Efficiency, gives a reasonable measure to compare different systems, since higher efficiencies are usually related to the higher level of energy management and utilization. The concept of energy and exergy efficiencies is also discussed in Section 5.1.3. In this section, this concept is used to find expressions for the efficiencies of the integrated systems.

5.3.1 Residential Hybrid PV-Fuel Cell-Battery System

The energy input to the residential hybrid PV-fuel cell-battery system is solar irradiance. Although solar energy is not available during night hours and cloudy days, the system operates solely on solar energy, thanks to the storage options considered in the integrated system. The main output of the system is electricity, which is fed to a house to supply its power demand. Heat recovery from the SOFC stack gas is another output of the system. Moreover, the integrated system is sized to supply the electricity demand throughout the year independent from the local grid. Therefore, the storage tank size should always contain enough hydrogen to feed the fuel cell, when required. In a year round basis, hydrogen production is set to be more than hydrogen consumption. Thus, the remaining hydrogen in the storage tank is another output of the system. The following equations illustrate the overall energy and exergy efficiencies of the residential hybrid PV-fuel cell-battery system:

$$\eta_{\text{System 1}} = \frac{W_{\text{demand}} + Q_{\text{HRSG}} + \Delta m_{\text{H}_2} LHV}{E_{\text{solar}}} \tag{5.143}$$

$$\psi_{\text{System 1}} = \frac{W_{\text{demand}} + Ex_{\text{q,HRSG}} + \Delta m_{\text{H}_2} ex_{\text{ch,H}_2}}{Ex_{\text{solar}}} \tag{5.144}$$

where W_{demand} is the annual electricity demand of the house in kWh, Q_{HRSG} is the total heat recovered from the fuel cell stack gas, Δm_{H_2} is the difference between

production and consumption of hydrogen on a yearly basis, and E_{solar} is the annual solar energy received by the PV system. The notations in Eq. 5.144 explain the exergy terms of the same concepts.

5.3.2 Integrated Renewable Energy-based System for Baseload Power Generation

The main output of the integrated renewable energy-based system is to supply baseload electric power. The system takes advantage of heat recovery to maximize energy utilization. Since the energy resources are renewable but intermittent, the recovered heat is stored as hot water in thermal energy storage systems. The inputs to the integrated system are wind and solar energy and biomass. The following equations give the overall energy and exergy efficiencies of the integrated renewable energy-based system for baseload power generation:

$$\eta_{\text{System 2}} = \frac{W_{\text{demand}} + Q_{\text{HRSG}} + \Delta m_{\text{H}_2} LHV_{\text{H}_2}}{E_{\text{solar}} + E_{\text{Wind}} + m_{\text{bm}} LHV_{\text{bm}}} \tag{5.145}$$

$$\psi_{\text{System 2}} = \frac{W_{\text{demand}} + Ex_{\text{q,HRSG}} + \Delta m_{\text{H}_2} ex_{\text{ch,H}_2}}{Ex_{\text{solar}} + Ex_{\text{Wind}} + m_{\text{bm}} ex_{\text{ch,bm}}} \tag{5.146}$$

where $W_{\text{demand}}, Ex_{\text{q,HRSG}},$ and Δm_{H_2}account for the total annual electric energy demand, total annual heat recovery from all the available waste heat sources, and the difference between production and consumption of hydrogen on a yearly basis, respectively. The energy inputs in the denominator of the efficiency equations are also considered on a yearly basis.

5.3.3 Hybrid PV-biomass System with Thermal Desalination and Energy Storage Options

The hybrid PV-biomass system with thermal desalination is proposed to supply power demand of a coastal area, where solar energy is abundant and potable water demand is high. The system uses solar energy and biomass to generate electricity in a PV system and a biomass-fuel cell-micro gas turbine system. Energy is stored in forms of compressed air and hydrogen. Heat recovery from compressed air during charging of the compressed air energy storage system is also considered. Moreover, heat is recovered from micro gas turbine exhaust gas for hot water usage. The following equations give the overall energy and exergy efficiencies of the hybrid PV-biomass system with energy storage options:

$$\eta_{\text{System 3}} = \frac{W_{\text{demand}} + Q_{\text{HRSG}} + \Delta m_{\text{H}_2} LHV_{\text{H}_2}}{E_{\text{solar}} + m_{\text{bm}} LHV_{\text{bm}}} \quad (5.147)$$

$$\psi_{\text{System 3}} = \frac{W_{\text{demand}} + Ex_{\text{q,HRSG}} + \Delta m_{\text{H}_2} ex_{\text{ch,H}_2}}{Ex_{\text{solar}} + m_{\text{bm}} ex_{\text{ch,bm}}} \quad (5.148)$$

The thermal water desalination system has its own terminology in defining its effectiveness. The ratio of desalinated water mass flow rate to the steam required for desalination process is called Performance Ratio (PR) (Hosseini et al., 2013a). For commercial, available plants, the PR varies from 4 to 7, which means that for 1 kg of feed steam to the thermal desalination system production of 4 to 7 kg of fresh water is expected.

5.4 Exergoeconomic Analyses of Integrated Renewable Energy-Based Systems

The application of energy and exergy equations in the components of the three proposed, novel systems were presented and discussed in Section 5.3. The mentioned relations provide the exergy flows of streams and materials in the systems, which are used for exergoeconomic analysis. In addition, the capacities of the components are obtained using the energy equations for the components, which are essential for calculating the levelized costs of the components. In this section, the exergoeconomic concepts presented in Section 5.1.4 are applied to the developed systems. Since exergoeconomic balance equations are related for the components of the systems, the schematics of the systems are repeated, for better illustration.

5.4.1 Exergoeconomic Analysis of System 1

The exergy flows through the main components of the hybrid system are shown in Figure 5.8. For each component, the inlet and outlet exergy flows are illustrated with arrows, and proper descriptions are given. For instance, the inlet exergy to the PV system is the solar irradiance exergy, and the outlet exergy is the PV electric exergy output. c_1 and c_2 are the respective unit exergy costs of the PV system.

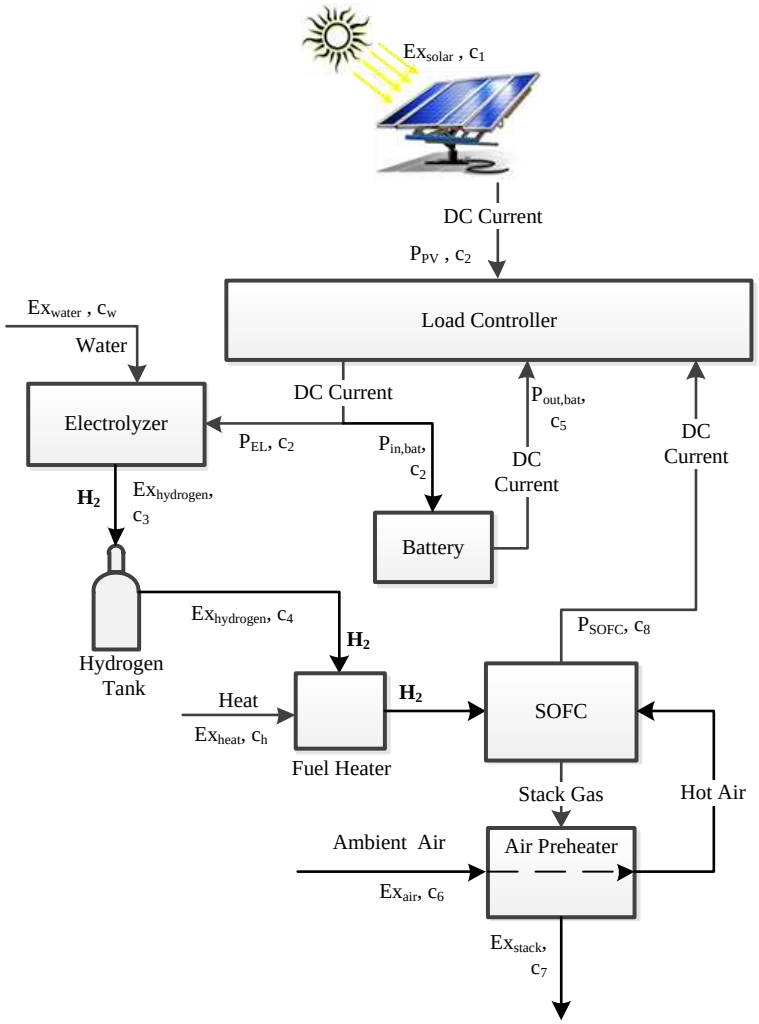

Figure 5.8: Exergy flow and accounted unit cost of exergy flows of the main components of the residential hybrid PV-fuel cell-battery system

For every component there is an associated levelized capital and operation and maintenance cost. Applying the exergoeconomic balance equation, Eq. 5.14, to the flows shown in Figure 5.8 results in the following equations:

$$c_1 \dot{E}x_{\mathrm{solar}} + \dot{Z}_{\mathrm{PV}} = c_2 P_{\mathrm{PV}} \tag{5.149}$$

Having known the exergy flow rates ($\dot{E}x_{\mathrm{solar}}$ and P_{PV}) and cost rates associated with levelized capital investments and O&M ($\dot{Z}_{\mathrm{PV}}$) costs, the unit cost of electric exergy generated by the PV system, c_2 is calculated using the above equation.

The relevant exergoeconomic balance equations for the electrolyser and the SOFC follow:

$$c_{\mathrm{w}} \dot{E}x_{\mathrm{water}} + c_2 P_{\mathrm{EL}} + \dot{Z}_{\mathrm{EL}} + \dot{Z}_{\mathrm{H_2-tank}} = c_4 \dot{E}x_{\mathrm{H_2}} \tag{5.150}$$

$$c_4\dot{E}x_{\mathrm{H_2}} + c_6\dot{E}x_{\mathrm{air}} + c_{\mathrm{h}}\dot{E}x_{\mathrm{heat-H_2}} - c_7\dot{E}x_{\mathrm{hot\,gas}} + \dot{Z}_{\mathrm{SOFC}} = c_8P_{\mathrm{SOFC}} \quad (5.151)$$

where unit cost of exergy of the electrolyser electricity consumption equals the cost of electricity generation in the PV system. c_w is found based on water exergy cost available in literature. c_4 gives the unit cost of produced hydrogen in the electrolyser after considering the hydrogen storage costs. In Eq. 5.151, $c_6 = 0$ since ambient air is free. Also, c_{h} and c_7 are considered equal to the unit exergy cost of hydrogen (c_4). c_8 is the unit exergy cost of the SOFC electric power output.

Equation 5.152 provides the exergoeconomic balance equation for the battery, which is used to calculate the unit exergy cost of electricity stored in the battery (c_5):

$$c_2P_{\mathrm{in,bat}} + \dot{Z}_{\mathrm{bat}} = c_5P_{\mathrm{out,bat}} \quad (5.152)$$

The exergoeconomic factor is given by Eq. 5.16, which is applied to the main components of System 1. The exergoeconomic factor of the PV system is obtained using

$$f_{\mathrm{PV}} = \frac{\dot{Z}_{\mathrm{PV}}}{\dot{Z}_{\mathrm{PV}} + c_{\mathrm{f}}\dot{I}_{\mathrm{PV}}} \quad (5.153)$$

where $\dot{I}_{\mathrm{PV}}$ accounts for irreversibility in the PV modules. The following equations relate the exergoeconomic factor to the capital cost and irreversibility of the electrolyser and the SOFC, respectively:

$$f_{\mathrm{EL}} = \frac{\dot{Z}_{\mathrm{EL}}}{\dot{Z}_{\mathrm{EL}} + c_2\dot{I}_{\mathrm{EL}}} \quad (5.154)$$

$$f_{\mathrm{SOFC}} = \frac{\dot{Z}_{\mathrm{SOFC}}}{\dot{Z}_{\mathrm{SOFC}} + c_4\dot{I}_{\mathrm{SOFC}}} \quad (5.155)$$

The relative cost difference of the electrolyser, the fuel cell, and the battery are calculated based as follows:

$$r_{\mathrm{EL}} = \frac{\mathrm{c}_4 - c_2}{\mathrm{c}_2} \quad (5.156)$$

$$r_{\mathrm{SOFC}} = \frac{\mathrm{c}_8 - c_4}{\mathrm{c}_4} \quad (5.157)$$

$$r_{\mathrm{bat}} = \frac{\mathrm{c}_5 - c_2}{\mathrm{c}_2} \quad (5.158)$$

where c_2, c_4, and c_8 are the unit exergy cost of the PV electricity output, the produced hydrogen by the electrolyser, and the electricity output of the SOFC, respectively.

5.4.2 Exergoeconomic Analysis of System 2

System 2 consists of three separate renewable power generation systems. Similar approaches are followed to express the cost related functions for the unit exergy of the products of the wind park, the compressed air energy storage, and the biomass-SOFC-MGT systems. The performance of the PV-fuel cell system is similar to the hybrid PV-fuel cell system of System 1 and its exergoeconomic equations, as presented in Section 5.4.1.

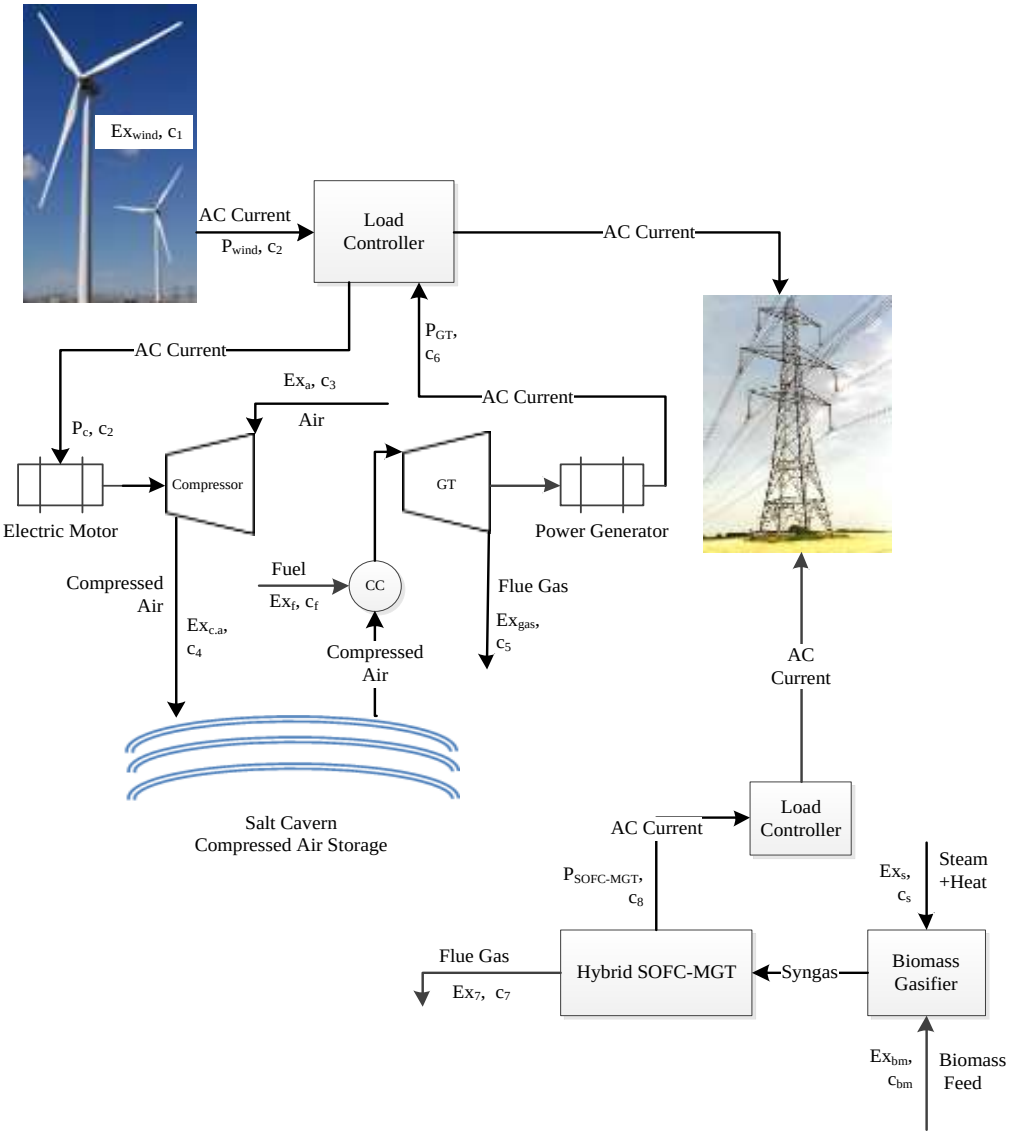

Figure 5.9: Exergy flow and accounted unit cost of exergy flows of the main components of the wind-CAES and the biomass-SOFC-GT systems

Here, the exergoeconomic equations of the wind-CAES and the biomass-SOFC-MGT systems are presented, separately. Figure 5.9 shows the exergy flow and the

notations of the unit exergy costs of flows in the wind-CAES and biomass-SOFC-MGT systems. The unit exergy cost of electricity generation by the wind park is calculated using

$$c_2 = \frac{c_1 \dot{E}x_{\text{wind}} + \dot{Z}_{\text{WP}}}{P_{\text{WP}}} \tag{5.159}$$

where c_2 is the unit exergy cost of electricity generation by the wind park and $\dot{Z}_{\text{WP}}$ and P_{WP} are the wind park levelized costs and the power generation, respectively. The following equation is used to calculate the unit exergy cost of the compressed air:

$$c_4 = \frac{c_2 P_c + \dot{Z}_{\text{CAES}}}{\dot{E}x_{\text{c.a}}} \tag{5.160}$$

where c_4 is unit exergy cost of the compressed stored air in the air storage caverns, P_{c} is energy consumption by the air compressors, and $\dot{E}x_{\text{c.a}}$ is exergy of the compressed air stored in the cavern.

The unit cost of generated electricity by the gas turbine of the CAES system is calculated using

$$c_6 = \frac{(c\dot{E}x)_{\text{c.a}} + c_{\text{f}}\dot{E}x_{\text{fuel}} - c_5\dot{E}x_{\text{gas}} + \dot{Z}_{\text{GT}}}{P_{\text{GT}}} \tag{5.161}$$

where c_6 is the unit exergy cost of the generated electricity by the gas turbine of the CAES system, $c_{\text{f}}\dot{E}x_{\text{fuel}}$ is the cost associated with fuel consumption of the gas turbine, and $c_5\dot{E}x_{\text{gas}}$ is the exergy cost of the high temperature exhaust gas from the gas turbine.

The exergoeconomic balance equation is applied to the biomass-SOFC-GT system to obtain a relation for the unit exergy cost of electricity generation by this system:

$$c_8 = \frac{c_{\text{s}}\dot{E}x_{\text{s}} + c_{\text{bm}}\dot{E}x_{\text{bm}} - c_7\dot{E}x_7 + \dot{Z}_{\text{biomass-SOFC-GT}}}{P_{\text{SOFC-GT}}} \tag{5.162}$$

Exergoeconomic factors are calculated using the following equations:

$$f_{\text{WP}} = \frac{\dot{Z}_{\text{WP}}}{\dot{Z}_{\text{WP}} + c_1\dot{I}_{\text{WP}}} \tag{5.163}$$

$$f_{\text{CAES}} = \frac{\dot{Z}_{\text{CAES}}}{\dot{Z}_{\text{CAES}} + c_2\dot{I}_{\text{CAES}}} \tag{5.164}$$

$$f_{\text{GT}} = \frac{\dot{Z}_{\text{GT}}}{\dot{Z}_{\text{GT}} + c_{\text{c.a}}\dot{I}_{\text{GT}}} \tag{5.165}$$

$$f_{\text{biomass-SOFC-GT}} = \left(\frac{\dot{Z}}{\dot{Z}+c_{\text{bm}}\dot{I}}\right)_{\text{biomass-SOFC-GT}} \quad (5.166)$$

The relative cost differences are given by

$$r_{\text{WP}} = \frac{c_2 - c_1}{c_1} \quad (5.167)$$

$$r_{\text{CAES}} = \frac{c_2 - c_4}{c_2} \quad (5.168)$$

$$r_{\text{GT}} = \frac{c_4 - c_6}{c_4} \quad (5.169)$$

$$r_{\text{biomass-SOFC-GT}} = \frac{c_8 - c_{\text{bm}}}{c_{\text{bm}}} \quad (5.170)$$

5.4.3 Exergoeconomic Analysis of System 3

Figure 5.10 shows the exergy and the accounted unit exergy of flows in the main components of System 3, the hybrid solar PV-biomass system with energy storage option. The concept of exergoeconomics is applied to the exergy flows and the unit exergy flows of the products of the components are calculated, accordingly.

Equations 5.171-173 are obtained from applying the exergoeconomic balance equation (Eq. 5.14) to the PV, the electrolyser, and the compressed air energy storage system of System 3. These sets of equations are used to calculate unit exergy costs of the generated electricity by the photovoltaic system, the compressed air stored in the air storage tank, and the hydrogen produced by the electrolyser, respectively:

$$c_1 = \frac{(c\dot{E}x)_{\text{solar}} + \dot{Z}_{\text{PV}}}{P_{\text{PV}}} \quad (5.171)$$

$$c_2 = \frac{c_1 P_{\text{c}} + \dot{Z}_{\text{CAES}}}{\dot{E}x_{\text{c.a}}} \quad (5.172)$$

$$c_3 = \frac{c_1 P_{EL} + \dot{Z}_{\text{EL}}}{\dot{E}x_{\text{H}_2}} \quad (5.173)$$

The unit cost of generated electricity by the gas turbine of the CAES system is calculated using

$$c_{\text{GT1}} = \frac{c_2 \dot{E}x_{\text{c.a}} + c_3 \dot{E}x_{\text{H}_2} - c_4 \dot{E}x_{\text{hot gas}} + \dot{Z}_{\text{GT}}}{P_{\text{GT1}}} \quad (5.174)$$

where c_{GT1} is the unit exergy cost of the generated electricity by the gas turbine of the CAES system, $c_3\dot{E}x_{\text{H}_2}$ is the cost associated with fuel consumption of the gas turbine,

and $c_4\dot{E}x_{\text{hot gas}}$ is the exergy cost of the high temperature exhaust gas from the gas turbine.

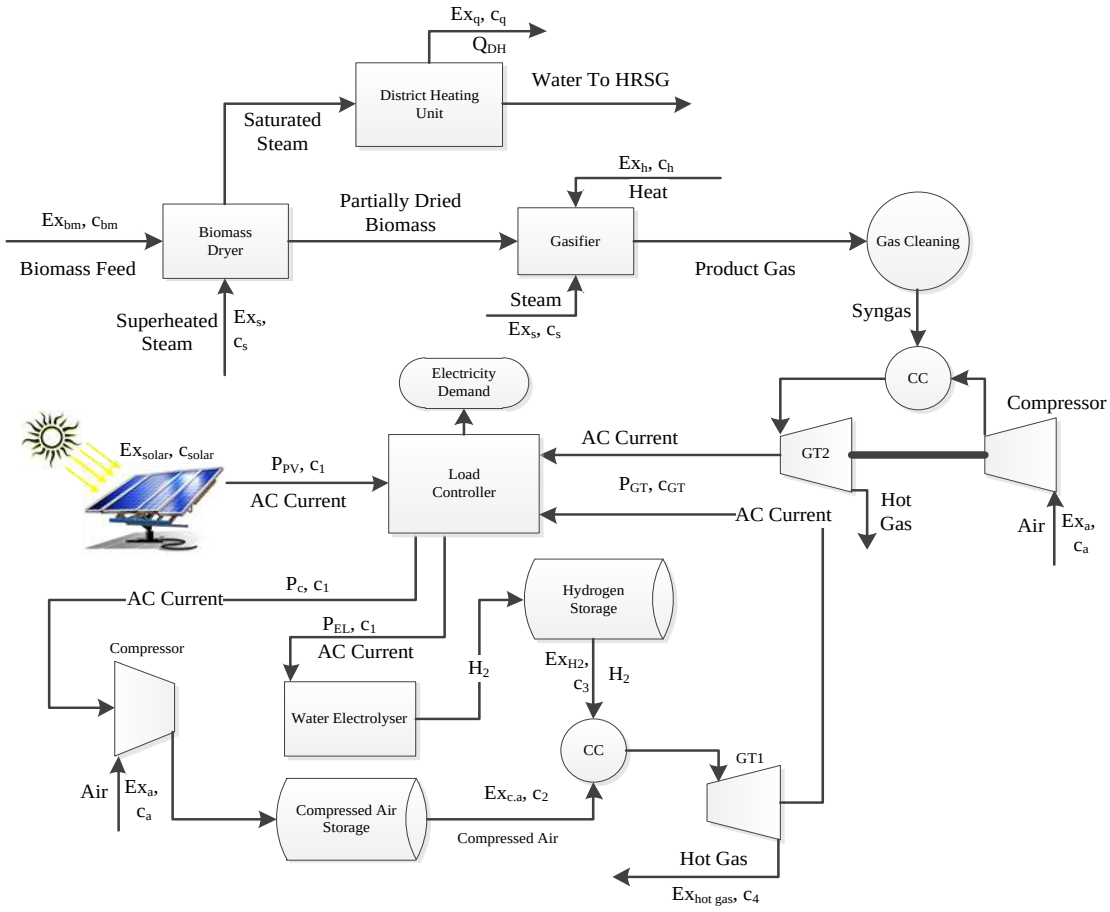

Figure 5.10: Exergy flows and accounted unit exergy costs to the products of the main components of the hybrid PV-biomass system with energy storage options

The exergoeconomic balance equation is applied to the biomass-GT system to obtain a relation for the unit exergy cost of electricity generation by this system, c_{GT2}:

$$c_{\text{GT2}} = \frac{c_s\dot{E}x_s + c_h\dot{E}x_h + c_{bm}\dot{E}x_{\text{bm}} - c_q\dot{E}x_{\text{q}} + \dot{Z}_{\text{biomass-GT}}}{P_{\text{GT2}}} \tag{5.175}$$

The exergoeconomic factors are calculated using the following equations:

$$f_{\text{PV}} = \frac{\dot{Z}_{\text{Pv}}}{\dot{Z}_{\text{PV}} + c_{\text{solar}}\dot{I}_{\text{PV}}} \tag{5.176}$$

$$f_{\text{CAES}} = \frac{\dot{Z}_{\text{CAES}}}{\dot{Z}_{\text{CAES}} + c_1\dot{I}_{\text{CAES}}} \tag{5.177}$$

$$f_{\text{GT}} = \frac{\dot{Z}_{\text{GT}}}{\dot{Z}_{\text{GT}} + c_3\dot{I}_{\text{GT}}} \tag{5.178}$$

$$f_{\text{biomass-GT}} = \left(\frac{\dot{Z}}{\dot{Z}+c_{\text{bm}}\dot{I}}\right)_{\text{biomass-SOFC-MGT}} \quad (5.179)$$

Equation 5.14 is used to calculate the relative cost difference of the main components of System 3. The following equations are obtained and used in the analyses:

$$r_{\text{PV}} = \frac{c_{\text{solar}}-c_1}{c_1} \quad (5.180)$$

$$r_{\text{CAES}} = \frac{c_2-c_1}{c_1} \quad (5.181)$$

$$r_{\text{GT}} = \frac{c_{\text{GT}}-c_3}{c_3} \quad (5.182)$$

$$r_{\text{biomass-SOFC-MGT}} = \frac{c_{\text{GT}}-c_{\text{bm}}}{c_{\text{bm}}} \quad (5.183)$$

The previously presented and discussed sections provide the energy, exergy and exergoeconomic equations and tools for the analyses of the three novel, renewable energy-based systems. These systems are developed to use renewable energy for electricity generation. Energy storage options are added to increase energy utilization and to compensate for temporal behaviour of renewable resources. The analyses are used to investigate the performance of the systems, to calculate their efficiencies and inefficiencies, and their share in taking steps toward environmental sustainability by decreasing the levels of greenhouse gas emission. The next section of this chapter discusses a brief introduction to exergoeconomic optimization and its application to the Systems that are studied here.

5.5 Exergoeconomic Optimization

The aim of exergoeconomic optimization is to minimize the costs associated with exergy flows, especially costs of inefficiencies. Selection of equipment type, size, and the configurations of the equipment in the processes, along with the temperature and pressure range of operation of these components are the goals of an optimization analysis.

Several considerations should be made when conducting an optimization analysis. Defining the system boundary is a first step. All the important and effective parameters should be inside the system boundary. For complex energy systems, it is

suggested that the system is broken down into subsystems. The optimization criterion is the next important step in optimization analysis of energy systems. Economy, thermodynamics, and environment can each be the basis from which the system is evaluated and optimized. Another essential element is the selection of variables. The variables on which the optimization is performed must be independent and address the characteristics of the system or process. These variables should be the important parameters that affect the performance and cost effectiveness of the system. Moreover, they should be distinguished from parameters of minor importance. The variables that are selected for optimization are subject to change and considered as decision variables, and should be distinguished from fixed value parameters of the system or the process. The next step in optimization analysis of an energy system is to select a mathematical model for the analysis. The mathematical model relates the variables and defines how the independent variables affect the system performance. The model consists of objective functions and some technical constraints. As an instance, the objective function can be the minimization of the product cost. Minimization of exergy loss or destruction could be another objective function.

In this research the mathematical model is the exergoeconomic approach. Details of regulations, assumptions and the optimization procedure are presented by Bejan et al. (1996). According to them, in thermal systems, the main goal is to optimize the system in general. The idea is that optimizing a sole component of the system may not lead to an overall optimized system. The optimization methods aim at finding an optimum operating parameter (or operating parameters depending on the number of decision variables). There is no absolute answer to an optimization problem, especially when there are many variables involved. For example, the exergy efficiency can be maximized, and thereby minimizing the environmental impact of the system, while the unit exergy cost of the product reaches its maximum value. In extreme cases of maximum exergy efficiency, the product cost may not be feasible.

Objective functions, that are set to be optimized, may contain only a single or multiple decision variables. They may also be linear or non-linear. When optimizing a single-variable objective function, graphical, direct, and indirect methods can be used. Graphing a number of the objective function values, and finding the optimum value is referred to as graphical method. In the indirect methods, the optimum (global or local) is found by finding the first and the second derivative of objective function. Newton’s

method and Secant methods are among those. Finally, comparing the objective function values in an interval (of the decision variables) is called the direct method. The Fibonacci method is one of the most efficient direct methods in optimization of single-variable objective functions.

Depending on the linearity of the objective functions, optimization of multivariable functions is performed using unconstrained multivariable optimization, linear programming optimization, and nonlinear programming with constrains (Bejan et al., 1996). In energy systems, the objective functions may include exergy efficiency, unit exergy cost of products, and environmental impact of the overall system. These functions usually conflict with each other, and finding an optimum operating/design condition of the system is an asset. Finding the extrema of the aforementioned functions is possible using search techniques. In this research, a genetic algorithm is used since it requires no initial conditions, works with multiple design variables, finds global optima (as opposed to local optima), utilizes populations (as opposed to individuals) and uses objective function formation (as opposed to derivatives).

The main idea behind genetic algorithm (GA) arises from nature, where offspring gain certain characteristics determined by genetic levels of chromosome combination of the parents. The variables and the values of the objective functions are formed in strings called chromosome, and the recombination of these strings is evaluated using crossover and mutation concepts. In the optimization procedure, strings which have higher fitness (into a certain condition or objective) are selected. The selected springs will have more opportunity to breed, or in engineering words, to be chosen as the basis for the next evaluation/searching criteria. If the algorithm is run for a reasonable time period, the strings (chromosomes) with higher fitness will eventually contain optimum operating parameters (genes). This means that the system will have its optimum performance if the conditions obtained by the GA optimization are applied. The time period in which genetic algorithm is run has no limit, according to Mitchell (1999). Among different methods, setting a limit on the number of iterations (runs), and setting a limit on the time in which the optimization is run are the two simple and possible termination criteria.

5.5.1 Objective Functions

The objective functions that are required to be optimized are the exergy efficiency, and total capital cost rate. These functions are optimized within the constraints of the decision variables.

Section 5.3 provides the exergy efficiency relations of the proposed systems. Obviously, the efficiency functions are meant to be maximized, while the total cost rate of system products is minimized. The total cost rate of the integrated systems is an objective function to be minimized in this study. The cost rate accounts for the total purchase cost of the system. In this function, the costs associated with equipment purchase and maintenance are calculated according to manufacturers' database. The total cost rate is illustrated by

$$\mathrm{Z} = \sum_{\mathrm{i}} c_{\mathrm{i}} P_{\mathrm{i}} \tag{5.184}$$

where Z is the purchase cost of the system, and c_{i} is the specific unit cost of component i, and P_{i} is the nominal power capacity of the component.

The integrated system uses renewable energy resources, which are more environmentally friendly, compared to fossil fuels, during their operation. Therefore, generating electricity and heat by renewable energy helps prevent the release of greenhouse gas emissions. Enhancing the integrated systems in terms of energy utilization and management reduces the rate of carbon dioxide in a greater level. It is possible to calculate the environmental impact savings of the integrated systems by calculating the equivalent carbon dioxide rate emitted by conventional power plants.

5.5.2 Decision Variables

Decision variables are the parameters that when varied allow objective functions to be optimized. For each of the integrated systems, some decision variables are considered as follows:

5.5.2.1 Residential hybrid PV-fuel cell-battery system

The following decision variables are utilized in the optimization of System 1:

- Solid oxide fuel cell stack temperature
- Solid oxide fuel cell nominal capacity
- Fuel utilization of the solid oxide fuel cell

The fuel cell temperature plays a significant effect on its performance. In higher stack temperatures voltage losses are lower. However, according to the Nernst equation, the open circuit voltage of the cells will be lower (Larminie and Dicks, 2003). Thus the operating temperature of the fuel cell becomes a decision variable in this research. The zirconia-based solid oxide fuel cells have an operating temperature range of 800 to 1100°C (Larminie and Dicks, 2003), which is used as the constraint of the decision variable in this study.

The first layout in this study includes a combination of fuel cells and batteries to supply electricity demand of the residential area on demand. The nominal capacity of the fuel cell plays a major role in sizing the components. The fuel cell can be selected to supply the minimum power demand of the house, which the rest of the electricity demand is met by the batteries. On the other limit, the fuel cell can provide the maximum power demand of the house, while the battery has its minimum contribution. Therefore, the lower and upper boundaries of the fuel cell nominal capacity to be optimized in the system are chosen to be the lowest and the highest electricity demand of the house.

Fuel utilization is the ratio of the amount of the fuel which is consumed by the fuel cell to the mass flow rate of the fuel entering the fuel cell stack. In ideal scenarios, fuel utilization (U_f) should be 1, meaning that all the fuel (e.g. hydrogen) entering the fuel cell stack participates in the electrochemical electricity generation process. However, the cell length is usually long (150 cm in tubular SOFCs), and the end of the cell may not receive adequate amount of fuel. Therefore, fuel cells are designed with the fuel utilization values less than 1. Depending on the type of the fuel cell, and the manufacturer, fuel utilization may change from 0.6 to 0.9. In this research, U_f is changed within the pre-mentioned range to investigate its effect on the system performance.

5.5.2.2 Integrated renewable energy-based system for baseload power generation

In the optimization of System 2, the following decision variables are utilized:

- Solid oxide fuel cell stack temperature
- Storage hours of the Compressed air energy storage
- Gas turbine expansion ratio
- Gas turbine isentropic efficiency

- Compression ratio of the air compressor

The zirconia-based solid oxide fuel cells have an operating temperature range of 800 to 1100°C (Larminie and Dicks, 2003), which is used as the constraint of the decision variable in this study.

The second novel integrated system is proposed to provide a constant rate of electric power; although it is fully supplied by renewable energy resources. There is a possibility that the renewable energy resources are unavailable for an undetermined period of time. Therefore, it is important to make sure that the storage system is large enough to back up the power supply. The size of the compressed air storage system will be changed to provide compressed air for the gas turbine on a continuous basis from 3 to 7 days. This significantly affects the size of the wind park, and the capital investment cost of the hybrid system. Operating pressure of the gas turbine of the CAES system is another decision variable. The gas turbine will be assumed to have a pressure equal or less than the high pressure, stored air in the storage system. Since, two expansion stages are considered, the expansion ratios will be varied from 6 to 8 for each expansion stage.

The isentropic efficiency of the gas turbine is related to the mechanical perfectness of the blades and the turbine set-up. Pressure drops, heat transfer to the surrounding, and many other factors will deviate the operation of the gas turbine from the isentropic state. The cost of the gas turbine and its actual power output are related to its isentropic efficiency. For optimization purposes, the isentropic efficiency is changed from 60 to 90%.

The pressure of the compressed air which is stored as the energy carrier is another parameter that is changed for the optimization analysis of the system. Two compression pressure stages are considered, each with 6 to 9 bar/bar pressure ratio.

5.5.2.3 Hybrid PV-biomass system with thermal desalination

In the optimization of System 3, the following decision variables are utilized:

- Steam-to-carbon ratio of the biomass gasification process (*SC*)
- Gas turbine expansion ratio (r_{GT})
- Gas turbine inlet temperature (*TIT*)
- Compression ratio of the air compressor (r_c)

- Gas turbine isentropic efficiency

System 3, hybrid renewable energy-based system provides electricity and distilled water. Steam-to-carbon ratio of the biomass gasifier affects the system's performance, and it is changed from, 1 mol/mol to 3 mol/mol to find an optimize value.

The system utilizes compressed air energy storage system as an energy storage option. The decision variables for the optimization process have the same characteristics described for the second system. Since, two expansion stages are considered, the expansion ratios will be varied from 6 to 8 for each expansion stage.

The gas turbine inlet temperature plays a major rule in its fuel consumption and energy output rate. The *TIT* of the gas turbine is changed from 1200 to 1400 K.

The isentropic efficiency of the gas turbine is related to the mechanical perfectness of the blades and the turbine set-up. Pressure drops, heat transfer to the surrounding, and many other factors will deviate the operation of the gas turbine from the isentropic state. The cost of the gas turbine and its actual power output are related to its isentropic efficiency. For optimization purposes, the isentropic efficiency is changed from 60 to 90%.

The pressure of the compressed air which is stored as the energy carrier is another parameter that is changed for the optimization analysis of the system. Two compression pressure stages are considered, each with 6 to 9 bar/bar pressure ratio.

Chapter 6: Results and Discussion

In this research, three novel integrated systems are proposed. The systems utilize renewable energy resources and are equipped with different types of energy storage options. Each of the proposed integrated systems is intended to supply electricity for a specific purpose. The concept of energy storage is investigated alongside with the corresponding integrated systems, since energy storage is a subdivision of larger energy systems. In this chapter, the results of the investigation of the integrated renewable energy-based systems are presented. The results are presented for each system separately.

6.1 System 1: Residential PV-Fuel Cell-Battery System

The residential PV-fuel cell-battery (PV-FC-battery) system described in chapter 4 is modeled and analyzed based on the equations presented in chapter 5. In this section, first the assumptions and data use are illustrated, and PV cell characteristics curves are presented, next. Daily performance of the hybrid system forms another part of the results presented, and economic evaluation, exergoeconomic analyses and hybrid system optimization based on exergy efficiency and total system cost rate form the last parts of this section.

6.1.1 Assumptions and Data

The thermodynamic and cost analyses are based on the following assumptions and data:

- Heat losses from the system boundaries are negligible.
- The data for solar irradiance, as well as the load variations, are for one hour time periods.
- Possible sources of data noise, e.g. sudden changes in solar irradiance and electric power demand, are not considered in the analyses (i.e. average hourly values are used).

- The solar irradiance is based on a monthly average in Toronto in 2011. The calculations are for each month, separately.
- The proton exchange membrane (PEM) electrolyser operates at 30 bar with 65% efficiency.
- The hydrogen generated by the electrolyser is stored at 25 bar on a seasonal storage basis. The size of the storage tank is determined based on the seasonal need for hydrogen.
- The fuel cell is an atmospheric SOFC.
- The nominal power output of each PV module is 210 W, at standard test conditions (STCs).

Tables 1 and 2 list the modeling data for the PV and the fuel cell systems. The solar irradiance data in Toronto, Canada is used in the analyses, since the electric power demand of a Canadian house is considered (UTM, 2012). The average hourly data over the course of each month of the year 2011 are taken as the input to the PV system. The same procedure is used for obtaining the electric power demand. Figure 6.1 shows the variation of average daily solar irradiance during each month. As expected, solar irradiance is a highest in summer months and lowest in winter months.

Table 6.1: PV system specifications

Short circuit current (I_{sc}), A	5.75
Open circuit voltage (V_{oc}), V	47.7
Maximum point current (I_{mp}), A	5.25
Maximum point voltage (V_{mp}), V	40.0
Array area, m^2	1.244
Number of cells in module	72
Temperature coefficient of short-circuit current, A/°C	2.03×10^{-3}
Temperature coefficient of open-circuit voltage, V/°C	-1.35×10^{-1}
Reference light current ($I_{L,ref}$), A	5.66
Reference reverse saturation current ($I_{0,ref}$), A	4.63×10^{-11}
Reference Conditions	
Total irradiance (G_{ref}), W/m^2	1000
Wind speed, m/s	5
Ambient temperature (T_a), °C	25

Source: SunPower (2012)

Here, c-Si photovoltaic modules manufactured by SunPower Corporation, with specifications shown in Table 6.1, are selected for analysis. The SOFC electrolyte is made of Y_2O_3-stabilized zirconia (YSZ), the anode material is YSZ with a coating of nickel, and the cathode is made of Sr-doped $LaMnO_3$ (LSM) + YSZ (Braun et al., 2011). The major input parameters to the SOFC are presented in Table 6.2. The internal consumption of the balance of plant of the SOFC is considered to be 4% of the generated power, and this is accounted for in efficiency calculations. The efficiency of the DC/AC inverter is taken to be 96% (Motahar and Alemrajabi, 2009).

Table 6.2: Input parameters to the SOFC model

Inlet air temperature, °C	25
Stack temperature, °C	900*
Activation area, cm^2	834*
Cell current density, A/cm	0.350
Fuel utilization	0.850*

*Source: Motahar and Alemrajabi (2009)

The electric power demand of a Canadian detached house with 210 m^2 floor space is illustrated in Figure 6.2.

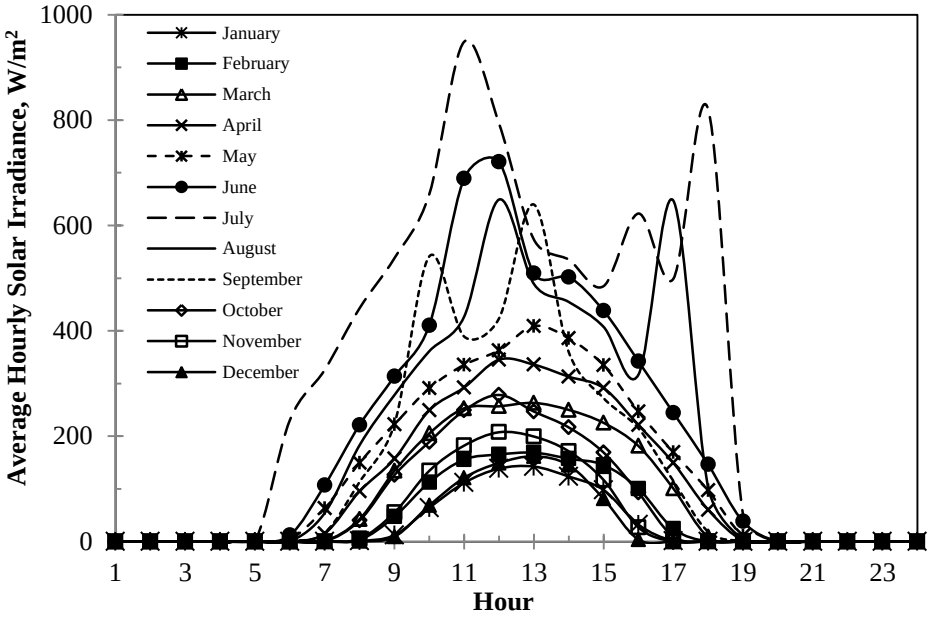

Figure 6.1: Average hourly solar irradiance for Toronto in 2011 (adapted from UTM, 2012)

The demand includes the power consumption of appliances, lighting, the furnace, and the air conditioning system (Saldanha and Beausoleil-Morrison, 2012). The house has maximum demand in July due to the considerable demand for air conditioning. However the demand exhibits similar trend for each month of the year, as there is a greater demand for electricity during night hours. Due to earlier sunset in fall-winter months the maximum demand occurs between 6 and 8 pm, rather than 8 to 10 pm as is the case for the spring-summer months.

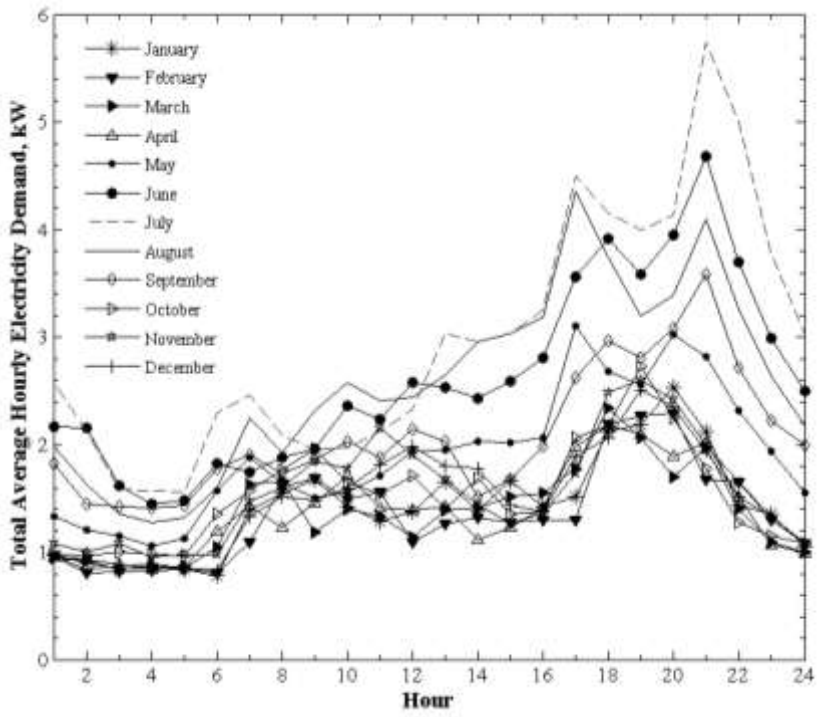

Figure 6.2: Daily average electricity demand by month, (data from Saldanha and Beausoleil, 2012)

6.1.2 Results and Discussion

A code is developed based on the modeling equations and thermodynamic analyses presented in chapter 5 to perform energy, exergy, and exergoeconomic analyses of the residential hybrid PV-fuel cell-battery system for a Canadian detached house. The code is run with a fuel cell of 2 kW nominal power capacity to determine the size of the other main components of the system. The capacity of the PV unit, the electrolyser, the hydrogen tank, and the battery are calculated in order to provide a positive accumulation of hydrogen content in the storage tank.

The developed code is validated with either manufacturer data or with literature regarding the main components of the system. The PV system model is validated

through comparison with the I-V characteristics of SunPower solar PV panel; SPR-210-BL. Figure 6.3 shows the I-V characteristic of the PV system for various values of solar irradiance.

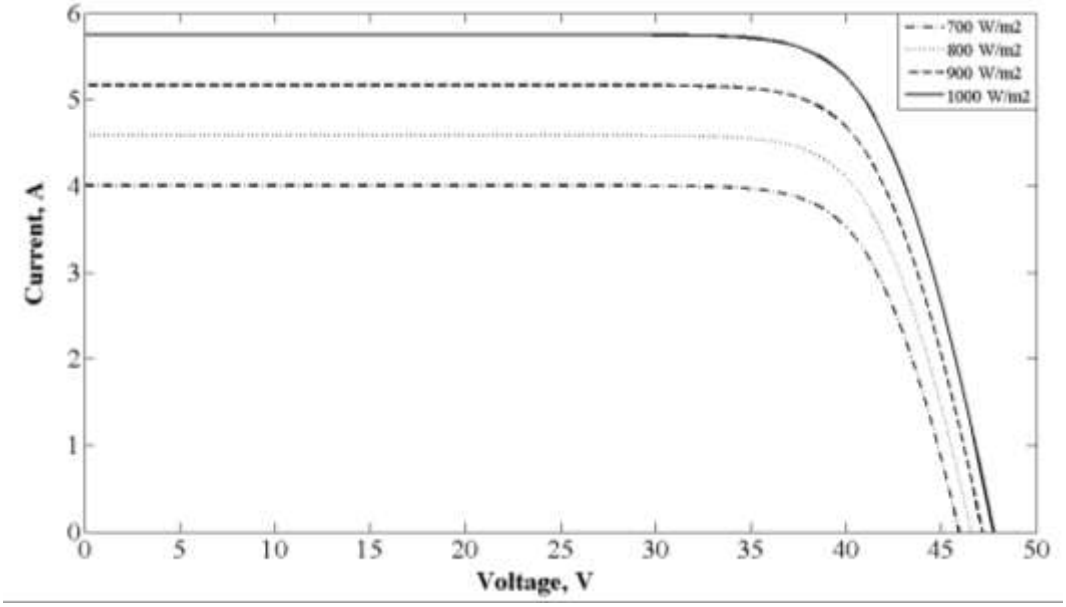

Figure 6.3: Effects of solar irradiance on I-V characteristics

The system characteristic considerably deviates from the design condition (solar irradiance = 1000 W/m^2) as solar irradiance decreases. According to Figure 6.4, the power output of the PV module has a maximum point, after which the power drops significantly.

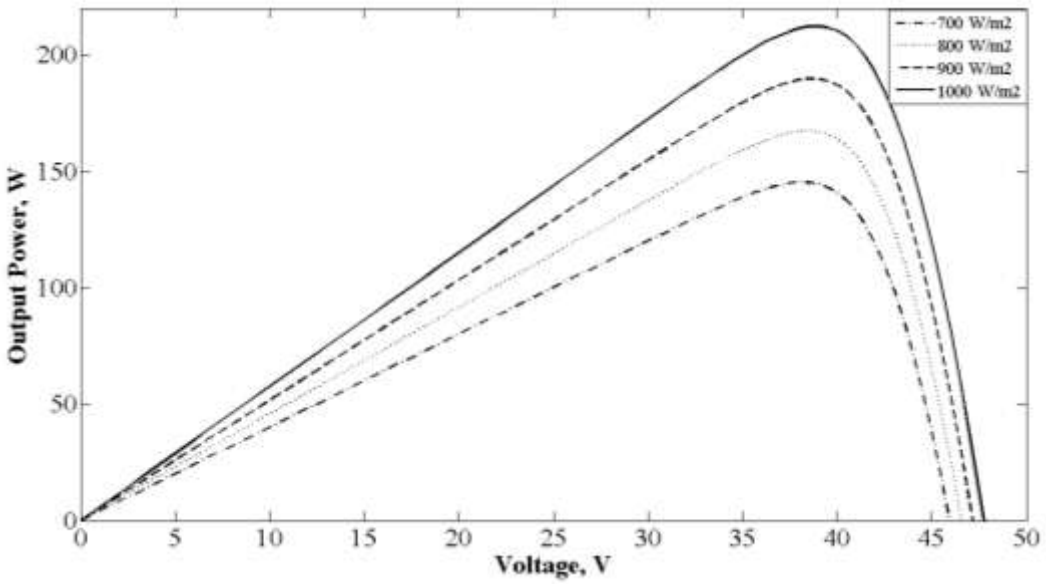

Figure 6.4: Effects of solar irradiance on power-voltage characteristics

Novel PV systems are designed to operate at the maximum power point with the change in solar irradiance. The results of the PV model are compared to the SunPower 210 solar panel's I-V characteristic curves for the standard test condition (STC) 1000 W/m^2, and 25°C. The obtained maximum power point at STC is only 2.4% different from the manufacturer's reported value.

Table 6.3 presents a comparison between the PV maximum power and efficiency, and the SOFC cell power output and efficiency with the manufacturer data or literature.

Table 6.3: Comparison of PV and SOFC models with manufacturer/ literature data

Parameter	PV maximum power[a], W/module	PV energy efficiency[a], %	SOFC power[b], W/cell	SOFC electric efficiency[b], %
Current model	215	16.88	27	47.6
Manufacturer/Literature	210	16.71	25[c]	50.0[d]

[a] SunPower (2012), 1000 W/m^2 solar irradiance, 25°C
[b] Colpan et al., (2007)
[c] 0.35 A/cm^2 current density, and 0.3 recirculation factor
[d] 0.35 A/cm^2 current density, and 0.85 fuel utilization

Figures 6.5-6.6 show that the efficiencies of the PV system follow the same trend as the power output: higher efficiencies are obtained for higher solar irradiances.

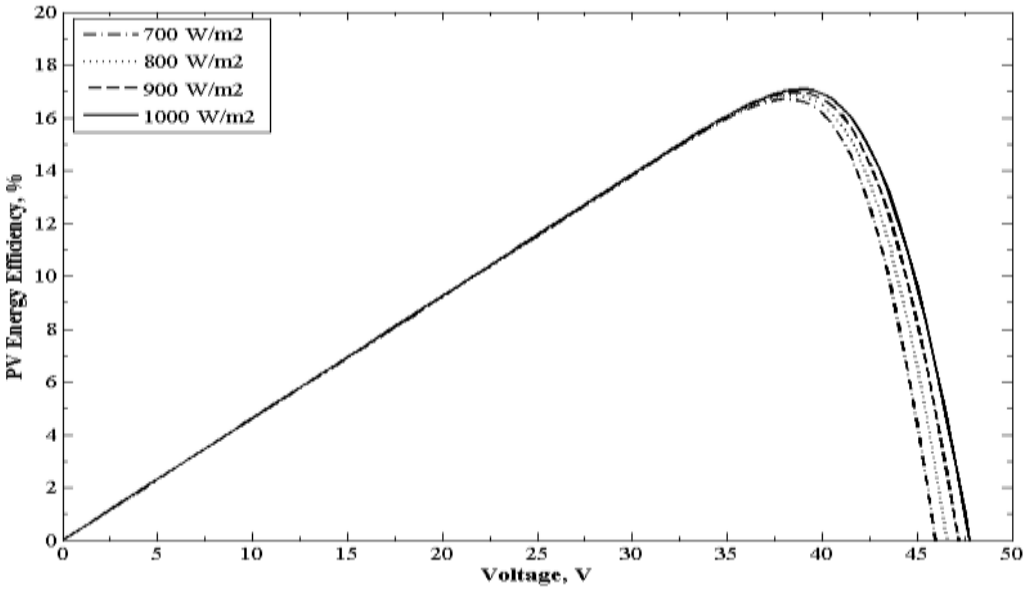

Figure 6.5: PV energy efficiency vs. voltage with various solar irradiance

The exergy efficiency at the maximum power output is higher than the corresponding energy efficiency, which can be defined by Eqs. 5.26-5.27. While the

energy and exergy values of the PV electric power output are the same, the exergy of solar irradiance is less than its energy value. Since the latter term is present in the denominator of Eq. 5.27, the exergy efficiency is higher than the energy.

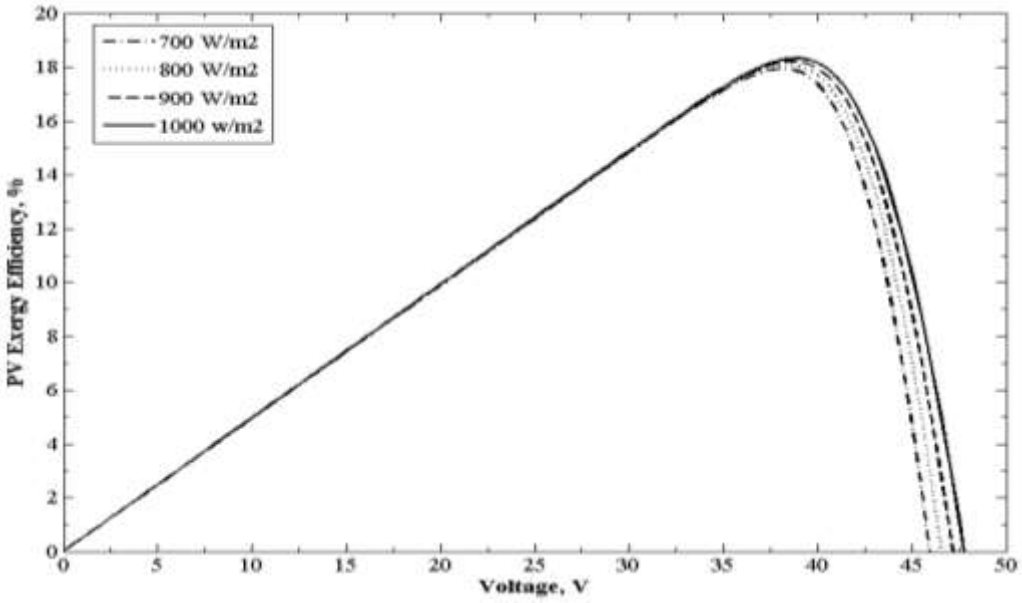

Figure 6.6: PV exergy efficiency vs. voltage with various solar irradiance

The SOFC model is validated with the results presented by Colpan et al. (2007) and Motahar and Alemrajabi (2009).

6.1.2.1 Energy and exergy results

System 1 is developed to supply the electricity demand of a house. Since the solar irradiance, which is the main and only source of energy input to the system, depends on the geographical location, nominal capacities of the main components vary with demand profile and location of the house. The electricity demand profile of a Canadian detached-house and solar irradiance in Toronto are considered as the inputs to the system. In Chapter 4, nominal capacities of the PV, electrolyser, SOFC, and the battery pack were predicted. Those values were calculated based on 1000 W/m^2 solar irradiance, 5.75 kW steady electricity demand, and a fuel cell with 2 kW power output. However, according to Figure 6.1, maximum solar irradiance in 2011 in Toronto is less than the manufacturer test condition. Therefore, power output of the PV system is less than the nominal capacity, and the required size of electrolyser and the battery pack varies, accordingly. Table 6.4 presents the nominal capacities of the main components of System 1.

Table 6.4: Nominal capacities of main components of System 1

Component	PV	Electrolyser	SOFC	Battery
Nominal Capacity	37.5 kW	31.7 kW	2 kW	12.4 kWh

A quick comparison of Table 6.4 with the data predicted in Table 4.1 reveals the major effect of temporal behaviour of solar irradiance on the nominal capacities. 18.4 kW PV capacity was predicted; however, the analysis shows that the PV size should be 37.5 kW for System 1 to be able to supply the electricity demand of the house. Table 6.5 presents the annual mass and energy flows in the components of System 1.

Table 6.5: Annual mass, energy and exergy flows in the residential PV-FC-battery system

Parameter	Annual cumulative value
Electrolyser hydrogen production, kg/year	538
Fuel cell hydrogen consumption, kg/year	535
Storage tank net hydrogen content, kg/year	3
PV electricity generation, MWh/year	36.,2
Electrolyser electricity consumption, MWh/year	27.7
SOFC electricity generation, MWh/year	769
Battery electricity supply, MWh/year	121
HRSG steam generation, MWh	218
Exergy of HRSG generated steam, MWh/year	594
Hydrogen storage tank size, kg	169
Total exergy destruction, MWh/year	190
Electricity demand, MWh/year	16.3
Solar irradiance (energy basis), MWh/year	220
Solar irradiance (exergy basis), MWh/year	205
PV power penetration, %	45.4
SOFC power penetration, %	47.2
Battery power penetration, %	7.4
PV total hours of operation, h/year	4505
Electrolyser total hours of operation, h/year	3423
SOFC total hours of operation, h/year	3769
Battery total hours of operation, h/year	1592
System 1 Energy efficiency, %	8.2
System 1 Exergy efficiency %	8.3

One may note that the components of System 1 do not always operate at full load. For instance, the SOFC does not operate during the hours with abundant solar availability, at which the PV supplies the power demand of the house. In contrast, the PV generates no electricity during night hours or cloudy periods. Therefore, to better present the mass and energy flows in the residential PV-FC-battery system, the cumulative values over a course of one year operation are given in Table 6.5. Table 6.5 presents the total, annual flows in the system components. To illustrate the hourly performance of the hybrid system, the power and hydrogen generation or consumption of the main components are presented for two typical days in summer and winter.

The results are obtained based on the hourly power demand and solar irradiance. Figure 6.7 shows the electricity demand of the house, and the PV unit, the fuel cell, and the battery power outputs during a summer day. The same data are presented in Figure 6.8 for a winter day.

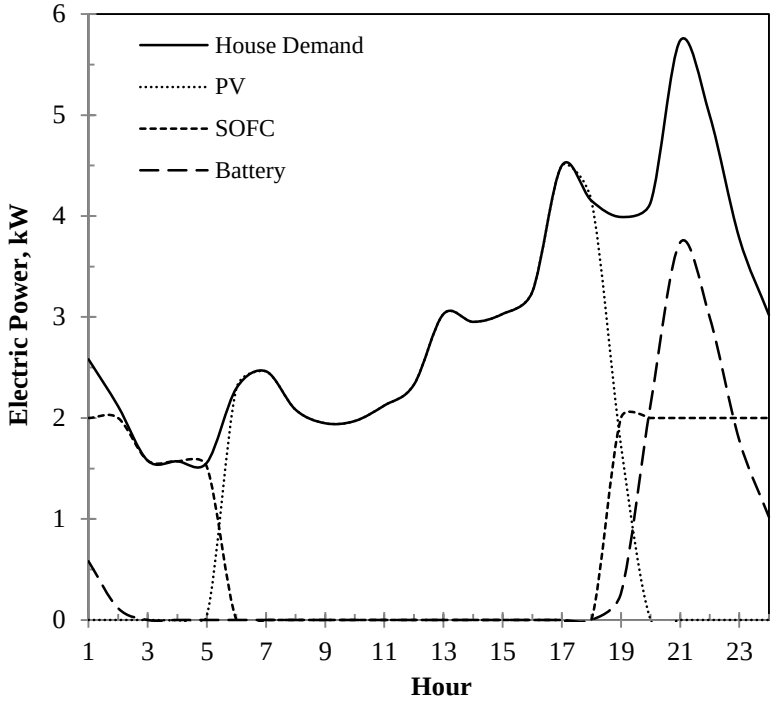

Figure 6.7: Electric power demand of the house and the power outputs of the PV unit, the fuel cell and the battery, for a typical summer day

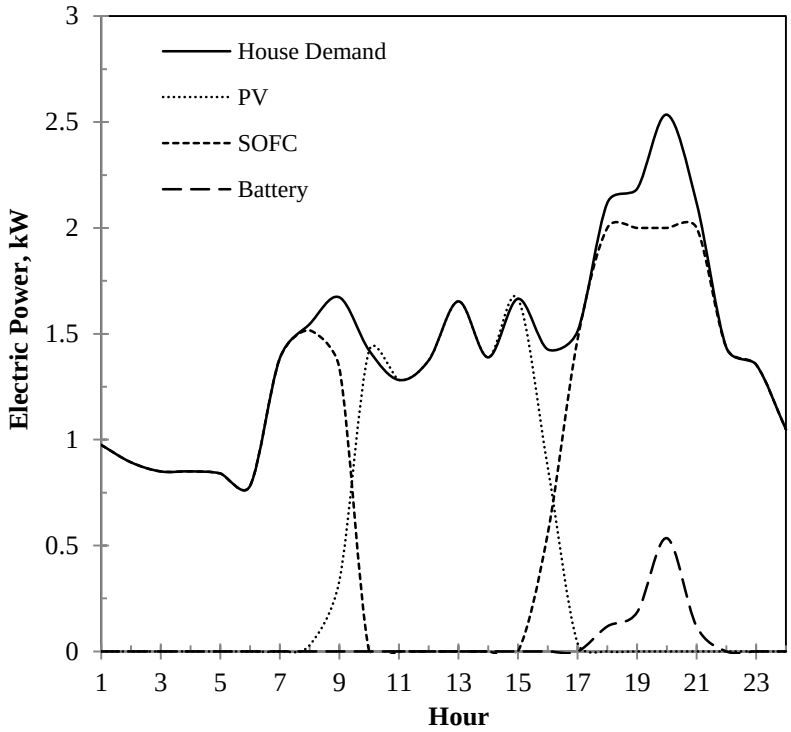

Figure 6.8: Electric power demand of the house and the power outputs of the PV unit, the fuel cell and the battery, for a typical winter day

According to Figures 6.7 and 6.8, the performance of the fuel cell and the battery depends on the electricity demand, since the operating aim is to supply the demand during the times of solar unavailability. For a typical summer day, the greatest demand occurs between 8 and 10 pm, and is higher than the fuel cell nominal capacity. Therefore, not only does the SOFC operate at full load, but also the battery is in service to cover the demand. Between 6 am and 6 pm, there is enough solar radiation to power the house with electricity, and both the SOFC and battery are in stand-by.

The maximum demand of the house for the typical winter day is observed in Figure 6.8 to occur between 6 and 8 pm. However, the demand is not much greater than the fuel cell nominal power. The battery provides a small portion of the demand, and the fuel cell is in operation for almost 19 hours throughout the day.

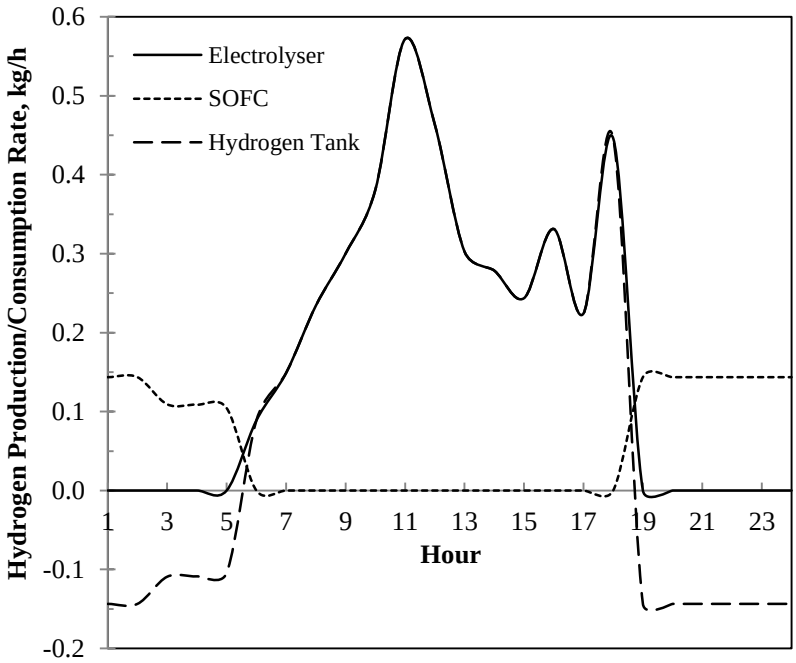

Figure 6.9: Hourly rates of hydrogen production and consumption for a typical summer day

The hourly rates of hydrogen production and consumption for the summer day are presented in Figure 6.9. The solid line in Figure 6.9 represents the hydrogen production rate by the electrolyser. During times of solar availability (6 am-6 pm), almost all of the hydrogen produced is stored in the hydrogen tank.

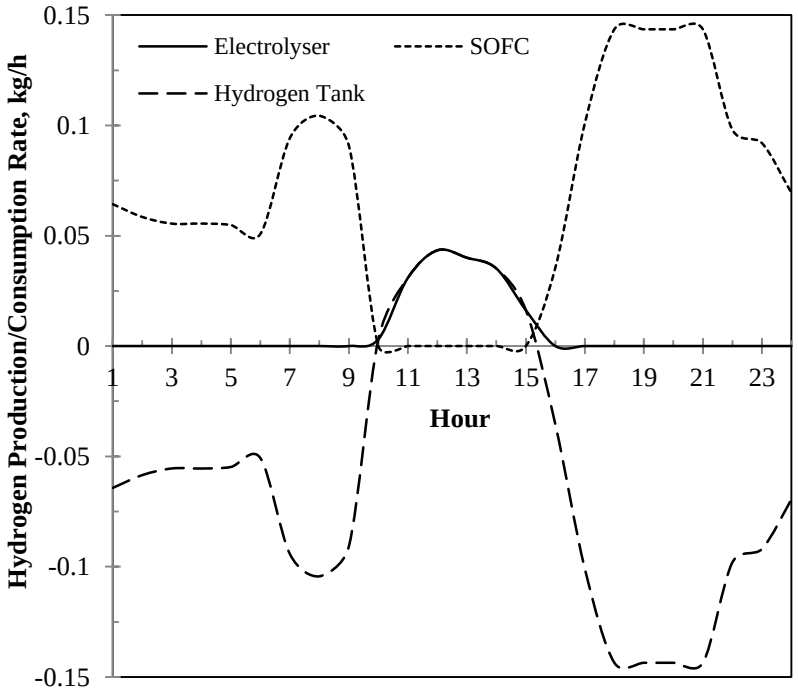

Figure 6.10: Hourly rate of hydrogen production and consumption for a typical winter day

This is the case when the PV power output is high enough to not only supply the demand, but also to feed the electrolyser for hydrogen production. For the time frame between 6 pm and 6 am the SOFC is in operation and is fuelled by the hydrogen stored in the storage tank. Figure 6.10 shows that during the winter day, hydrogen production and storage is less than the rate of hydrogen consumption by the fuel cell. The 19 hours running time of the fuel cell consumes 9.2 times more hydrogen than the amount produced by the electrolyser. Therefore, care should be exercised when sizing the PV-FC-battery system in order to produce and store enough hydrogen to cover the annual consumption rate.

Heat recovery from the fuel cell stack gas is connected to its operation scheme. The change in the pattern of the fuel cell performance affects the rate of the heat recovery, as illustrated in Figure 6.11 for the two typical days discussed above. When the fuel cell operates at its nominal capacity (2 kW), 5.6 kWh thermal energy is recovered from its stack gas (Figure 6.11).

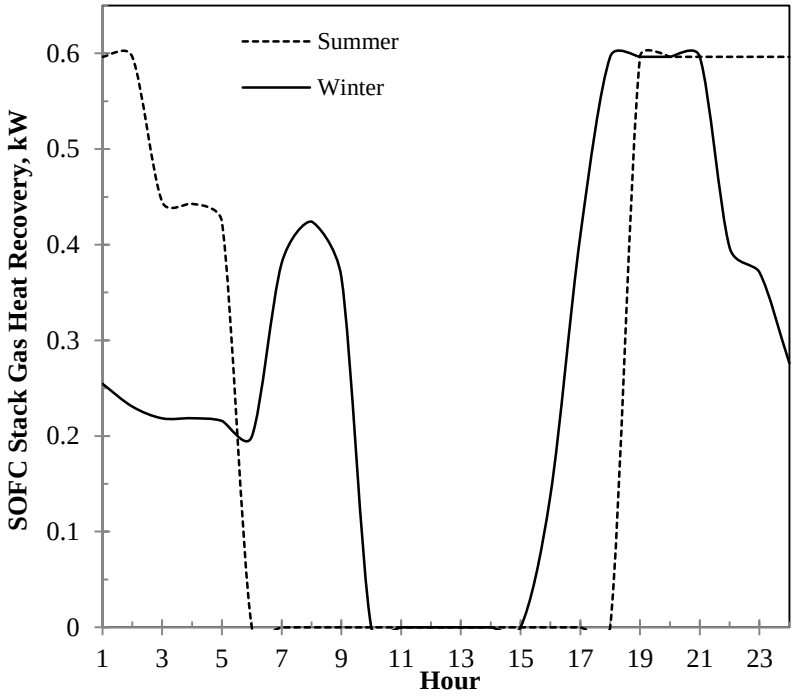

Figure 6.11: Heat recovery from the fuel cell stack gas in two typical days

A performance analysis of the hybrid system on an hourly (or even minute-by-minute) basis is possible using the data for the solar irradiance and electricity demand of the house. To simplify the analysis, average monthly data are used and the results of electricity and hydrogen generation are presented. The fuel cell nominal capacity is

2 kW, which covers almost the entire power demand in the winter day during its operation. The size of the battery is selected based on the maximum need for its power, which is 3.4 kW during the summer day.

With the increase in solar irradiance in the summer months (Figure 6.1), the PV electric power output increases significantly. Therefore, most of the electricity demand is directly met by the PV output, and the fuel cell supplies its lowest share of the demand. Moreover, during periods of solar unavailability, the electricity demand is higher than the fuel cell nominal power, so the battery meets the remaining load. This behaviour is more significant in the warmer months, when there is a greater demand for electricity by the AC system. To quantify the significant difference in the share of these components supplying the demand, the power penetrations of the PV system, the fuel cell, and the battery are shown in Figure 6.12. Due to the lower solar irradiance in the Fall-Winter months, the fuel cell penetration in demand supply is as high as 68% in January and December.

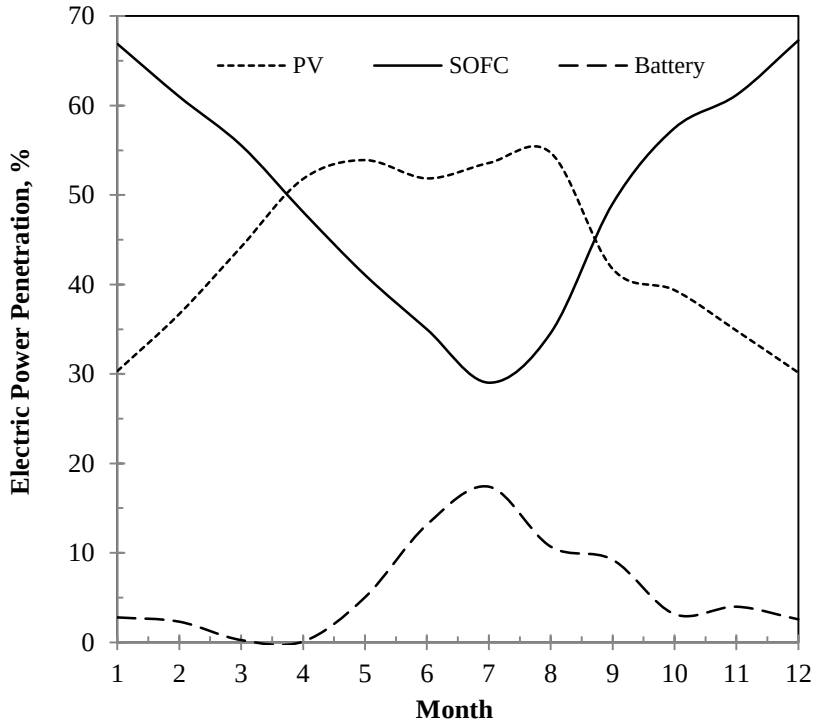

Figure 6.12: PV and SOFC-battery average power penetration

The supply share of the fuel cell decreases with the rise in solar availability in summer months, where the PV unit then reaches its maximum value of share in supply. The share of the battery in power supply depends on the trend of demand and

the capacity of the fuel cell. Figure 6.12 clearly shows the significant contribution of energy storage in the reliability of electricity supply to the residential area.

The power demand and solar irradiance determine the hydrogen flow in the system. With the increased solar irradiance in summer, more hydrogen is generated in the electrolyser, as illustrated in Figure 6.13 (black solid bars). The amount of the stored hydrogen depends on the fuel cell consumption rate. As shown in Figure 6.13, the electrolyser is not capable of producing enough hydrogen to feed the fuel cell demand during the fall-winter months, so the fuel cell is fed by the storage tank. The hybrid system is also analyzed based on exergy. The exergy results show that the PV system has the greatest exergy destruction among the three main components. Due to its lower exergy efficiency relative to the electrolyser and the fuel cell, the PV system is responsible for the greatest share of the exergy destruction of the hybrid system. This is illustrated in Table 6.6, which is based on yearly cumulative exergy destruction. Improving the performance of PV cells and decreasing the operating temperature of the fuel cell are some of the steps that can be taken to reduce the exergy destruction.

Aside from electric energy generation by the residential PV-fuel cell-battery system, heat recovery from the SOFC stack gases is possible with a heat recovery unit.

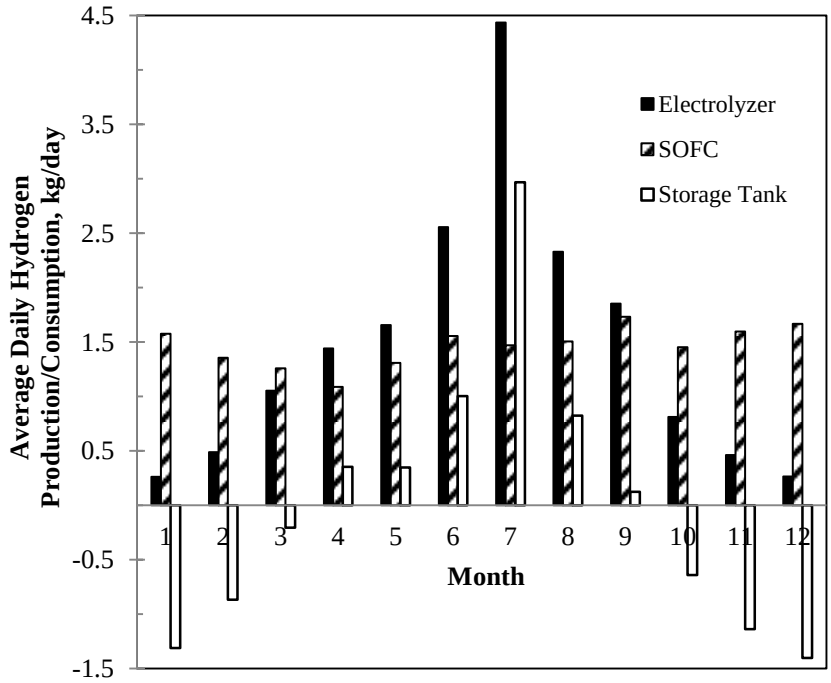

Figure 6.13: Hydrogen production and consumption

Table 6.6: Share of each component of total exergy destruction in the hybrid PV-fuel cell-battery system

Component	Photovoltaic System	Electrolyser	SOFC
Annual exergy destruction, %	89	5.0	6.0

The developed model for System 1 also calculates heat recovery rate from the fuel cell, which depends on its power output. Since the fuel cell power output varies with time, the quantity of generated steam by the heat recovery steam generator varies. A TES system is suggested to store the recovered heat in a hot water tank. The residential hot water demand can be supplied by the stored thermal energy. The TES in System 1 is assessed based on nominal capacity to obtain the maximum water and heat flow rates during the three main phases and the results are presented in Figure 6.14.

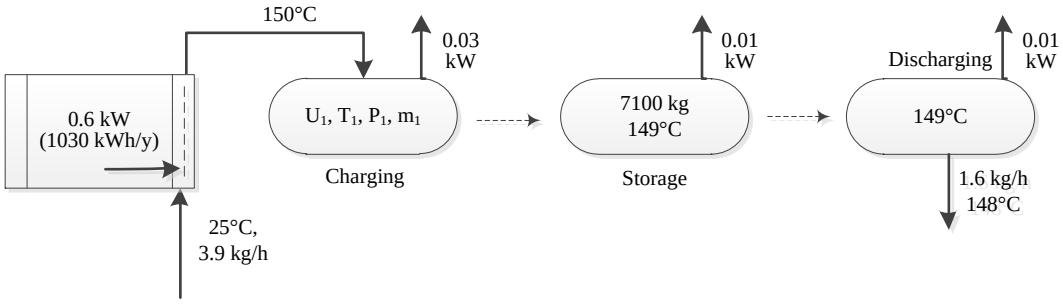

Figure 6.14: Storage medium and heat flow rates in the TES system

According to Figure 6.14, the maximum heat recovery rate from the fuel cell is 0.6 kW, of which 5% is wasted through the system's boundary. The maximum storage capacity of the storage tank is 7100 kg, and the stored hot water is supplied to the house on a continuous rate of 1.6 kg/hr. Heat loss through the tank boundary is lesser during the discharging rate due to the lower water discharge rate.

Figure 6.15 presents the total monthly heat recovery from the SOFC stack gases (solid line with circular markers). The accumulative stored energy in the TES system is also shown in Figure 6.15 as "TES heat content" during the charging phase. The dashed lines with square markers represent the thermal energy stored in the TES system during the months at which the hot water tank is charged. The accumulated heat during spring-summer months is stored in the form of hot water in the storage tank, and it is discharged to supply a part of the hot water demand of the house during fall-winter months. The discharging phase is shown with the square markers in Figure

6.15. The storage tank is discharged continuously starting November through March. The house is then supplied with hot water throughout fall-winter months with an almost constant feed, as represented by the solid line with rectangular markers in Figure 6.15.

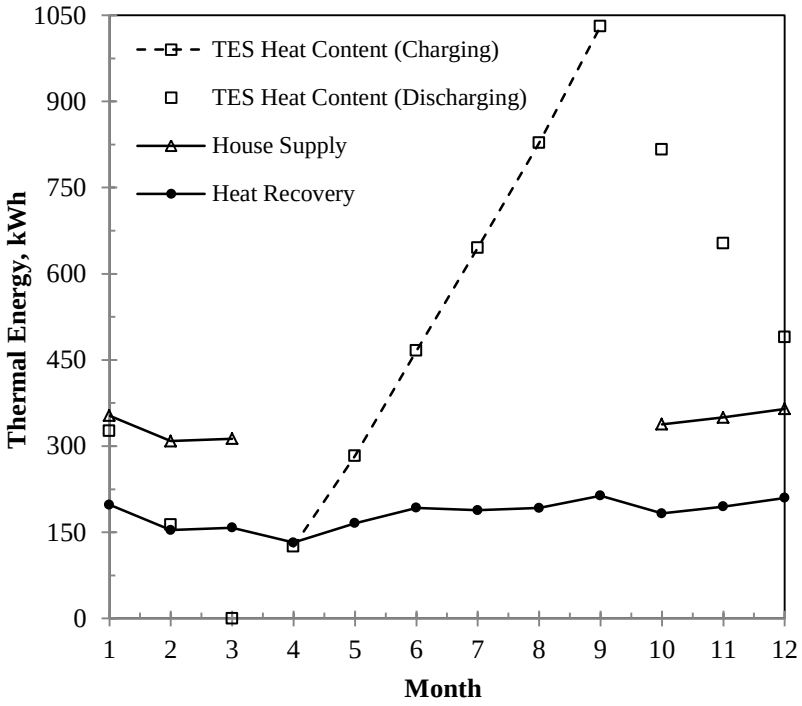

Figure 6.15: Total monthly heat recovery, storage, and supply by the TES

Figure 6.16 presents the same concepts, only based on exergy. From Figure 6.16 one can see that thermal exergy has significantly lower quantities than the corresponding thermal energy values reported in Figure 6.15. Table 6.7 presents the overall heat recovery and efficiencies of the thermal energy storage system of the residential PV-fuel cell-battery system. The annual thermal energy supply to the house is 2028 kWh/year, which is provided as hot water at 130°C. The seasonal heat loss from the TES system is assumed to be 5%, and pressure losses are neglected. The exergy of the supplied hot water is 502 kWh/year, and the overall exergy efficiency of the TES is 85%.

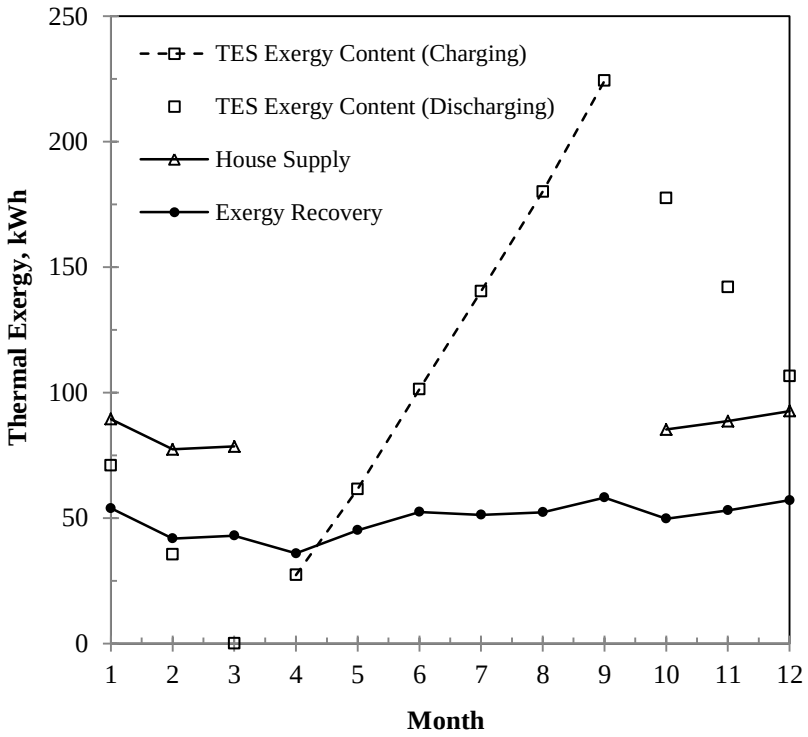

Figure 6.16: Total monthly thermal exergy recovery, storage, and supply by the TES

Table 6.7: Energy and exergy flows and efficiencies in the TES system

Energy			Exergy		
Heat recovery, kWh/year	Heat supply to the house, kWh/year	Overall TES energy efficiency, %	Thermal exergy recovery, kWh/year	Thermal exergy supply to the house, kWh/year	Overall TES exergy efficiency, %
2183	2028	93	594	502	85

6.1.2.2 Cost evaluation

Table 6.7 shows the results of the component sizing and their relevant costs. The costs per unit of energy ($/kW) presented in Table 6.8 are based on data from the literature. Although efforts have been made to use appropriate values for the costs of operation and maintenance, the values used are approximate and are in US dollars.

The unit cost of electricity depends on the total estimated cost and the total amount of electricity generated over the lifetime of the system. The system is sized to supply the total electricity demand of the house, which for the present case study are the surfaces under the graphs in Figure 6.2. Therefore the unit cost of electricity is calculated to be 0.84 $/kWh. The unit cost of electricity depends on system size, location, annual solar availability, land use, interest rates, and many other factors.

However, a similar range was obtained by Lagorse et al. (2008). They perform their economic analysis for a site located in France, and the predicted electricity cost is 0.9 $/kWh, based on 2008 currency exchange rates. The major difference between the systems is the use of PEM fuel cells in the model by Lagorse et al. (2008) and SOFCs in the present work.

Table 6.8: Equipment purchase and operation and maintenance costs

System and component	Nominal size	Unit cost	Cost ($\times 10^3$)
PV system[*]			
PV modules	37.17 kW	5156 $/kW	$ 191.6
O&M[**]		47 $/kW. year	1.747 $/year
Fuel Cell system[***]			
SOFC	2 kW	2297 $/kW	$ 4.594
O&M		5% of purchase	0.200 $/year
Hydrogen storage			
Stored hydrogen	168.86 kg (5623.04 kWh)		
Hydrogen storage tank	83.68 m^3 at 25 bar, 300 K	4 $/kWh	$ 22.51
O&M		3% of purchase	0.676 $/year
Electrolyser			
PEM electrolyser, installation	29.74 kW	587 $/kW	$ 17.44
O&M		5% of purchase	0.872 $/year
Battery			
Battery, installation	12.38 kWh	650 $/kWh	$ 8.050
O&M		3% of purchase	0.403 $/year
Total hybrid system capital cost			$ **244.2**
Operation and maintenance			3.897 $/year
Total O&M cost over the system lifetime (25 years)			$ **97.43**
Total estimated system cost over 25 years			$ **341.6**

[*]Source: SunPower (2012)
[**]Source: Enbar (2010)
[***]Source: Braun et al. (2011)

6.1.2.3 Exergoeconomic results

The results of the energy and exergy analyses in section 6.1.2 are utilized to perform an exergoeconomic analysis of the hybrid PV-fuel cell-battery system for a Canadian detached house. Table 6.9 presents the unit cost of the products of the main components of the hybrid system. The products of the PV unit and fuel cell are

electricity, while the electrolyser produces hydrogen. Table 6.9 also shows the relative cost increase and exergoeconomic factor. According to Eqs. 5.156-5.158, the relative cost increase (r) is calculated in relation to the unit cost of the fuel consumed by the component. The fuel (exergy input) to the PV system is solar irradiance, which is available abundantly, and free of charge. Thus it would make no sense to calculate r for the PV system.

However, to illustrate how economically effective the PV systems are, the relative cost increase is calculated based on the common unit cost of electricity in the market. An average 12.6 ¢/kWh in Ontario (DirectEnergy, 2012) is used in the calculation for the PV system. Therefore, unit cost of the generated electricity by the PV system is compared with this value. Table 6.9 shows a significant difference between the PV output electricity price and the price of electricity by conventional power plants.

Table 6.9: Exergoeconomic evaluation of the main component of System 1 (2 kW SOFC)

Component	PV	Electrolyser	SOFC
Unit cost of product, $/kWh	0.268	0.505	1.47
Levelized capital cost rate, 10^3 $/year	8.41	0.736	1.55
Annual cost of exergy destruction, 10^3 $/year	2.86	2.67	5.64
Relative cost increase (r)	1.13	0.88	1.92
Exergoeconomic factor (f)	0.772	0.370	0.231

The unit costs of electricity generation are considerably higher than the prices for electricity generated using conventional, commercial methods. Moreover, due to the sequential increase of the unit costs, the relative cost increase differs significantly for the main components. The exergoeconomic factor, f provides useful information about the cost effectiveness of the system components. Since the PV system has the highest exergy destruction rate among the three main components of the residential hybrid PV-fuel cell-battery system (Table 6.6), its exergy destruction cost rate is significant enough comparing to its capital cost rate. However, the specific purchase costs of the photovoltaic panels are still expensive, despite recent developments in technology. Therefore, higher values are obtained for exergoeconomic factor of the PV system. This is well illustrated by exergoeconomic factor of 0.772. The exergoeconomic values of the electrolyser and the SOFC explain a similar characteristic of these components; cost of exergy destruction is significant.

Figure 6.17 shows the product unit cost of the main components (in dollars per unit of exergy) during each month of the year. Figure 6.17 illustrates the significant effect of the intermittency of the renewable energy resource. The hybrid system components are selected to work at their nominal capacities. However, due to the nature of the demand and the daily solar irradiance pattern, they have lower power/product outputs. This affects corresponding product costs. For example, the PV system performs best during months with higher solar irradiance, and its power output is closer to its nominal capacity. Therefore, it appears that the purchase cost is paid-off at a higher rate when the PV has its better performance.

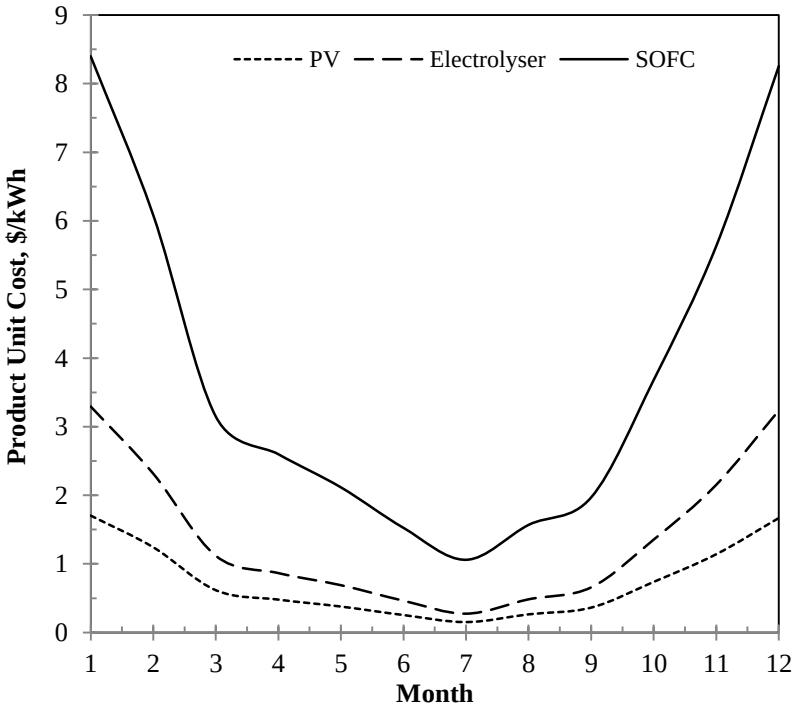

Figure 6.17: Unit exergy cost of products of the main components of the hybrid system for each month of operation (with an SOFC capacity of 2 kW)

The unit cost of hydrogen produced in the electrolyser is a function of the cost of the electricity generated by the photovoltaic system. This is the reason that the hydrogen production cost is lesser during the spring-summer months. Although the fuel cell is more active during the fall-winter months, the cost of the electricity generated by the SOFC is higher than the cost in spring-summer months. The reason for this is related to the increased cost of the hydrogen produced in the electrolyser.

6.1.2.4 Effect of SOFC nominal capacity

The changes in the capacities of the PV and battery systems with increasing fuel cell nominal power capacity are shown in Figure 6.18. A larger fuel cell capacity implies higher rates of hydrogen consumption. To supply the hydrogen demand, the sizes of the PV unit, the electrolyser and the hydrogen storage tank should be larger. However, the need for the battery power output decreases with the size of the fuel cell.

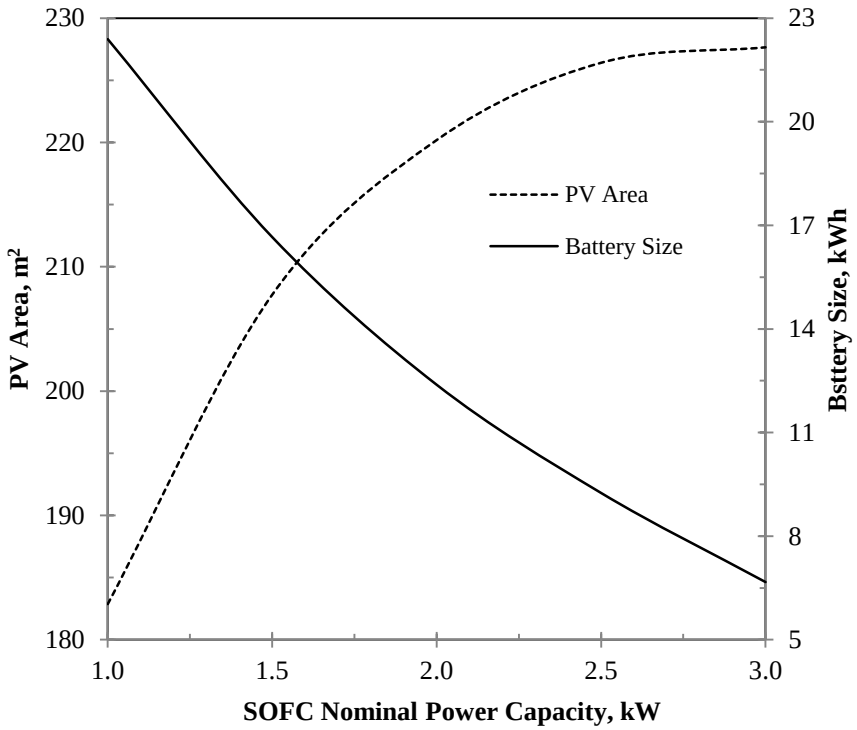

Figure 6.18: Variations of PV and battery capacities with SOFC nominal capacity

The unit cost of electricity and hydrogen varies as the nominal capacities of the components change with the fuel cell size. Although the PV size increases with fuel cell capacity, the unit cost of electricity produced by the PV system remains almost unchanged. The cost of hydrogen production by the electrolyser slightly decreases. Figure 6.19 shows that the fuel cell responds differently to a change in its nominal capacity. At 1.7 kW power capacity, the unit cost of electricity generated by the SOFC reaches its lowest value. The cost of electricity and hydrogen presented in Figure 6.19 are highly dependent on the power demand and solar irradiance trends. According to the exergoeconomic cost balance, unit cost of a purchased component decreases if it is in operation more frequently.

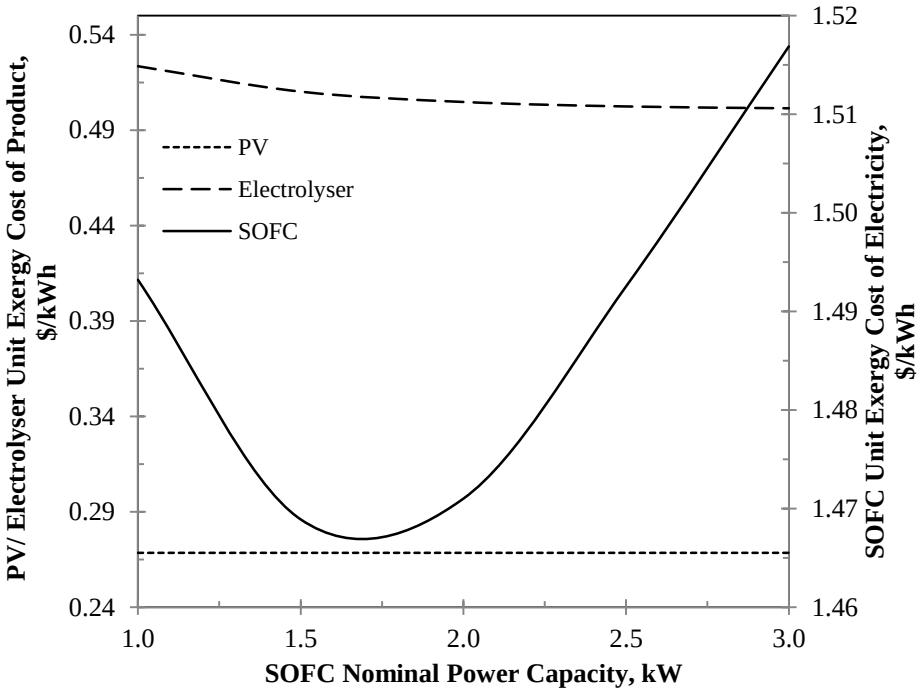

Figure 6.19: Effects of SOFC capacity on product unit costs components of System 1

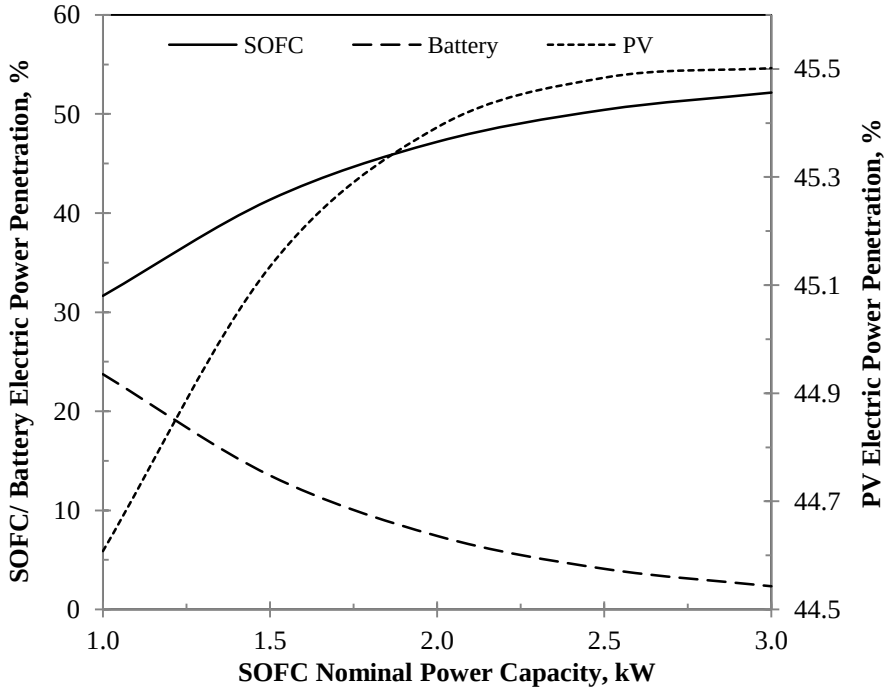

Figure 6.20: Power penetration share of the hybrid PV-fuel cell-battery system vs. the nominal capacity of the SOFC

To explain this, power penetrations of the power production components are presented in Figure 6.20. There is a slight increase in the share of the PV in supplying the demand, from 44.6 to 45.5%. However, the SOFC share increases significantly

(by 20%). The battery share in supplying the demand decreases as the share of the fuel cell increases, since the battery is used as a back-up for the fuel cell.

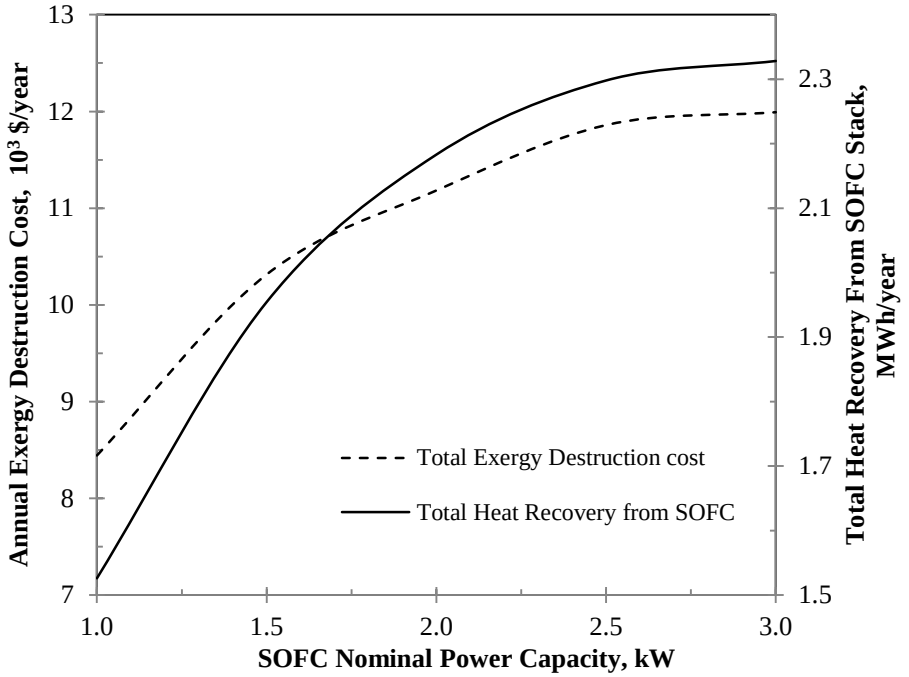

Figure 6.21: Effects of SOFC nominal capacity on the total annual cost of exergy destruction and total annual heat recovery from the fuel cell stack

One advantage of utilizing a fuel cell with a larger capacity is the extent of heat recovery from the stack gases. As shown in Figure 6.21, heat recovery from the stack gases increases in a larger size fuel cell, primarily due to the increase in the stack gas mass flow rate. However, the total annual exergy destruction cost of the hybrid system increases with the size of the fuel cell. There may be a trade-off between these parameters. Higher heat recovery is an advantage in supplying the house with hot water or heat; however, an increasing cost of exergy destruction should normally be avoided.

The components of the hybrid system are connected through the exergoeconomic analysis. The unit cost of hydrogen production slightly decreases with increasing fuel cell capacity, while the exergoeconomic factor of the fuel cell increases from 0.17 to 0.30 (Figure 6.22). Values closer to 0.5 for the exergoeconomic factor suggest that the capital costs and the exergy destructions are reasonably balanced. The fuel cell lifetime is as short as 20,000-40,000 hours; a complete overhaul is thus required every 3.5 years (20,000 hours lifetime), involving changing the cells and some of the hardware. Increasing the fuel cells' lifetime, decreasing the purchase cost, and

improving ion and electron transfers in the cells all improve the exergoeconomic factor.

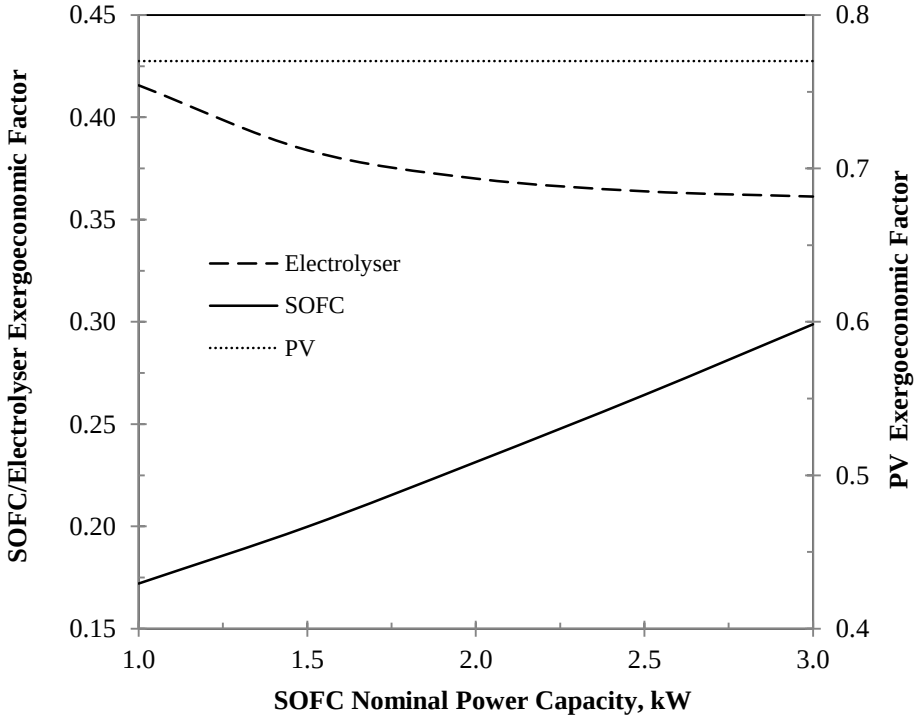

Figure 6.22: Variation of exergoeconomic factor with SOFC nominal size

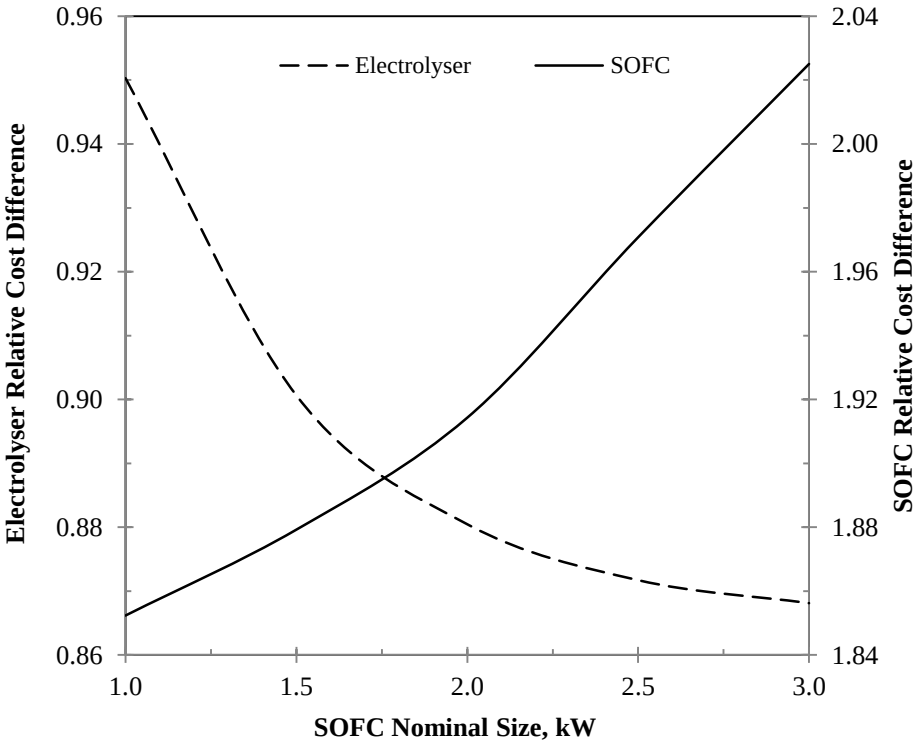

Figure 6.23: Variations of relative cost difference with SOFC nominal size

The exergoeconomic factor of the electrolyser decreases as the capacity of the fuel cell increases, due to the increase in the capacity (and therefore the increase in the purchase cost) of the electrolyser. The nominal power capacity of the fuel cell has a positive effect on the hydrogen production cost in terms of relative cost difference of the electrolyser. Figure 6.23 shows that the cost difference between the input electricity to the electrolyser (as fuel) and the generated hydrogen (as product) decreases when the fuel cell has a larger capacity. However, the relative cost difference of the fuel cell increases.

6.1.3 Optimization of System 1

According to the above mentioned graphs, the performance of the residential hybrid PV-fuel cell-battery system is a function of the fuel cell nominal capacity. Other parameters such as the SOFC stack temperature and fuel utilization have effects on the fuel cell performance and on the hybrid system in general. Therefore, these three main parameters are considered as decision variables to find optimal points of design and operation of System 1. The hybrid system's exergy efficiency and total purchase cost are considered as the objective functions. The bounds of the decision variables are discussed and presented in Chapter 5.

The fuel cell nominal capacity is changed from 1 to 3 kW, its stack temperature varies between 820 and 1020°C, and the fuel utilization is changed from 0.6 to 0.9. The obtained optimal points based on the objective functions form a Pareto frontier, which is presented in Figure 6.24, which shows that exergy efficiency varies between 9.2-12%. All the points in Figure 6.24 represent an optimal point, and are non-dominant in respect to each other. Table 6.10 presents the optimal values of the decision variables at three important points on the Pareto frontier. These three points are named A, B, and C on Figure 6.24. Point A shows minimum total purchase cost (minimum exergy efficiency), while point B is an optimal point at which the exergy efficiency is a maximum (maximum total purchase cost). In some optimization problems, variations of the efficiency and cost are significant and a decision should be made regarding choosing one of the optimal points presented by the Pareto frontier. Both the optimal total purchase cost and the exergy efficiency of System 1 vary considerably. This mainly is due to the size and expensive capital cost and of the PV panel. Selecting an optimal point at which the hybrid system has its best operating

specifications is in the designers' hands. Another objective function based on which an optimum stack temperature can be selected is the heat recovery potential from the fuel cell.

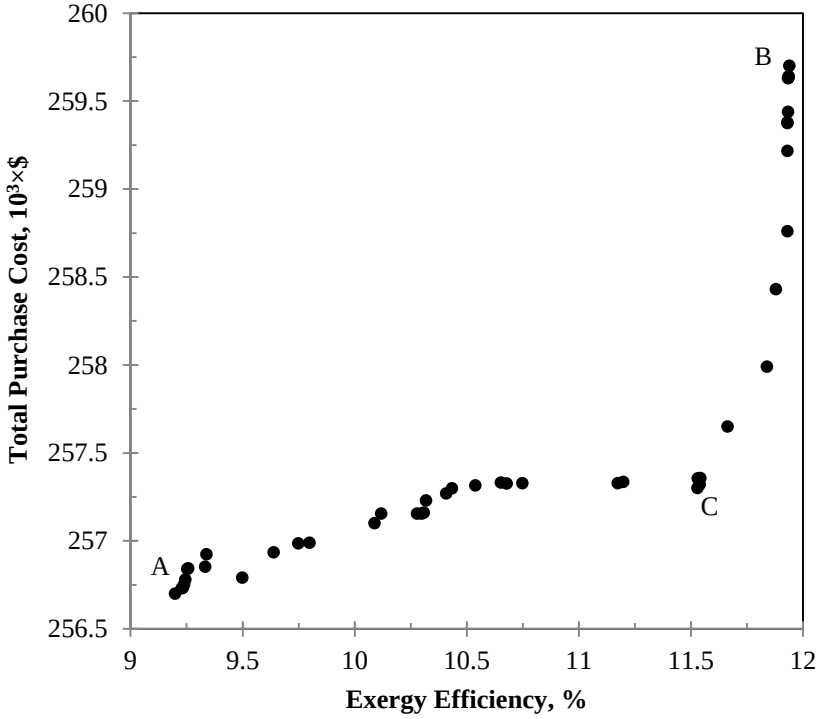

Figure 6.24: Pareto frontier; optimal values of exergy efficiency and total purchase cost of the residential PV-fuel cell-battery system

Table 6.10 shows that point A has a higher stack temperature. Therefore, the hybrid system has higher heat recovery potential at point A, although its exergy efficiency is lower. Point C on Figure 6.24 is the closest point to the equilibrium point. The equilibrium point is where both objective functions have their absolute optimal points. For instance, the exergy efficiency is at a maximum and the total purchase cost is at a minimum at the equilibrium point.

Table 6.10: Optimization results for the residential hybrid PV-fuel cell-battery system at three optimal points

Optimal point	Decision variables			Energy efficiency, %	Exergy efficiency, %	Total purchase cost, 10^3×$	c_{SOFC}, ¢/kWh	Q_{hrsg}, MWh/y
	SOFC capacity, kW	Fuel utilization	Stack temperature, K					
A	1.3	0.9	1140	10.5	9.2	256.7	139.6	3.5
B	1.9	0.83	1105	12.3	11.9	259.7	141.4	3.3
C	1.6	0.72	1132	12.1	11.5	257.3	140.4	3.4

According to Table 6.10, the unit exergy cost of electricity generation by the fuel cell is higher at point B since heat recovery potential at this point is less than points A and C. In addition, higher energy efficiencies are achieved than exergy due to the lower exergy content of the recovered heat.

A comparison is performed between the residential hybrid PV-fuel-cell-battery system, which utilizes energy storage options, and two other systems: a simple PV-fuel cell system that does not benefit from energy storage, and a stand-alone PV-battery system. The simple PV-fuel cell system is only composed of a solar photovoltaic system and a fuel cell stack, in which the PV system operates when solar energy is available and the fuel cell system powers the residential area during the hours of PV power unavailability. This system benefits from no energy storage, and the fuel cell is fed by natural gas. Li-ion battery is the only energy storage option in the stand-alone PV-battery system, which stores the excess electricity generated by the PV during solar irradiance availability. The stand-alone PV-battery system has a seasonal storage characteristic. Table 6.11 presents the comparison between these three systems, which are distinguished as System 1, simple PV-FC system, and stand-alone PV-battery. When considering the simple PV-fuel cell system, the nominal capacities of the PV and the SOFC are selected to meet the maximum electric demand of the house. This strategy increases the share of the photovoltaic system in the power supply.

Table 6.11: Comparison of System 1 with a simple PV-fuel cell with no energy storage options, and a PV-battery system

Parameter	Simple PV-FC system	PV-Battery	System 1
PV nominal capacity, kW	5.7	17.9	37.2
SOFC nominal capacity, kW	5.7	0	1.6
Battery nominal capacity, kWh	0	3037	12.4
PV annual power penetration, %	30.2	42	46
SOFC/battery annual power penetration, %	69.8	58**	54*
Fossil fuel consumption, kg/year	1796	0	0
CO_2 emission, 103 kg- CO_2/year	5.6	0	0
Energy efficiency, %	33.2	15.4	12.1
Exergy efficiency, %	29.9	16.5	11.5
Cost of electricity, $/kWh	0.27	25	0.84

*SOFC+battery
**Battery only

According to Table 6.11, the simple PV-FC system consumes almost 1800 kg of natural gas per year, which is accountable for the release of 5.6 tonnes of CO_2. Both systems are considered to power a Canadian detached-house with an annual 16 MWh electricity consumption. The developed residential PV-fuel cell-battery system benefits from hydrogen and thermal energy storage options and is driven solely by renewable solar energy. As indicated in Table 6.11, the power penetration of the PV system is 46%, which is 16.2% and 9.5% higher than the power penetration of the simple PV-FC and the stand-alone PV-battery systems, respectively. The stand-alone PV-battery system meets the same electricity demand; however, its cost of electricity generation is significantly higher. This is due to the expensive purchase cost (650 $/kWh) and short lifetime (almost 5 years) of the battery. The calculated value for the cost of electricity generation by the stand-alone PV-battery system may be surprisingly high; however, similar results are obtained by Lazou and Papatsoris (2000). They report up to 11.6 $/kWh for electricity generation by a similar system operating in different regions of Europe based on 150 $/kWh as the purchase cost of lead acid batteries in 1998. Other studies report the unit cost of electricity generation of grid-integrated PV-battery systems, which eliminates the need for seasonal electricity generation, around 1.8 $/kWh.

6.1.4 Closure

Several useful insights are obtained via the exergoeconomic analysis of a hybrid photovoltaic-fuel-cell-battery system that supplies the electricity demand of a Canadian detached house and provides a part of the thermal demand through heat recovery from the fuel cell stack gases. The energy and exergy analyses results are based on a system with a fuel cell having a 2 kW nominal capacity. The electricity demand of the house in the spring-summer months exceeds the demand in the fall-winter months. The battery supplies a considerable share of the demand on a typical summer day (maximum 3.6 kW power rate), while on a typical winter day its share is less than 0.5 kW. The hydrogen production and consumption rates are dependent on the power demand and solar availability. For solar irradiance data for Toronto in 2011 and electricity demand of a Canadian house, a 37.17 kW PV module is selected. The electrolyser is capable of producing 4.5 kg/day hydrogen on a typical day. Most of the hydrogen produced by the electrolyser during spring-summer days is stored in a seasonal storage tank. The economic investigation of the hybrid system reports an

average cost of electricity to be 0.84 $/kWh for 25 years of operation. Since the economic analysis does not consider the costs of irreversibility, the exergoeconomic analyses are performed to estimate the cost of the electricity and hydrogen. The electricity and hydrogen unit costs are observed to vary with solar availability and demand pattern. The minimum costs occur during the spring-summer months, when the systems operate at their maximum capacities. Also, the size of the fuel cell has a considerable effect on the exergoeconomic results. The nominal capacity of the fuel cell at an optimal point is found to be 1.6 kW, based on the optimization results. The optimal exergy efficiency varies from 9.2 to 11.9%.

6.2 System 2: Integrated Renewable Energy-Based System for Baseload Power Generation

The results of energy, exergy and exergoeconomic analyses are presented here for System 2, which is an integrated renewable energy-based system for baseload power generation. The system is comprehensively described in Chapter 4, and the required equations for the analyses are presented in Chapter 5. This system is composed of three separate renewable energy-based power generation sub-systems. These systems are Wind-CAES, PV-hydrogen-fuel cell (PV-H_2-FC), and biomass-solid oxide fuel cell-micro gas turbine (biomass-SOFC-MGT). The results of the analysis of each individual system are presented here. Also, the performance of the overall, integrated system is studies based on energy and exergy flows of the sub-systems. Moreover, optimal points of design and operation are obtained in an optimization process.

6.2.1 Assumptions and Data

The modeling and analyses are performed based on the following assumptions and data.

- Transient behaviour of the systems is not considered, although the weather data has transient characteristics.
- The wind turbine power output is 3.5 MW (12.3 m/s rated wind speed), with $700/kW capital cost (Greenblatt et al., 2007).
- The CAES system is considered to have 168 hours of air storage capacity.
- The equivalent natural gas price (natural gas plus carbon dioxide emission price) is $5/GJ.

- The compression pressure range for the parametric study is 81, 64, and 49 bar.
- The expansion pressure range for the parametric study is 64, 49 and 36 bar.
- Hourly wind speed data of Port Colbourne, Ontario, Canada are used for wind power calculations (NCDIA, 2011).
- Hourly solar irradiance data of Toronto, Ontario, Canada are used for PV power calculations (UTM, 2012).
- The reference environment state, taken as similar to the ambient condition, for the exergy analysis is set to 1 bar and 298 K.

The economic and exergoeconomic analyses are performed based on data presented in Table 6.12.

Table 6.12: Unit costs of components

Component	Wind turbine	Air compressor	Gas turbine	PV	SOFC	Electrolyser	Bio-SOFC-GT
Capital cost, $/kW	700[a]	175[a]	185[a]	5400[b]	2300[c]	590[d]	3800[e]

[a]Data adapted from Greenblatt et al. (2007)
[b]Data adapted from Enbar (2010); SunPower (2012)
[c]Data adapted from Braun et al. (2011); McIlveen-Wright et al. (2011)
[d]Data adapted from NREL (2009)
[e]Data adapted from McIlveen-Wright et al. (2011)

6.2.2 Results and Discussion

Investigation of the integrated renewable energy-based baseload power generation system is performed for 5 MW solar PV and 25 MW biomass-SOFC-GT power outputs. Since each sub-power generation system is independent from the rest, the results are presented separately. In this section the results of modeling, and energy and exergy economic analyses of the systems are presented. When discussing the monthly performance of the Wind-CAES system, the compression ratio of the compressor stages is set to 8, while the expansion ratio of each stage of the gas turbine is considered to be 6. The pressure difference between the compressed air storage system and the gas turbine operating pressure is regulated by a pressure regulator, considering the pressure losses in the pathways and pipelines (Greenblatt et al., 2007).

6.2.2.1 Wind-CAES system

The Wind-CAES system power output accounts for 94% of the baseload power supply. However, since wind power is inherently intermittent, the shares of the wind park and the CAES systems in providing the grid with electricity vary.

Table 6.13: Nominal capacity and annual flows in the components of the Wind-CAES system

Parameter	Value
Wind turbines nominal capacity, MW	1246
Air compressor nominal capacity, MW	606
GT nominal capacity, MW	470
Compressed air storage, 10^6 kg/year	4449
Gas turbine air consumption, 10^6 kg/year	4226
Gas turbine fuel consumption, 10^6 kg/year	105
Wind turbines power output, TWh/year	4.74
Share of wind turbines in supplying the demand, TWh/year	3.93*
Air compressor electricity consumption, TWh/year	0.817
Gas turbine electric power generation, TWh/year	1.36
Thermal exergy recovery from intercoolers, TWh/year	0.247
Thermal exergy of GT flue gas, TWh/year	0.059
Exergy of the stored air, TWh/year	0.173
Carbon dioxide emission, 10^6 kg/year	95
Electricity demand, TWh/year	4.12
Wind power penetration, %	95*
Gas turbine power penetration, %	33
Energy efficiency, %	37
Exergy efficiency, %	33

*Wind turbines excess electricity generation is fed to the local grid. In some scenarios, if the CAES system is fully charged the excess electricity generation by the wind turbines is dumped. Here, otherwise is considered.

The mass, energy, and exergy flows in the Wind-CAES system of System 2 are presented in Tables 6.13 on an annual basis. The annual flows are given here since the integrated systems are powered by renewable energy resources. These sources of energy have temporal behaviour, and the system components may not operate at their full load.

Comparing the required wind power generation by the Wind-CAES system with the predicted value in Table 4.3 signifies the negative impact of the wind intermittency on the system size. Due to the variation in wind speed, 1246 GW wind

power is necessary for the Wind-CAES to supply 470 MW baseload electric power. If the wind speed was always available at the wind turbine rated power (12.3 m/s), only 662 MW wind power would be required. The intermittency of wind energy also affects the required capacities of the air compressor. Moreover, the data of Table 6.13 is used to validate the results of the developed model. According to Greenblatt et al. (2007) the ratio of GT power output to the air compressor power input is almost 1.5, which in the current research is 1.6. The slight difference is due to the difference in pressure ratios considered in the analyses. Moreover, they report the unit cost of electricity by the Wind-CAES system as 6 ¢/kWh based on the currency value in 2007. The current research reports 7 ¢/kWh for the unit cost of electricity production.

Figure 6.25 shows the energy flows of the CAES system for 1 MW GT electric power output. According to this figure, 0.66 MW electric power and 1.23 MW fuel consumption are required to generate 1 MW electricity by the gas turbine. Heat recovery potential from the compressed air and the gas turbine exhaust gases are also presented in Figure 6.24.

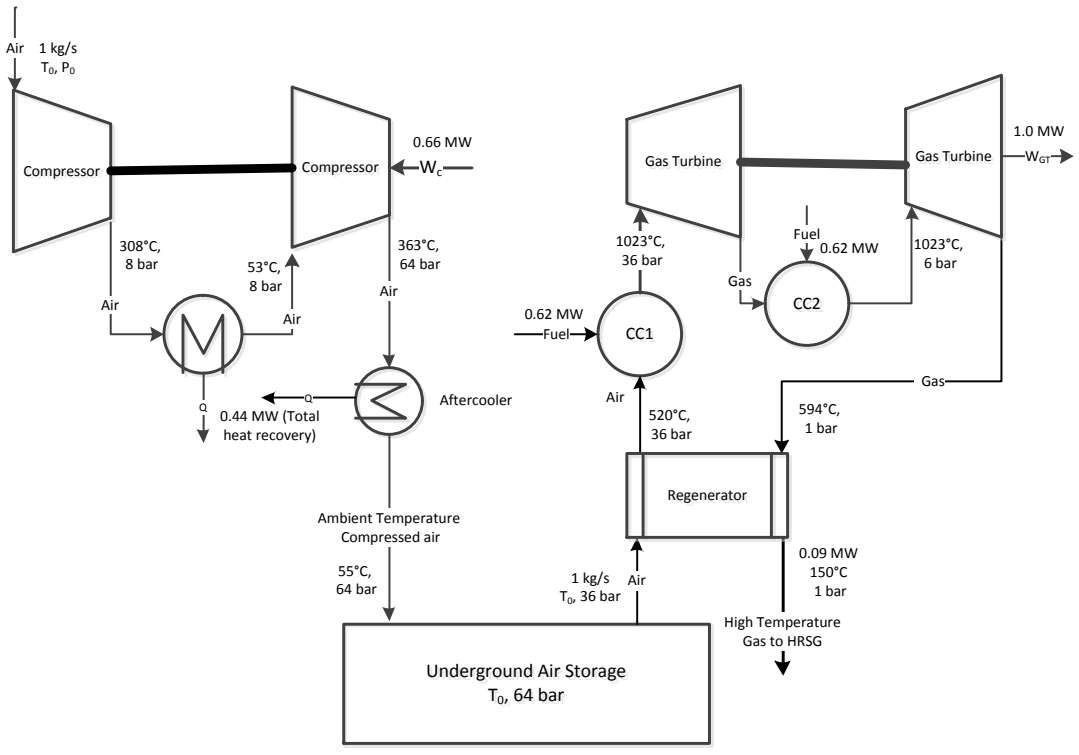

Figure 6.25: Energy flows in the CAES-GT system

Therefore, round-trip efficiency of the CAES-GT system is $\frac{1}{0.65+1.23} = 53\%$. This calculation is regardless of the heat recovery potentials from the compressor and the gas turbine, which raises the energy efficiency to 77%. However, thermal energy and electricity have different qualities, based on exergy concepts. Thus, the exergy efficiency is calculated to obtain a better insight of the nominal round-trip efficiency of the CAES-GT system. The thermal exergy recovery from the CAES system with 1 MW power output is 0.17 MW, which results in 62% exergy efficiency.

Since the available wind power varies with time, the performance of the Wind-CAES system is investigated on an hourly basis, and the results are presented for each month of the year. Power penetration is the ratio of the electricity provided by the system to the electricity demand. Power penetrations for the wind park and the CAES system are shown in Figure 6.26.

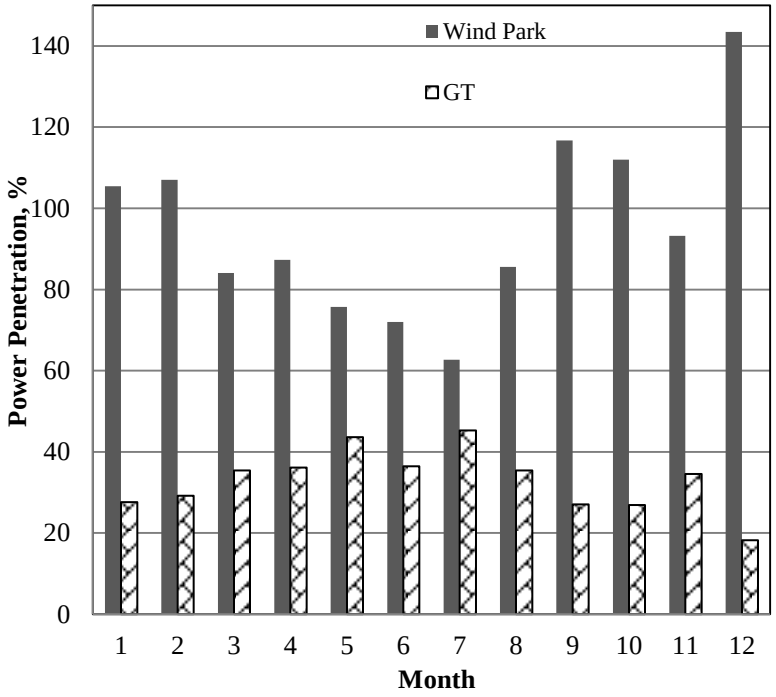

Figure 6.26: Monthly power penetration of wind park and GT (r_c = 8, r_{GT} = 6, h_s = 168)

There is no specific trend to the shares of the two power supply systems, since they strongly depend on the wind resource. However, the wind park plays a major role in the Fall-Winter months. Figure 6.26 also shows that power penetration of the wind park for some months of the year is more than 100%. During these months, the power output of the wind park exceeds the demand; however, the CAES system is fully charged, so there is no need to compress air with the electricity. In some analyses, the

wind park's excess electricity is dissipated or used for space heating unless there is the possibility of selling the electricity to the grid.

The CAES system is charged (refilled with compressed air) when the wind park power output exceeds the electricity demand. It is discharged when there is a need for power production otherwise met by the gas turbine. Therefore, the charging/discharging rates change as illustrated in Figure 6.27. The system component (wind turbines, air compressor, gas turbine) capacities are selected to maintain a net positive quantity of stored air in the cavern throughout the year. The data in Figure 6.27 is presented in million kg of compressed air per month, to quantify the differences between storage and consumption for each month.

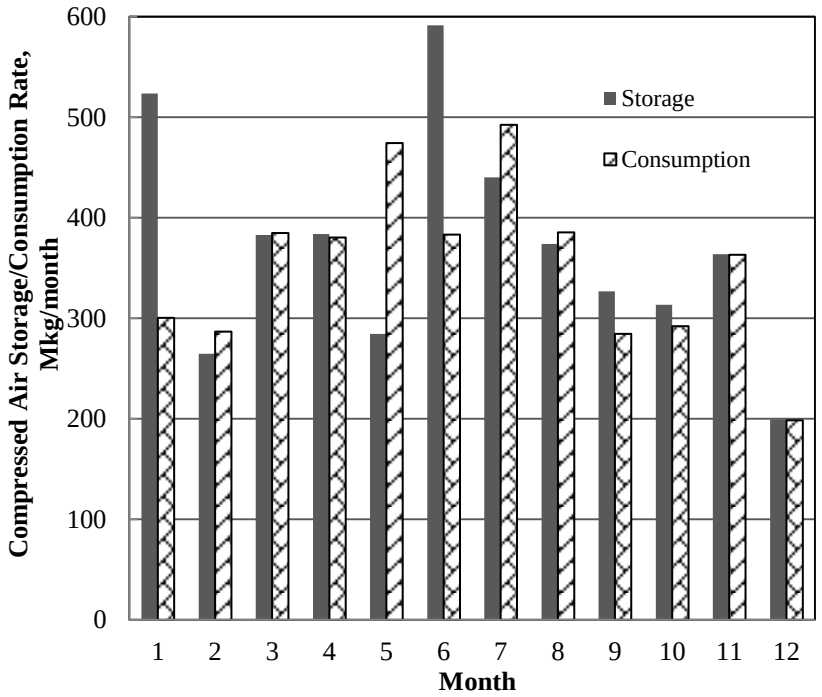

Figure 6.27: Charging and discharging of CAES system (r_c = 8, r_{GT} = 6, h_s = 168)

Wind-CAES systems are generally not carbon emission-free power generation plants. In fact, if the compressed air is heated by combustion, some levels of carbon and other greenhouse gas emissions are released. In this paper, the compressed air undergoes a combustion process with methane. Figure 6.28 illustrates monthly changes in fuel consumption and carbon dioxide emissions. They are proportional to the gas turbine operation and the need for excess power generation. With the performance of the Wind-CAES system described, a parametric study is performed considering changes in the compressor and gas turbine pressure ratios. For a fixed

storage cavern pressure of 64 bar (implying a compressor stage pressure ratio of 8 since two compression stages are considered), the change in the wind power penetration is shown in Figure 6.29, for various gas turbine pressure ratios.

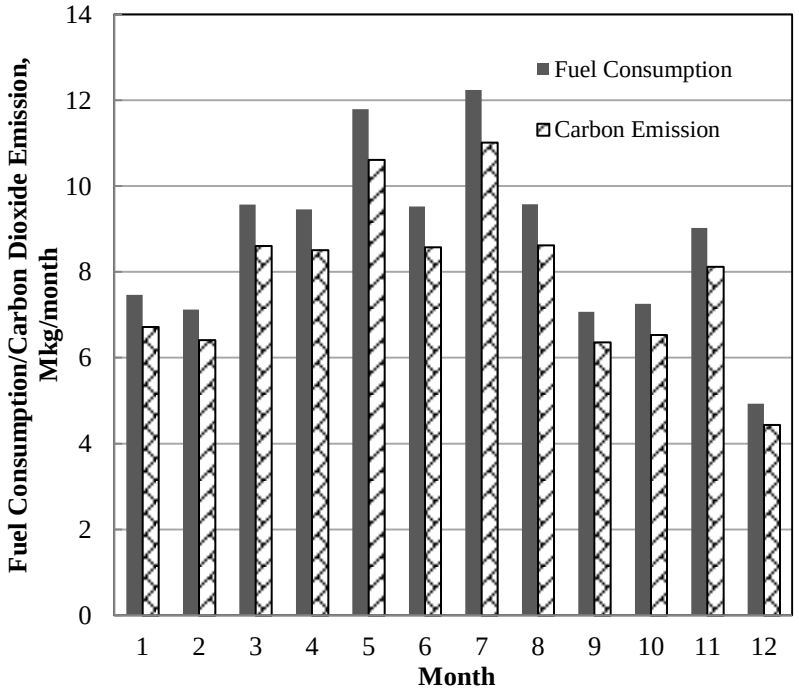

Figure 6.28: Fuel consumption and CO_2 emission rates (r_c = 8, r_{GT} = 6, h_s = 168)

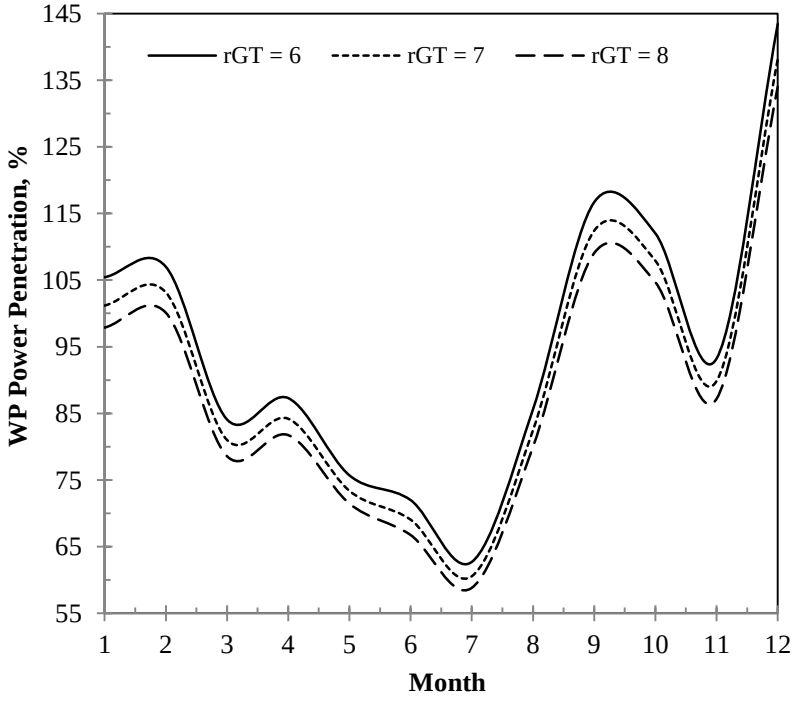

Figure 6.29: Power penetration of WP with various GT expansion ratios (r_c = 8, h_s = 168)

The power penetration of the wind park decreases as the gas turbine pressure ratio increases. A higher pressure ratio in the gas turbine results in a higher specific power output. Therefore, fewer wind turbines are required for the wind park and the share of the gas turbine in meeting the electricity demand increases (Figure 6.30).

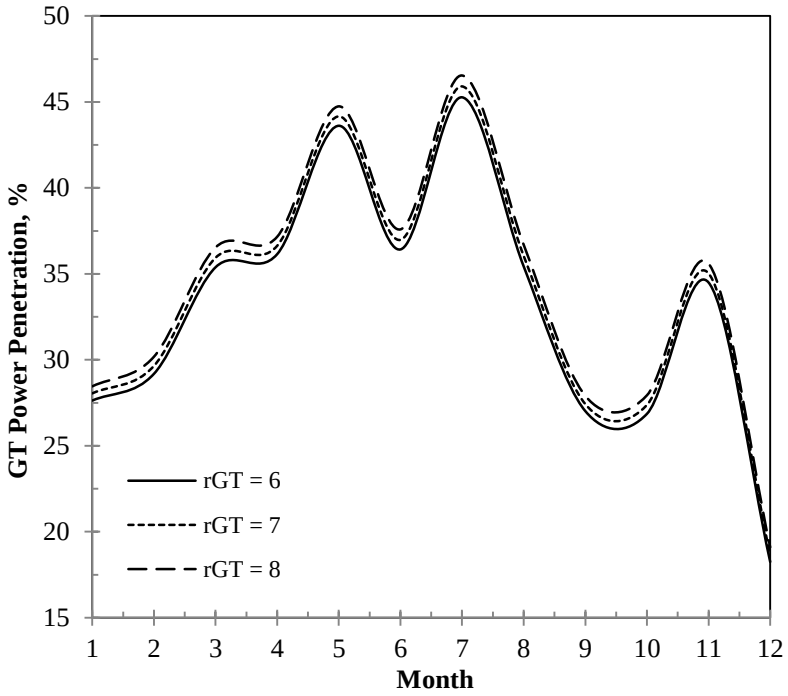

Figure 6.30: Power penetration of GT for various GT expansion ratios (r_c = 8, h_s = 168)

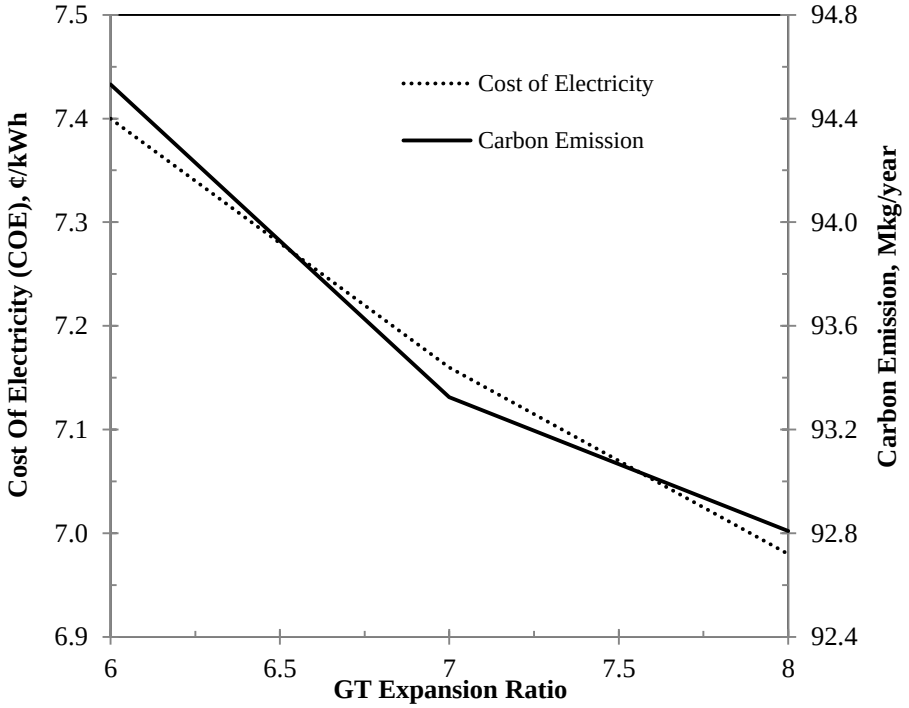

Figure 6.31: COE and annual carbon emission vs. GT expansion ratio (r_c = 8, h_s = 168)

The gas turbine expansion ratio impacts the capacity of the main components of the Wind-CAES system, which affects related system costs. The unit cost of electricity is a function of the system's total capital and maintenance costs and the total generated power by the system during its lifetime. Figure 6.31 shows that increasing the GT expansion ratio decreases the unit cost of generated electricity by the Wind-CAES system. According to Figure 6.31, the unit cost of electricity drops from 7.4 to 7.0 ¢/kWh as the GT expansion ratio increases from 6 to 8. For a fixed GT capacity, a higher specific power output leads to lower air and fuel consumption. A decrease in the fuel consumption due to the increase in turbine expansion ratio results in a reduction in the yearly carbon dioxide emissions, as also illustrated in Figure 6.31. Moreover, decreasing the pressure difference between the gas turbine inlet pressure and the pressure of the air storage cavern (i.e., increasing the gas turbine expansion ratio), increases the overall energy and exergy efficiencies of the Wind-CAES system, as observed in Table 6.14.

Table 6.14: Effects of gas turbine expansion ratio of overall energy and exergy efficiencies of the Wind-CAES system (r_c=8, h_s=168)

Gas turbine expansion ratio	6	7	8
Wind-CAES energy efficiency, %	37.2	37.9	37.6
Wind-CEAS exergy efficiency, %	32.8	33.9	34.7

As discussed in Figure 6.30 and illustrated in Figure 6.32, the GT power output increases if the pressure of the air entering the turbine cascade is closer to the compressed air pressure (decreasing the level of pressure loss in the air cavern). Although Figure 6.31 shows that the annual carbon emission rate decreases with increasing gas turbine pressure ratio, the specific carbon dioxide emission in g/kWh increases due to the increase in the share of the wind park in providing the grid with electricity.

The exergoeconomic method is used to calculate the unit cost of exergy of the system components. Here, the unit cost of generated electricity by the gas turbine is presented. The compressed air pressure affects the electricity cost of the Wind-CAES system, mainly due to the changes in the system components' capacities. The variations of the unit cost of GT electricity output with a change in the pressure of the stored air and the expansion ratio of the gas turbine is shown in Figure 6.33.

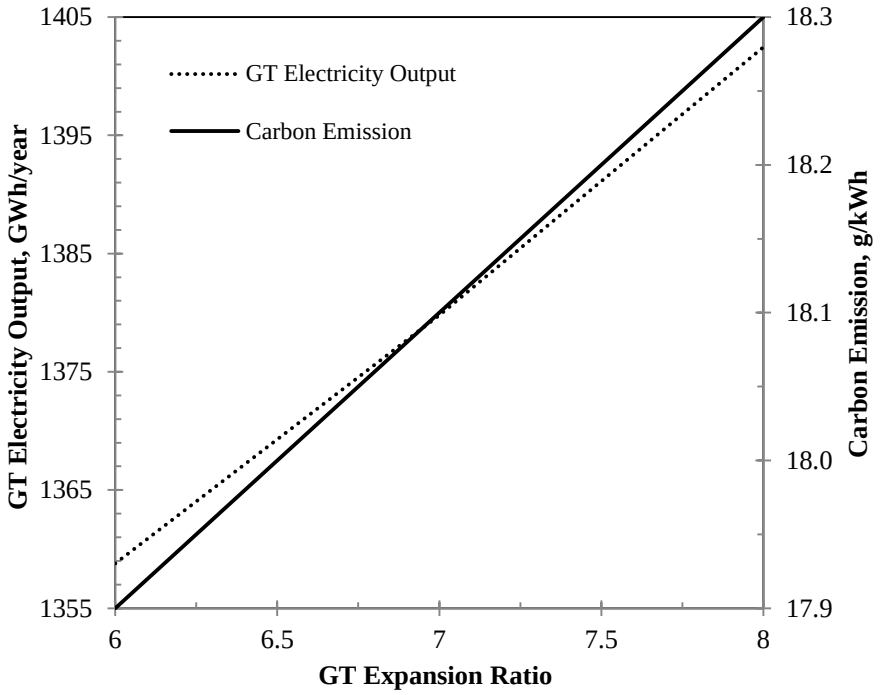

Figure 6.32: GT electric power output and carbon emission per unit of Wind-CAES electric power vs. GT expansion ratio (r_C = 8, h_s = 168)

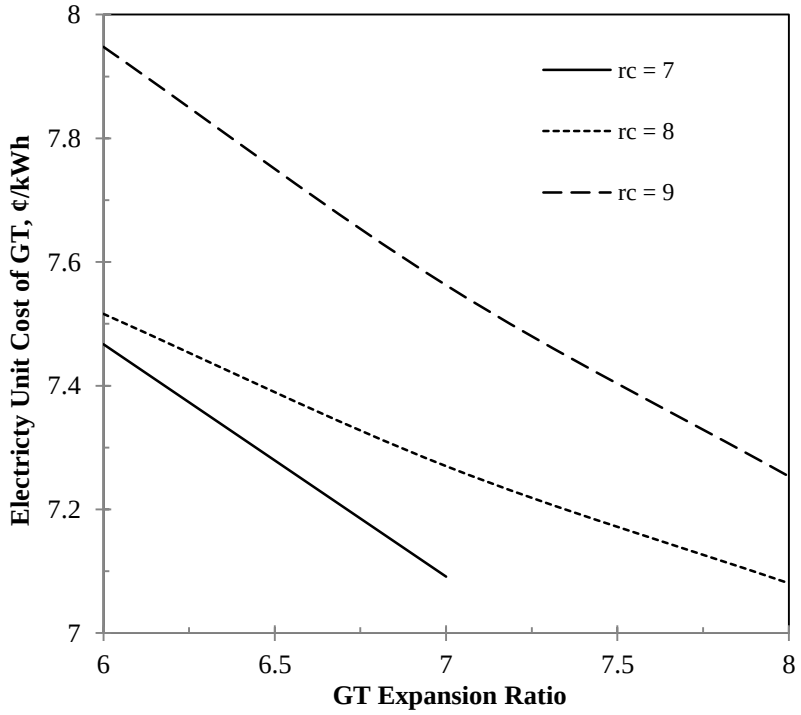

Figure 6.33: Variations of GT unit cost of electric exergy with the compressed air pressure ratio and the gas turbine expansion ratio

The highest price is for the case when the difference between the compressed air pressure and the turbine inlet pressure is a maximum. According to Figure 6.33, if

there is no pressure difference between the storage system and the gas turbine inlet pressure, the unit cost of GT electricity output is a minimum. The maximum expansion ratio that the GT can have is the compression ratio of the compressor, which explains the inconsistency in the lines in Figure 6.33. For example, when the compression ratio of the compressor is 7, the GT's expansion ratio can vary of up to the same value.

6.2.2.2 PV-H_2-FC system

Hydrogen is produced by water electrolysis, using surplus generated electricity by the PV system, and is consumed by the solid oxide fuel cell when the PV power is below the demand.

Table 6.15: Nominal capacities, and annual flows in the components of the PV-H_2-FC system

Parameter	Annual cumulative value
PV nominal capacity, MW	112
Electrolyser nominal capacity, MW	90
SOFC nominal capacity, MW	5
Hydrogen storage tank size, 10^3kg	527
Electrolyser hydrogen production, 10^3kg /year	1482
Fuel cell hydrogen consumption, 10^3kg /year	1481
Storage tank net hydrogen content, 10^3kg /year	0.8
PV electricity generation, GWh/year	93
Electrolyser electricity consumption, GWh/year	76
SOFC electricity generation, GWh/year	26
HRSG steam generation, GWh	12
Exergy of HRSG generated steam, GWh/year	8.1
Total exergy destruction, GWh/year	561
Electricity demand, GWh/year	44
Solar irradiance (energy basis), GWh/year	603
Solar irradiance (exergy basis), GWh/year	560
PV power penetration, %	40
SOFC power penetration, %	60
PV total hours of operation, h/year	3849
Electrolyser total hours of operation, h/year	3105
SOFC total hours of operation, h/year	5654
PV-H_2-FC Energy efficiency, %	9.0
Pv-H_2-FC Exergy efficiency %	9.1

If solar energy was always available at 1000 W/m^2 solar irradiance, only 28 MW solar PV would be required to supply a 5 MW baseload electricity. The size of the electrolyser in this case is reported as 23 MW, according to Table 4.4. However, solar energy is intermittent, and the required capacities of the PV and the electrolyser are 112 and 90 MW, respectively. This is presented in Table 6.15.

Hourly solar irradiance data are the input to the PV-H_2-FC system, and the results of mass, energy, and exergy flows are obtained for each time step. The annual flows are calculated as the cumulative values of the results, and given in Table 6.15. To understand the temporal behaviour of the renewable energy-based system, and to address the values more clearly, the cumulative monthly values are presented here. The production/consumption pattern of hydrogen depends on the temporal variations of the solar irradiance.

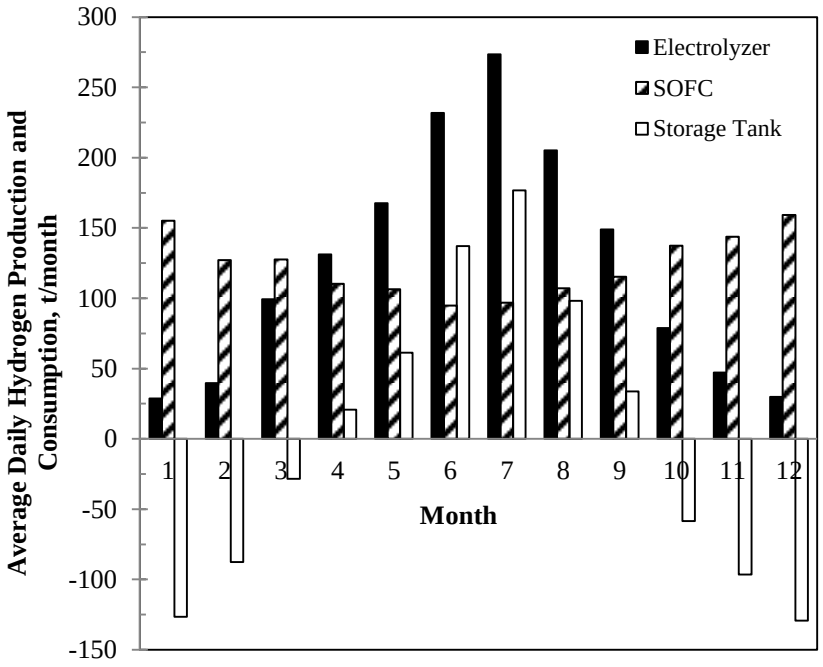

Figure 6.34: Monthly flow rate of hydrogen production and consumption

Figure 6.34 shows more production of hydrogen during high irradiance months (Spring-Summer) than Fall-Winter months. But, the SOFC consumes more hydrogen during low solar irradiance months. The system components are sized to have positive cumulative hydrogen in the storage tank throughout the year. The hydrogen production/consumption pattern is observed to be proportional to the PV and fuel cell power outputs (as shown in Figure 6.35).

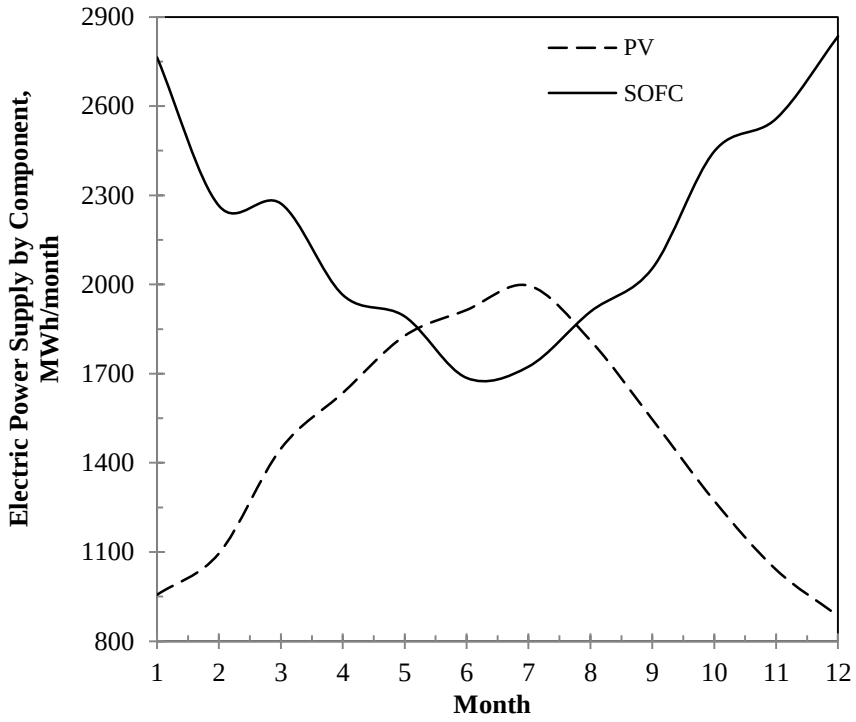

Figure 6.35: PV and SOFC share in electric power supply

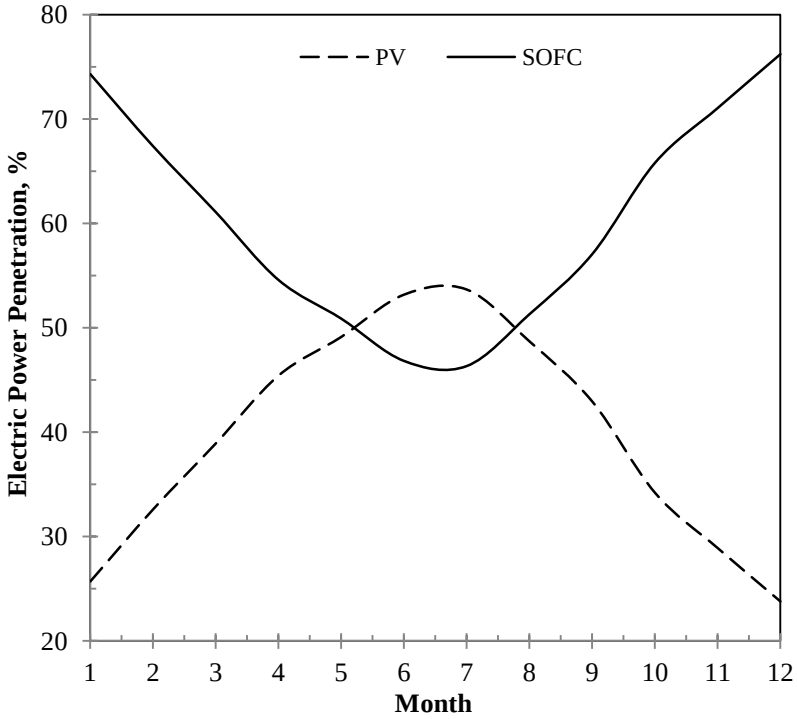

Figure 6.36: Electric power penetration of PV and SOFC system in meeting the demand

A better understanding of the PV and fuel cell shares in power production is observed in Figure 6.36. The power penetration of the PV system exceeds that of the fuel cell in spring-summer months, and exhibits an opposite trend in fall-winter

months. A graphical illustration of the contributions of the PV-H_2-FC system main components to the total exergy destruction (Figure 6.37) shows that the PV accounts for almost 85% of the annual exergy destruction. This is mainly associated with internal irreversibility.

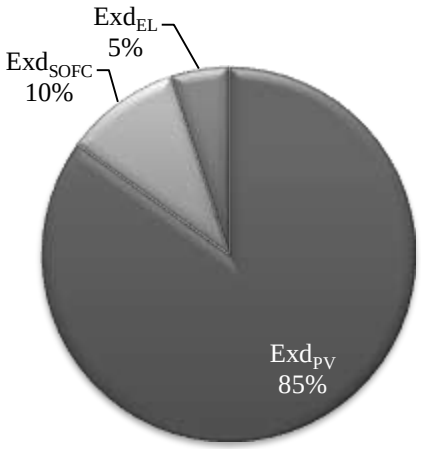

Figure 6.37: Annual exergy destruction breakdown for the main components of the PV-H_2-FC system

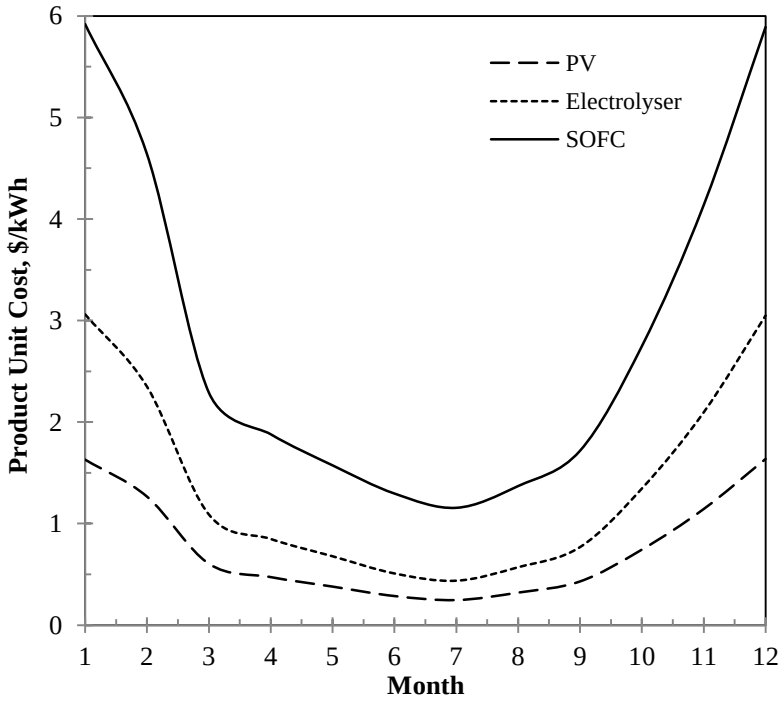

Figure 6.38: Unit cost of exergy for PV-H_2-FC components' products

Since the performance of the PV-H_2-FC system depends on the weather condition, for the exergoeconomic analysis, the unit cost of exergy of the products of the main components are determined on a monthly basis. Figure 6.38 shows during the months

with high solar irradiance, the cost of generated electricity by the PV and fuel cell systems is minimal. The PV electricity generation is significantly below its rated power during fall-winter months, causing a significant increase in the unit costs of the products. Although the fuel cell operates closer to its nominal capacity during this period of time, the generated electricity is still expensive due to the higher price for hydrogen production in months with low solar irradiance.

6.2.2.3 Integrated renewable energy-based power generation system

The energy and exergy results of the sub-systems of System 2 were presented and discussed above. Here these results are presented for the integrated system.

The PV system has a high exergoeconomic factor, demonstrating its expensive capital costs, according to Table 6.16. The SOFC in the PV-H_2-FC system has the minimum exergoeconomic factor due to its high exergy destruction and low capacity factor. Moreover, the costs associated with exergy destruction are functions of the unit exergy of fuel of the system. The fuel cell consumes the produced hydrogen by the electrolyser, which is considerably expensive. Therefore, the exergy destruction cost is higher than the levelized fuel cell purchased cost. The exergoeconomic factors of the other main components of the integrated renewable energy-based system are also presented in Table 6.16.

Table 6.16: Exergoeconomic factor for the main components of the integrated CHP system

Component	PV-H_2-FC			Wind-CAES			Biomass-SOFC-GT
	PV system	Electrolyser	SOFC	Wind park	Air compressor	Gas turbine	
Exergoeconomic factor	0.77	0.36	0.12	0.62	0.55	0.89	0.17

Table 6.17 provides information regarding heat recovery potential from the components of the integrated system. Moreover, the ratios of the heat recovered to the electric power input (output) of the components are presented. The results show that there is a good potential for heat recovery from the compressed air during compression and storage of air in the CAES system. The extent of heat recovery from the SOFC-GT system integrated with biomass gasification is significant, since heat can be recovered from the gasification process, the fuel cell and the micro gas turbine.

Table 6.17: Heat recovery from the integrated system components

Component	CAES[a]		PV-H_2-FC	Biomass-SOFC-GT
	Compressor	GT		
Heat recovery, GWh/y (GWhth/GWhe)	694 (0.85)	100 (0.07)	11.6 (0.3)	149 (0.7)
Energy consumption, GWh/y	817	1459	12.0[b]	687 (biomass)
Electric power output, GWh/y	NA	1359	43.8	219

[a] r_c = 8, h_s = 168, r_{GT} = 6
[b] Energy for pre-heating the hydrogen feed to the SOFC

Table 6.18: Energy and flows and efficiencies of the integrated system components

Parameter	Wind-CEAS	PV-H_2-FC	Biomass-SOFC-GT	Integrated System
E_{in}, TWh/y	13.6	0.614	0.610	14.8
E_{out}, TWh/y	5.06	0.056	0.368	5.48
η, %	37.2	9.0	60.3	37.0
Ex_{in}, TWh/y	13.9	0.569	0.646	15.1
Ex_{out}, TWh/y	4.49	0.052	0.274	4.82
ψ, %	32.3	9.1	42.4	31.9

The total energy and exergy flows in the integrated renewable energy-based system are listed in Table 6.18. These values are reported for each sub-system and for the overall system, separately. Values of energy and exergy efficiencies are reported. Table 6.18 shows that the overall energy and exergy efficiencies of the integrated system are 37.0 and 31.9%, respectively. A lower exergy value of recovered heat is the main reason for the lower overall exergy efficiency, compared to the energy efficiency.

Table 6.19: Unit cost of generated electricity by each sub-system of the integrated system.

Sub-system	Wind-CAES	PV-H_2-FC	Biomass-SOFC-GT
Unit cost of electricity, ¢/kWh	7.4[a]	89[b]	17[c]

[a] r_c = 8, h_s = 168, r_{GT} = 6, P_{GT}=470 MW
[b] P=5 MW
[c] P=25 MW, TIT=1300 K, T_{stack}=1173 K

Each sub-system of the integrated renewable energy-based system generates electricity, however with a different unit cost of electricity. Table 6.19 reports the unit cost of electricity generation by the integrated system. Results of the exergoeconomic analyses show the unit cost of electricity generated by the Wind-CAES system is 7.4

¢/kWh, while it is 89 and 17 ¢/kWh for the PV-H_2-SOFC and the biomass-SOFC-GT systems, respectively.

6.2.3 Optimization of System 2

The performance of the Wind-CAES system of the integrated renewable energy-based system is strongly dependent on the operating and design parameters. The optimization process provides a trade-off between the objective functions.

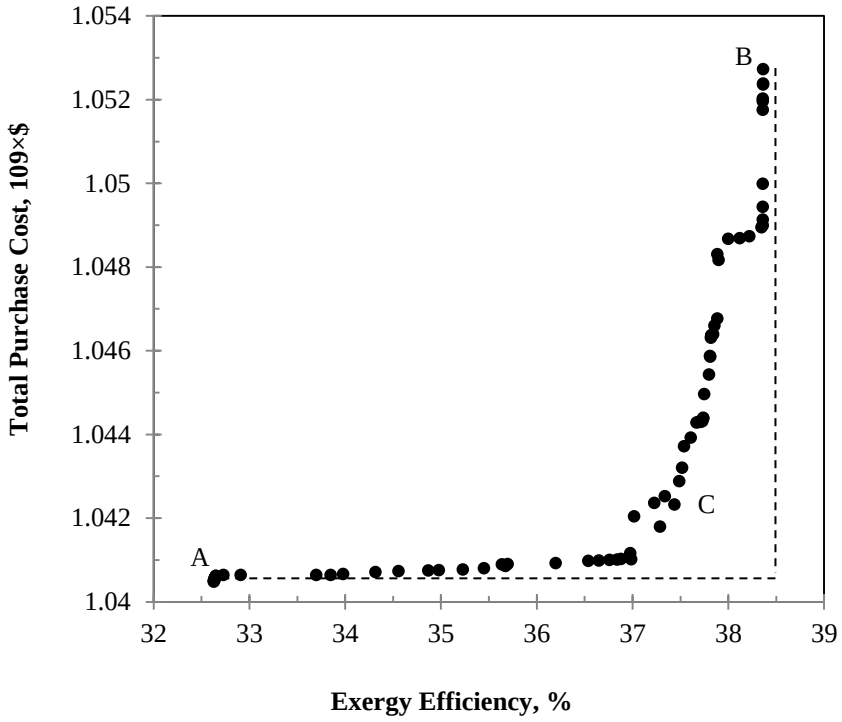

Figure 6.39: Pareto frontier: best trade-off values for the total purchase cost and exergy efficiency of the Wind-CAES system

Figure 6.39 shows the best trade-off values for the total purchase cost and exergy efficiency. The trade-off presents 72 points at which the system has its optimum performance in terms of exergy efficiency, while the total purchase cost is a minimum. Each of the points on Figure 6.39 present an optimal behaviour of the Wind-CAES system; however, selecting a point can be dependent on whether maximum efficiency (maximum total cost) or minimum total cost (minimum efficiency) is important. Table 6.20 presents the data representing points A, B, and C. Point C is the closest point to a hypothetical, so-called equilibrium point, at which both objective functions have their optimal points.

Table 6.20: Optimal decision parameters of the Wind-CAES system at three different points

Optimal point	r_{GT}	*TIT*, K	r_c	h_s, hr
A	6.87	1381	8	220
B	6.14	1388	8	240
C	6.50	1398	8	232

Various parameters are reported in Table 6.21, when the optimal decision parameters are applied to the Wind-CAES system. Table 6.21 shows the values for total exergy destruction, annual carbon dioxide emission, energy and exergy efficiency and some other parameters of the Wind-CAES system.

Table 6.21: Results of some parameters of the Wind-CAES at the optimal points

Optimal point	Ex_d	$(CO_2)_y$	η	Ψ	Ex_q	c_{GT}	f_{GT}	WP_{pen}	GT_{pen}
A	2857	104.7	39.7	32.6	423.4	7.12	0.82	75.7	36.1
B	2771	105.9	43.7	38.4	435.4	7.39	0.80	77.0	35.7
C	2812	105.2	43.1	37.3	428.94	7.25	0.81	76.4	35.9

Ex_d: Annual exergy destruction, GWh
$(CO_2)_y$: Annual carbon dioxide emission, 10^6kg/y
η: Energy efficiency, %
Ψ: Exergy efficiency, %
Ex_q: Annual heat recovery (thermal exergy), GWh
c_{GT}: Unit exergy cost of electricity generated by the gas turbine of the Wind-CAES system, ¢/kWh
f_{GT}: Exergoeconomic factor of the gas turbine
WP_{pen}: Electric power penetration of the wind park, %
GT_{pen}: Electric power penetration of the gas turbine, %

Points A, B, and C refer to Figure 6.39, and are three optimal points shown by the Pareto frontier. The energy and exergy efficiencies of the Wind-CEAS system are maximum are point B, according to Table 6.21; however, annual carbon dioxide emissions are highest at this point (105.9×10^6 kg/y). Table 6.21 shows that point C, which is the closest point to the equilibrium point on the Pareto frontier, has moderate values compared to the reported values for points A and B.

The values of decision variables at point C are introduced to the integrated system as inputs. The results of energy and exergy flows and efficiencies of the system components are obtained and presented in Table 6.22. Therefore, according to Table 6.22, the overall energy and exergy efficiencies of System 2 are reported as 42.3 and 39.0%, respectively, at the optimal point C.

Table 6.22: Energy and exergy flows and efficiencies of the integrated renewable energy based system for baseload power generation at an optimal point

Parameter	Wind-CAES	PV-H2-FC	Biomass-SOFC-GT	Integrated System
Ein, TWh/y	11.9,	0.614	0.610	13.1
Eout, TWh/y	5.12	0.0555	0.368	5.54
η, %	43.0	9.0	60.3	42.3
Exin, TWh/y	11.,7	0.569	0.647	12.0
Exout, TWh/y	4.38	0.0520	0.274	4.68
ψ, %	37.4	9.14	42.4	39.0

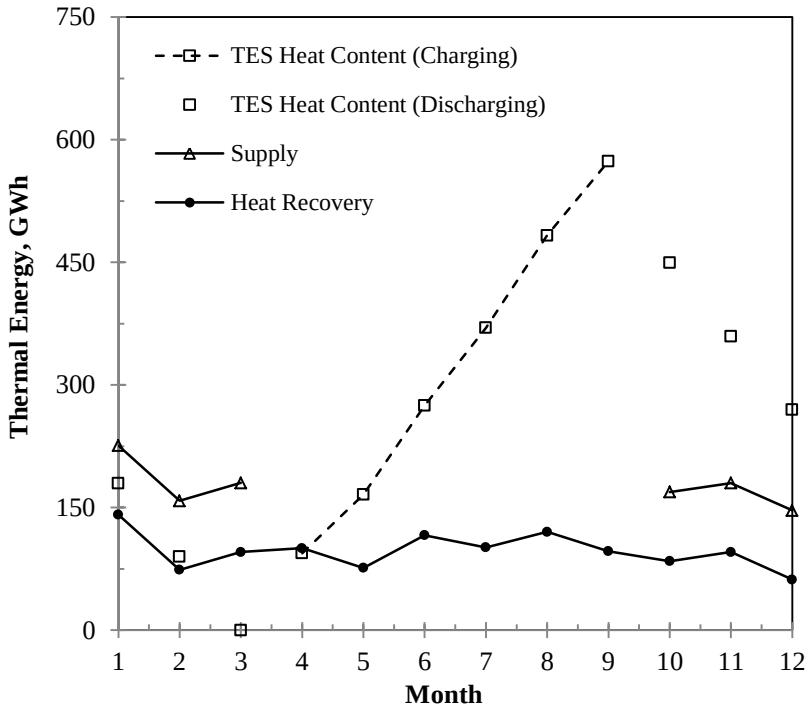

Figure 6.40: Total monthly heat recovery, storage and supply by the TES of System 2

The total monthly heat recovery from the components of the integrated system is calculated as shown in Figure 6.40 by the solid line with circular markers. The results are obtained considering the values of the decision variables at point C. This figure also presents the accumulated thermal energy content in the thermal energy storage system (square markers on Figure 6.40). The thermal energy content is shown for both charging and discharging phases of the storage process. The energy stored during the charging months (spring-summer) in the TES system is equally discharged through fall-winter months. With this strategy an almost constant thermal energy is supplied to the local community (solid line with the rectangular markers). The overall energy

efficiency of the TES system is 91%, which accounts for heat losses during the storage phases.

Figure 6.41 presents the corresponding exergy values of the parameters discussed in Figure 6.40. The overall exergy efficiency is 70%, which reveals the levels of exergy loss and destruction in the thermal energy storage system. Lower energy and exergy efficiencies are achieved compared to the results obtained for the TES of System 2. This mainly occurs due to the different temperature levels of the available heat.

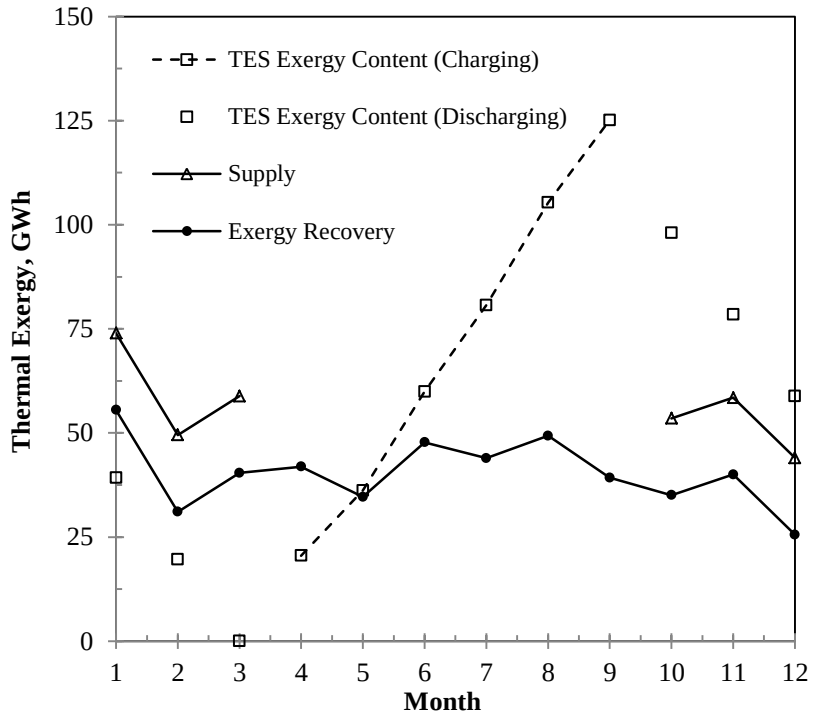

Figure 6.41: Total monthly thermal exergy recovery, storage and supply by the TES system of System 2

The integrated renewable energy-based system benefits from energy storage options to provide baseload electric power. For example, excess electricity is generated and stored in the compressed air energy storage system. The stored energy in the CAES is utilized when wind power is not sufficiently available. Moreover, heat is recovered during air compression and storage in the CAES system and stored in the thermal energy storage system. The stored thermal energy is utilized during fall-winter months for heating or hot water production purposes.

Other power generating sub-systems include energy storage systems. It is reasonable to perform a comparison between the novel, integrated system (System 2) and a simple power generation system that does not benefit from energy storage options. The wind park is no longer equipped with the compressed air energy storage system and a simple gas turbine cycle is considered to meet the electric power demand during wind power unavailability.

Table 6.23: Comparison of System 2 with a simple system without energy storage options

Parameter	Simple baseload power generation system	System 2
Renewable energy penetration, %	52	88
CO_2 emission, 10^6 kg/year	1250	455
Energy efficiency, %	38	42
Exergy efficiency, %	37	37

In addition, the PV-H_2-FC system, which has a hydrogen production and storage system, is simplified to a PV-FC system. Therefore, the solid oxide fuel cell is fed with natural gas instead of hydrogen. Moreover, the photovoltaic system is sized to meet the power demand and no longer generates excess electricity for hydrogen production. Table 6.23 compares System 2 with a simple renewable energy baseload power generation system. Renewable energy penetration is 88% in System 2, which uses energy storage options to provide baseload power generation, while the renewable energy penetration of the simple baseload power generation system is 52%. As illustrated in Table 6.23 the level of carbon dioxide emissions of the novel, integrated renewable energy-based system is almost one-third of the emissions of the system without storage options. Table 6.23 also shows the energy and exergy efficiencies of the systems.

Other storage options could be integrated with the renewable energy resources for baseload power generation. The main reasoning of the considered storage options was discussed in Section 4.2; nevertheless, an assessment is performed for an integrated system that utilizes hydrogen storage instead of CAES. System 2 has a CAES system to compensate for temporal power output of the wind park. The CAES system stores the excess electricity generation by the wind park, and generates electricity when the required. Here, the Wind-CAES system is compared with a Wind-hydrogen-GT system, which uses hydrogen storage produced in a water electrolyser to cover for the

wind park power loss. The excess generated electricity by the wind park is directed to a water electrolyser, and the produced hydrogen is stored in hydrogen tanks. When required, hydrogen is extracted from the storage tanks and is combusted with air in the combustion chamber of a gas turbine. The combustion gases are expanded in the gas turbine to produce mechanical work. The gas turbine is connected to an electricity generator, and the generated electricity is fed to the power grid. 168 hours of storage is considered to have a consistent comparison with the wind-CAES system. The results of the comparison are presented in Table 6.24.

Table 6.24: Comparison of the Wind-CAES system with a Wind-hydrogen-GT system

	Wind-CAES	Wind-hydrogen-GT
Wind park nominal capacity, GW	1.25	2.11
Compressor nominal capacity, GW	0.606	0.421
GT nominal capacity, GW	0.470	0.891
Electrolyser nominal capacity, GW	0	1.30
Storage capacity, h	168 (compressed air)	168 (hydrogen)
Share of WP in demand supply, TWh/year	3.93	3.06
Share of ES in demand supply, TWh/year	1.36	1.06
Heat recovery, TWh/year	0.247	2.01
Carbon dioxide emission, 10^6 kg/year	95	0
Cost of electricity generation, ¢/kWh	7	12
Energy efficiency, %	37	31
Exergy efficiency, %	33	25

Comparing the results reveals this fact that compressed air energy storage is economically more viable than using hydrogen for wind energy storage (7 vs. 12 ¢/kWh). Moreover, the nominal capacity of the wind park of the Wind-CAES is almost half of the Wind-hydrogen-GT system. However, the Wind-CAES system consumes natural gas to power the gas turbine, while the Wind-hydrogen-GT system is a carbon free power generation system. Moreover, higher efficiencies are reported for the Wind-CAES system due to lower number of the wind turbines (both systems have the same power output as 470 MW).

6.2.4 Closure

Integrated renewable energy-based systems have the potential for baseload power generation. The novel integrated system presented in this study utilizes wind, solar

and biomass energy resources, and provides 500 MW baseload power. The performance of the integrated system depends on weather conditions and the system component design parameters. For a 64 bar compressed air storage system, and a 36 bar gas turbine inlet air pressure, 356 3.5-MW rated power wind turbines are required to generate 470 MW baseload power. The compressed air storage will have a 3300 m^3 in volume and an energy storage capacity of 79 GWh (i.e., 7 days storage capacity at the gas turbine rated power). The lower the pressure difference between the compressed air in the cavern and the gas turbine inlet air pressure, the fewer wind turbines required in the Wind-CAES system. This results in higher penetration for the gas turbine.

The results also show that 5.4×10^5 PV modules (covering 0.66 Mm^2 of land) are required to generate 5 MW of baseload electric power. The capacity of the SOFC of the PV-H_2-FC system is 5 MW with 11.6 GWh annual heat-recovery potential. The PV system accounts for almost 85% of the annual exergy destruction due to its internal irreversibility.

Optimization of the integrated renewable energy-based system for baseload power generation provides a range of optimal points at which the exergy efficiency and the total purchase cost of the system are optimum. These optimal points are related to some specific values for the decision variables, which are considered to be the compression pressure rate, expansion pressure ratio, gas turbine isentropic efficiency, and the CAES system storage capacity. At one of the optimal points, which is the closest point to the equilibrium point on the Pareto frontier, the overall exergy efficiency of the integrated system is reported as 38.9%. At this point, the optimal compression ratio is 8, the optimal expansion ratio of the gas turbine is 6.5, and the optimal storage capacity of the CAES system is reported as 232 h.

6.3 System 3: Hybrid PV-biomass System with Thermal Desalination and Energy Storage Options

System 3 integrates biomass gasification with a gas turbine on one side, and solar PV and water electrolysis, on the other side. These two systems are combined in a hybrid system through energy storage. The power output of the solar photovoltaic system is temporal and during solar unavailability there is no electricity generation by

the PV system. Fortunately, energy storage can overcome this shortcoming; with an oversized solar PV system more electricity is generated during high solar irradiance hours to be stored and consumed when needed. The excess generated electricity is stored in the form of hydrogen. The produced and stored hydrogen participates in a combustion process with air in the combustion chamber of a gas turbine. The air for the combustion process is supplied by a compressed air energy storage system (CAES). Energy is provided for the CAES system via excess electricity generation by the integrated biomass-gas turbine (biomass-GT) system. Therefore, the hybrid system is capable of supplying electricity for a community throughout the whole day. This system is analyzed based on energy, exergy and exergoeconomics, and the results are presented here. Also, the optimal operation points of the system are determined through an optimization process.

6.3.1 Assumptions and Data

The energy and exergy analyses, along with the exergoeconomic analysis of the hybrid PV-biomass system with energy storage options are performed based on the following assumptions and data:

- Heat losses from the system boundaries are negligible.
- The data for solar irradiance, as well as the load variations, are for one hour time periods.
- Possible sources of data noise, e.g. sudden changes in solar irradiance and wind speed, are not considered in the analyses (i.e. average hourly values are used).
- The solar irradiance is based on hourly average rates in Toronto in 2011.
- A proton exchange membrane (PEM) electrolyser is used, and operates at 30 bar and 65% efficiency.

Average hourly solar irradiance data in Toronto, Canada in 2011 are used as the energy input to the photovoltaic system. The data are presented in a previous paper by the authors (Hosseini et al., 2013b). A developed computer code receives the solar irradiance data for each hour of the day. The PV maximum power point is calculated, and is reported as the electric power output of the photovoltaic system. Accordingly, the rate of exergy destruction is obtained by the computer code. The total electricity generation by the PV system is estimated as the summation of the energy output

throughout the year. In the meanwhile, the developed computer code provides an average daily power generation of the PV system on a monthly basis.

Straw or cereal plants, husk, wood, and scrap are only examples of available biomass types for biofuel production (Basu, 2010), each has its own chemical formula and heating value. Burning biomass releases the carbon dioxide which was originally absorbed by the plant during photosynthesis. Using biomass as fuel adds no net carbon dioxide to the environment (Basu, 2010). Therefore, biomass is considered a carbon neutral (on a net basis) renewable energy resource. In this paper, saw dust with the chemical formula of $C_{4.643}H_{6.019}O_{2.368}N_{0.021}$ is used as the biomass feed (Rao et al., 2004), and superheated steam at 10 bar and 400°C is provided to the gasification process. The gasification heat requirement is assumed to be supplied by an external heat source (Hosseini et al., 2012). Table 6.25 provides the input data to the biomass gasification and gas turbine systems. The input data to the CAES system are presented in Table 6.26.

Table 6.25: Input parameters for the gasification and gas turbine system

Parameter	Value
Dryer	
Superheated steam pressure, bar	3
Superheated steam temperature, °C	200
Moisture fraction of feed biomass, $kg_{moisture}/kg_{WB}$	0.5[a]
Gasifier	
Steam pressure, bar	10[a]
Steam temperature, °C	400
Steam-to-carbon ratio (*SC*), mol/mol	2[a]
Gas turbine	
Compressor inlet air temperature (T_0), ˚C	25
Air compressor isentropic efficiency, %	85[b]
Gas turbine isentropic efficiency, %	87[b]
Gas turbine inlet temperature (*TIT*), ˚C	1027[c]
Compressor pressure ratio (r_c)	8

[a]Adapted from Basu (2010)
[b]Adapted from Dincer et al. (2009)
[c]Adapted from Akkaya et al. (2008); Colpan et al. (2007)

Table 6.26: Input data to the compressed air energy storage system

Parameter	Value
Compression ratio (r_c), bar/bar	8
Expansion ratio (r_{GT}), bar/bar	7
Number of compression/expansion ratio	2
Gas turbine inlet temperature (*TIT*), ˚C	1027[a]
Air cavern storage capacity (h_s), hr	72

[a]Adapted from Dincer et al. (2009)

Table 6.27: Annual mass, energy and exergy flows in the main components of System 3

Parameter	Value
Electrolyser hydrogen production, 10^3 kg/year	276
CAES-GT hydrogen consumption, 10^3 kg/year	276
Compressed air storage, 10^6 kg/year	26.5
CAES-GT compressed air consumption, 10^6 kg/year	26.5
Biomass consumption, 10^6 kg/year	19.8
PV electric energy generation, GWh/year	21.2
Electrolyser electric energy consumption, GWh/year	14.2
Biomass-GT electric energy generation, GWh/year	76.5
Air compressor electric energy consumption, GWh/year	4.80
CAES-GT electric energy generation, GWh/year	8.90
Heat recovery from biomass-GT system, GWh/year	3.84
Heat recovery from CAES-GT system, GWh/year	4.86
Thermal exergy recovered from biomass-GT system, GWh/year	1.40
Thermal exergy recovered from CAES-GT system, GWh/year	2.20
Total exergy destruction, GWh/year	202
Specific CO_2 emission, g/kWh	845
Solar energy input, GWh/year	137
Solar exergy input, GWh/year	127
Total electric energy demand, GWh/year	87.6
PV power penetration, %	8.0
Biomass-GT power penetration, %	82
CAES-GT power penetration, %	10
System 3 energy and exergy efficiency, %	34.8, 34.1

6.3.2 Results and Discussion

The hybrid PV-biomass system is analyzed based on energy, exergy and exergoeconomics. The system provides 10 MW baseload electric power, and uses

energy storage and heat recovery. The biomass-GT system meets 80% of the electricity demand and also feeds the air compressor of the CAES system for compressed air storage. The size of the PV system is selected to meet 20% of the electricity demand during solar availability.

However, the intermittent characteristic of solar energy results in a demand-supply mismatch by the photovoltaic system, which is compensated by the gas turbine of the CAES system. Table 6.27 presents the annual mass, energy and exergy flows in the main components of System 3. The data in Table 6.27 are obtained considering the assumptions and data use explained before. The annual share of the solar PV system in meeting the electricity demand is 8%, while this value is 10% for the CAES-GT system. Therefore, the total contribution of energy storage systems (hydrogen and compressed air) in supplying the power demand is 18%.

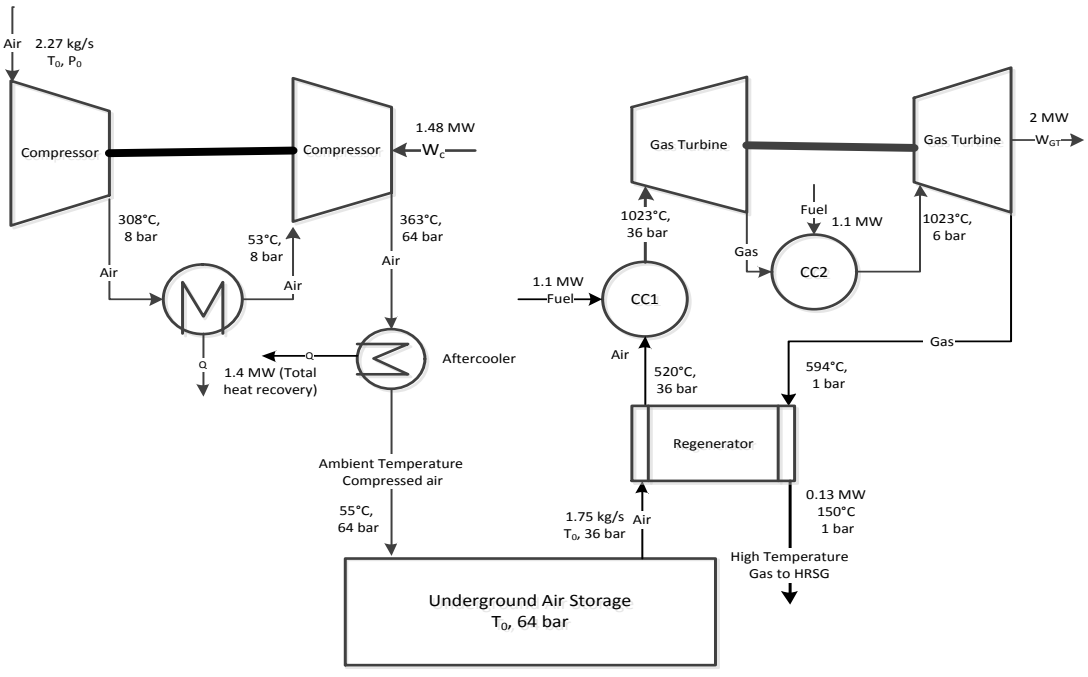

Figure 6.42: Energy flows in the CAES-GT system

Figure 6.42 shows the nominal mass and energy flow rates in the components of the CAES system; 1.48 MW electricity and 2.2 MW hydrogen feed is required to eventually generate 2 MW electric power in the gas turbine. The round-trip efficiency based on only electricity generation aspect of the system is 54%. Therefore, the overall round-trip efficiency of the CAES system considering heat recovery from the

compression and the expansion processes is 98%, and the relevant exergy efficiency is 75%.

In this section, average daily performance of the hybrid system is reported. The results are presented for each month, due to the significant variation of the solar radiation throughout the year. Average daily hydrogen production, consumption and storage during each month are illustrated in Figure 6.43. The electrolyser produces most of the annual hydrogen production during months with high-solar irradiance (spring-summer). The gas turbine of the CAES system burns hydrogen during fall-winter months at higher rates.

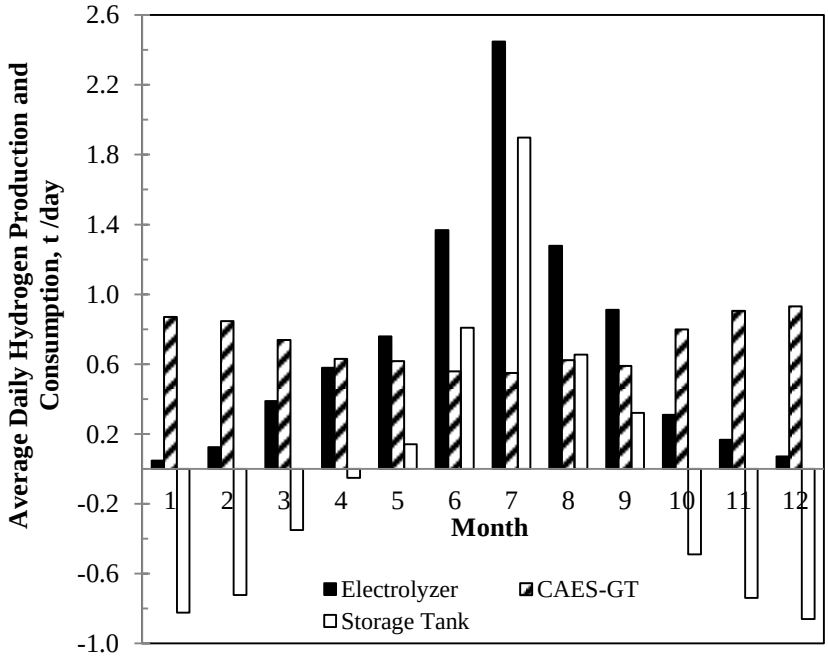

Figure 6.43: Average daily hydrogen production and consumption for each month

The negative values for hydrogen storage (blank bars) represent higher hydrogen consumption than production during the corresponding months, which explains the unavoidable need for seasonal hydrogen storage; more hydrogen should be produced by the electrolyser when solar irradiance is abundant. A hydrogen tank with 120,000 kg storage capacity is required to meet the hydrogen consumption requirement of the gas turbine throughout the year. The size of the storage tank will be approximately 100 m^3 in volume with a pressure of 30 bar.

A similar trend is observed in the CAES system. Indeed, the consumption patterns of the stored hydrogen and compressed air are related, since they both are consumed by the gas turbine of the CAES system. Ambient air is compressed and stored in the

CAES system during high-solar irradiance months and is utilized by the gas turbine when needed. The production, consumption and storage of compressed air are presented in Figure 6.44.

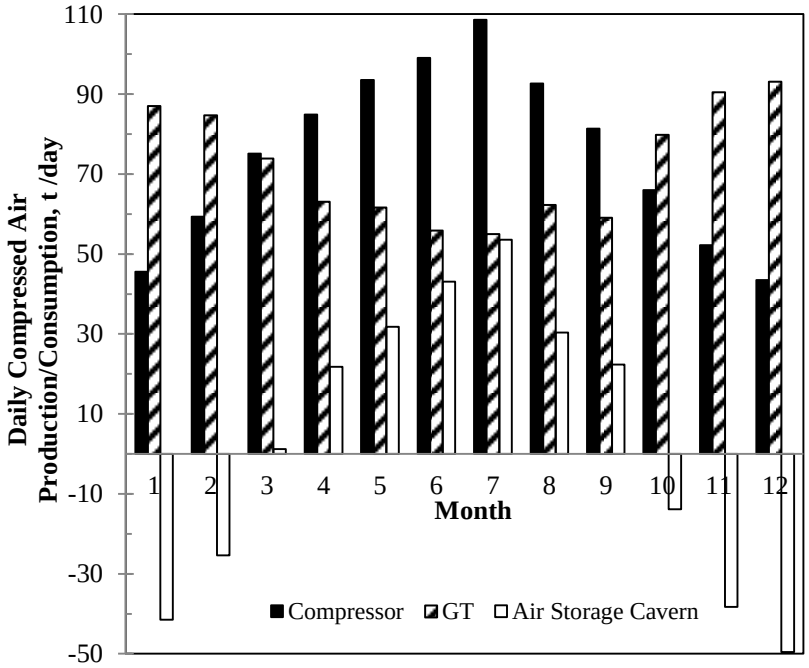

Figure 6.44: Average daily compressed air production, consumption and storage of the CAES-GT system

The average daily electric energy outputs of the PV and CAES-GT systems are shown in Figure 6.45. The PV system reaches its maximum energy output in summer, while the gas turbine of the CAES has its maximum share in meeting the electricity demand during fall-winter months. These two systems compensate for each other to maintain a baseload power generation.

The main components of the CAES system are the air compressor and the gas turbine, which depends on the time of day, one may operate while the other one is not in service. In spring-summer months, the biomass-GT system feeds the compressor of the CAES, and in fall-winter months, the gas turbine of the CAES system generates electricity to meet the demand. Figure 6.46 presents a graphical explanation of this trend.

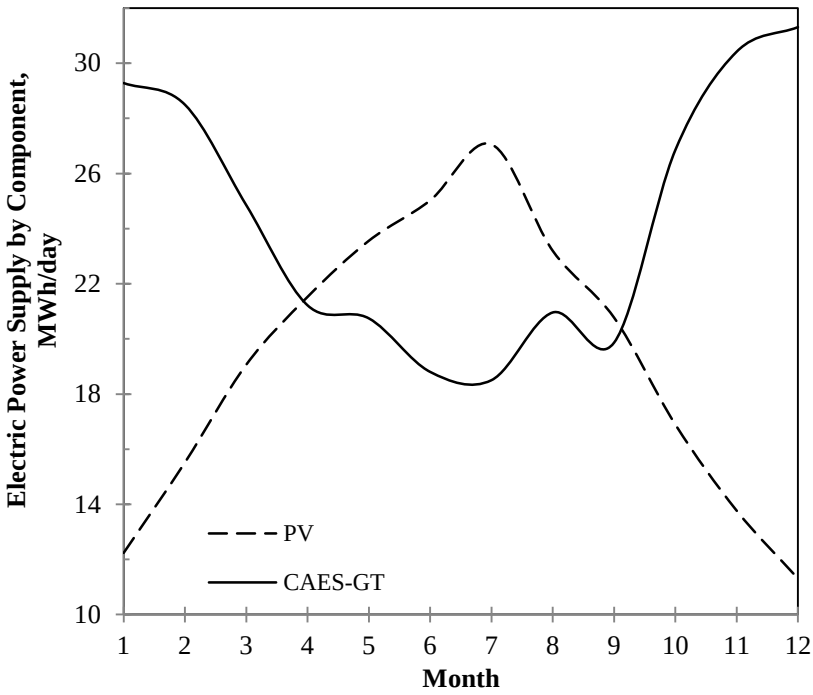

Figure 6.45: Average daily electric power supply by the PV and CAES-GT systems

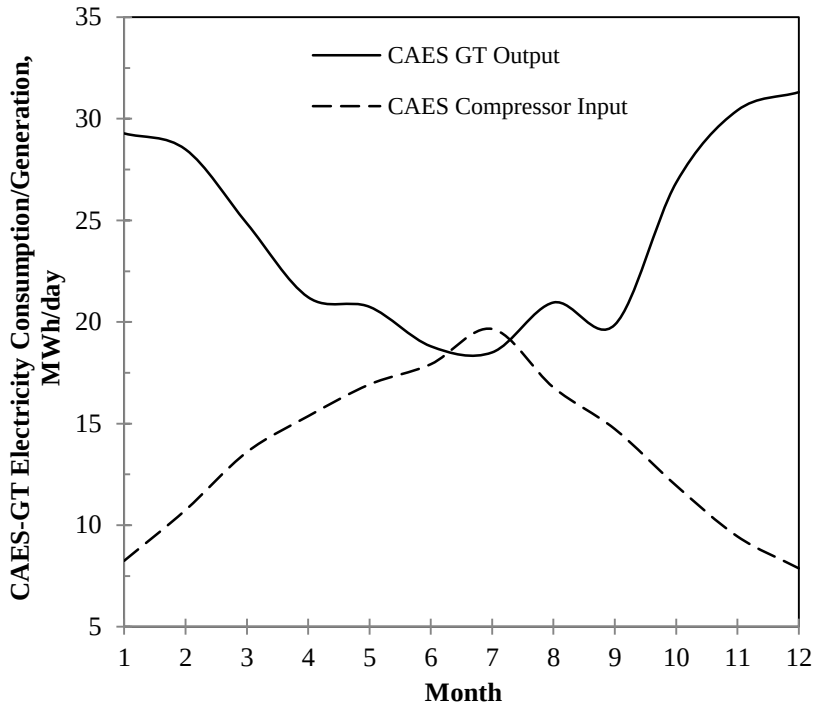

Figure 6.46: Average electricity consumption/generation of the CAES-GT system

According to Figure 6.47, the biomass-GT system supplies an almost fixed ratio of the electricity demand. The electric power penetration of the photovoltaic and the CAES-GT systems are inter-related, which is also shown in Figure 6.47.

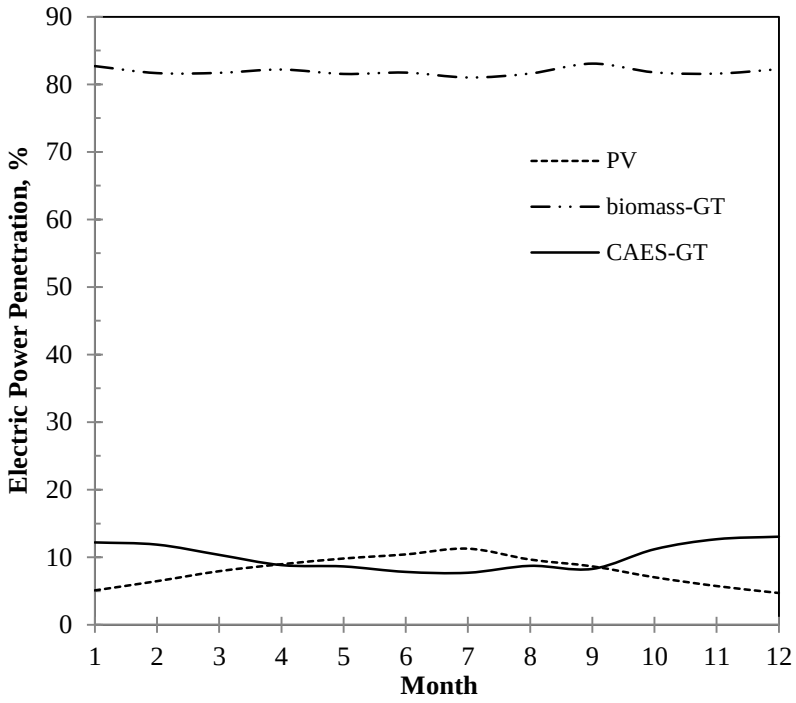

Figure 6.47: Electric power penetration of the electricity generation components of the hybrid PV-biomass system

The PV has its maximum power penetration percentage in July, while the gas turbine of the CAES system is taking some time off. The power output of energy systems depends on the rates of energy inputs and the effectiveness of the system components. Exergy destruction represents the ineffectiveness of the system in converting the input energy flows to useful high quality output.

Solar energy is abundant, free, and environment-friendly; however the current, fairly economical PV systems are not capable of converting it to electricity with high efficiencies. Figure 6.48 shows that the PV system accounts for 56% of the annual exergy destruction in the hybrid system, since the average exergy efficiency of the PV systems is hardly 17%. Figure 6.48 also expresses that 38% of the annual exergy destruction occurs in the biomass-GT system. This is mainly due to the chemical reactions in the gasifier and the combustion chamber of the GT.

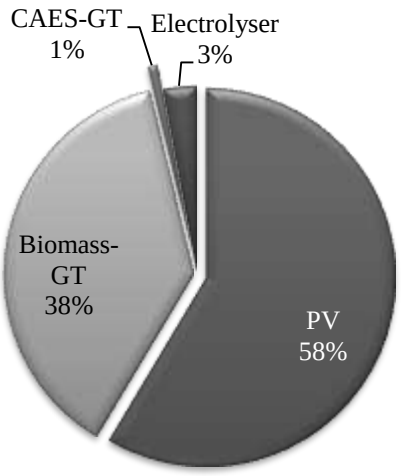

Figure 6.48: Average exergy destruction percentage of the integrated system components

Table 6.28: Energy and exergy flows and efficiencies of the hybrid system components

Component	PV	Electrolyser	CAES-GT	Biomass-GT
Energy input, MWh/y	1.37×10^5	1.42×10^4	4.80×10^3 (electricity) 9.20×10^3 (hydrogen)	1.40×10^5
Exergy Input, MWh/y	1.27×10^5	1.42×10^4	4.80×10^3 (electricity) 9.06×10^3 (hydrogen)	1.40×10^5
Energy output, MWh/y	2.12×10^4	9.20×10^3	8.89×10^3 (electricity) 3.89×10^3 (heat)	7.65×10^4 (electricity) 3.84×10^3 (heat)
Exergy output, MWh/y	2.12×10^4	9.06×10^3	8.89×10^3 (electricity) 2.19×10^3 (heat)	7.65×10^4 (electricity) 1.40×10^3 (heat)
Energy efficiency, %	15.5	64.9	91.3	57.2
Exergy efficiency, %	16.7	64.0	86.6	55.6
Overall energy efficiency, %		34.8		
Overall exergy efficiency, %		34.1		

Table 6.28 provides the total annual energy and exergy flows in the components of the hybrid system. Table 6.28 also provides the extent of heat recovery from the system components. The overall energy and exergy efficiencies of the hybrid PV-biomass system with energy storage options are 34.8 and 34.1%, respectively. These values are highly competitive with the overall efficiencies of conventional power plants, which fall between 35% for gas-fired steam power plants to 55% for modern combined cycles.

6.3.2.1 Parametric analysis

The hybrid PV-biomass system with energy storage options was analyzed based on energy, exergy and exergoeconomics for a specific set of inputs presented in Tables 6.25-6.26.

It is of interest to investigate the system by changing some of the major design and operating parameters. For example, steam-to-carbon ratio plays a major role in biomass gasification. Specific heat requirement and produced syngas molar fractions are affected by the change in *SC,* which is varied from 1 to 3 mol/mol, but the optimum value depends on the configuration and other design parameters of the gasification system. As shown in Figure 6.49, increasing *SC* has a positive effect on both the energy and exergy efficiencies of the hybrid PV-biomass system.

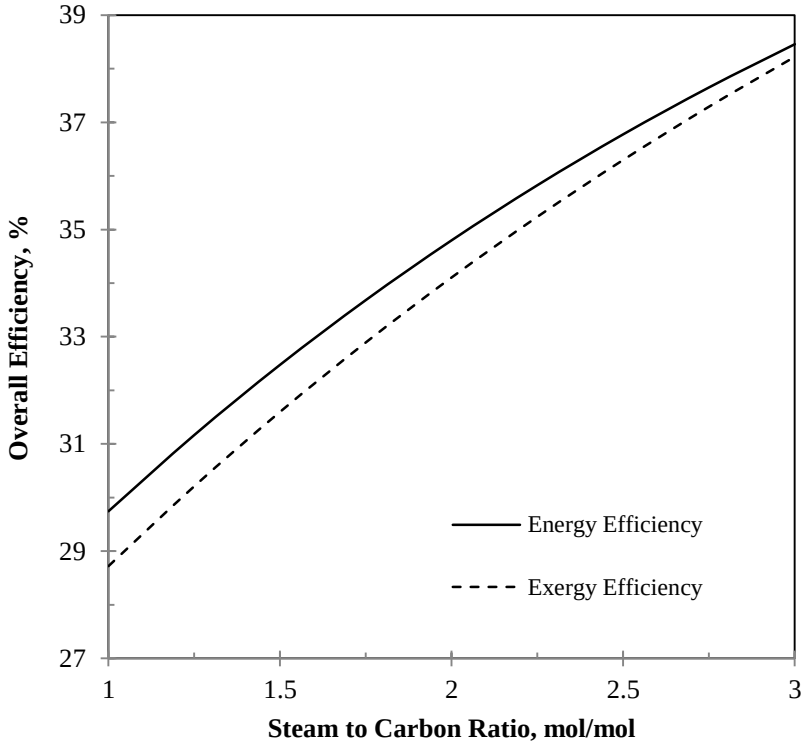

Figure 6.49: Effects of *SC* on the overall efficiency of the integrated PV-biomass system

The increasing in *SC* leads to an increase in the steam requirement for the gasification process. As reported by the authors in a previous paper, the gasification heat requirement and the syngas molar heating value decrease with *SC*; however, the molar heating value decreases (Hosseini et al., 2012). More steam is fed to the gasifier when increasing the steam-to-carbon ratio, which leads to a higher mass flow rate of the product gas. The gasification system is integrated with a gas turbine, which

utilizes the syngas produced by the gasifier. The net electricity generation by the gas turbine is higher when more fuel is consumed. That is, for a fixed GT electric power output, less biomass is required by the gasification process. In other words, for a constant electric power output of the gas turbine, less biomass is utilized by the gasification process, since *SC* has already increased the total mass flow entering the combustion chamber of the GT.

This is clarified in Figure 6.50, which illustrates the variations in the specific biomass consumption to the hybrid PV-biomass system electric energy output. More steam and less heat is required for the gasification process to be initiated and maintained if *SC* is increased, both of which have negative impact on the heat recovery potential from the hybrid PV-biomass system. This is shown in Figure 6.51, along with the variations of the specific exergy destruction with the change in *SC*.

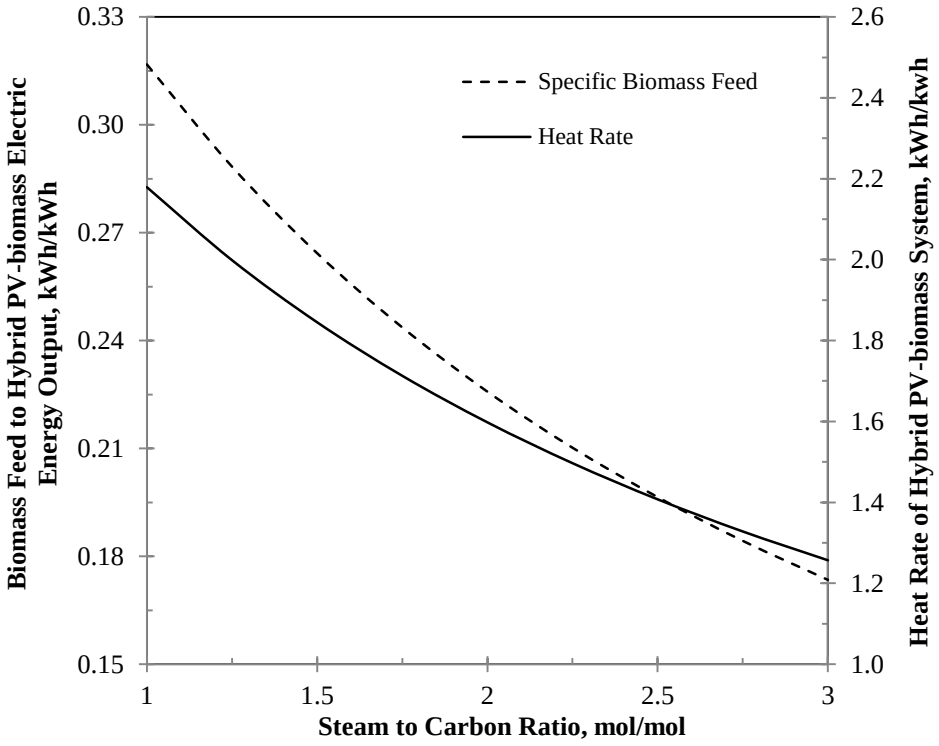

Figure 6.50: Variations of specific biomass consumption and biomass-GT heat rate with *SC*

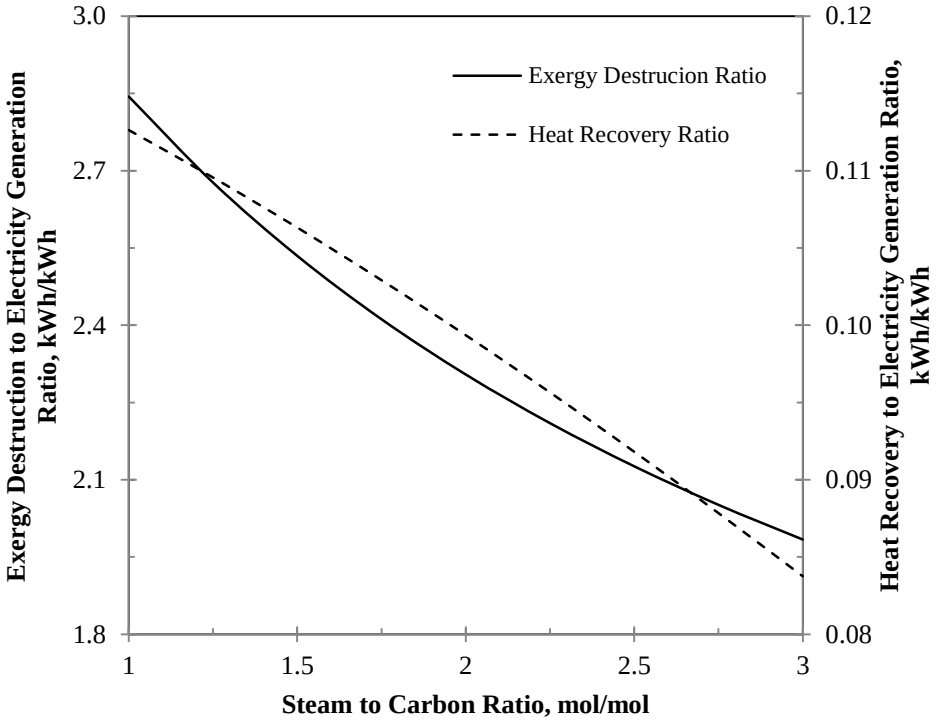

Figure 6.51: Variations of the specific exergy destruction and heat recovery with *SC*

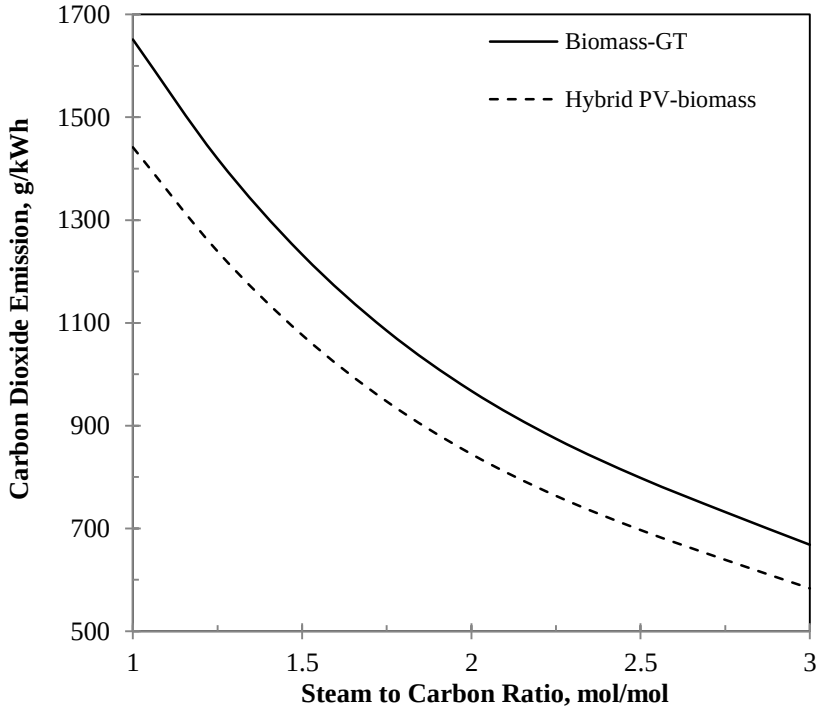

Figure 6.52: Specific carbon dioxide emission vs. steam-to-carbon ratio

Besides the positive improvement in the hybrid PV-biomass system energy and exergy efficiencies, as shown in Figure 6.49, increasing steam-to-carbon ratio of the biomass gasification system decreases the level of carbon dioxide emissions from

both the biomass-GT system (as a sub-system) and the hybrid PV-biomass system (as an overall hybrid system). The corresponding changes are shown in Figure 6.52. Carbon dioxide emissions decrease from 1441 to 583 g/kWh when *SC* is changed from 1 to 3 mol/mol. Therefore, when they are integrated with a biomass-GT system, the overall carbon emission of the hybrid system are less than the biomass-GT system itself, since more electricity is generated with the same level of greenhouse gas emission.

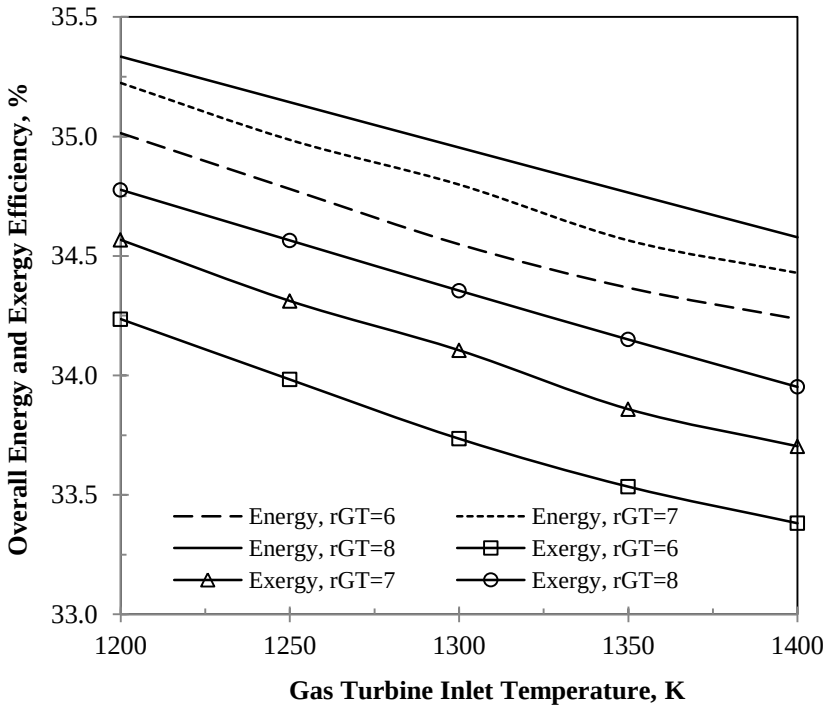

Figure 6.53: Effects of gas turbine inlet temperature and expansion ratio on the overall energy and exergy efficiencies of the hybrid PV-biomass system

Other important parameters that affect the performance of the hybrid PV-biomass system with energy storage options are the gas turbine inlet temperature and expansion ratio. In this research, results are presented for the variations of overall system energy and exergy efficiencies with the change in *TIT* and r_{GT} of the gas turbine of the CAES system. The *TIT* and r_{GT} of the gas turbine of the biomass-GT are considered constant throughout this analysis.

Figure 6.53 shows that, for r_{GT}=6, the overall energy and exergy efficiencies decrease by 2.2 and 2.4%, respectively, when *TIT* increases from 1200 to 1400 K. The gas turbine expansion ratio, however, has positive effects on the hybrid PV-biomass system, as seen in Figure 6.53. Although the increase in turbine inlet temperature

reduces the efficiency of the hybrid system, carbon dioxide emissions decrease as shown in Figure 6.54.

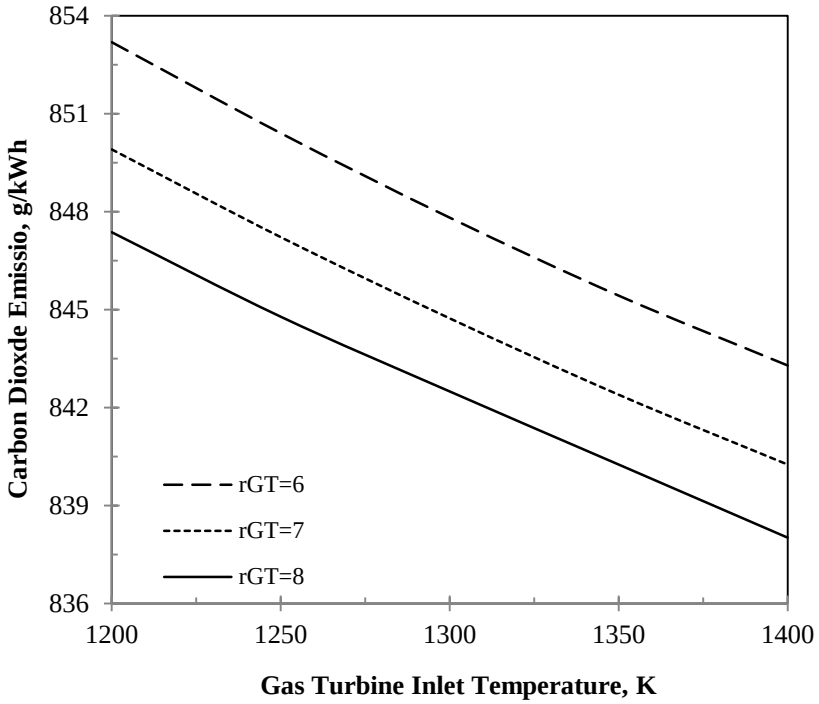

Figure 6.54: Reductions in CO_2 emission with GT inlet temperature and expansion ratio

6.3.2.2 Exergoeconomic analysis

The results of the energy and exergy analyses were presented and discussed in the previous sections. Exergoeconomics provides useful information about unit exergy cost of products, cost of exergy destruction, and relative cost difference of products. The unit exergy cost of products is calculated based on the annual capital, and operation and maintenance costs of the hybrid PV-biomass system as well as the total exergy of products (electricity) in a year. Figure 6.55 presents the variations of unit exergy cost of products of the main components of the hybrid system with the increase in *SC*.

Figure 6.55 presents the exergoeconomic results for electricity generation by the PV, the biomass-GT, and the CAES-GT systems, and for hydrogen generation by the water electrolyser. The unit exergy cost of electricity generation by the biomass-GT system decreases with the change in *SC* from 1 to 3 mol/mol. Indeed, *SC* has its highest effect on the biomass-GT system, and the CAES-GT system unit exergy cost of product decreases very insignificantly. The decrease in c_{GT2} is due to the reduction in the biomass feed and system's heat rates when *SC* is changed between 1-3 mol/mol.

This was previously depicted and discussed in Figure 6.50. The unit costs of electricity and hydrogen production by the PV and electrolyser systems, respectively, are not affected by the steam-to-carbon ratio.

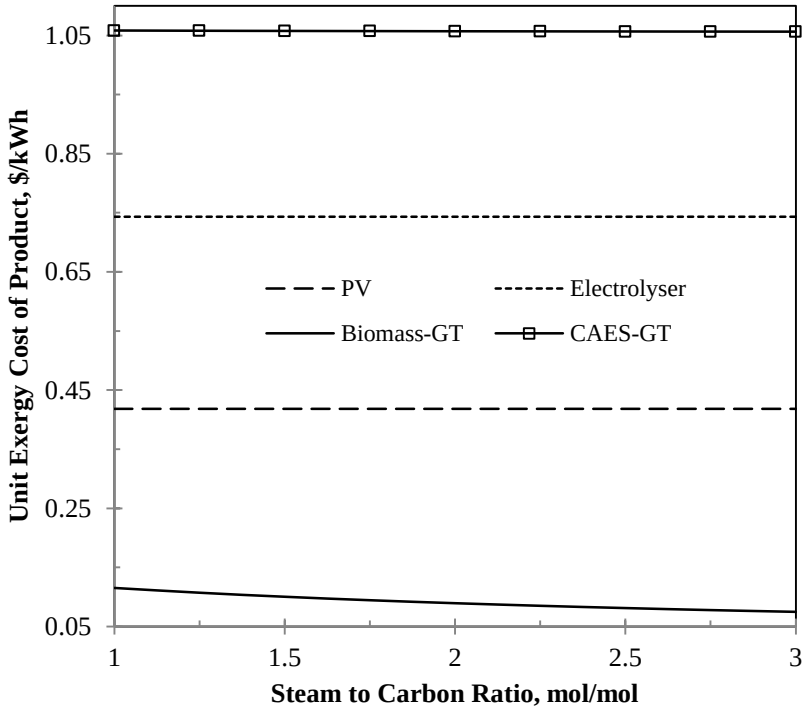

Figure 6.55: Variations of unit exergy cost of product of the main components of System 3

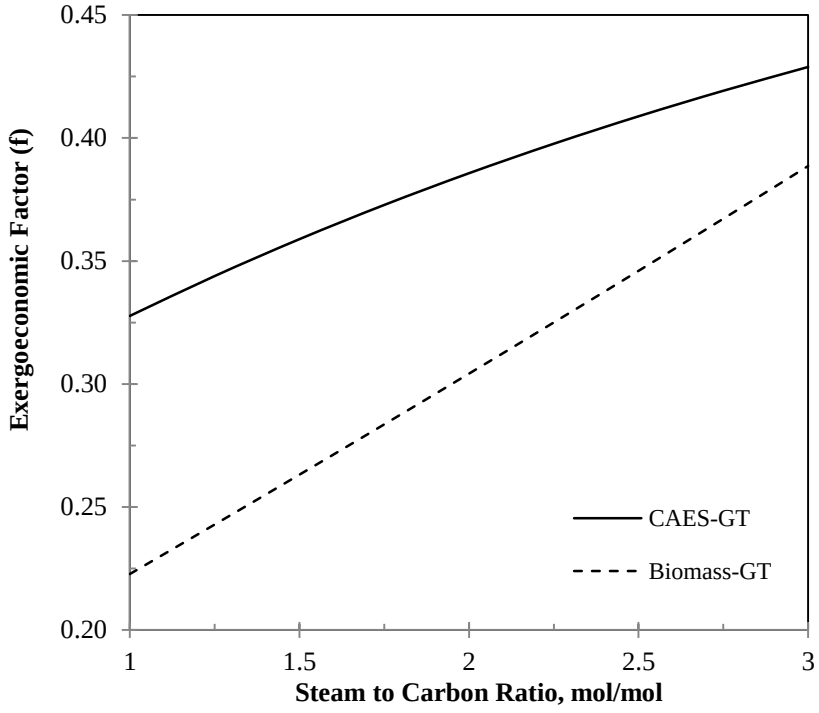

Figure 6.56: Exergoeconomic factor and its change with the increase in *SC*

According to Figure 6.51, specific exergy destruction of the hybrid PV-biomass system with energy storage options decreases with the increase in *SC*. On the other hand, the levelized cost rate of the hybrid system remains constant, since steam-to-carbon ratio does not affect equipment sizes. Therefore, the exergoeconomic factor will be only a function of the exergy destruction and unit exergy cost of product of each component. Thus, the biomass-GT and CAES-GT systems will have higher exergoeconomic factors when *SC* is changed from 1 to 3 mol/mol. Figure 6.56 shows the variations of exergoeconomic factor (*f*) with SC. The CAES-GT system has higher exergoeconomic factor due to its lower exergy destruction rate comparing to its capital and O&M costs. Low values of the exergoeconomic factor of the biomass-GT system reveal its improvement potentials in terms of exergy destruction. The steam-to-carbon ratio also affects the relative cost difference of the biomass-GT and CAES-GT systems. The unit exergy cost of the generated electricity by the CAES-GT system is almost constant when SC is changed (Figure 6.55).

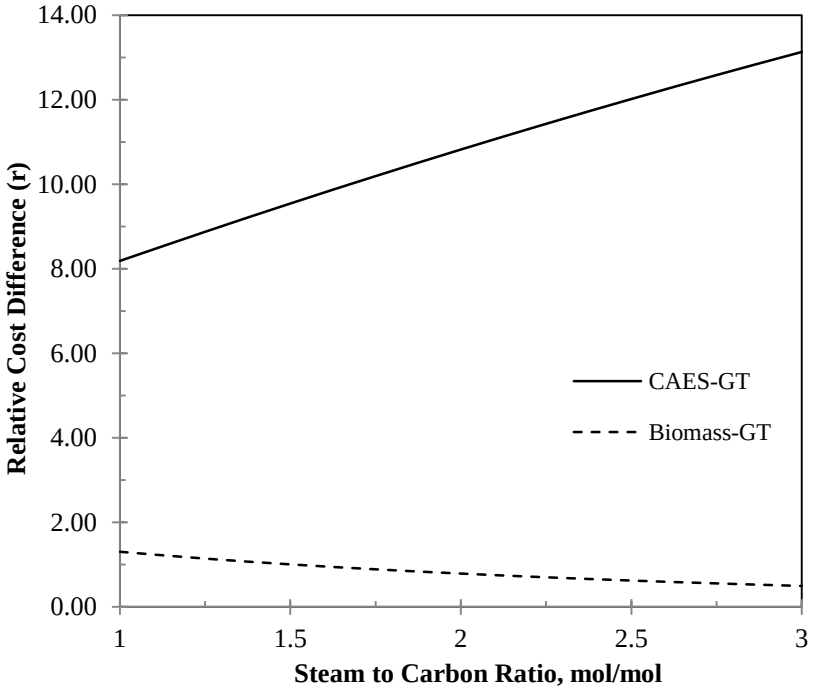

Figure 6.57: Variations of the relative cost difference of the biomass-GT and CAES-GT systems with the increase in steam-to-carbon ratio.

Therefore, by the increase in the unit exergy cost of the generated electricity by the biomass-GT system, the relative cost difference of the CAES-GT system increases, as a result (Figure 6.57). The relative cost difference of the CAES-GT system is calculated considering the generated electricity as product, and the input electricity

from the biomass-GT system as fuel. One may consider the unit cost of hydrogen feed as the fuel to the CAES-GT system. In that case, the results of the relative cost difference $r_{\mathrm{CAES-GT}}$ would be different.

The relative cost difference of the biomass-GT system is calculated considering the biomass feed as the fuel and the generated electricity as the product. Since the unit cost of the biomass feed is constant, $r_{\mathrm{biomass-GT}}$ decreases with the decrease in the unit exergy cost of the generated electricity by the biomass-GT system.

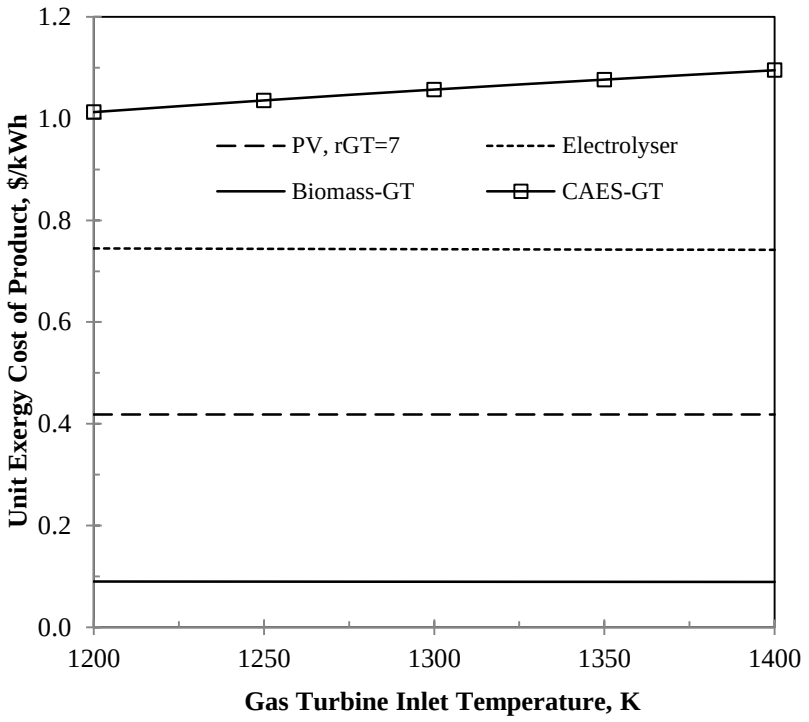

Figure 6.58: Effects on gas turbine inlet temperature on the unit exergy cost of products of the components of the hybrid PV-biomass system with energy storage options

A higher gas turbine inlet temperature leads to an increased hydrogen feed consumption rate. The gas turbine hydrogen feed is produced by the water electrolyser in the PV-electrolyser system. Therefore, a higher *TIT* results in larger PV and electrolyser nominal capacities. These all impact the unit exergy cost of the products of the hybrid system components, due to the subsequent increase in the capital and purchase costs. However, Figure 6.58 shows *TIT* has a major effect on the unit cost of generated electricity by the CAES-GT system. A better picture of this effect is presented by Figure 6.59, which illustrates variations of the unit exergy cost of the generated electricity by the gas turbine of the CAES-GT system.

More than 8% increase in the unit cost of electricity is observed; with the change in TIT from 1200 to 1400 K. Figure 6.59 also shows the variations of the unit cost of electricity generation by the CAES-GT system with the gas turbine expansion ratio. The higher the gas turbine expansion ratio (r_{GT}), the lower the cost of electricity. In obtaining the results of this part, the pressure ratio of the compressor is kept constant at $r_{\mathrm{GT}} = 8$. Therefore, any increase in the gas turbine expansion ratio implies lower pressure difference between the air storage cavern and the gas turbine.

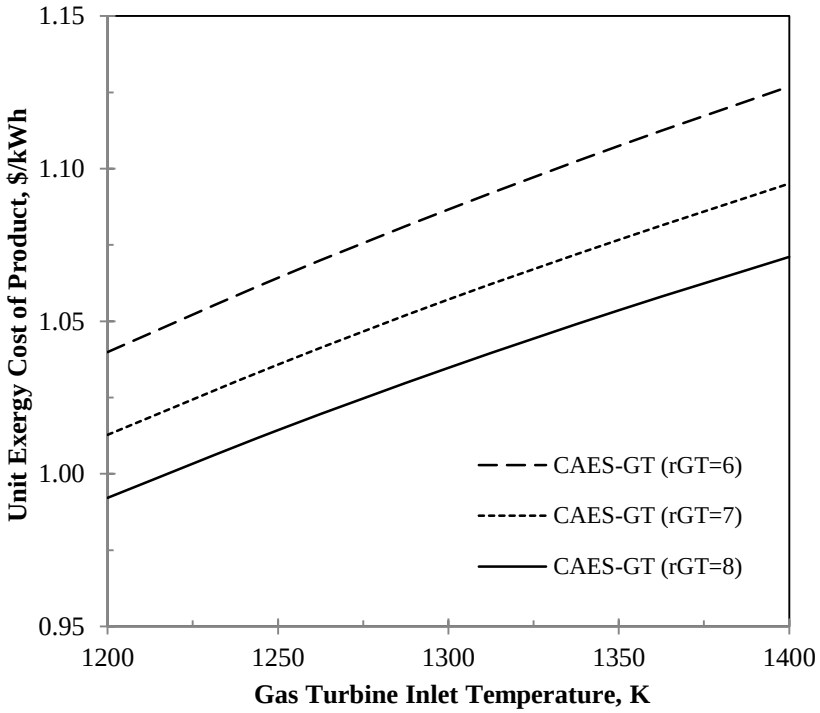

Figure 6.59: Variations of the unit cost of electricity generation by the CAES-GT system with the gas turbine inlet temperature, for different gas turbine expansion ratios

The relative cost difference, thus, is affected by the change in the gas turbine inlet temperature. As shown in Figure 6.60, the relative cost difference decreases around 0.1% and 2% for the electrolyser and the biomass-GT system. This level of change may seem negligible when comparing with 10% increase in the relative cost difference of the generated electricity by the CAES-GT system. Higher values of relative cost difference reveals the fact that the product of the system is more expansive than the fuel consumed.

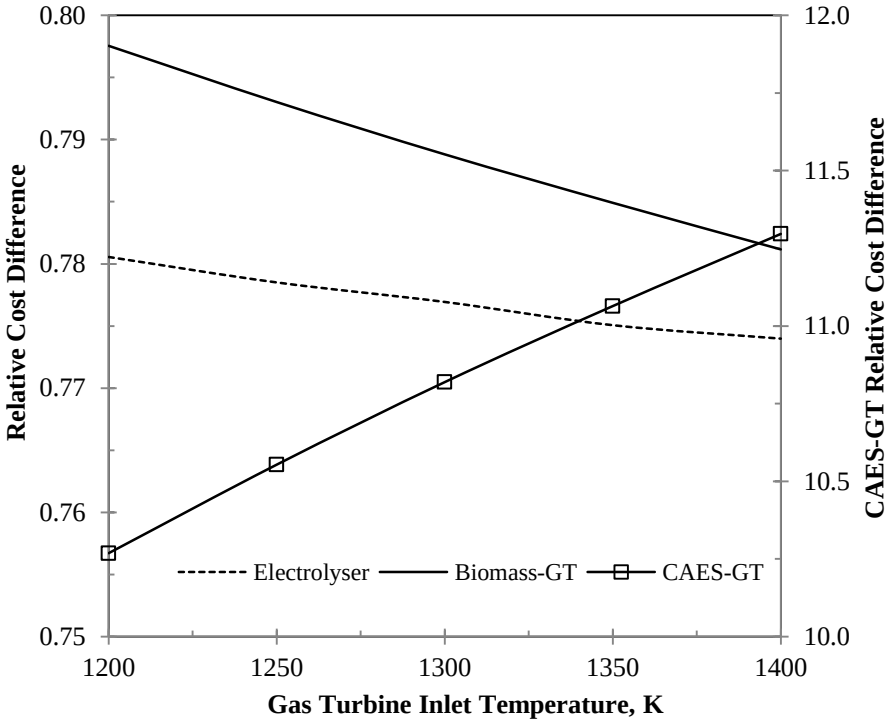

Figure 6.60: Effect of gas turbine inlet temperature on the relative cost difference of the products of the hybrid PV-biomass system ($r_{\mathrm{GT}} = 7$).

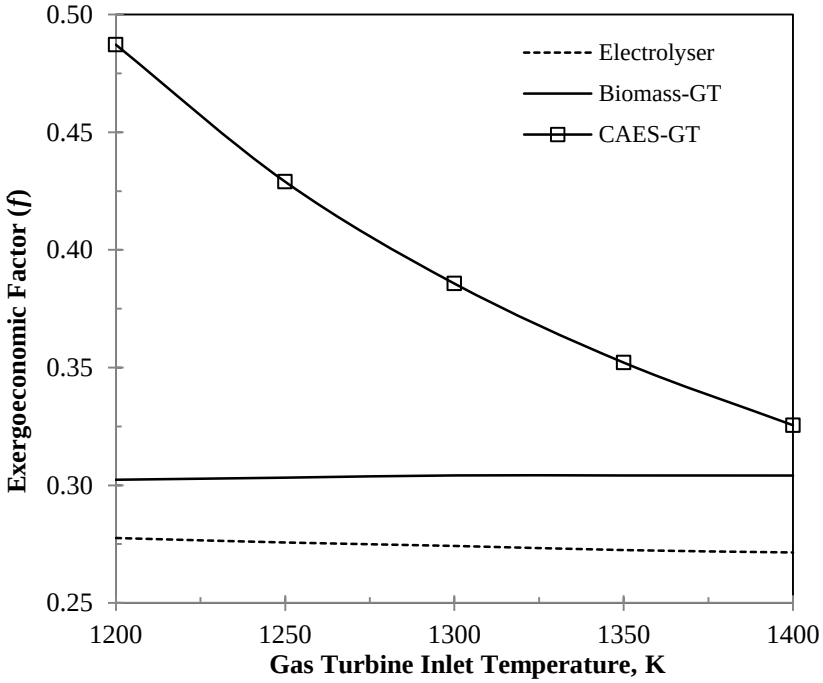

Figure 6.61: Effect of gas turbine inlet temperature on exergoeconomic factor of the components of the hybrid PV-biomass system ($r_{\mathrm{GT}} = 7$)

This may be due to expensive equipment purchase costs or due to exergy destruction rates in the system. This can be illustrated by the exergoeconomic factor of the components of the hybrid PV-biomass system in Figure 6.61. As is seen in

Figure 6.61, the exergoeconomic factor of the CAES-GT system drops significantly from 0.487 at 1200 K to 0.326 at 1400 K. aside from the increase in the levelized capital cost of the system, the significant increase in the exergy destruction in the CAES-GT system is the main cause of the decrease in its exergoeconomic factor.

6.3.3 Optimization of System 3

The effects of various parameters on the performance of the integrated solar PV-biomass system were discussed in the previous sections. The steam-to-carbon ratio of the biomass gasification system affects the unit exergy cost of electricity generation by the biomass-GT system and an increase in the gas turbine inlet temperature results in a higher unit cost of electricity generation by the CAES-GT system. Other parameters such as compressor pressure ratio and gas turbine expansion ratio affect the performance of System 3. In order to determine optimal points of operation and design of the integrated system, an optimization process is applied to the system. The objective functions are the overall exergy efficiency and the total purchase cost of the integrated system. The decision variables are also introduced and discussed in Chapter 5, which include the steam-to-carbon ration, turbine inlet temperature, compressor pressure ratio, gas turbine expansion ratio and isentropic efficiency. The ranges of the changes of the decision variables are presented in Table 6.29

Table 6.29: Decision variables and their range of change in the optimization process

Parameter	Steam-to-carbon ratio (*SC*), mol/mol	Turbine inlet temperature (*TIT*), K	Compressor pressure ratio (r_c), bar/bar	Gas turbine expansion ratio (r_{GT}), bar/bar	Gas turbine isentropic efficiency, %
Range of Change	1-3	1200-1400	7-9	6-8	65-85

Optimization of the energy systems may provide different optimal points or it can present one point as the best, optimum point of design and operation based on the objective functions. Pareto frontier is the locus of the optimal points given by the optimization process. Each point on the Pareto frontier represent optimal values of the objective functions, with specific set of values of the decision variables. The Pareto frontier for the hybrid solar PV-biomass system, with energy storage options, is presented in Figure 6.62

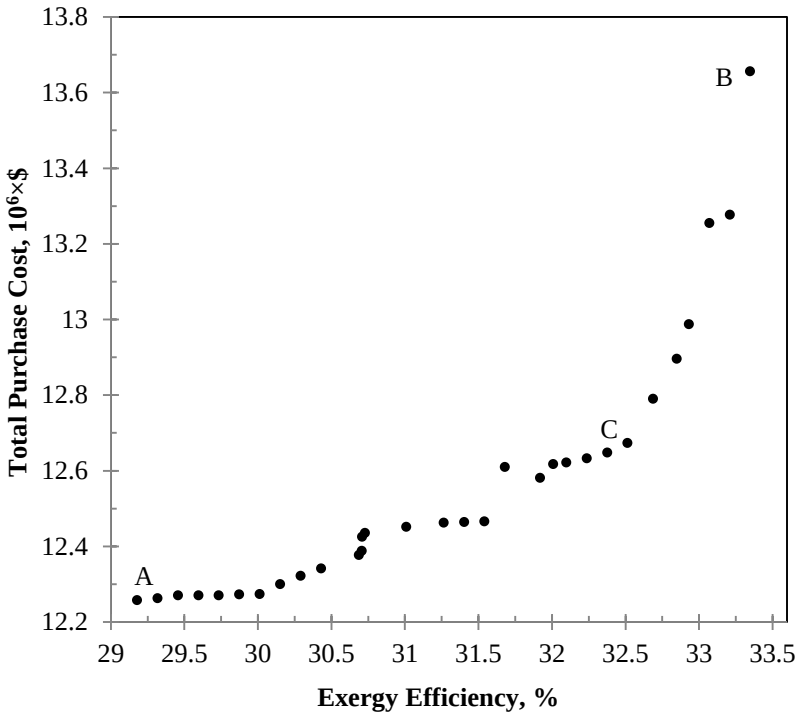

Figure 6.62: Pareto frontier: optimal points based on overall exergy efficiency and total purchase cost of the hybrid system

Points A and B are marked on Pareto frontier of System 3 as the points with minimum total purchase cost (minimum exergy efficiency), maximum exergy efficiency (maximum total purchase cost), respectively. Point C is the closest point to the equilibrium point which is characterized with maximum exergy efficiency and minimum total purchase cost. The values of the decision variables at each of these three optimal points are introduced to the hybrid system to obtain the extents of exergy destruction, carbon dioxide emission, energy efficiency, and unit exergy cost of the generated electricity by the biomass-GT system. These results are presented in Table 6.30.

When applying the values of the decision variables at the selected optimal point to the integrated system, the total heat recovery from the hybrid PV-biomass system is obtained as well. The recovered heat is introduced to the thermal water desalination system as the feed steam. Table 6.30 presents the obtained results from modeling and analysis of the water desalination system.

The results shown in Table 6.31 present the distilled water production cost by the hybrid PV-biomass system. The MED system has four evaporation/condensation effects and a condenser, where the total required heat transfer area is 1350 m^2. The

plant nominal capacity is 270 m^3/day. These systems are more economically feasible when the seawater is fed to the system. In this analysis, the salinity of Lake Ontario is considered in the calculation, since the hybrid system is evaluated based on the weather conditions of Toronto, Canada.

Table 6.30: Results of some parameters of the hybrid solar PV-biomass system at optimal points

Optimal point	Ex_d	$(CO_2)_y$	η	Ψ	Ex_q	c_{GT}	f_{GT}
A	243	0.107	29.9	29.2	136	11.4	0.22
B	207	0.070	33.9	33.3	99.5	9.3	0.28
C	213	0.076	33.1	32.5	106	9.7	0.27

Ex_d: Annual exergy destruction, GWh
$(CO_2)_y$: Annual carbon dioxide emission, 10^6×kg/y
η: Energy efficiency, %
Ψ: Exergy efficiency, %
Ex_q: Annual heat recovery (thermal exergy), GWh
c_{GT}: Unit exergy cost of electricity generated by the gas turbine of the Wind-CAES system, ¢/kWh
f_{GT}: Exergoeconomic factor of the gas turbine
WP_{pen}: Electric power penetration of the wind park, %
GT_{pen}: Electric power penetration of the gas turbine, %

Table 6.31: Distilled water production by heat recovery from the hybrid PV-biomass system

Parameter	Steam feed flow rate, kg/s	MED plant nominal capacity, kg/s	Heat transfer area, m^2	Performance ratio (PR), kg/kg	Distilled water price, \$/m^3
Values	0.46	3.1	1350	6.5	2.8

The results of energy assessment of the TES for System 3 are shown in Figure 6.63, which are obtained based on the maximum heat recovery availability from the CAES-GT system. A 1.5 MW thermal energy is recoverable, which is stored as hot water with a total capacity of 1.5×10^3 kg. The heat loss from the TES system boundary is 0.16 MW, and the overall energy efficiency is 89%.

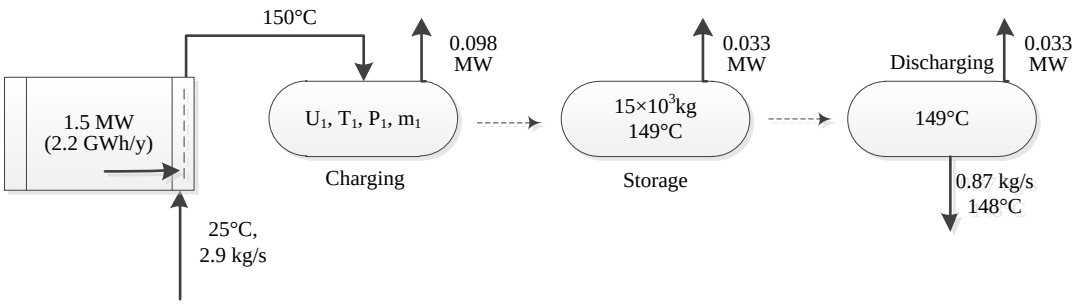

Figure 6.63: Storage medium and heat flow rates in the TES system

When investigating the hybrid PV-biomass system for its thermal energy recovery potentials based on the optimal point C on the Pareto frontier, the results illustrated in Figure 6.64 are obtained.

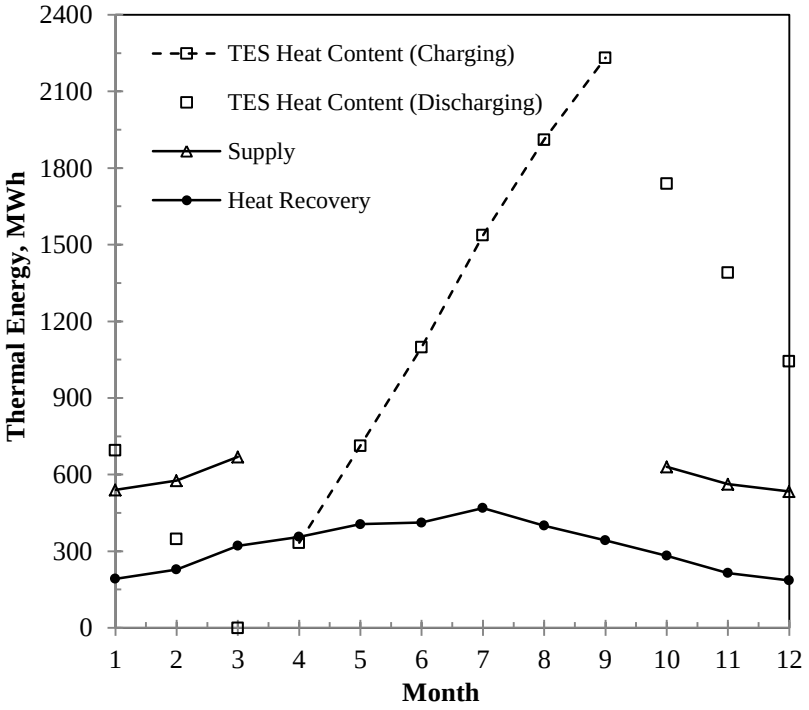

Figure 6.64: Thermal energy recovery, storage and supply by the TES system

It is shown that 2200 MWh thermal energy is accumulated in the thermal storage tanks throughout the charging phases and 600 MWh/month thermal energy is supplied to the district heating system on average. The solid line with circular markers shows the total monthly heat recovery from the CAES-GT system. The charging phase of the energy storage process is presented by the dashed line with square markers. In fact, the square markers show the discharging phase, while the thermal energy supply is shown as the solid line with rectangular markers. Figure 6.65 presents the corresponding values in exergy terms. Overall energy and exergy efficiencies are obtained as 92 and 72%, respectively.

System 3 is a hybrid solar PV-biomass system, which generates 10 MW baseload power using hydrogen and compressed air energy storage options. To investigate the importance of energy storage options in generating renewable energy-based electricity a comparison is reported. System 3 is compared with two systems: a simple PV-

biomass system, which has no energy storage options, and a hybrid PV-biomass system that uses pumped-hydro (PH) as the energy storage option.

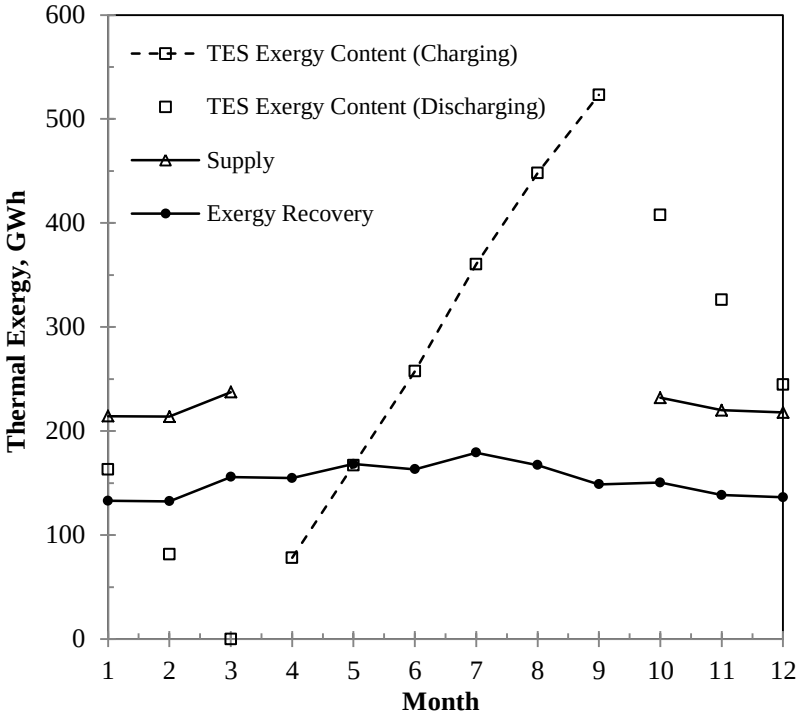

Figure 6.65: Thermal exergy recovery, storage and supply by the TES system

The PV modules of the simple system generate up to 2 MW electricity while the rest of the demand is met by a biomass-GT system. During the hours of solar power unavailability the biomass-GT operates and generates electricity, considering there is no CAES system involved. The operation of the PV-biomass-PH system is similar to the one of System 3. However, the CAES system is substituted with a pumped hydro system. When excess electricity is available from the PV-biomass system, a pump displaces water from a downstream storage pool (dam) or an upstream one. Therefore electric energy is stored in the form of potential energy of the elevated water. The height distance between the two water reservoirs is set as 200 m (Namgyel, 2004). When solar power is unavailable or insufficient, the stored water is directed to a hydro turbine, which generates electricity by converting potential energy to rotational energy.

Table 6.32 reveals that if hydrogen and compressed air energy storage options are not used in the PV-biomass system, 50% more biomass is required annually to generate 96% of the electricity demand. Moreover, the electric power penetrations of

the solar PV system, which is a carbon-free electricity generation system, are 4 and 10% for the simple and System 3, respectively. The greenhouse gas emission level of the integrated system reduces from 99×10^6 to 88×10^6 kg-CO_2/year, when energy storage options are used.

Table 6.32: Comparison of System 3 with a system without energy storage options

Parameter	Simple PV-biomass system	PV-biomass-PH	Hybrid PV-biomass system with ES options
Biomass consumption, 10^6 kg/year	45	20	22
PV electric power penetration, %	4	7.7	8
Biomass-GT electric power penetration, %	96	82.2	82
ES electric power penetration, %	0	10.1	10
CO_2 emission, g/kWh	1126	848	1008
CO_2 emission, 10^6kg/year	99	72.3	88
energy efficiency, %	29	65	33
exergy efficiency, %	27	63	33

The results of the comparison are also presented for the PV-biomass-PH system. Higher efficiencies are achieved due to the higher efficiencies of the pump and hydro turbine compared to the air compressor and the gas turbine of the CAES system. However, a cost evaluation presents the unit cost of electricity generation by the PV-biomass-PH system as 19.8 ¢/kWh, while the corresponding value for System 3 is 11 ¢/kWh. In economic calculations the values presented by Namgyel (2004) are used (2500 $/kW cost of PH storage system).

6.3.4 Closure

The hybrid PV-biomass system with energy storage options was investigated based on energy, exergy, and exergoeconomics. The hybrid system consists of an integrated biomass-based gas turbine cycle (biomass-GT), which generates electricity, and provides heat recovery. As another sub-part of the hybrid system, a PV-electrolyser module is integrated with a compressed air energy storage system. The overall hybrid system supplies 10 MW baseload electric power, and an annual 7730 MWh thermal energy. The exergy analysis results show that the PV system accounts for 56% of the annual exergy destruction in the hybrid system and 38% of the annual exergy destruction occurs in the biomass-GT system. The overall energy and exergy

efficiencies of the hybrid PV-biomass system with energy storage options are 34.8 and 34.1%, respectively. The hybrid PV-biomass system is sensitive to some parameters such as the steam-to-carbon ratio of the biomass gasifier, and the gas turbine inlet temperature and expansion ratio. A 29% increase in energy and exergy efficiencies is reported with the increase in *SC* from 1 to 3 mol/mol. The related reduction in the specific carbon dioxide emission is from 1441 to 583 g/kWh. Moreover, the gasifier steam-to-carbon ratio positively affects the unit exergy cost of products of the hybrid system components. In contrast to *SC*, the increase in the GT inlet temperature has a negative effect on the overall energy and exergy efficiencies, and it does not make a significant contribution to the reduction in the specific carbon dioxide emission. However, higher GT expansion ratios result in higher energy efficiencies and lower CO_2 emissions. The relative cost difference decreases around 0.1% and 2% for the electrolyser and the biomass-GT system, when the GT inlet temperature is increases from 1200 to 1400 K.

6.4 Final Comparison and Generalization

In this research three novel, integrated renewable energy-based systems were developed and analyzed. The aim of the analyses was to investigate ESSs in the integrated systems. System 1 is a residential photovoltaic-fuel-cell-battery system that is developed to meet the power requirement of a house. This system is emission free, and if properly sized and configured can reliably meet the electric demand of the house. It also provides the residential area with thermal energy, with the aim of seasonal thermal storage.

System 2 is a baseload power plant that integrates different renewable energy resources. Hydrogen and compressed air energy storage are considered in the integrated system to overcome the temporal availability of the renewable resources. Thermal energy storage is also included to increase energy utilization.

System 3 is a hybrid solar photovoltaic-biomass system that is developed to supply 10 MW electricity to a small community. It is also integrated with a thermal desalination plant for distilled (potable) water production. Hydrogen, compressed air energy storage, and thermal energy storage are the energy storage options considered in System 3.

Each of the systems is developed for a specific purpose. However, they all have one thing in common; renewable energy is the main source of energy. Systems 1 and 3 operate solely on renewable energy, and System 2 consumes natural gas only to cover for wind power unavailability.

Comparison of the three developed systems is possible through heat recovery potential, exergy destruction ratio, and specific carbon dioxide emissions. The heat recovery potential is estimated through the ratio of the annual heat recovery from the system to the annual electric energy generation by the system. Higher heat recovery potential improves energy utilization and is driving interest towards multi-generation system.

Exergy destruction ratio is the ratio of the annual exergy destruction within the system boundary to the annual electric energy generation by the system. The lesser the values of exergy destruction ratio, the better the renewable energy use. Specific carbon dioxide emissions are obtained as the ratio of the annual carbon dioxide emissions to the annual electric energy generation. This parameter is only presented to compare the systems in terms of renewable energy use, since the sources of energy are emission free, except for System 2, which consumes natural gas. The results are presented in Table 6.33.

Table 6.33: Comparison of the systems based on heat recovery potential, exergy destruction ratio, and CO_2 emission

Parameter	System 1	System 2	System 3
Electric energy generation, GWh/year	0.016	4380	87.6
Heat recovery, GWh/year	0.0034	1163	8.05
Heat recovery potential, %	21	27	9.2
Exergy destruction, GWh/year	0.17	7579	213
Exergy destruction ratio, GWh/GWh	10.6	1.7	2.44
CO_2 emission, g/kWh	0	104	1008

Table 6.33 shows the heat recovery potential of System 2 is the greatest and System 3 has the least potential. System 1 has the highest exergy destruction ratio due to the significant exergy destruction in the photovoltaic system. System 3 is ranked second in terms of exergy destruction ratio since it uses both solar PV and biomass gasification, which have considerable exergy destruction. Moreover, System 3 consumes biomass to generate electricity and the CO_2 emissions of the gasification

process and the combustion process in the gas turbine result in 1008 g/kWh emission. The emission level of system one is zero, since solar energy is the only source of energy in this system.

The developed systems were investigated based on the solar irradiance and wind speed data of Toronto, Canada. The results will apply to any other location with the same weather condition and data. However, the application of the systems is not limited to Toronto, as their configurations and component selection are independent from geographical locations. Different weather data will only result in different nominal capacities of the system components. For instance, higher average solar irradiance in a location leads to smaller PV modules. Also, lesser number of wind turbines is required in System 2 if the average wind speed is higher.

Chapter 7: Conclusions and Recommendations

7.1 Conclusions

In this study, hydrogen storage, compressed air energy storage, thermal energy storage and battery energy storage are considered for three novel integrated energy systems. These integrated renewable energy-based systems are developed to accommodate different storage options. In this regard, solar, wind and biomass are the main energy sources to the integrated systems.

System 1 is a residential photovoltaic-fuel cell-battery system that is developed to meet the power requirement of a house. System 2 is a baseload power plant that integrates different renewable energy resources. Hydrogen and compressed air energy storage are considered in the integrated system to overcome the temporal availability of the renewable resources. System 3 is a hybrid solar photovoltaic-biomass system that is developed to supply 10 MW electricity to a small community. It is also integrated with a thermal desalination plant for distilled (potable) water production.

The energy, exergy and exergoeconomic analyses are performed and applied to the components to calculate the rates of energy and exergy flows, the efficiencies and the unit exergy cost of flows in the components. The present systems are also optimized based on exergy efficiency and total purchase cost as the objective functions. The following conclusions are made for the developed systems.

7.1.1 For System 1:

The following concluding remarks are drawn from this study:

- The capacities and performances of the components of System 1 depend on the weather data and the pattern of electricity demand of the house.
- The PV electric power output exceeds demand, during months with high-solar irradiance (spring-summer months in Canada). Also, the PV power penetration is higher during these months. Therefore, most of the hydrogen

produced by the electrolyser during high-irradiance months is stored in the storage tank (rather than consumed by the fuel cell).

- The results of the investigation prove the capability and reliability of solid oxide fuel cells in load following and generating electricity when needed. This is achieved through protecting the fuel cell by a fast response power supply system, the batteries. When abrupt changes in demand are sensed, the battery meets the electricity demand until the fuel cell adjusts itself to the new situation.
- System 1 is investigated based on the weather data in Toronto, and electricity demand of a Canadian house. However, the system is applicable to any other location around the globe, since the configuration is developed to supply off-grid electricity for a house. Geographical location and different demand patterns will only affect the component sizing.
- The unit cost of electricity generation by the hybrid PV-FC-battery system is 84 ¢/kWh (2 kW fuel cell capacity, 25 years system lifetime), which is comparable to the results obtained in the literature (90 ¢/kWh by Lagorse et al. (2008)).
- According to the exergoeconomic results, the minimum values of unit exergy costs of hydrogen production and electricity generation occur during the high-irradiance months, when the system operates at maximum capacity.
- The nominal capacity of the fuel cell affects the capacities of the PV and the electrolyser. For the case study in this research, 1.5 kW is an optimal capacity for the fuel cell. This is obtained through an optimization process. The optimum fuel cell capacity depends on the demand pattern.
- The optimum exergy efficiency of System 1 is 9.94%, and the PV system has the highest share in exergy destruction among the components of the hybrid system.

7.1.2 For System 2:

The following conclusions can be made from System 2:

- The novel integrated system presented in this study uses wind, solar and biomass energy resources to generate baseload electric power. The capacities

and performances of the integrated system depend on weather data and on the design parameters of the system components.

- For 64 bar compressed air pressure, 36 bar gas turbine inlet pressure, and 3.5 MW wind turbine nominal power, 356 wind turbines are required to supply 470 MW baseload electric power.
- The ratio of the electric energy output of the gas turbine to the energy consumption of the air compressor is 1.6, which is validated through the literature.
- The decrease in pressure drop, between the compressed air storage system and the pressure of the air entering the gas turbine, improves the performance of the CAES-GT system. As a result, a lesser number of wind turbines are required, and the power penetration of the gas turbine increases.
- The PV-H_2-FC system of System 2 is aimed at meeting a part of the baseload electric power demand through solar energy use and storage. In this research, this share is 5 MW; however, it is the designer's decision to make. The decision would be based on solar energy data of the site location.
- The PV-H_2-FC system accounts for 7% of total exergy destruction of the integrated renewable energy-based system. The results show higher exergy destruction for the PV-H_2-FC than the biomass-SOFC-GT system, although the power output of the latter system is higher. Low-efficient PV cells are responsible for high exergy destruction of the solar energy-based systems.
- The optimal gas turbine temperature is 1399 K with 36 bar/bar GT expansion ratio, according to the optimization results. The optimization of System 2 reveals 42 and 37% energy and exergy efficiencies, respectively.
- System 2 has 27% heat recovery potential, which can be related to 27% decrease in fossil fuel consumption for thermal energy production.
- Although the CAES-GT system uses natural gas as fuel, the carbon dioxide emission of the integrated system is comparably low. The emission of System 2 is only 104 g/kWh, which is by far less than the modern gas-fired power plants (440 g/kWh).

7.1.3 For System 3:

The investigation of System 2 leads to the following concluding remarks:

- The hybrid system supplies 10 MW baseload electric power and 7730 MWh thermal energy. However, its heat recovery potential is comparably less than System 2 (9% vs. 27%, respectively).
- The PV system is the source of 57% of total exergy destruction and 38% of the annual exergy destruction in the biomass-GT system.
- The overall energy and exergy efficiencies of System 3 are 33.1 and 32.5%, respectively.
- The hybrid PV-biomass system is sensitive to some parameters such as steam-to-carbon ratio of the biomass gasifier, and the gas turbine inlet temperature and expansion ratio. A 29% increase in energy and exergy efficiencies is reported with an increase in *SC* from 1 to 3 mol/mol. The related specific carbon dioxide emission reduction is from 1441 to 583 g/kWh.
- Moreover, the gasifier steam to carbon ratio positively affects the unit exergy cost of products of the hybrid system components. In contrast to *SC*, the increased gas turbine inlet temperature has a negative effect on the overall energy and exergy efficiencies, and does not make a significant contribution to the reduction in specific carbon dioxide emission.
- Using hydrogen and compressed air energy storage options decreases biomass consumption of System 3 by 50%. Moreover, the contribution of solar energy in the integrated system increases from 4 to 10%, when energy storage options are used. The greenhouse gas emission level of the integrated system reduces from 99-88×10^6 kg-CO2/year, when energy storage options are used.

7.2 Recommendations

The results obtained from this research also suggest several areas for future studies, as summarized below:

- The conducted analyses could be used to compare the developed systems with other power generation systems: conventional or renewable energy-based.

- The current research could help with better understanding of the applications of ESS in renewable energy-based systems.
- The developed systems could be applied to any geographical locations and electric power demand.
- The developed models could be used to individually investigate the components of the integrated systems. The models can be used to analyze the components based on energy, exergy, and exergoeconomics. The performance characteristics can also be obtained.
- The models can also be used to help decision makers in selecting the optimum size and/or efficiencies of the components when designing renewable power generation systems.

References

Abhat, A., 1983, "Low temperature latent heat thermal energy storage: Heat storage materials", Solar Energy, 30, pp. 313-332.

Abuadala, A., and Dincer, I., 2010, "Efficiency evaluation of dry hydrogen production from biomass gasification", Thermochimica Acta, 507–508, pp. 127-134.

Abuadala, A., and Dincer, I., 2012, "A review on biomass-based hydrogen production and potential applications", International Journal of Energy Research, 36, pp. 415-455.

Abuadala, A., Dincer, I., and Naterer, G. F., 2010, "Exergy analysis of hydrogen production from biomass gasification", International Journal of Hydrogen Energy, 35, pp. 4981-4990.

Ahluwalia, R. K., Hua, T. Q., and Peng, J. K., 2012, "On-board and Off-board performance of hydrogen storage options for light-duty vehicles", International Journal of Hydrogen Energy, 37, pp. 2891-2910.

Akkaya, A. V., Sahin, B., and Huseyin Erdem, H., 2008, "An analysis of SOFC/GT CHP system based on exergetic performance criteria", International Journal of Hydrogen Energy, 33, pp. 2566-2577.

Ameri, M., and Hejazi, S. H., 2004, "The study of capacity enhancement of the Chabahar gas turbine installation using an absorption chiller", Applied Thermal Engineering, 24, pp. 59-68.

Arias, D. A., McMahan, A. C., and Klein, S. A., 2008, "Sensitivity of long-term performance simulations of solar energy systems to the degree of stratification in the thermal storage unit", International Journal of Energy Research, 32, pp. 242-254.

Baker, C. R., and Shaner, R. L., 1978, "A study of the efficiency of hydrogen liquefaction", International Journal of Hydrogen Energy, 3, pp. 321-334.

Basu, P., 2010, Biomass gasification and pyrolysis: practical design and theory, Elsevier, Oxford.

Beaudin, M., Zareipour, H., Schellenberglabe, A., and Rosehart, W., 2010, "Energy storage for mitigating the variability of renewable electricity sources: An updated review", Energy for Sustainable Development, 14, pp. 302-314.

Begić, F., and Afgan, N. H., 2007, "Sustainability assessment tool for the decision making in selection of energy system—Bosnian case", Energy, 32, pp. 1979-1985.

Bejan, A., Tsatsaronis, G., and Moran, M., 1996, Thermal Design and Optimization, John Wiley and Sons, New York.

Blackwell, R., 2013, "Wind power's prevailing direction in Canada? Big and foreign-owned", http://www.theglobeandmail.com/report-on-business/industry-news/energy-and-resources, June 5 2013.

Borgnakke, C., and Sonntag, R. E., 2008, Fundamentals of Thermodynamics, Wiley, Hoboken.

Braun, R. J., Klein, S. A., and Reindl, D. T., 2011, "Assessment of solid oxide fuel cells in building applications, phase 1: modeling and preliminary analyses", No. 207-R, Energy Center of Wisconsin.

Calderón, M., Calderón, A. J., Ramiro, A., and González, J. F., 2010, "Weather data and energy balance of a hybrid photovoltaic-wind system with hydrogen storage", International Journal of Hydrogen Energy, 35, pp. 7706-7715.

Caliskan, H., Hepbasli, A., and Dincer, I., 2011, "Exergy analysis and sustainability assessment of a solar-ground based heat pump with thermal energy storage", Journal of Solar Energy Engineering, 133, pp. 011005-011005.

CanWEA, 2008, "WindVision 2025: powering Canada's future", http://www.canwea.ca/windvision_e.php, June 5 2013.

Cavallo, A. J., 2001, "Energy storage technologies for utility scale intermittent renewable energy systems", Journal of Solar Energy Engineering, 123, pp. 387-389.

Cavallo, A. J., 2007, "Controllable and affordable utility-scale electricity from intermittent wind resources and compressed air energy storage (CAES)", Energy, 32, pp. 120-127.

CEC, 2004, "Failure modes and effects analysis for hydrogen refueling options", No. TR-03-177, California Energy Commision, California.

Chenni, R., Makhlouf, M., Kerbache, T., and Bouzid, A., 2007, "A detailed modeling method for photovoltaic cells", Energy, 32, pp. 1724-1730.

Chidambaram, L. A., Ramana, A. S., Kamaraj, G., and Velraj, R., 2011, "Review of solar cooling methods and thermal storage options", Renewable and Sustainable Energy Reviews, 15, pp. 3220-3228.

Clark, W., and Isherwood, W., 2004, "Distributed generation: remote power systems with advanced storage technologies", Energy Policy, 32, pp. 1573-1589.

Clarke, R. E., Giddey, S., Ciacchi, F. T., Badwal, S. P. S., Paul, B., and Andrews, J., 2009, "Direct coupling of an electrolyser to a solar PV system for generating hydrogen", International Journal of Hydrogen Energy, 34, pp. 2531-2542.

Cohce, M. K., Dincer, I., and Rosen, M. A., 2010, "Thermodynamic analysis of hydrogen production from biomass gasification", International Journal of Hydrogen Energy, 35, pp. 4970-4980.

Colpan, C. O., Dincer, I., and Hamdullahpur, F., 2007, "Thermodynamic modeling of direct internal reforming solid oxide fuel cells operating with syngas", International Journal of Hydrogen Energy, 32, pp. 787-795.

Colpan, C. O., Hamdullahpur, F., Dincer, I., and Yoo, Y., 2010, "Effect of gasification agent on the performance of solid oxide fuel cell and biomass gasification systems", International Journal of Hydrogen Energy, 35, pp. 5001-5009.

Dell, R. M., and Rand, D. A. J., 2001, "Energy storage — a key technology for global energy sustainability", Journal of Power Sources, 100, pp. 2-17.

Denholm, P., Ela, E., Kirby, B., and Milligan, M., 2010, "The role of energy storage with renewable electricity generation", No. NREL/TP-6A2-47187, National Renewable Energy Laboratory (NREL), US.

Denholm, P., and Kulcinski, G. L., 2004, "Life cycle energy requirements and greenhouse gas emissions from large scale energy storage systems", Energy Conversion and Management, 45, pp. 2153-2172.

Di Profio, P., Arca, S., Rossi, F., and Filipponi, M., 2009, "Comparison of hydrogen hydrates with existing hydrogen storage technologies: Energetic and economic evaluations", International Journal of Hydrogen Energy, 34, pp. 9173-9180.

Dicken, C. J. B., and Mérida, W., 2007, "Measured effects of filling time and initial mass on the temperature distribution within a hydrogen cylinder during refuelling", Journal of Power Sources, 165, pp. 324-336.

Dincer, I., and Dost, S., 1996, "A perspective on thermal energy storage systems for solar energy applications", International Journal of Energy Research, 20, pp. 547-557.

Dincer, I., and Rosen, M. A., 2007, Exergy: Energy, Environment and Sustainable Development, Elsevier.

Dincer, I., and Rosen, M. A., 2011a, "Energy and exergy analysis of thermal energy storage systems", in Thermal energy stoage: systems and applications, John Wiley & Sons, Singapore.

Dincer, I., and Rosen, M. A., 2011b, "Sustainability aspects of hydrogen and fuel cell systems", Energy for Sustainable Development, 15, pp. 137-146.

Dincer, I., and Rosen, M. A., 2011c, Thermal energy storage, systems and applications, John Wiley & Sons, Chichester.

Dincer, I., Rosen, M. A., and Zamfirescu, C., 2009, "Exergetic performance analysis of a gas turbine cycle integrated with solid oxide fuel cells", Journal of Energy Resources Technology, 131, pp. 032001-0320011.

DirectEnergy, 2012, "Price comparison for residential rlectricity consumers ", https://www1.directenergy.com/ONProgramDocs/ON_PC_Elec_RES_ONER910_Oct18.12.pdf, July 2, 2013.

Divya, K. C., and Østergaard, J., 2009, "Battery energy storage technology for power systems—An overview", Electric Power Systems Research, 79, pp. 511-520.

Dunn, S., 2002, "Hydrogen futures: toward a sustainable energy system", International Journal of Hydrogen Energy, 27, pp. 235-264.

EERE, 2008a, "Gaseous and liquid hydrogen storage", http://www1.eere.energy.gov/hydrogenandfuelcells/storage/hydrogen_storage.html, June 19, 2013.

EERE, 2008b, "Technical assessment: cryo-compressed hydrogen storage for vehicular applications", US Department of Energy Hydrogen Program.

Enbar, N., 2010, "PV O&M best practices", Utility/Lab Workshop on PV Technology and Systems, Tempe, Arizona, November 8-9, 2010.

Evans, A., Strezov, V., and Evans, T. J., 2009, "Assessment of sustainability indicators for renewable energy technologies", Renewable and Sustainable Energy Reviews, 13, pp. 1082-1088.

Gaines, L., and Cuenca, R., 2000, "Costs of lithium-ion batteries for vehicles", No. ANL/ESD-42, Argonne National Laboratory.

GCEP, 2006, "An assessment of solar energy conversion technologies and research opportunities", Stanford University.

Gibson, T. L., and Kelly, N. A., 2008, "Optimization of solar powered hydrogen production using photovoltaic electrolysis devices", International Journal of Hydrogen Energy, 33, pp. 5931-5940.

Grazzini, G., and Milazzo, A., 2008, "Thermodynamic analysis of CAES/TES systems for renewable energy plants", Renewable Energy, 33, pp. 1998-2006.

Green, M. A., Emery, K., Hishikawa, Y., Warta, W., and Dunlop, E. D., 2012, "Solar cell efficiency tables (version 39)", Progress in Photovoltaics: Research and Applications, 20, pp. 12-20.

Greenblatt, J. B., Succar, S., Denkenberger, D. C., Williams, R. H., and Socolow, R. H., 2007, "Baseload wind energy: modeling the competition between gas turbines and compressed air energy storage for supplemental generation", Energy Policy, 35, pp. 1474-1492.

Hacatoglu, K., Dincer, I., and Rosen, M. A., 2011a, "Exergy analysis of a hybrid solar hydrogen system with activated carbon storage", International Journal of Hydrogen Energy, 36, pp. 3273-3282.

Hacatoglu, K., McLellan, P. J., and Layzell, D. B., 2011b, "Feasibility study of a Great Lakes bioenergy system", Bioresource Technology, 102, pp. 1087-1094.

Haji Abedin, A., 2010, "Thermochemical energy storage systems: modelling, analysis and design", MSc Thesis, University of Ontario Institute of Technology, Oshawa, ON.

Hawkes, A. D., Aguiar, P., Croxford, B., Leach, M. A., Adjiman, C. S., and Brandon, N. P., 2007, "Solid oxide fuel cell micro combined heat and power system operating strategy: Options for provision of residential space and water heating", Journal of Power Sources, 164, pp. 260-271.

Hirscher, M., 2010, "Storage of hydrogen in the pure form", in Handbook of hydrogen storage: new materials for future energy storage, M. Hirscher, ed., Wiley-VCH, Weinheim.

Hosseini, M., Dincer, I., Ahmadi, P., Avval, H. B., and Ziaasharhagh, M., 2013a, "Thermodynamic modelling of an integrated solid oxide fuel cell and micro gas turbine system for desalination purposes", International Journal of Energy Research, 37, pp. 426-434.

Hosseini, M., Dincer, I., and Rosen, M. A., 2012, "Thermodynamic analysis of a cycle integrating a solid oxide fuel cell and micro gas turbine with biomass gasification", 11th International Conference on Sustainable Energy Technologies (SET 2012) Vancouver, September 2-5, 2012.

Hosseini, M., Dincer, I., and Rosen, M. A., 2013b, "Hybrid solar–fuel cell combined heat and power systems for residential applications: Energy and exergy analyses", Journal of Power Sources, 221, pp. 372-380.

Hua, T. Q., Ahluwalia, R. K., Peng, J. K., Kromer, M., Lasher, S., McKenney, K., Law, K., and Sinha, J., 2011, "Technical assessment of compressed hydrogen storage tank systems for automotive applications", International Journal of Hydrogen Energy, 36, pp. 3037-3049.

IEA, 2012, "Renewable energy outlook", in World Energy Outlook 2012, International Energy Agency.

Ismail, K. A. R., and de Jesus, A. B., 2001, "Parametric study of solidification of PCM around a cylinder for ice-bank applications", International Journal of Refrigeration, 24, pp. 809-822.

Jacobsen, R. T., Leachman, J. W., Penoncello, S. G., and Lemmon, E. W., 2007, "Current status of thermodynamic properties of hydrogen", Int J Thermophys, 28, pp. 758-772.

Javani, N., 2011, "Investigation of energy storage options for thermal management in hybrid electric vehicles", PhD Candidacy Thesis Proposal, University of Ontario Institute of Technology, Oshawa, ON.

Jensen, J. O., Vestbø, A. P., Li, Q., and Bjerrum, N. J., 2007, "The energy efficiency of onboard hydrogen storage", Journal of Alloys and Compounds, 446–447, pp. 723-728.

Kamimoto, M., Abe, Y., Sawata, S., Tani, T., and Ozawa, T., "Latent heat storage unit using form-stable high density polyethylene for solar thermal applications", Proc. International Symposium on Thermal Application of Solar Energy, Kanagawa, Japan.

Klell, M., Kindermann, H., and Jogl, C., "Thermodynamics of gaseous and liquid hydrogen storage", Proc. Proceedings International Hydrogen Energy Congress and Exhibition IHEC 2007, Istanbul, 13-15 July 2007.

Krainz, G., Bartlok, G., Bodner, P., Casapicola, P., Doeller, C., Hofmeister, F., Neubacher, E., and Zieger, A., "Development of automotive liquid hydrogen storage systems," Proc. Advances in cryogenic engineering: Transactions of the cryogenic engineering conference - CEC, Anchorage, Alaska (USA), 22-26 Sept. 2003, pp. 35-40.

Krein, P., 2007, "Battery management for maximum performance in plug-in electric and hybrid vehicles", Vehicle Power and Propulsion Conference, Arlington, 9-12 Sept. 2007, pp. 2-5.

Lagorse, J., Simões, M. G., Miraoui, A., and Costerg, P., 2008, "Energy cost analysis of a solar-hydrogen hybrid energy system for stand-alone applications", International Journal of Hydrogen Energy, 33, pp. 2871-2879.

Lane, G. A., 1983, Solar heat storage: latent heat material, CRC Press, Florida.

Larminie, J., and Dicks, A., 2003, "Fuel cell systems explained", John Wiley & Sons Ltd, Wiltshire.

Lazou, A. A., and Papatsoris, A. D., 2000, "The economics of photovoltaic stand-alone residential households: A case study for various European and Mediterranean locations", Solar Energy Materials and Solar Cells, 62, pp. 411-427.

Lemmon, E. W., and Jacobsen, R. T., 2005, "A new functional form and new fitting techniques for equations of state with application to pentafluoroethane (HFC-125)", Journal of Physics and Chemistry, 34, pp. 69-108.

López, E., Isorna, F., and Rosa, F., 2007, "Optimization of a solar hydrogen storage system: Exergetic considerations", International Journal of Hydrogen Energy, 32, pp. 1537-1541.

Lu, L., and Yang, H. X., 2010, "Environmental payback time analysis of a roof-mounted building-integrated photovoltaic (BIPV) system in Hong Kong", Applied Energy, 87, pp. 3625-3631.

Lund, H., 2005, "Large-scale integration of wind power into different energy systems", Energy, 30, pp. 2402-2412.

Lund, H., and Salgi, G., 2009, "The role of compressed air energy storage (CAES) in future sustainable energy systems", Energy Conversion and Management, 50, pp. 1172-1179.

Lund, H., Salgi, G., Elmegaard, B., and Andersen, A. N., 2009, "Optimal operation strategies of compressed air energy storage (CAES) on electricity spot markets with fluctuating prices", Applied Thermal Engineering, 29, pp. 799-806.

Madlener, R., and Latz, J., 2013, "Economics of centralized and decentralized compressed air energy storage for enhanced grid integration of wind power", Applied Energy, 101, pp. 299-309.

Martinot, E., 2013, "Renewables, global futures report (GFR)", Renewable Rnergy Policy Network for 21st Century (REN21).

Maus, S., Hapke, J., Ranong, C. N., Wüchner, E., Friedlmeier, G., and Wenger, D., 2008, "Filling procedure for vehicles with compressed hydrogen tanks", International Journal of Hydrogen Energy, 33, pp. 4612-4621.

McDowall, J., 2006, "Integrating energy storage with wind power in weak electricity grids", Journal of Power Sources, 162, pp. 959-964.

McIlveen-Wright, D. R., Moglie, M., Rezvani, S., Huang, Y., Anderson, M., Redpath, D., Dave, A., and Hewitt, N. J., 2011, "A techno-economic analysis of biomass gasifiers integrated with high and intermediate temperature solid oxide fuel cells", International Journal of Energy Research, 35, pp. 1037-1047.

Minh, N., 2002, "Solid oxide fuel-cell hybrid system", Second DOE/UN International Conference and Workshop on Hybrid Power Systems, Charlotte, April 16-17, 2002.

Mitchell, M., 1999, An introduction to genetic algorithms, MIT Press, Cambridge.

Mori, D., and Hirose, K., 2009, "Recent challenges of hydrogen storage technologies for fuel cell vehicles", International Journal of Hydrogen Energy, 34, pp. 4569-4574.

Motahar, S., and Alemrajabi, A. A., 2009, "Exergy based performance analysis of a solid oxide fuel cell and steam injected gas turbine hybrid power system", International Journal of Hydrogen Energy, 34, pp. 2396-2407.

Mueller, F., Brouwer, J., Jabbari, F., and Samuelsen, S., 2006, "Dynamic simulation of an integrated solid oxide fuel cell system including current-based fuel flow control", Fuel Cell Science, 3, pp. 144-154.

Munteanu, I., Bratcu, A. I., Cutululis, N. A., and Ceanga, E., 2008, Optimal control of wind energy systems toward a global approach, Springer.

Nair, N.-K. C., and Garimella, N., 2010, "Battery energy storage systems: Assessment for small-scale renewable energy integration", Energy and Buildings, 42, pp. 2124-2130.

Naish, C., McCubbin, I., Edberg, O., and Harfoot, M., 2007, "Outlook of energy storage technologies", No. IP/A/ITRE/ST/2007-07, European Parliament's committee on Industry, Research and Energy (ITRE).

Namgyel, D., 2004, "Wind following with pumped hydroelectric energy storage in New Brunswick", M.Sc, University of Rajasthan, India.

NCDIA, 2011, "Daily data report of Port Colborne", Environment Canada.

Nieminen, J., Dincer, I., and Naterer, G., 2010, "Comparative performance analysis of PEM and solid oxide steam electrolysers", International Journal of Hydrogen Energy, 35, pp. 10842-10850.

Nourai, A., 2007, "Installation of the first distributed energy storage system (DESS) at American electric power (AEP)", No. SAND2007-3580, Sandia National Laboratories.

NRC, 2008, "Energy efficiency trends in Canada - 1990 to 2005", http://oee.nrcan.gc.ca/publications/statistics/trends07/preface.cfm?attr=0, June 3, 2013.

NRC, 2011, "Solar photovoltaic energy", http://canmetenergy.nrcan.gc.ca/renewables/solar-photovoltaic/562, June 6, 2013.

NREL, 2009, "Current (2009) state-of-the-art hydrogen production cost estimate using water electrolysis", No. NREL/BK-6A1-46676, National Renewable Energy Laboratory.

OAGO, 2011, "2011 Annual report of the office of the auditor general of Ontario", Office of the Auditor General of Ontario.

Öztürk, H. H., 2004, "Comparison of energy and exergy efficiencies of an underground solar thermal storage system", International Journal of Energy Research, 28, pp. 341-353.

Peters, R., and Burda, C., 2007, "The basics on base load: meeting Ontario's base load electricity demand with renewable power sources", The Pembina Institute, Canada.

Ptasinski, K. J., Prins, M. J., and Pierik, A., 2007, "Exergetic evaluation of biomass gasification", Energy, 32, pp. 568-574.

Puig-Arnavat, M., Bruno, J. C., and Coronas, A., 2010, "Review and analysis of biomass gasification models", Renewable and Sustainable Energy Reviews, 14, pp. 2841-2851.

Radchik, A., Skryabin, I., Maisano, J., Novikov, A., and Gazarian, T., 2013, "Ensuring long term investment for large scale solar power stations: Hedging instruments for green power", Solar Energy.

Rao, M. S., Singh, S. P., Sodha, M. S., Dubey, A. K., and Shyam, M., 2004, "Stoichiometric, mass, energy and exergy balance analysis of countercurrent fixed-bed gasification of post-consumer residues", Biomass and Bioenergy, 27, pp. 155-171.

Rosen, M. A., Tang, R., and Dincer, I., 2004, "Effect of stratification on energy and exergy capacities in thermal storage systems", International Journal of Energy Research, 28, pp. 177-193.

Saldanha, N., and Beausoleil-Morrison, I., 2012, "Measured end-use electric load profiles for 12 Canadian houses at high temporal resolution", Energy and Buildings, 49, pp. 519-530.

Scott, D. S., 2007, Smelling land: the hydrogen defense against climate catastrophe, Canadian Hydrogen Association, Canada.

Shabani, B., Andrews, J., and Watkins, S., 2010, "Energy and cost analysis of a solar-hydrogen combined heat and power system for remote power supply using a computer simulation", Solar Energy, 84, pp. 144-155.

Shin, D., and Banerjee, D., "Enhanced thermal properties of PCM based Nanofluid for solar thermal energy storage", Proc. ASME 4th International Conference on Energy Sustainability, ASME, Phoenix, , May 17-22, 2010.

Sukamongkol, Y., Chungpaibulpatana, S., and Ongsakul, W., 2002, "A simulation model for predicting the performance of a solar photovoltaic system with alternating current loads", Renewable Energy, 27, pp. 237-258.

SunPower, 2012, "210 Solar panel", www.prevailingwindpower.com/sunpower.pdf, June 26, 2012.

Szargut, J., 2005, Exergy method: technical and ecological applications, WIT Press, Boston.

TamizhMani, G., Ji, L., Tang, Y., and Petacci, L., 2003, "Photovoltaic module thermal-wind performance: Long-term monitoring and model development for energy rating", No. NREL/CD-520-33586, NCPV and Solar Program Review Meeting 2003.

Tesfahunegn, S. G., Ulleberg, Ø., Vie, P. J. S., and Undeland, T. M., 2011, "Optimal shifting of photovoltaic and load fluctuations from fuel cell and electrolyzer to lead acid battery in a photovoltaic/hydrogen standalone power system for improved performance and life time", Journal of Power Sources, 196, pp. 10401-10414.

Tock, L., Gassner, M., and Maréchal, F., 2010, "Thermochemical production of liquid fuels from biomass: Thermo-economic modeling, process design and process integration analysis", Biomass and Bioenergy, 34, pp. 1838-1854.

UTM, 2012, "Weather data", University of Toronto Mississauga, University of Toronto Mississauga.

Uzunoglu, M., Onar, O. C., and Alam, M. S., 2009, "Modeling, control and simulation of a PV/FC/UC based hybrid power generation system for stand-alone applications", Renewable Energy, 34, pp. 509-520.

Van Thong, V., and Belmans, R., 2006, "Distributed generation overview: current status and challenges", International Review of Electrical Engineering, 1, pp. 178-189.

Wagner, L., 2007, "Overview of energy storage methods", Mora Associates.

Wang, S. Y., and Yu, J. L., 2012, "Optimal sizing of the CAES system in a power system with high wind power penetration", International Journal of Electrical Power & Energy Systems, 37, pp. 117-125.

Wang, Z., Naterer, G. F., Gabriel, K. S., Secnik, E., Gravelsins, R., and Daggupati, V., 2011, "Thermal design of a solar hydrogen plant with a copper–chlorine cycle and molten salt energy storage", International Journal of Hydrogen Energy, 36, pp. 11258-11272.

Yang, J. C., 2009, "A thermodynamic analysis of refueling of a hydrogen tank", International Journal of Hydrogen Energy, 34, pp. 6712-6721.

Yumrutaş, R., Kunduz, M., and Ayhan, T., 2003, "Investigation of thermal performance of a ground coupled heat pump system with a cylindrical energy storage tank", International Journal of Energy Research, 27, pp. 1051-1066.

Zalba, B., Marín, J. M., Cabeza, L. F., and Mehling, H., 2003, "Review on thermal energy storage with phase change: materials, heat transfer analysis and applications", Applied Thermal Engineering, 23, pp. 251-283.

Zhang, X., Chan, S. H., Li, G., Ho, H. K., Li, J., and Feng, Z., 2010, "A review of integration strategies for solid oxide fuel cells", Journal of Power Sources, 195, pp. 685-702.

Zurigat, Y. H., Maloney, K. J., and Ghajar, A. J., 1989, "A comparison study of one-dimensional models for stratified thermal storage tanks", Transactions of the ASME Journal of Solar Engineering, 111, pp. 204-211.